Atlas of Perioperative 3D Transesophageal Echocardiography

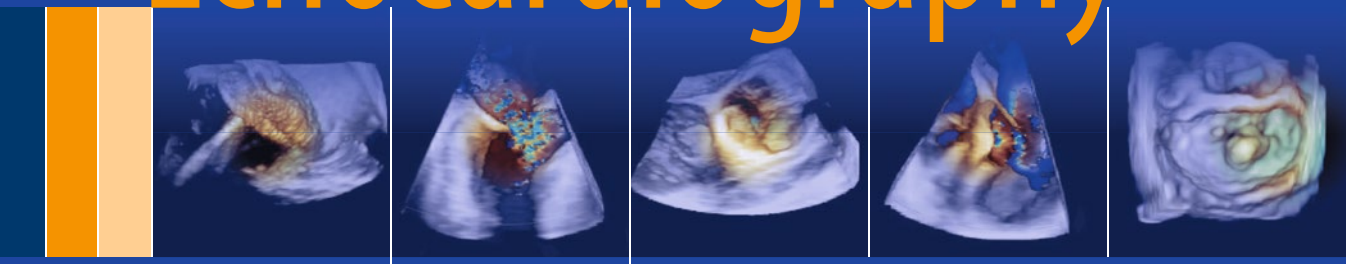

Cases and Videos

Wei-Hsian Yin
Ming-Chon Hsiung

EXTRAS ONLINE

Springer

Atlas of Perioperative 3D Transesophageal Echocardiography

Wei-Hsian Yin • Ming-Chon Hsiung

Atlas of Perioperative 3D Transesophageal Echocardiography

Cases and Videos

Springer

Wei-Hsian Yin
Division of Cardiology
Cheng-Hsin General Hospital
Taipei
Taiwan

Ming-Chon Hsiung
Division of Cardiology
Cheng-Hsin General Hospital
Taipei
Taiwan

ISBN 978-981-10-0586-2 ISBN 978-981-10-0587-9 (eBook)
DOI 10.1007/978-981-10-0587-9

Library of Congress Control Number: 2016940312

Printed on acid-free paper

This Springer imprint is published by Springer Nature
The registered company is Springer Science+Business Media Singapore Pte Ltd.

Preface

Transesophageal echocardiography plays a pivotal role in perioperative management of patients undergoing open-heart surgery and interventional transcatheter therapy. It provides information for therapeutic decisions and detection of patient after surgery. Advances in computer technology resulted in the development of 3D images of cardiac structures, which enhanced the usefulness of echocardiography during the operation and played the role of the third eye of the surgeon.

To become proficient at perioperative 3D transesophageal echocardiography, understanding of principles of echocardiography and the pathophysiology is essential. In addition, clinical experience in perioperative 3D transesophageal is the must. This book contains a series of over 50 interesting and unusual cases to enrich your knowledge. In each case, background information is followed by a step-by-step approach to patient diagnosis and postoperative outcomes. The highlight of this book is the large number of illustrations, over 600, which is mainly 3D transesophageal echocardiography combined with 2D transesophageal echocardiography, X ray, fluoroscopy, computed tomography, etc., to demonstrate the various cardiovascular pathologies. Since the echo images we obtain in clinic practice are moving images, we have also used over 400 videos, which serve as a supplement to the static illustrations in the casebook and are all freely available in the Internet.

The atlas is organized into 11 chapters. In Chaps. 1, 2 and 3 abnormalities affecting mitral, aortic, tricuspid, and pulmonary valves are described. Prosthetic valves are discussed in Chap. 4. Chapter 5 details abnormalities of aorta. Chapters 6, 7 and 8 cover coronary artery diseases, congenital heart diseases, and cardiomyopathies. Cases of infective endocarditis are provided in Chap. 9. Chapter 10 deals with tumors and mass lesions. And the other cases are classified in Chap. 11. It is our hope that this book will offer readers an insider's view of perioperative 3D transesophageal echocardiography and to refresh their clinical training.

Growing from conception to completion, this casebook mirrored many of the experiences of parenting, especially wise from the rearing of our previous book, *Practice of clinical echocardiography case study*. Thankfully, Cheng Hsin General Hospital, Taipei, Taiwan, provided us full clinical support. We also appreciate the Division of Cardiovascular and Division of

Cardiovascular Surgery for facilitating performance of perioperative 3D transesophageal echocardiography. Lastly, the entire Echocardiography Laboratory, especially Li-Na Lee, Fang-Chieh Lee, and Wei-Hsuan Chiang, is thanked for compiling the cases and delivering the new book to the public.

Taipei, Taiwan Wei-Hsian Yin, MD
Taipei, Taiwan Ming-Chon Hsiung, MD

Contents

Abbreviations

2D	Two-dimensional
3D	Three-dimensional
Af	Atrial fibrillation
AML	Anterior mitral leaflet
AO	Aorta
AR	Aortic regurgitation
AS	Aortic stenosis
ASD	Atrial septal defect
AV	Aortic valve or atrioventricular
AVR	Aortic valve replacement
BNP	Brain-natriuretic peptide
CABG	Coronary artery bypass graft
CCA	Common carotid artery
CT	Computed tomography
ECG	Electrocardiogram
FL	False lumen
HV	Hepatic vein
ICA	Internal carotid artery
IVC	Inferior vena cava
IVS	Interventricular septum
LA	Left atrial
LAA	Left atrial appendage
LAD	Left anterior descending coronary artery
LCC	Left coronary cusp
LCX	Left circumflex artery
LIMA	Left internal mammary artery
LV	Left ventricle
LVEF	Left ventricular ejection fraction
LVOT	Left ventricular outflow tract
MI	Myocardial infarction
MR	Mitral regurgitation
MRSA	Methicillin-resistant *Staphylococcus aureus*
MPA	Main pulmonary artery
MPG	Mean pressure gradient
MPR	Multi-planar reconstruction
MS	Mitral stenosis
MV	Mitral valve

MVR	Mitral valve replacement
NCC	Noncoronary cusp
OM	Obtuse marginal artery
PA	Pulmonary artery
PCI	Percutaneous coronary intervention
PFO	Patent foramen ovale
PML	Posterior mitral leaflet
PPG	Peak pressure gradient
PR	Pulmonary regurgitation
PS	Pulmonary stenosis
PTCA	Percutaneous transluminal coronary angioplasty
PV	Pulmonary valve
PVR	Pulmonary valve replacement
RA	Right atrial
RCA	Right coronary artery
RCC	Right coronary cusp
RV	Right ventricle
RVOT	Right ventricular outflow tract
SAM	Systolic anterior motion
SMA	Superior mesenteric artery
SVC	Superior vena cava
SVG	Saphenous vein graft
TAVI	Transcatheter aortic valve implantation
TEE	Transesophageal echocardiography
TH	Thrombus
TL	True lumen
TR	Tricuspid regurgitation
TS	Tricuspid stenosis
TV	Tricuspid valve
TVR	Tricuspid valve replacement
VSD	Ventricular septal defect

Brief Introduction of 3D TEE

The history of echocardiography started with A-mode images derived by a thin ultrasound beam and advanced to M-mode displays and then to 2D examination of the heart in motion. This was followed by Doppler, color Doppler, tissue Doppler, speckle imaging, 3D reconstruction, and ultimately the development of real-time 3D TEE. Echocardiography remains the most commonly requested imaging study of the heart. Combined with portability, non-invasion, low cost, and widespread availability, it is a tribute to decipher clinical problems in cardiac pathology.

The key differences between 2D and 3D ultrasound imaging are the arrangement of elements in the transducer and the image processing procedure. In conventional cardiac 2D transducer, 64–128 elements are arranged along a single row, whereas 3D ultrasound used a matrix array transducer containing over 2500 elements. This system could acquire volumetric data rather than single slices of data, which ultimately permitted the display of volumetric 3D images. The piezoelectric elements within the transducers are arranged in a matrix configuration and require a large number of digital channels for these fully sampled elements to be connected. To reduce both power consumption and the diameter of the connecting cable, several miniaturized circuit boards are incorporated into the transducer, allowing partial beam forming to be performed in the probe. The image quality using reconstructive techniques depend critically on the quality of the original 2D images where minor patient or transducer movements or irregular rhythms may result in artifacts. Technologic advances led to improve the acquisition of multiple, gated image planes using ECG and respiratory gating which limits the amount of motion artifacts.

To date, the 3D spatial modes may be summarized as follows: live 3D, 3D zoom, 3D full volume, and 3D color Doppler. First, live 3D is a real-time mode that displays a fixed pyramidal dataset which allows quick 3D imaging and live change of movement of the TEE probe. Second, 3D zoom displays a magnified but truncated pyramidal dataset of variable size. To optimize image quality, accurate placement and adjustment of the sector width are important. 3D zoom is preferentially used to display the MV, TV, or the LAA. The en face view of the MV mirrors the surgical view from the LA perspective providing careful information. Third, the 3D full volume mode allows the acquisition of a pyramidal dataset including a larger cardiac volume and composed by merging a predefined number of narrower live 3D pyramidal wedges obtained over one to six heartbeats. The full volume can be further processed

offline by rotating and cropping to visualize specific structures inside the pyramid. Lastly, 3D color Doppler is similar to the acquisition of a full volume mode while with a larger dataset. It displays the direction, the range, and the relationship with surrounding structures of the blood flow.

In conclusion, the 3D TEE technique improved anatomic definition, diagnostic confidence, and novel views of the complicated cardiovascular encountered in common clinical practice. In addition, live 3D TEE enhances the perioperative communication among cardiac surgeons, cardiac physicians, and anesthesiologists. Together with promptly quantify software, 3D TEE helps to present the modality in perioperative situations precisely.

Diseases of the Mitral Valve

1

Abstract

In this chapter, cases of mitral leaflets prolapse, flail, annulus calcification, rheumatic heart disease, and systolic anterior motion received mitral repair or replacement are presented.

The TEE assessment always begins with a systematic 2D examination of the MV regardless of the type of the disease. 3D en face view from LA down to the MV can mirror the surgeon's view and express the MV structure and function carefully. In addition, evaluation of repair in the operating room before chest closure allows further intervention if required therefore improves the outcome.

1.1 Prolapse of Posterior Mitral Leaflet Having Repair

A 59-year-old woman had valvular heart disease with severe MR suffered from intermittent palpitation and exertional dyspnea. Auscultation: regular heart beat with a grade 3 systolic murmur over apex. ECG: sinus rhythm and nonspecific ST-T change. Chest X ray: cardiomegaly. Operation: MV and TV repair.

Electronic supplementary material The online version of this chapter (doi:10.1007/978-981-10-0587-9_1) contains supplementary material, which is available to authorized users.

W.-H. Yin, M.-C. Hsiung, *Atlas of Perioperative 3D Transesophageal Echocardiography*,
DOI 10.1007/978-981-10-0587-9_1

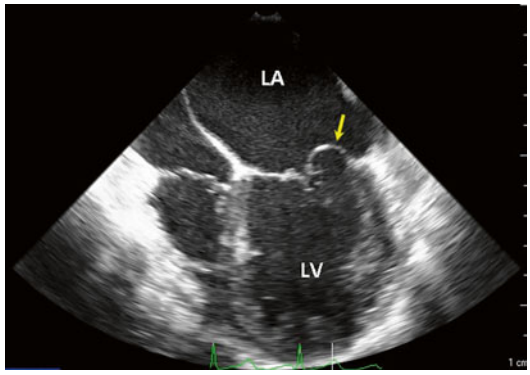

Fig. 1.1 Two-dimensional transesophageal echocardiography (2D TEE) image, four- chamber view, showed prolapse of posterior mitral leaflet (*arrow*) and LA dilatation

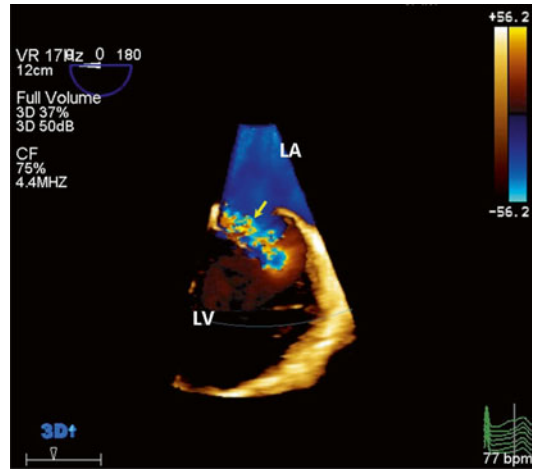

Fig. 1.4 3D TEE color Doppler, showed severe eccentric MR (*arrow*)

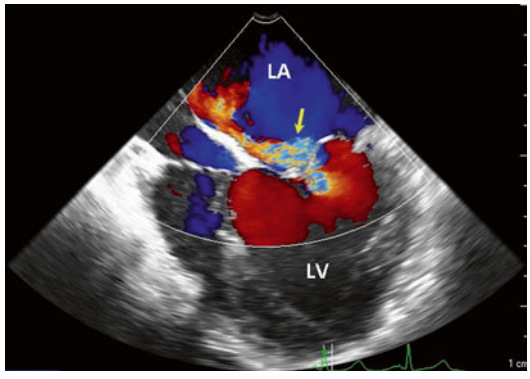

Fig. 1.2 2D TEE color Doppler, showed severe eccentric MR (*arrow*)

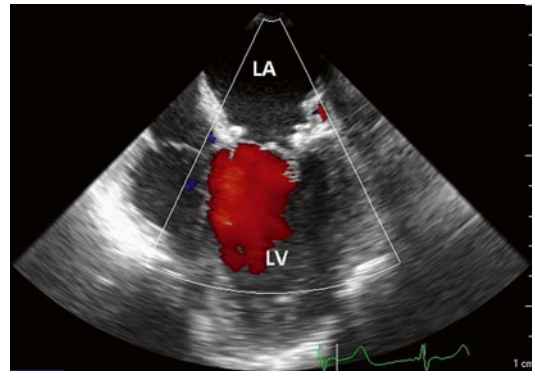

Fig. 1.5 2D TEE color Doppler, status post MV repair, showed well-closed MV without MR

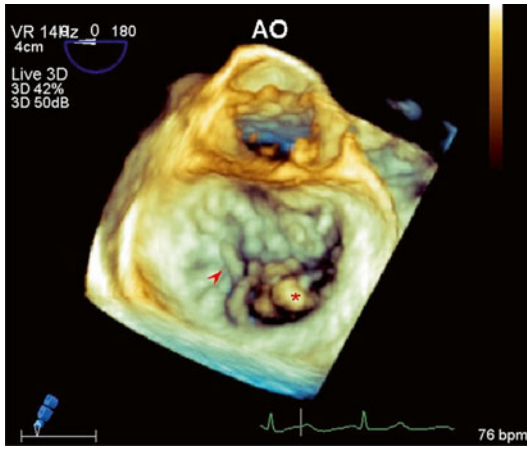

Fig. 1.3 3D TEE image, en face view, showed prolapse of P2 scallop (*) and chordae rupture (*arrow*)

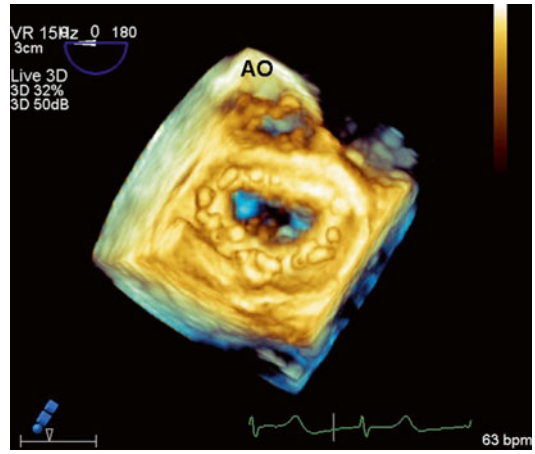

Fig. 1.6 3D TEE image, en face view, showed repaired MV with suture

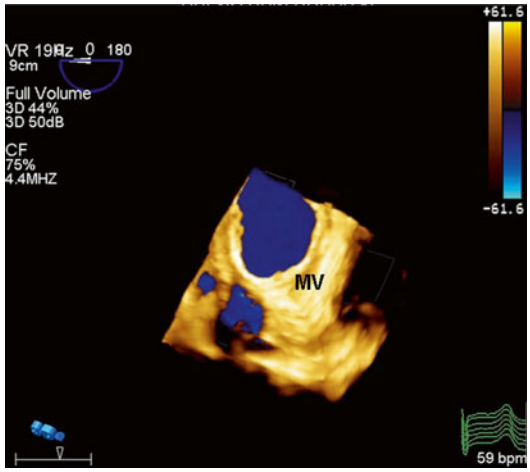

Fig. 1.7 3D TEE color Doppler, showed repaired MV without MR

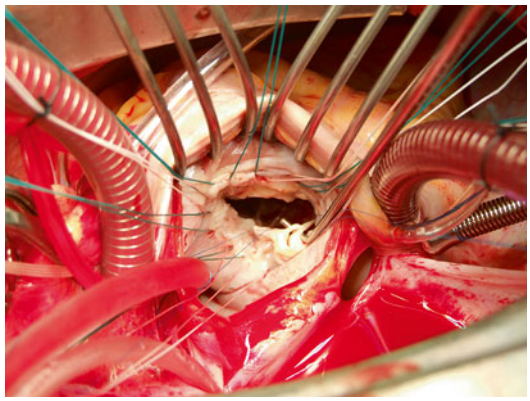

Fig. 1.8 Picture during MV repair showed prolapse of P2

Tips

Prolapse of P2 scallop is the most common structural causes of MR and it has a very high rate of successful repair.

1.2 Prolapse of Both Mitral Leaflets Having Mitral Replacement

A 73-year-old man has a 10-year-long valvuar heart disease history. He suffered dyspnea, shortness of breath and palpitation. Auscultation: irregular heart beat with a grade 2/6 systolic murmur over apex. ECG: atrial fibrillation with rapid ventricular response and LV hypertrophy. Chest X ray: cardiomegaly. Cardiac catheterization: severe MR, LVEF = 47 % with general hypokinesis and dilated LA. Operation: MV replacement, TV repair and atrial fibrillation ablation.

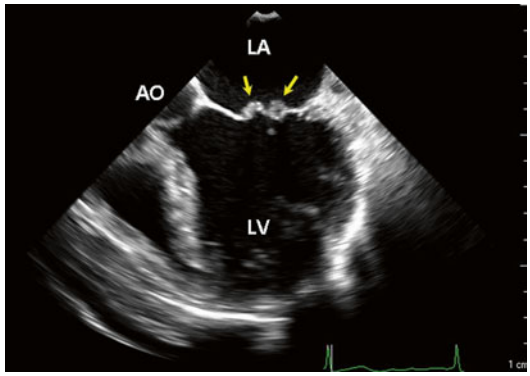

Fig. 1.9 Two-dimensional transesophageal echocardiography (2D TEE) image, five-chamber view, showed prolapse of both anterior and posterior mitral leaflets (*arrows*). Dilated LV and enlarged mitral annulus were also noted

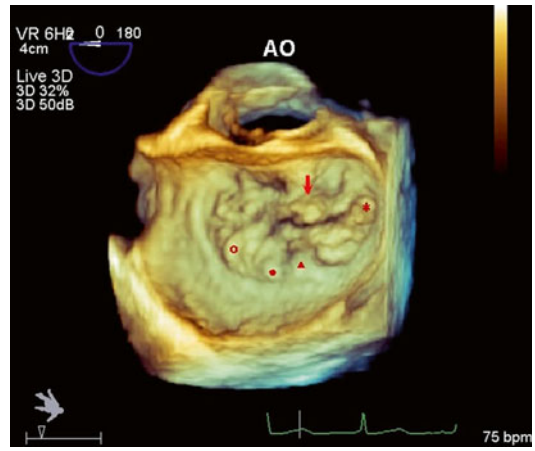

Fig. 1.11 3D TEE image, en face view, showed prolapse of A3 (*arrow*), P1 (***o***), P2 (.), P3 (▲) scallops and posteromedial commissure (*)

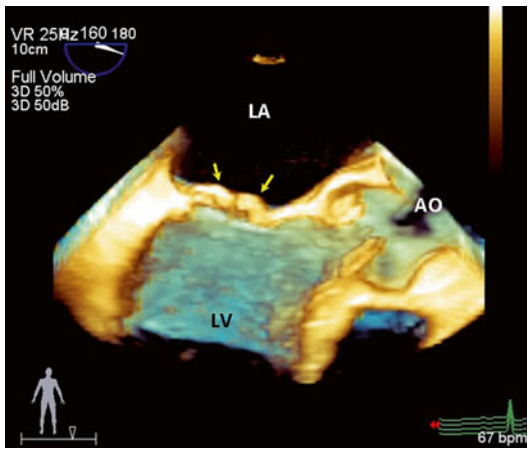

Fig. 1.10 3D TEE image, long-axis view, showed prolapse of both anterior and posterior mitral leaflets (*arrows*)

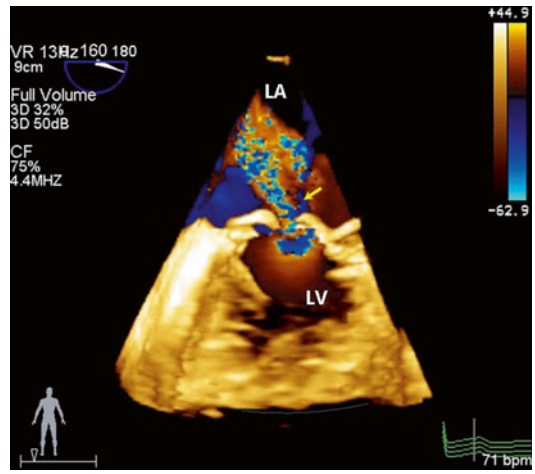

Fig. 1.12 3D TEE color Doppler, showed severe centric MR (*arrow*)

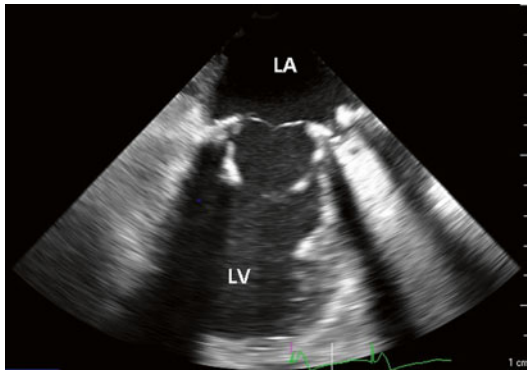

Fig. 1.13 2D TEE image, long-axis view, status post tissue MV replacement, showed normal closure of MV

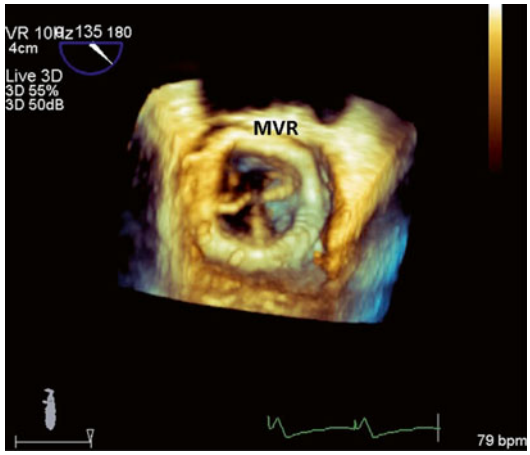

Fig. 1.14 3D TEE image, en face view, status post tissue MV replacement (*MVR*), showed normal closure of MV

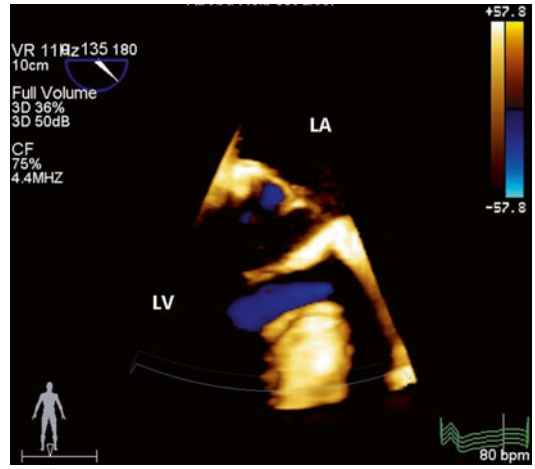

Fig. 1.15 3D TEE color Doppler, long-axis view, status post tissue MV replacement, showed no MR

Tips

The en face view of the MV is a view looks down at the valve from the LA perspective and is closest to the surgeon's actual view. By convention, the AML is at the top, the PML is at the bottom and the aorta is superior to the MV.

1.3 Barlow Syndrome

A 62-year-old man with medical-controlled hypertension suffered intermittent chest discomfort with dyspnea. Auscultation: regular heart beat with a grade 3 systolic murmur over apex. ECG: sinus rhythm and ventricular premature beats. Cardiac catheterization: double coronary artery disease and severe MR. Chest CT angiography: extensive atherosclerotic change of the aorta and bilateral iliac arteries, atherosclerotic calcifications at bilateral coronary arteries. Operation: MV replacement and CABG *x*2 (LAD, RCA)

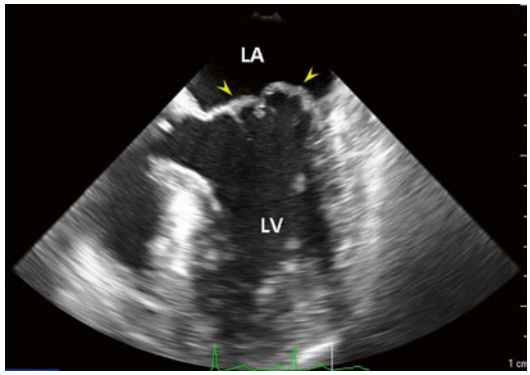

Fig. 1.16 Two-dimensional transesophageal echocardiography (2D TEE) image, five-chamber view, showed LA dilation and prolapse of both anterior and posterior mitral leaflet (*arrows*)

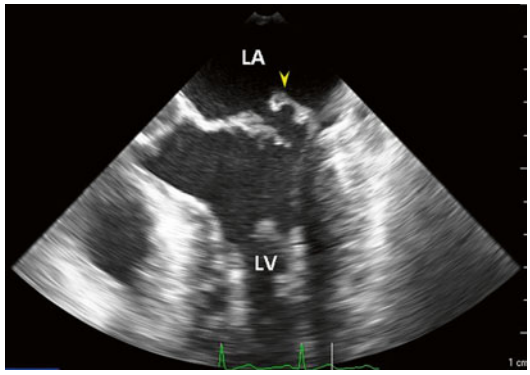

Fig. 1.17 2D TEE image, five-chamber view, showed flail of posterior mitral leaflet (*arrow*)

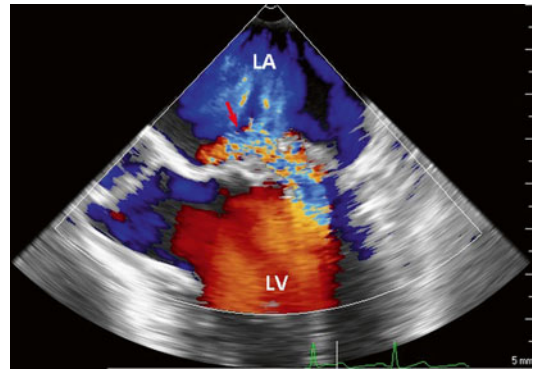

Fig. 1.18 2D TEE color Doppler, five-chamber view, showed severe eccentric MR (*arrow*)

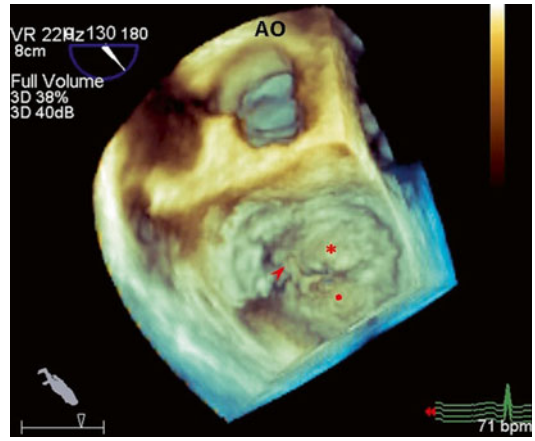

Fig. 1.19 3D TEE image, en face view, showed prolapse of both anterior (*) and posterior (.) mitral leaflet with chordae rupture (*arrow*)

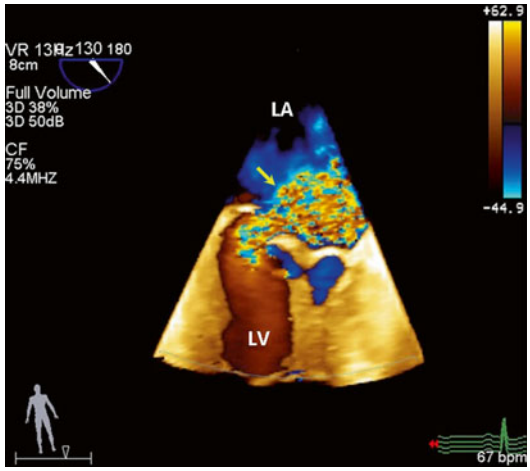

Fig. 1.20 3D TEE color Doppler, showed severe eccentric MR (*arrow*)

Tips

The Carpentier classification of MR is based on MV leaflets' motion. Type II is the result in this case as the leaflets extend beyond the annular plane in systole.

1.4 Flail of Anterior Mitral Leaflet Having Mitral Repair

The 73-year-old man with valvular heart disease refused surgical intervention. A year later, symptom of exertional dyspnea worsen. Auscultation: regular heart beat with a grade 3/6 systolic murmur. ECG: normal sinus rhythm, left axis deviation and LA enlargement. Cardiac catheterization: severe MR with huge LA, mild LV dysfunction and pulmonary hypertension. Operation: MV and TV repair and CABG x1 (SVG to RCA).

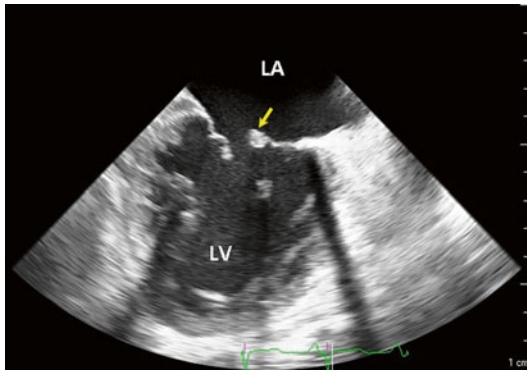

Fig. 1.21 Two-dimensional transesophageal echocardiography (2D TEE) image, two-chamber view, showed LA dilation and flail of AML (*arrow*) which floats independently

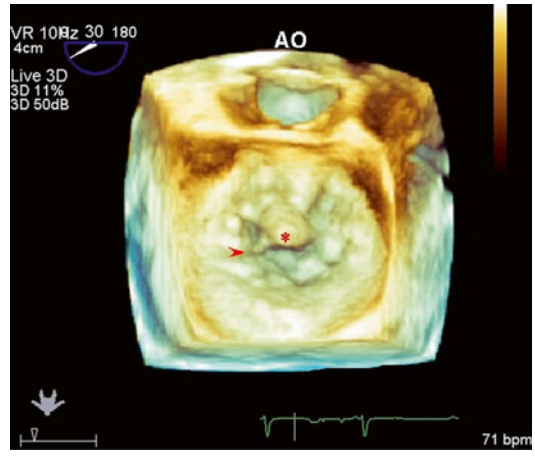

Fig. 1.23 3D TEE image, en face view, showed flail of A2 scallop (*) with chordae rupture (*arrow*)

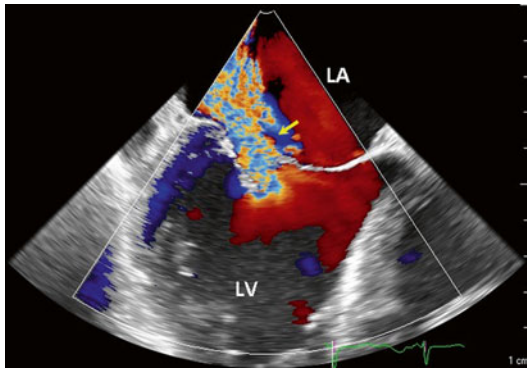

Fig. 1.22 2D TEE color Doppler, two-chamber view, showed severe eccentric MR (*arrow*)

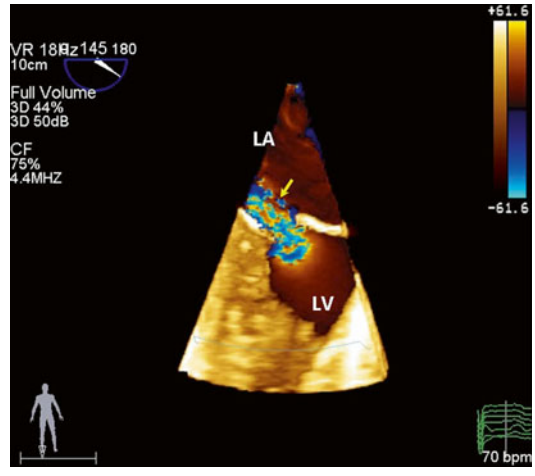

Fig. 1.24 3D TEE color Doppler, showed severe eccentric MR (*arrow*)

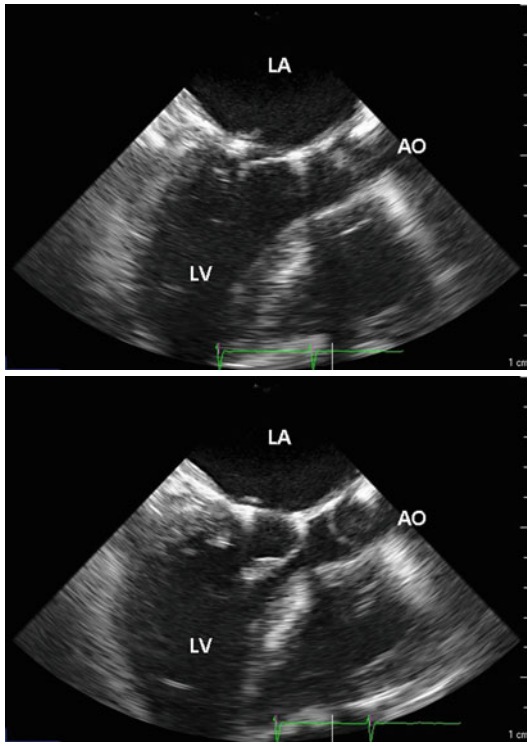

Figs. 1.25 and 1.26 2D TEE image, long-axis view, status post MV repair, showed normal MV function with cardiac cycle

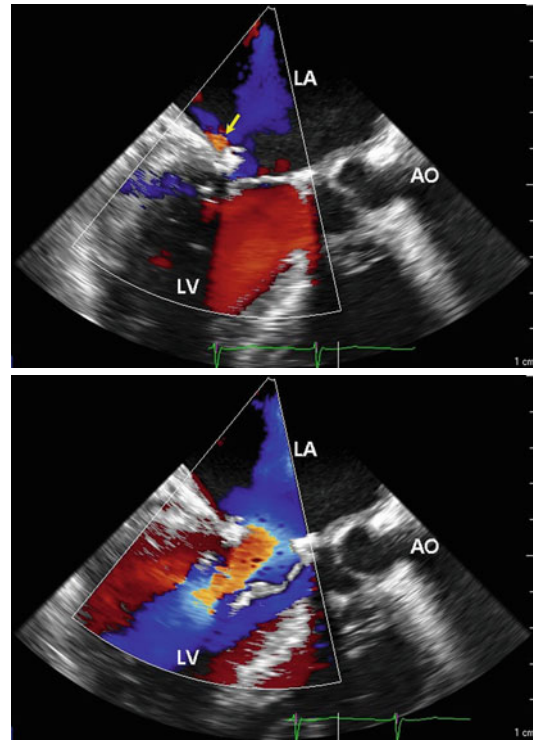

Figs. 1.27 and 1.28 2D color Doppler, status post MV repair, showed well-closed MV with trivial MR (*arrow*) and normal mitral inflow (*below*)

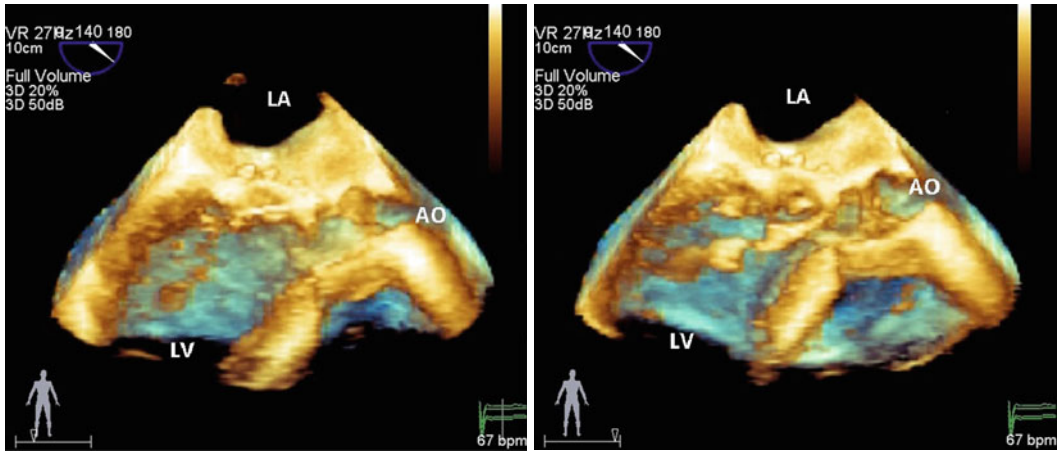

Figs. 1.29 and 1.30 3D TEE image, long-axis view, status post MV repair, showed MV normal closing and opening in systole (*left*) and in diastole (*right*)

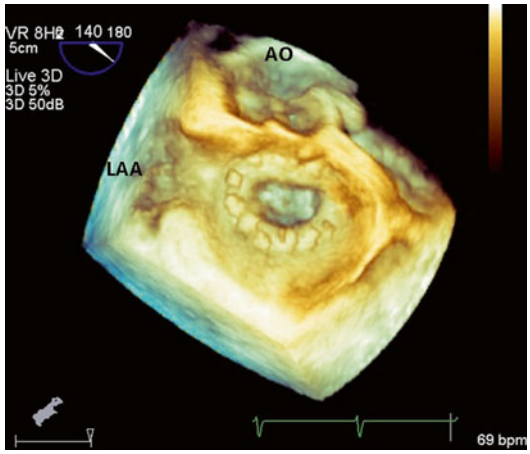

Fig. 1.31 3D TEE image, en face view, status post MV repair, showed MV with suture and left atrial appendage (*LAA*)

Tips

Flail is a situation where a leaflet float freely into the atrium in systole with one or more ruptured chordae.

1.5 Flail of Posterior Mitral Leaflet Having Mitral Replacement

A 72-year-old man with MV disorder, arrhythmia, heart failure and pulmonary edema suffered exertional dyspnea. Auscultation: irregular heart beat with a grade 3/6 systolic murmur. ECG: atrial fibrillation with moderate ventricular response and early repolarization. Chest X ray: cardiomegaly. Operation: MV replacement, TV repair and atrial fibrillation ablation.

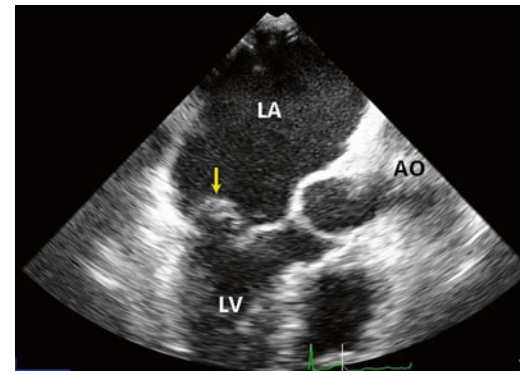

Fig. 1.32 Two-dimensional transesophageal echocardiography (2D TEE) image, long-axis view, showed LA dilatation and flail of posterior mitral leaflet (*arrow*)

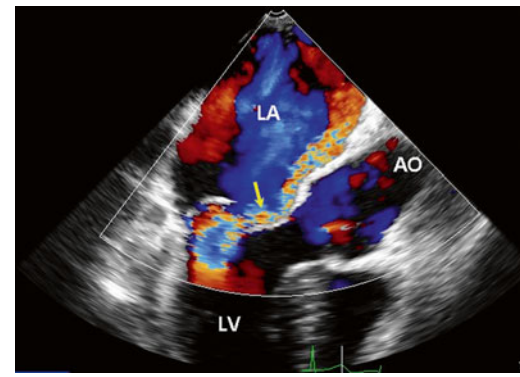

Fig. 1.33 2D TEE color Doppler, long- axis view, showed severe eccentric MR (*arrow*)

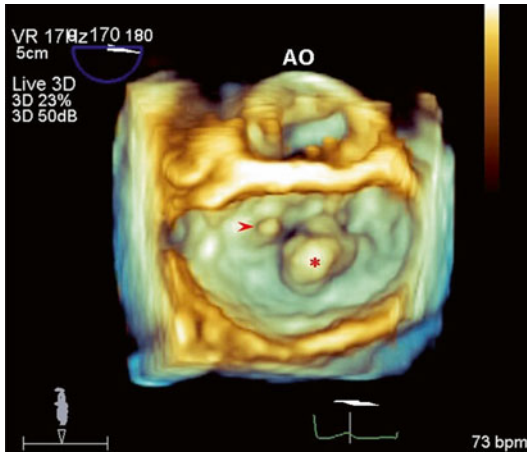

Fig. 1.34 3D TEE image, en face view, showed flail of P2 scallop (*) and ruptured chordae (*arrow*)

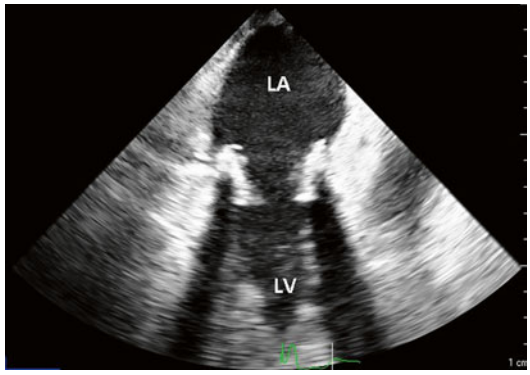

Fig. 1.35 2D TEE image, two-chamber view, status post tissue MV replacement, showed normal mitral prosthesis function

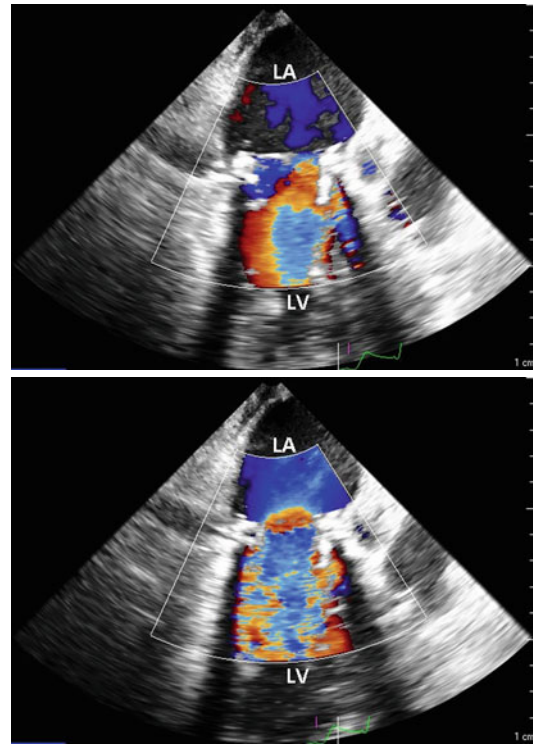

Figs. 1.36 and 1.37 2D TEE color Doppler, two-chamber view, status post tissue MV replacement, showed no MR in systole (*above*) and normal mitral prosthesis inflow (*below*)

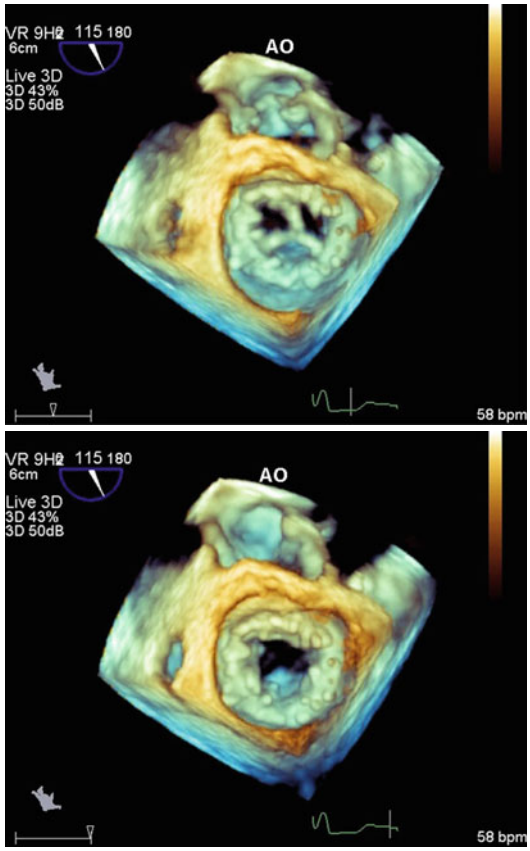

Figs. 1.38 and 1.39 3D TEE image, en face view, status post tissue MV replacement, showed mitral prosthesis normal closing and opening in systole (*above*) and in diastole (*below*)

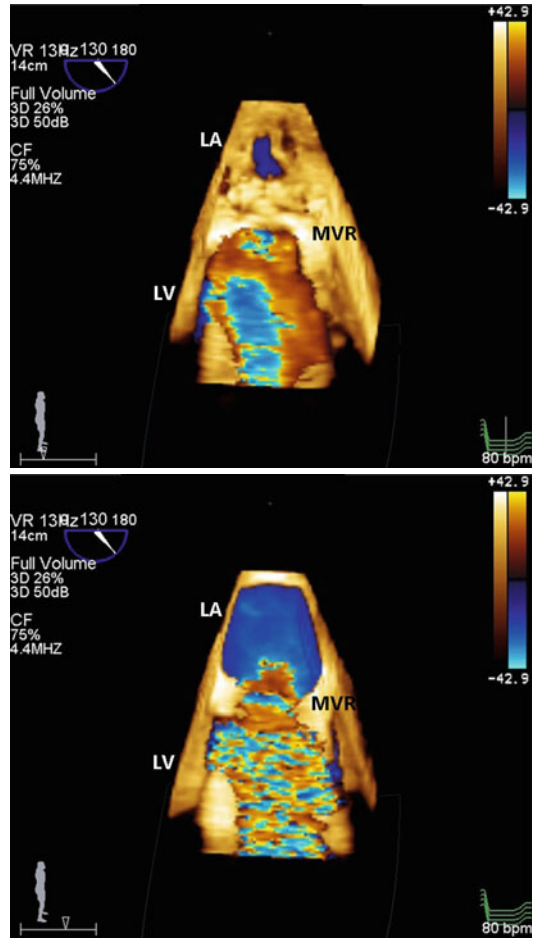

Figs. 1.40 and 1.41 3D TEE color Doppler, status post tissue MV replacement (*MVR*), showed no MR in systole (*above*) and slightly accelerated mitral inflow in diastole (*below*)

Tips

Eccentric MR jets usually suggest a structural MV abnormalities and need to be carefully investigated.

1.6 Mitral Annulus Calcification Having Mitral Replacement

A 74-year-old woman had a 10-year-long history of mitral regurgitation. She suffered exercise intolerance and generalize weakness. Auscultation: regular heart beat with a grade 3 low pitch murmur over left sternal border. ECG: sinus rhythm. Cardiac catheterization: severe mitral stenosis (PPG is 12 mmHg, MPG is 10 mmHg and MV area is 0.74 cm^2) with mild MR. Operation: MV replacement and TV repair.

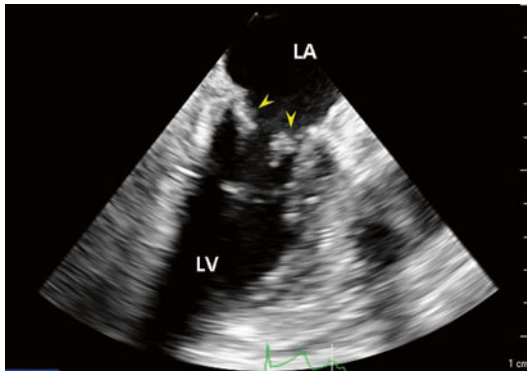

Fig. 1.42 Two-dimensional transesophageal echocardiography (2D TEE) image, showed thickened MV (*arrows*) with mitral annulus calcified

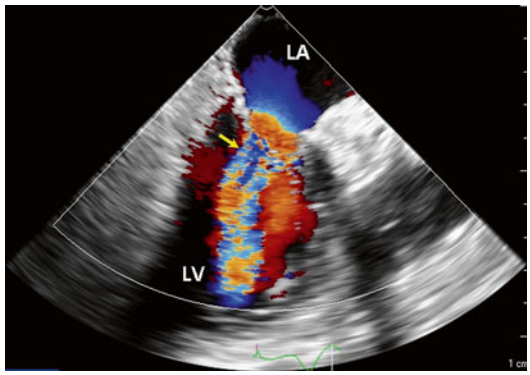

Fig. 1.43 2D TEE color Doppler, showed mitral stenosis with high-velocity mosaic mitral inflow (*arrow*)

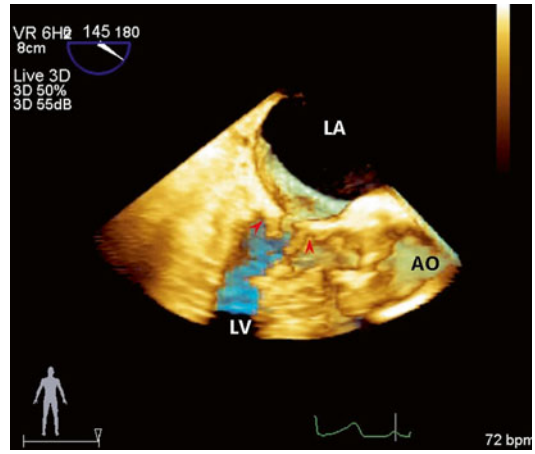

Fig. 1.44 3D TEE image, long-axis view, showed thickened MV with mitral annulus calcified (*arrows*)

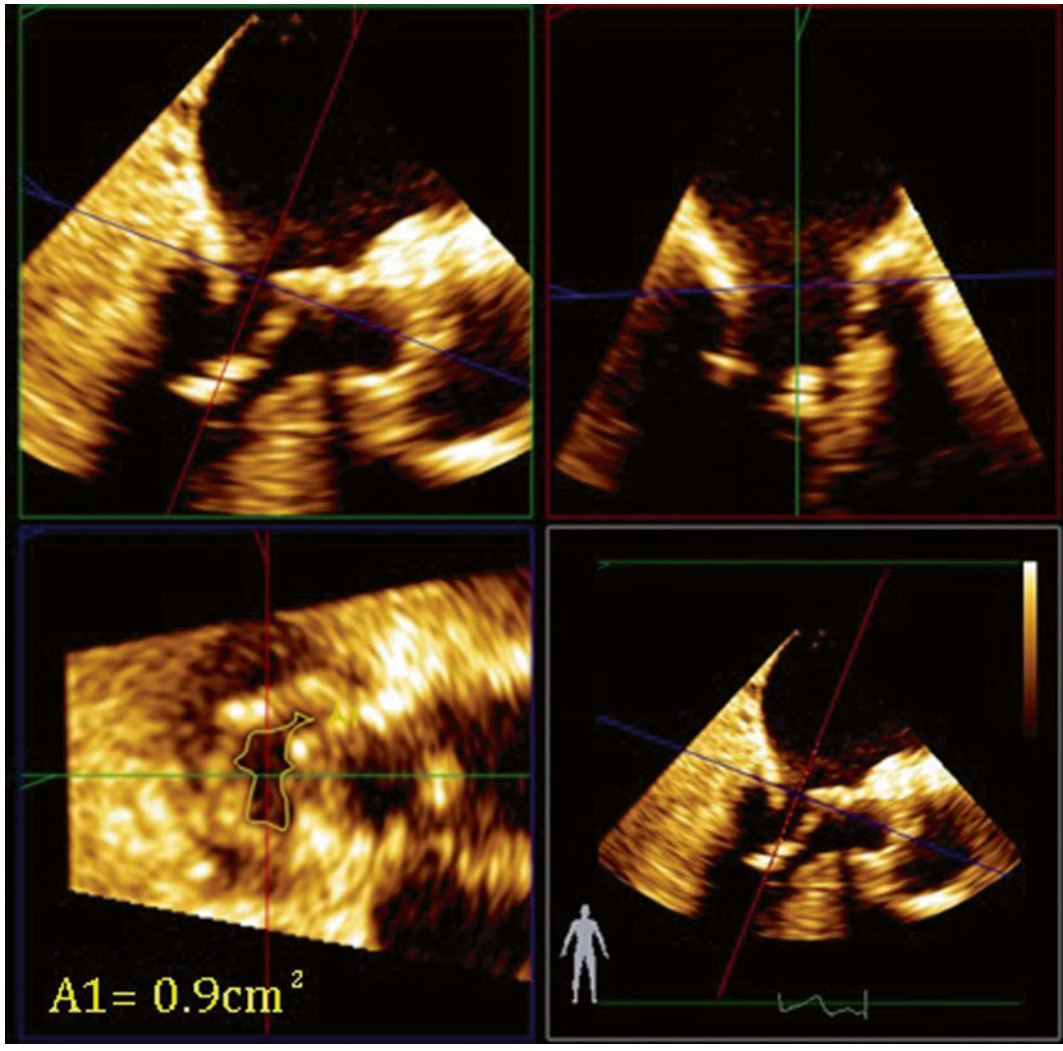

Fig. 1.45 Multi-planar reconstruction (*MPR*) of 3D TEE image, showed MV area is 0.9 cm^2

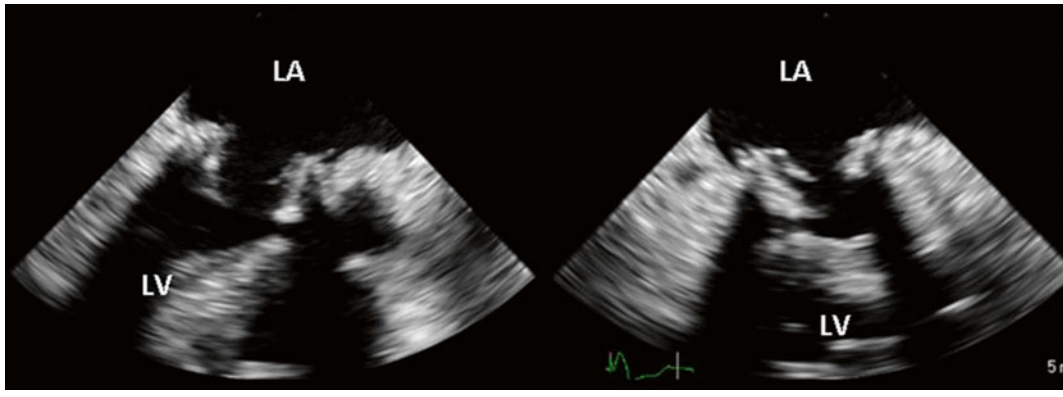

Fig. 1.46 2D TEE image, x-plane view, status post tissue MV replacement, showed normal prosthesis function

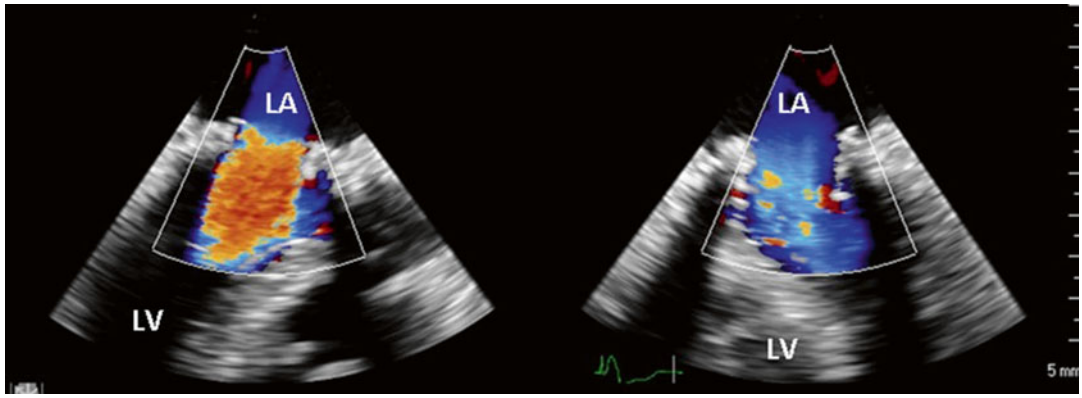

Fig. 1.47 2D TEE color Doppler, x-plane view, status post tissue MV replacement, showed normal mitral inflow

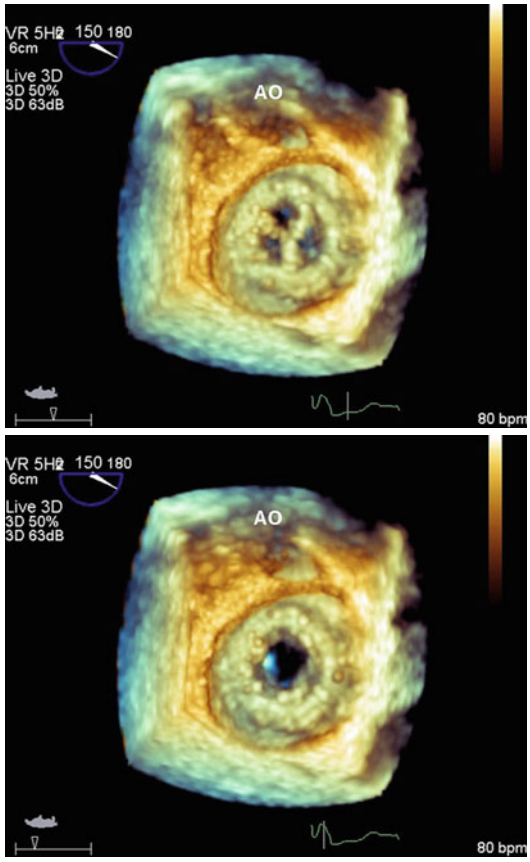

Figs. 1.48 and 1.49 3D TEE image, en face view, status post tissue MV replacement, showed normal mitral prosthesis closing in systole (*above*) and opening in diastole (*below*)

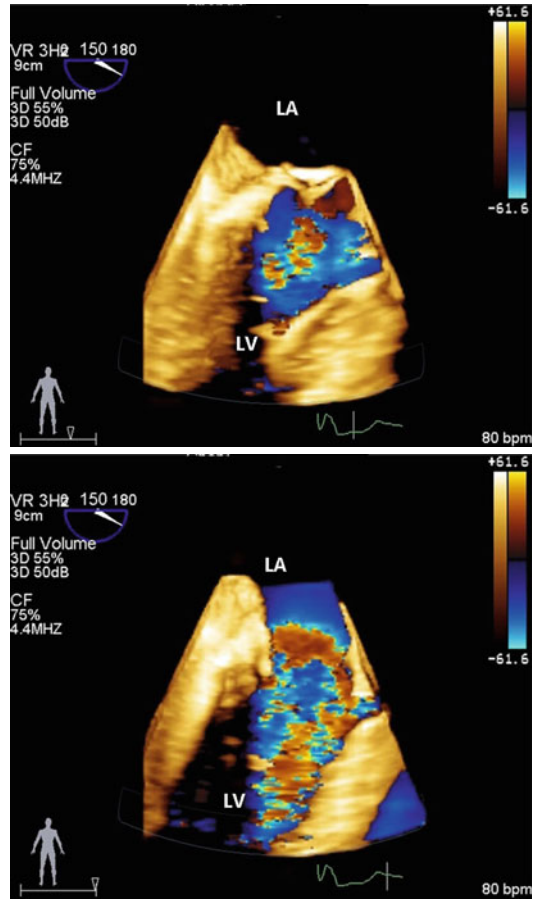

Figs. 1.50 and 1.51 3D TEE color Doppler, long-axis view, status post tissue MV replacement, showed no MR in systole (*above*) and normal mitral inflow in diastole (*below*)

Tips

Calcific stenosis is common in elderly patients who have mitral annulus calcification invading leaflets and leading to effective stenosis.

1.7 Rheumatic Heart Disease Having Mitral Replacement

A 45-year-old woman suffered dyspnea on exertion and cough. Rheumatic heart disease with mitral stenosis was told by other hospital. She admitted for surgical treatment. Auscultation: regular heart beat with a grade 4/6 systolic murmur over apex. Chest X ray: LA enlargement. Coronary CT: mild cardiomegaly. Operation: MV replacement and TV repair.

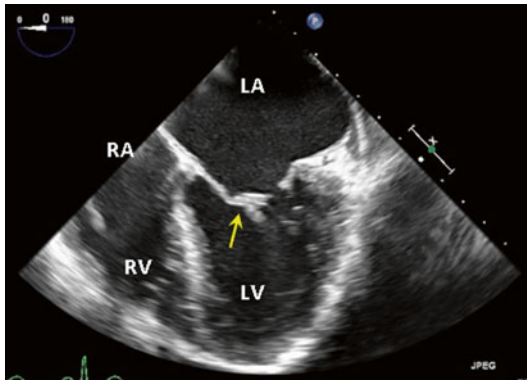

Fig. 1.52 Two-dimensional transesophageal echocardiography (2D TEE) image, four-chamber view, showed thickened MV with hockey sign (*arrow*). Dilated LA and enlarged mitral annulus were also noted

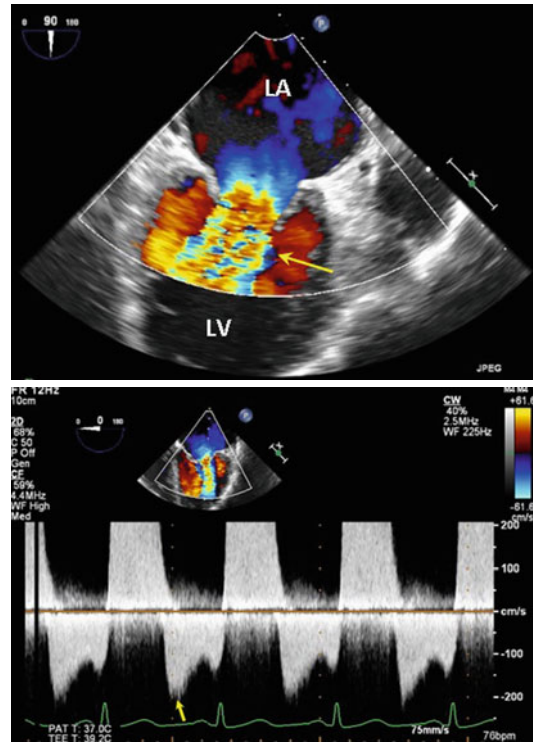

Figs. 1.53 and 1.54 2D TEE color Doppler (*above*) showed high-velocity mosaic flow in diastole (*arrow*) due to mitral stenosis (*MS*) and high pressure gradient (PPG is16 mmHg) was present by continuous-wave Doppler (*below*)

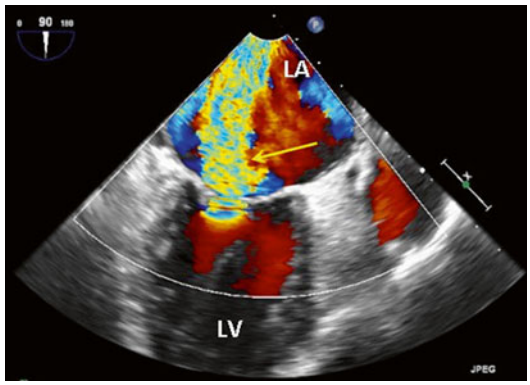

Fig. 1.55 2D TEE color Doppler, showed severe MR (*arrow*) in systole

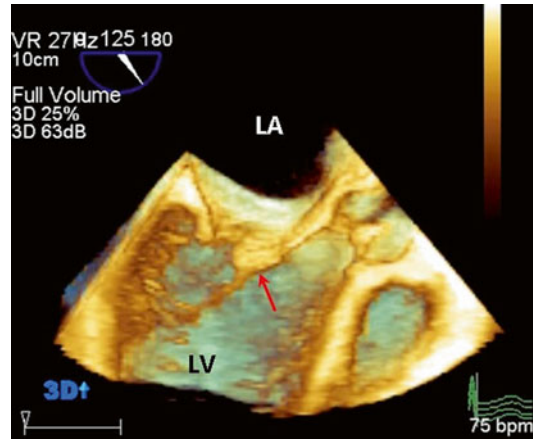

Fig. 1.56 3D TEE image, long-axis view, showed thickened MV with hockey sign (*arrow*)

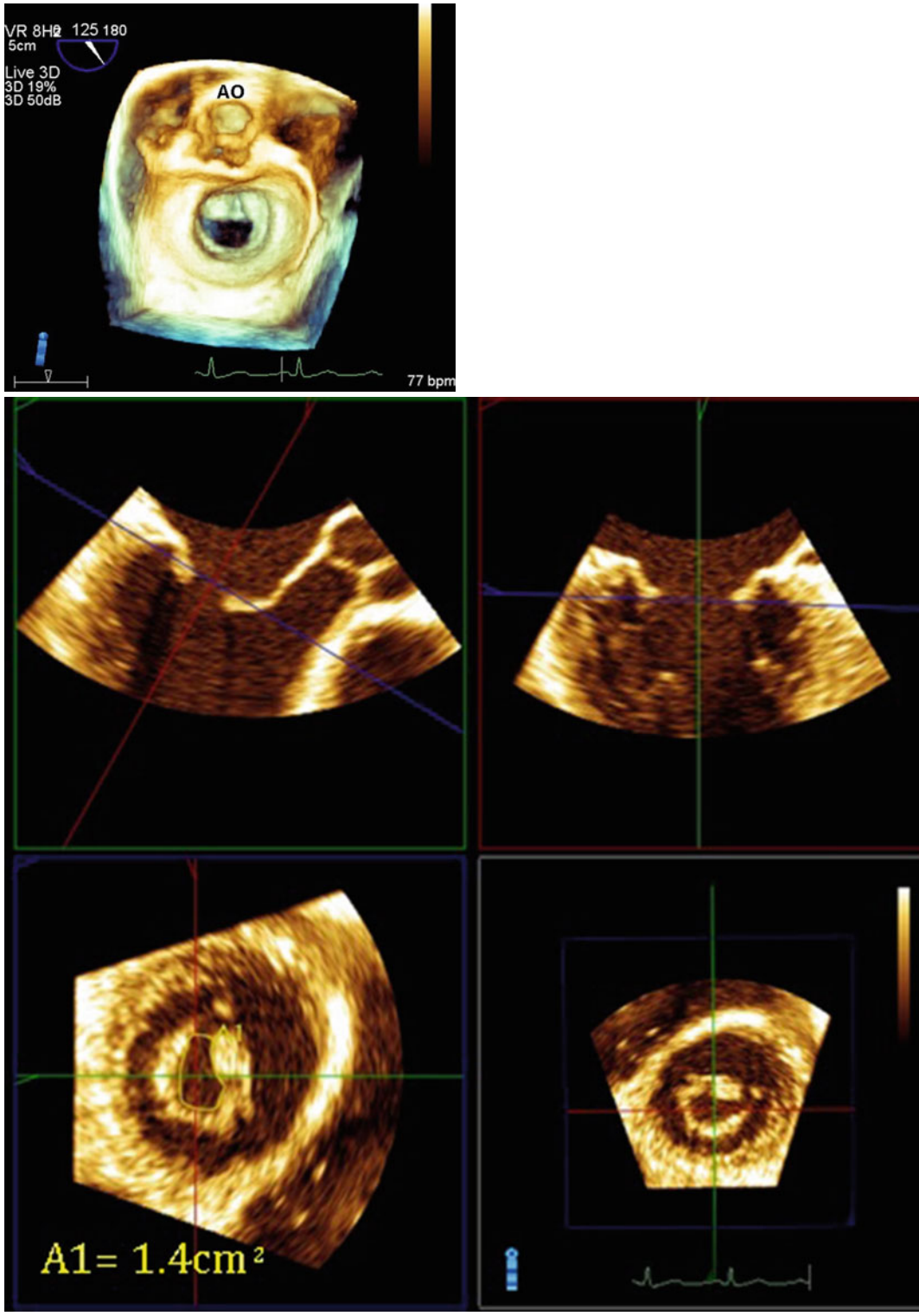

Figs. 1.57 and 1.58 3D TEE image, en face view (*left*) and Multi-planar reconstruction (*MPR*) (*right*), showed thickened MV and small mitral orifice with area is 1.4 cm^2

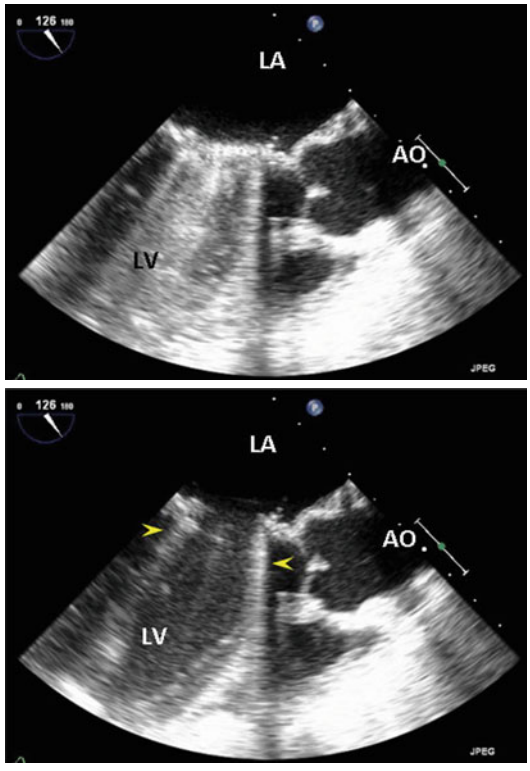

Figs. 1.59 and 1.60 2D TEE image, long-axis view, status post mechanical MV replacement, showed reverberation (*arrows*) from the valve and good function in systole (*above*) and diastole (*below*)

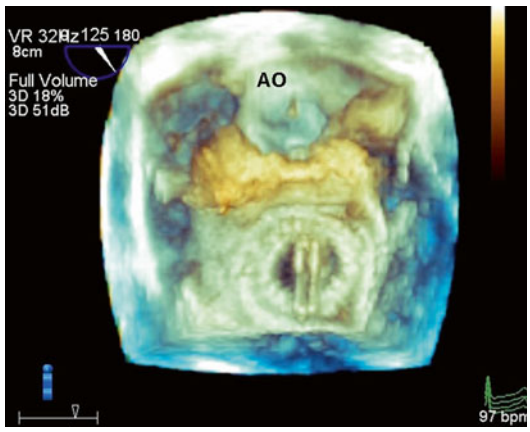

Fig. 1.61 3D TEE image, en face view, status post MV replacement, showed bileaflet mechanical mitral prosthesis with normal opening in diastole

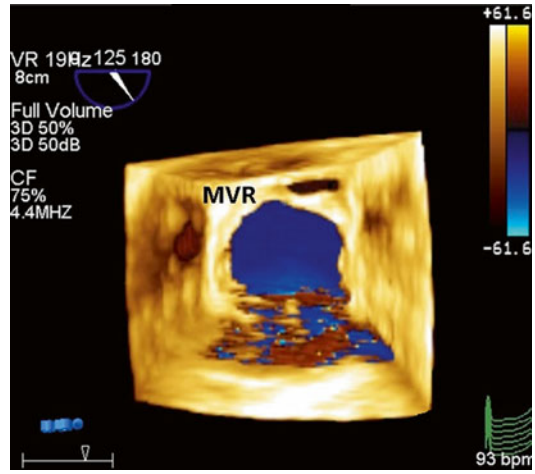

Fig. 1.62 3D TEE color Doppler, status post MV replacement (*MVR*), showed smooth mitral inflow

Tips

Rheumatic mitral stenosis usually presents with restricted mitral leaflets, commissural fusion, and calcification of the subvalvular appartus. Increase of diastolic grdients across the MV are also seen.

1.8 Systolic Anterior Motion After Mitral Valve Repair

A 77-year-old man had a history of severe MR, colon cancer status post operation, multiple cerebral infarctions and hypertension. Auscultation: regular heart beat with a grade 1/6 systolic murmur. ECG: sinus rhythm with occasional supraventricular premature complexes. Chest X ray: cardiomegaly. Cardiac catheterization: severe MR. Operation: attempted MV repair then MV replacement and TV repair.

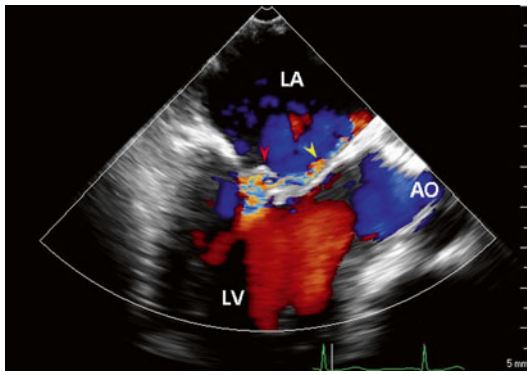

Fig. 1.63 Two-dimensional transesophageal echocardiography (2D TEE) color Doppler, long-axis view, showed prolapse of posterior mitral leaflet (*red arrow*) with severe eccentric MR (*yellow arrow*). LA dilation and LV hypertrophy were also noted

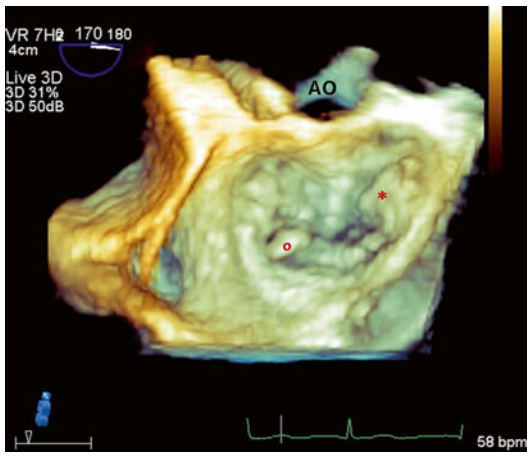

Fig. 1.64 3D TEE image, en face view, showed prolapse of P1 (***o***) and P3 (*)

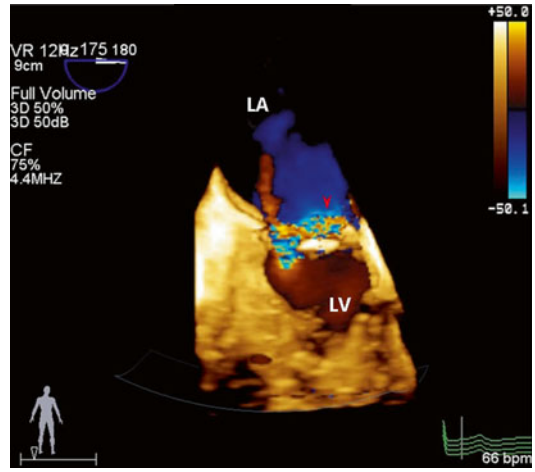

Fig. 1.65 3D TEE color Doppler, showed prolapse of PML with severe eccentric MR (*arrow*)

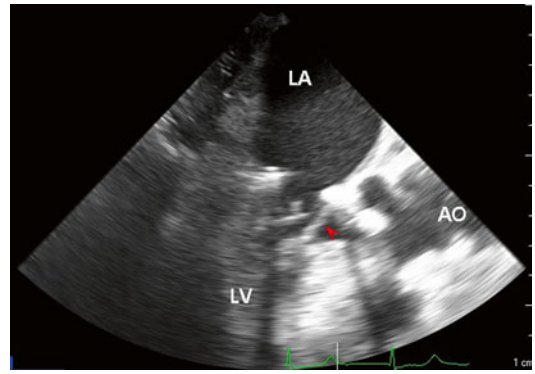

Fig. 1.66 2D TEE image, long-axis view, status post MV repair, showed intravnetricular septal hypertrophy with mitral leaflet systolic anterior motion (*arrow*) and LV outflow tract obstruction

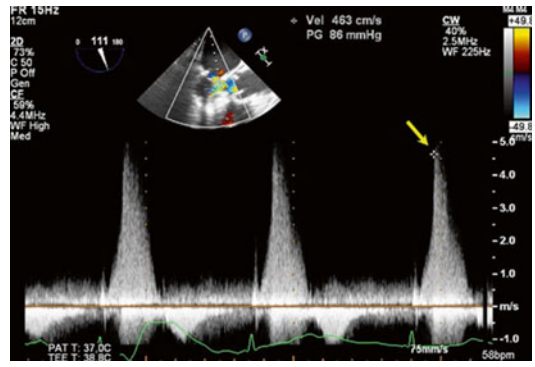

Fig. 1.67 2D TEE continuous-wave Doppler with the origin of the velocity at subaortic region, status post MV repair, showed a late-peaking, high-velocity gradient is 86 mmHg (*arrow*) due to LV outflow tract obstruction

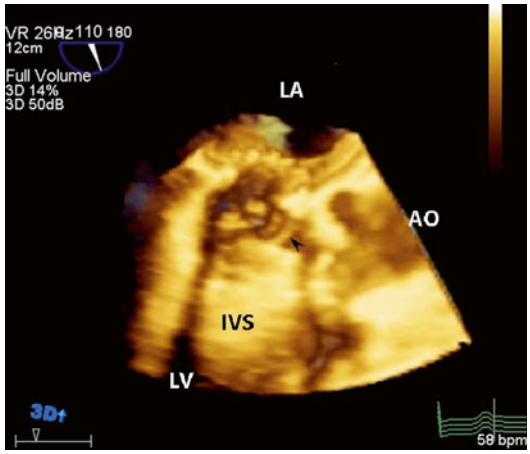

Fig. 1.68 3D TEE image, long-axis view, status post MV repair, showed interventricular septal (*IVS*) hypertrophy with mitral leaflet systolic anterior motion (*arrow*) and LV outflow tract obstruction

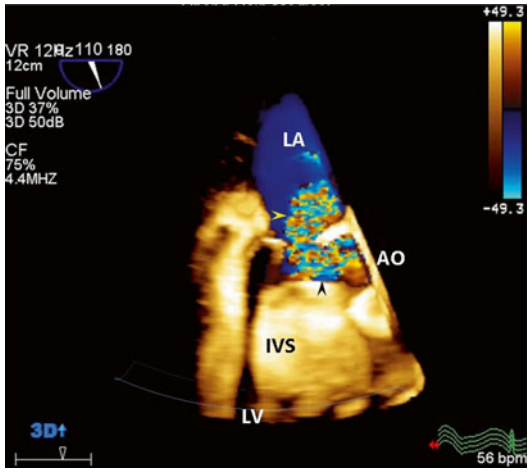

Fig. 1.69 3D TEE color Doppler, long-axis view, status post MV repair, showed severe MR (*yellow arrow*) due to mitral leaflet systolic anterior motion and turbulent LV outflow (*black arrow*) due to subaortic obstruction

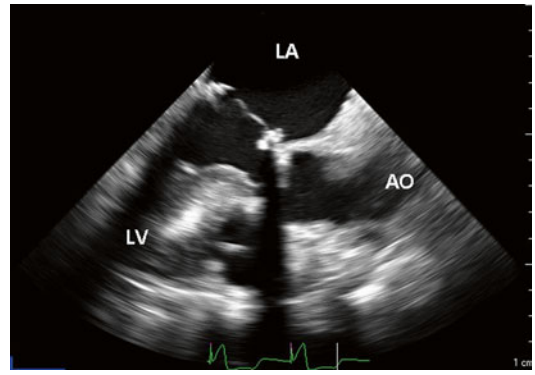

Fig. 1.70 2D TEE image, long-axis view, status post tissue MV replacement, showed normal prosthesis function without systolic anterior motion of mitral leaflet

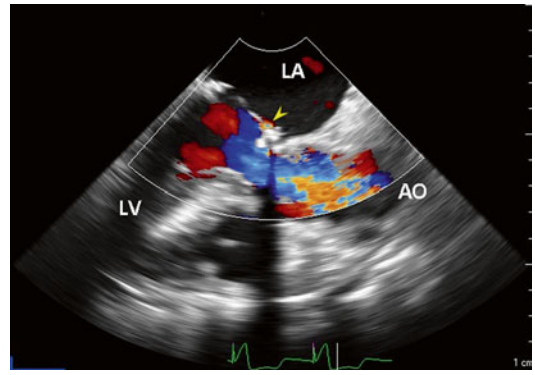

Fig. 1.71 2D TEE color Doppler, long- axis view, status post tissue MV replacement, showed trivial MR (*arrow*) and normal LV outflow

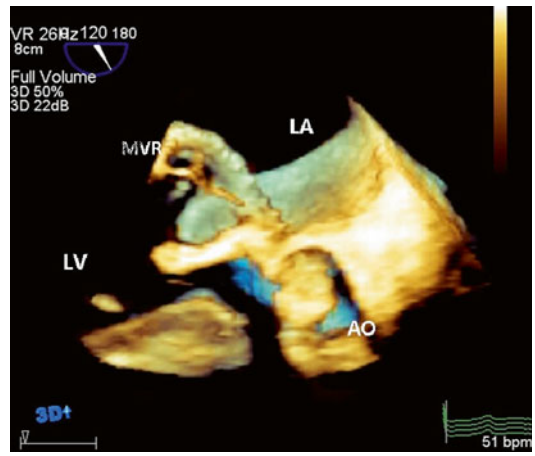

Fig. 1.72 3D TEE image, long-axis view, status post tissue MV replacement (*MVR*), showed normal prosthesis function without mitral leaflet systolic anterior motion

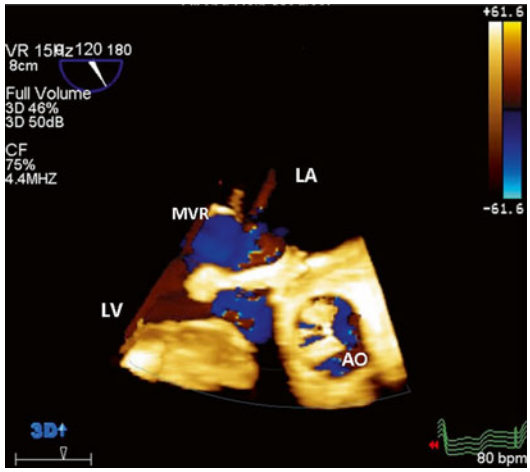

Fig. 1.73 3D TEE color Doppler, long-axis view, status post tissue MV replacement (*MVR*), showed trivial MR and normal LV outflow

Tips

Factors which develop systolic anterior motion after mitral repair include short anterior leaflet, long posterior leaflet, and small LV cavity, etc.

Suggested Reading

Addetia K, Mor-Avi V, Weinert L, et al. A new definition for an old entity: improved definition of mitral valve prolapse using three-dimensional echocardiography and color-coded parametric models. J Am Soc Echocardiogr. 2014;27(1):8–16.

Akhter N, Zhao Q, Andrei AC, et al. Identification of prolapsing mitral valve scallops by a three-dimensional multiplanar reconstruction method. Echocardiography. 2015;32(1):106–13.

Alfieri O, Lapenna E. Systolic anterior motion after mitral valve repair: where do we stand in 2015? Eur J Cardiothorac Surg. 2015;48(3):344–6.

Ben Zekry S, Spiegelstein D, Sternik L, et al. Simple repair approach for mitral regurgitation in Barlow disease. J Thorac Cardiovasc Surg. 2015;150(5):1071–1077.e1.

Butler TC, Sedgwick JF, Burstow DJ. 3-D assessment of infective endocarditis with anterior mitral valve perforation and flail posterior leaflet. Int J Cardiol. 2015;185:249.

Colli A, Manzan E, Zucchetta F, et al. Feasibility of anterior mitral leaflet flail repair with transapical beating-heart neochord implantation. JACC Cardiovasc Interv. 2014;7(11):1320–1.

Fucci C, Faggiano P, Nardi M, et al. Triple-orifice valve repair in severe Barlow disease with multiple-jet mitral regurgitation: report of mid-term experience. Int J Cardiol. 2013;167(6):2623–9.

Fusini L, Ghulam Ali S, Tamborini G, et al. Prevalence of calcification of the mitral valve annulus in patients undergoing surgical repair of mitral valve prolapse. Am J Cardiol. 2014;113(11):1867–73.

Mori M, Yoshimuta T, Ohira M, et al. Impact of real-time three-dimensional transesophageal echocardiography on procedural success for mitral valve repair. J Echocardiogr. 2015;13(3):100–6.

Mukit M, Kagalwala DZ, El-Eshmawi A, et al. Novel presentation of flail mitral valve. J Cardiothorac Vasc Anesth. 2015;29(5):1398–401.

Murugesan V, Pulimamidi VK, Rajappa M, Satheesh S, et al. Elevated fibrinogen and lowered homocysteine-vitamin determinants and their assodiation with left atrial thrombus in patients with rheumatic mitral stenosis. Br J Biomed Sci. 2015;72(3):102–6.

Nanda N, Hsiung MC, Miller AP, et al. Live/real time 3D echocardiography. Oxford: Wiley-Blackwell; 2010.

Otto CM. Textbook of clinical echocardiography. Philadelphia: W. B. Saunders Company; 2000.

Oxorn DC. Intraoperative echocardiography. Philadelphia: Elsevier Saunders; 2012.

Padala M, Sweet M, Hooson S, et al. Hemodynamic comparison of mitral valve repair: techniques for a flail anterior leaflet. J Heart Valve Dis. 2014;23(2):171–6.

Perrino A, Reeves S, Glas K. The practice of perioperative transesophageal echocardiography essential cases. Philadelphia: Lippincott Williams & Wilkins; 2011.

Pinheiro AC, Mancuso FJ, Hemerly DF, et al. Diagnostic value of color flow mapping and Doppler echocardiography in the quantification of mitral regurgitation in patients with mitral valve prolapse or rheumatic heart disease. J Am Soc Echocardiogr. 2007;20(10):1141–8.

Rostagno C, Droandi G, Rossi A, et al. Anatomic characteristics of bileaflet mitral valve prolapse--Barlow disease--in patients undergoing mitral valve repair. Ital J Anat Embryol. 2014a;119(1):20–8.

Rostagno C, Droandi G, Rossi A, et al. Anatomic characteristics of bileaflet mitral valve prolapse--Barlow disease--in patients undergoing mitral valve repair. Ital J Anat Embryol. 2014b;119(1):20–8.

Schaheen LW, Hayanga AJ, Badhwar V. Chordal relocation for repair of anterior mitral leaflet flail: a reproducible option. Multimed Man Cardiothorac Surg. 2014;2014:mmt021.

Sidebotham DA, Allen SJ, Gerber IL, et al. Intraoperative tranesophageal esophageal echocardiography for surgical repair of mitral regurgitation. J Am Soc Echocardiogr. 2014;27(4):345–66.

Diseases of the Aortic Valve

2

Abstract

This chapter described AV prolapse, bicuspid AV, rheumatic heart disease, and AS received proper treatments including aortic repair, replacement, or transcatheter AV implantation.

The best views for the AV examination are middle esophageal AV short- and long-axis views. 3D echocardiography compared with 2D can assess valvular morphology and provide additional information regarding AS severity with accurate multi-planer reconstruction of the anatomic AV orifice.

2.1 Prolapse of Noncoronary Cusp

A 58-year-old man had a history of type B Wolff-Parkinson-White syndrome, chronic obstructive pulmonary disease and severe AR with prolapse of NCC. He complained of frequent chest distress and exertional dyspnea recently. Auscultation: regular heart beat with a grade 2/6 diastolic murmur. Chest X ray: cardiomegaly. Operation: AV replacement.

Electronic supplementary material The online version of this chapter (doi:10.1007/978-981-10-0587-9_2) contains supplementary material, which is available to authorized users.

W.-H. Yin, M.-C. Hsiung, *Atlas of Perioperative 3D Transesophageal Echocardiography*,
DOI 10.1007/978-981-10-0587-9_2

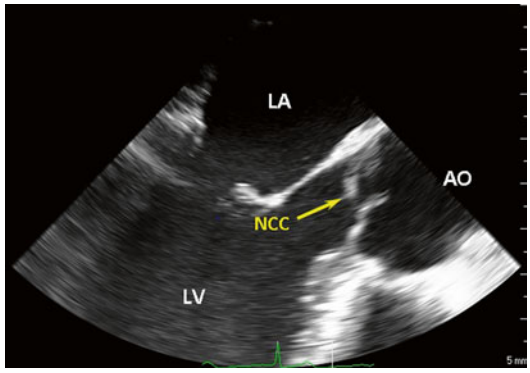

Fig. 2.1 Two-dimensional transesophageal echocardiography (2D TEE) image, long-axis view, showed NCC (*arrow*) prolapse into LV

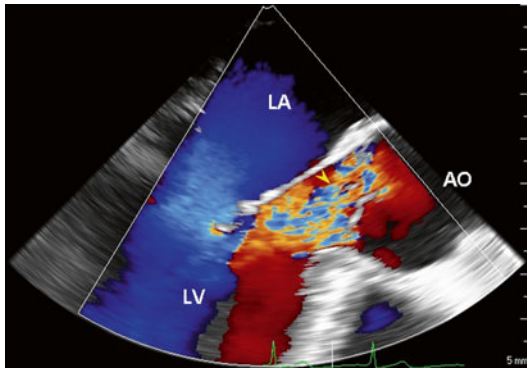

Fig. 2.2 2D TEE color Doppler, long-axis view, showed severe AR (*arrow*)

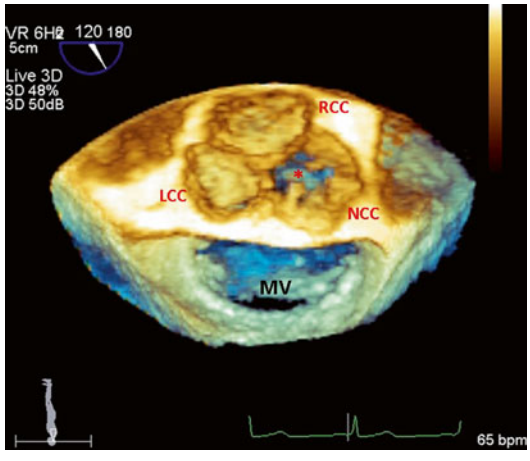

Fig. 2.3 3D TEE image, surgical view, showed NCC (*) prolapse into LV

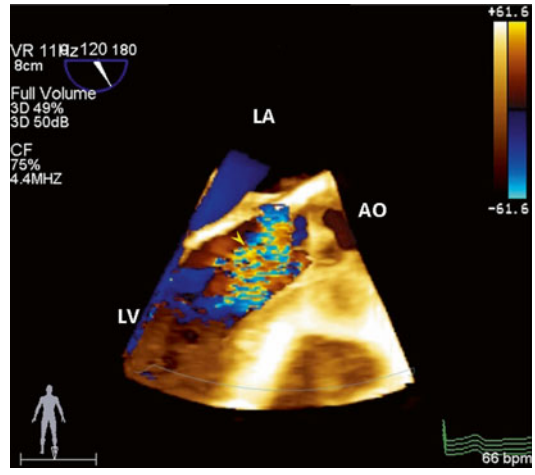

Fig. 2.4 3D TEE color Doppler, long-axis view, showed severe AR (*arrow*)

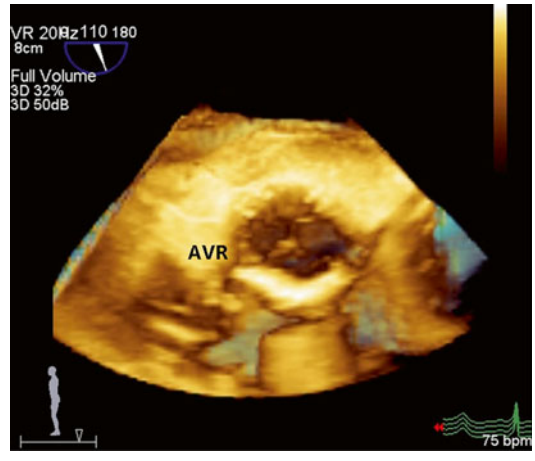

Fig. 2.5 3D TEE image, short-axis view, status post tissue AV replacement (*AVR*)

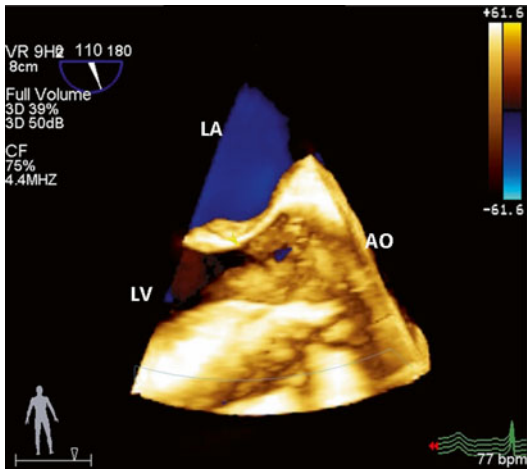

Fig. 2.6 3D TEE color Doppler, long-axis view, status post operation, showed trivial AR

Tips

AV prolapse has the aortic cusp extend beyond the annular plane resulting in eccentric AR in diastole.

2.2 Bicuspid Aortic Valve Having Aortic Valve Repair

A 24-year-old young man had a history of hypertension, bicuspid AV with AR under regular medical treatment. He suffered from shortness of breath, chest distress and malaise. Auscultation: regular heart beat with a grade 1/6 to and fro murmur over upper sternal border and a grade 1/6 systolic murmur over apex. ECG: sinus rhythm, counter clockwise rotation and LV hypertrophy. Cardiac catheterization: bicuspid AV and severe aortic regurgitation. Operation: AV repair and ventriculoaortic junction plasty.

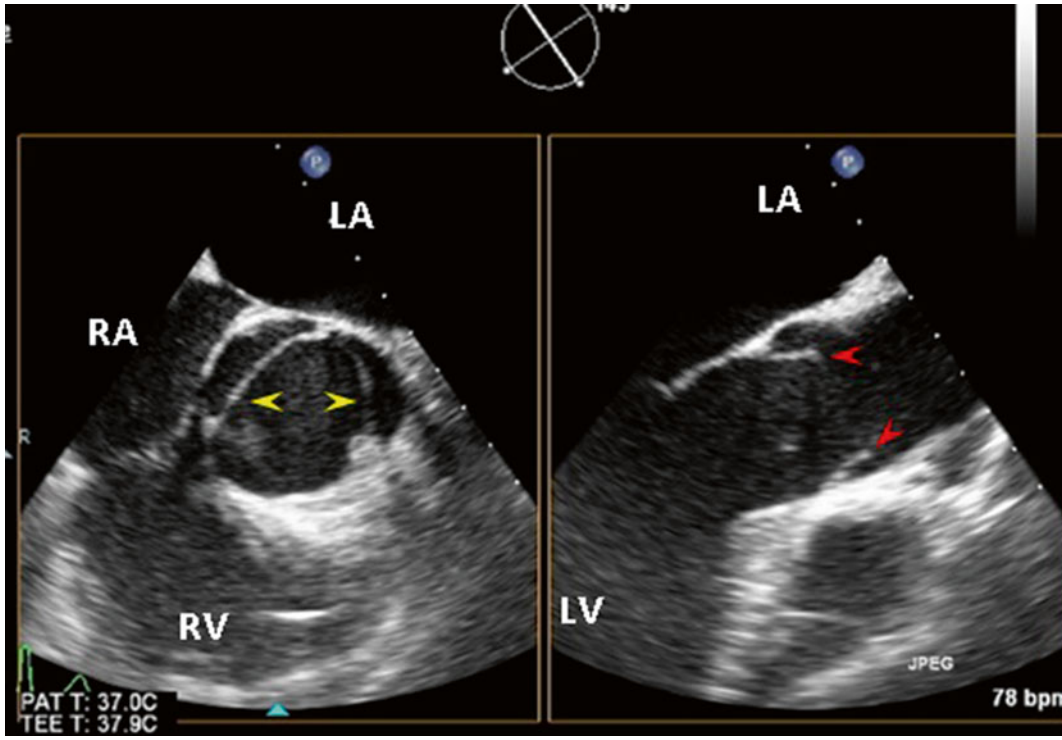

Fig. 2.7 Two-dimensional transesophageal echocardiography (2D TEE) image, x-plane view, showed bicuspid aortic valve (*yellow arrows*) with oval shape orifice and doming sign (*red arrows*) in systole

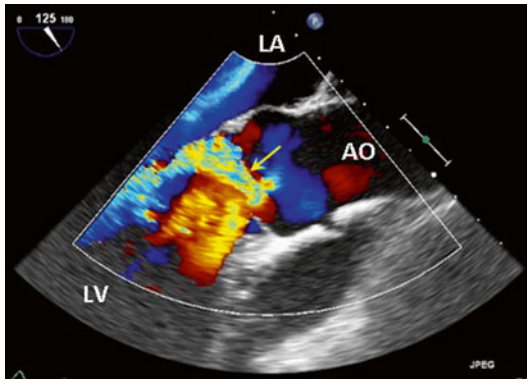

Fig. 2.8 2D TEE color Doppler, long-axis view, showed severe eccentric AR (*arrow*)

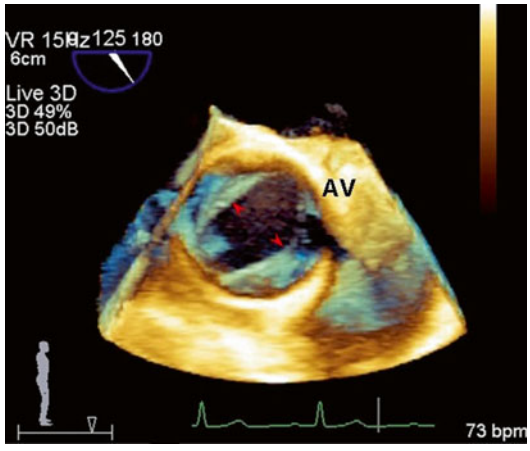

Fig. 2.9 3D TEE image, short-axis view, showed bicuspid AV with oval shape orifice (*arrows*)

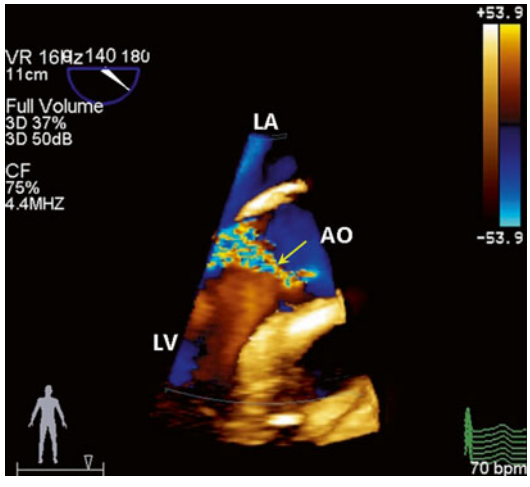

Fig. 2.10 3D TEE color Doppler, showed severe eccentric AR (*arrow*)

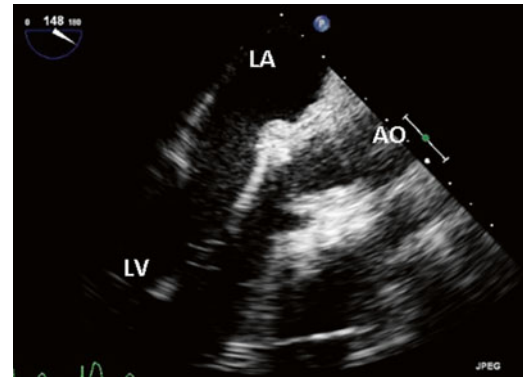

Fig. 2.11 2D TEE image, long-axis view, status post AV repair and ventriculoaorticplasty (*arrows*)

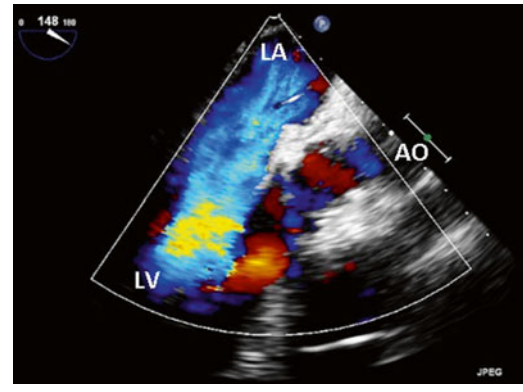

Fig. 2.12 2D TEE color Doppler, long-axis view, status post AV repair, showed no AR in diastole

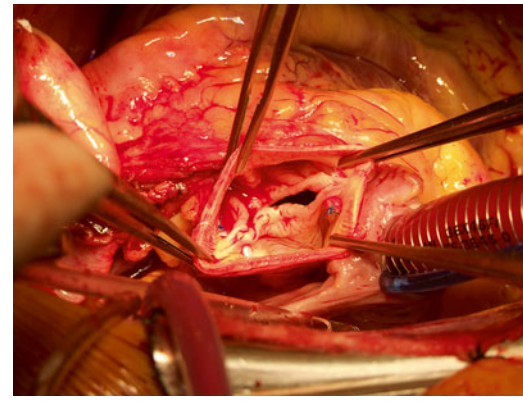

Fig. 2.13 Picture during operation showed the bicuspid AV

Tips

A thickened, doming valve is common in patients with bicuspid AV; however, a calcified valve is uncommon before age 30.

2.3 Bicuspid Aortic Valve Having Tissue Aortic Valve Replacement

A 61-year-old woman had poor physical activity and poor sleeping quality. She suffered from cough with shortness of breath. Auscultation: regular heart beat with a systolic murmur over apex. ECG: sinus rhythm and clockwise rotation. Chest X ray: mild cardiomegaly. Cardiac catheterization: critical AS with AV area is 0.6 cm^2. Operation: AV replacement.

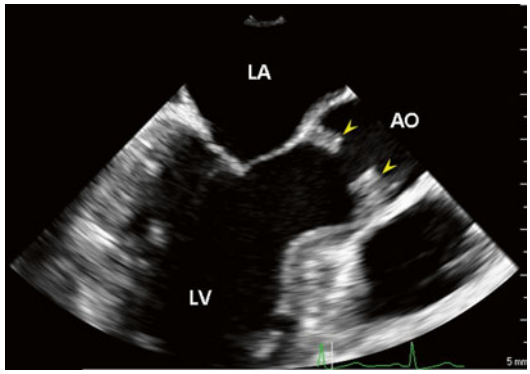

Fig. 2.14 Two-dimensional transesophageal echocardiography (2D TEE) image, long-axis view, showed the bicuspid AV with doming sign (*arrows*) in systole

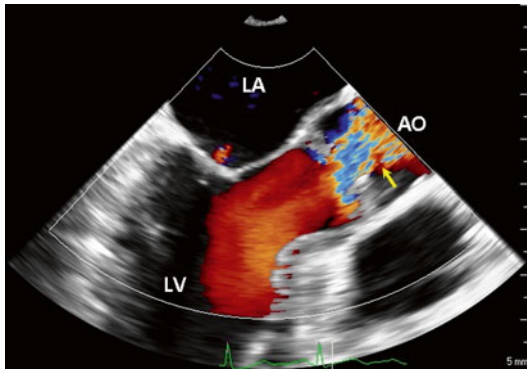

Fig. 2.15 2D TEE color Doppler, long-axis view, showed aortic stenosis (AS) with high-velocity LV outflow (*arrow*)

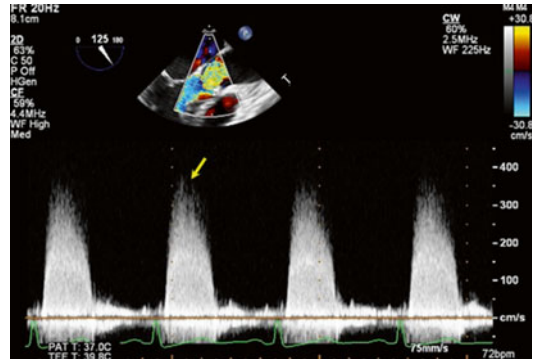

Fig. 2.16 2D TEE continuous-wave Doppler, AS with high pressure gradient (peak 60 mmHg) flow (*arrow*) was present

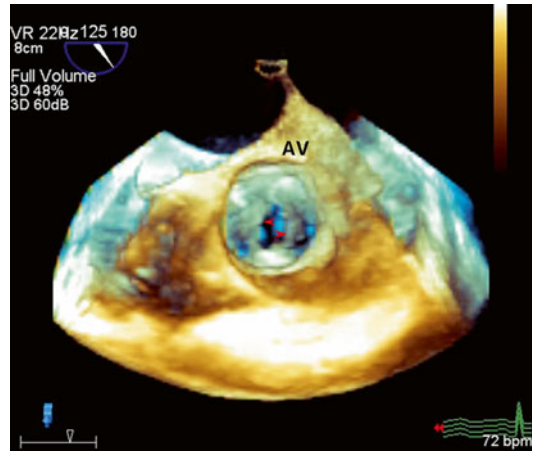

Fig. 2.17 3D TEE image, short-axis view, showed bicuspid AV (*arrows*) with small orifice

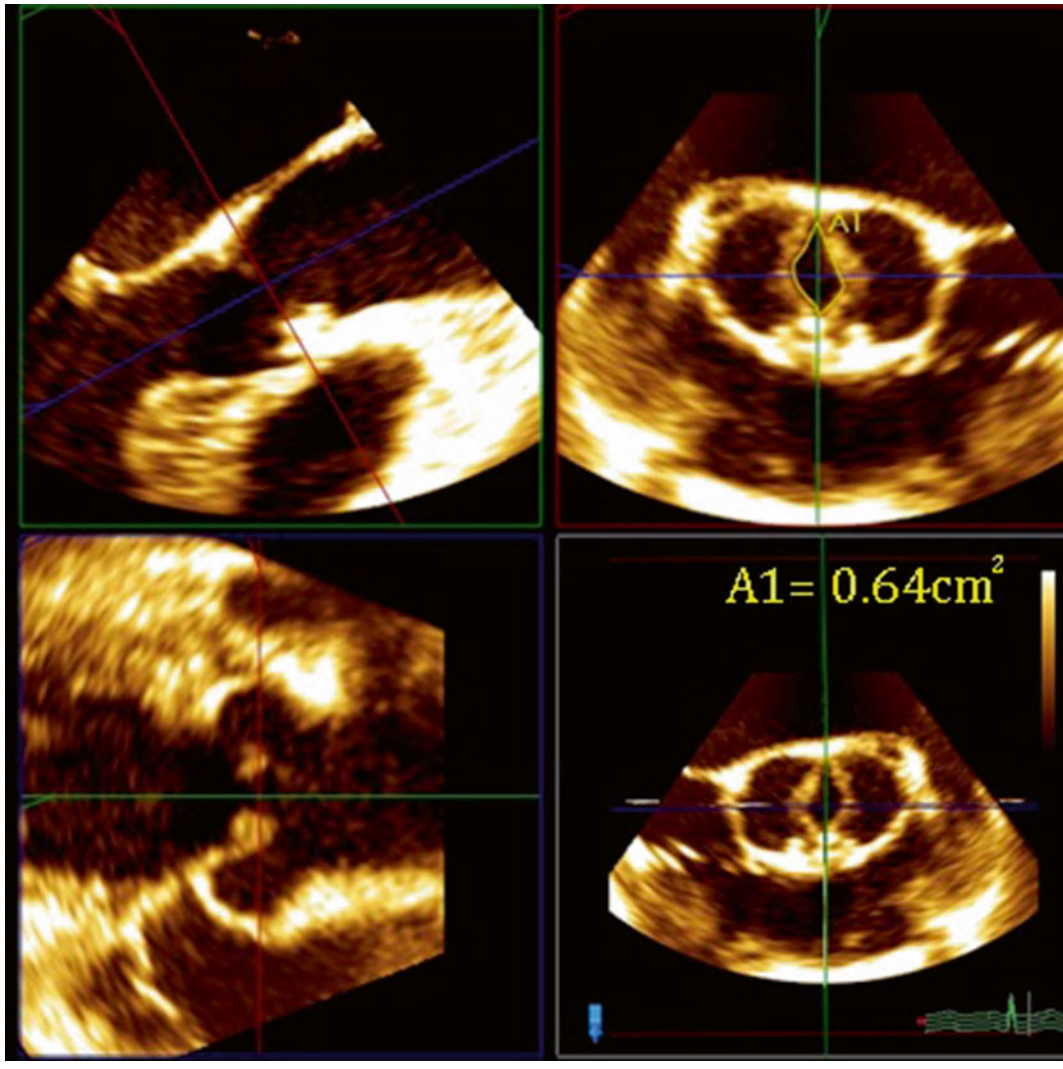

Fig. 2.18 Multi-planar reconstruction (MPR) of 3D TEE image, showed the AV area is 0.64 cm^2

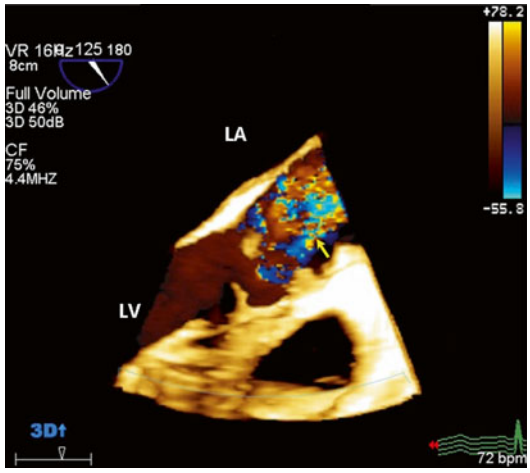

Fig. 2.19 3D TEE color Doppler, showed AS with high-velocity LV outflow (*arrow*)

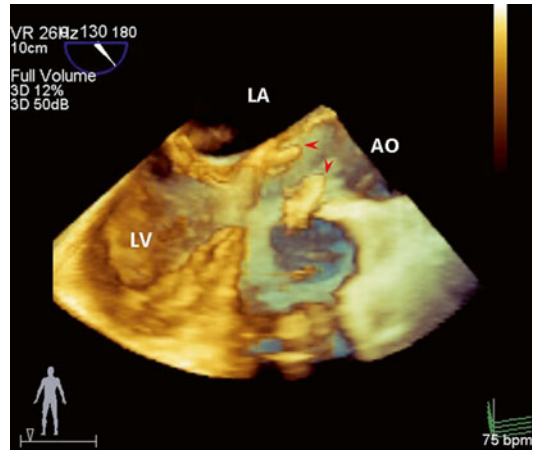

Fig. 2.22 3D TEE image, long-axis view, status post tissue AV replacement (*arrows*), showed good prosthesis function

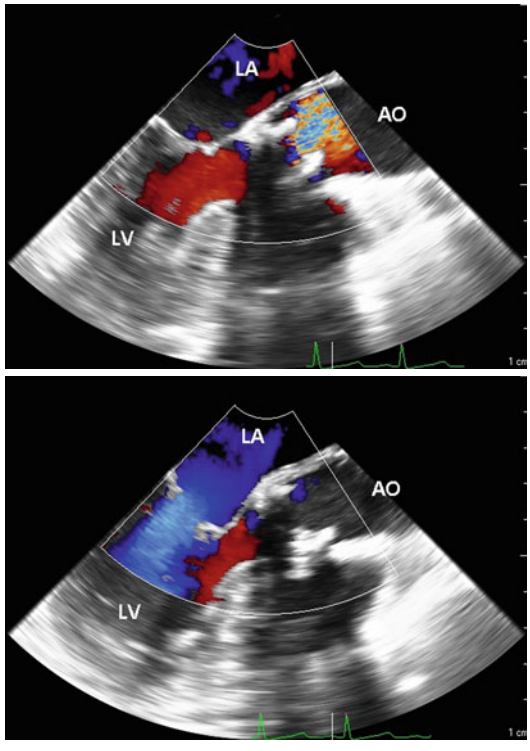

Figs. 2.20 and 2.21 2D TEE color Doppler, long-axis view, status post tissue AV replacement, showed slightly accelerated flow across the prosthesis in systole (*above*) and no AR in diastole (*below*)

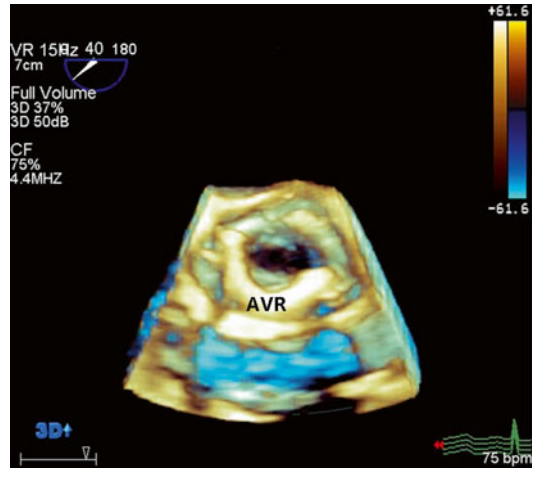

Fig. 2.23 3D TEE color suppressed image, en face view of AV, status post AV replacement (*AVR*), showed good prosthesis function

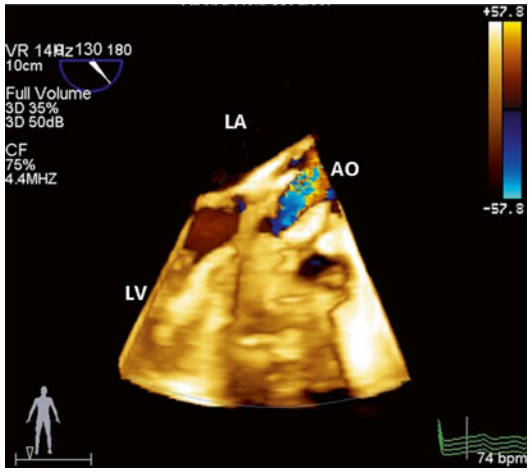

Fig. 2.24 3D TEE color Doppler, long- axis view, status post AV replacement, showed slightly accelerated flow across the prosthesis

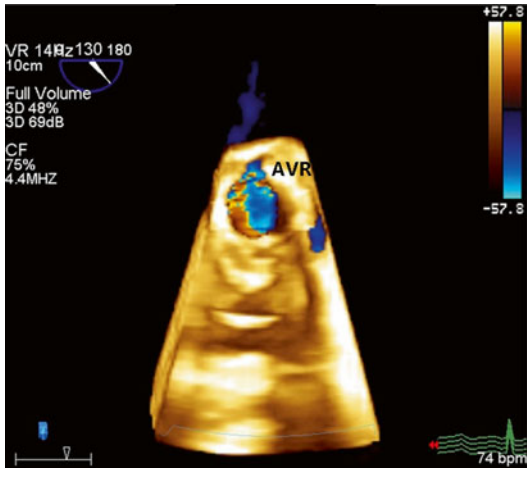

Fig. 2.25 3D TEE color Doppler, short-axis view, status post AV replacement, showed slightly accelerated flow across the prosthesis

Tips

Bicuspid AV is the most common congenital heart disease diagnosed in adults. It is asymptomatic in most patients but may develop AS or AR over the lifetime. Today, of valve replacement worldwide, tissue valves are used in 40 % or more, predominantly as stented porcine AV and bovine pericardial valves.

2.4 Bicuspid Aortic Valve Having Mechanical Aortic Valve Replacement

A 51-year-old woman with a history of schizophrenia, hepatitis C and intestinal adhesions had bicuspid AV and suffered progressive dyspnea on exertion for months. Auscultation: regular heart beat with a grade 2 systolic murmur over the aortic area and left sternal border. ECG: sinus bradycardia. Cardiac catheterization: congenital bicuspid AV with symptomatic critical stenosis. Operation: AV replacement.

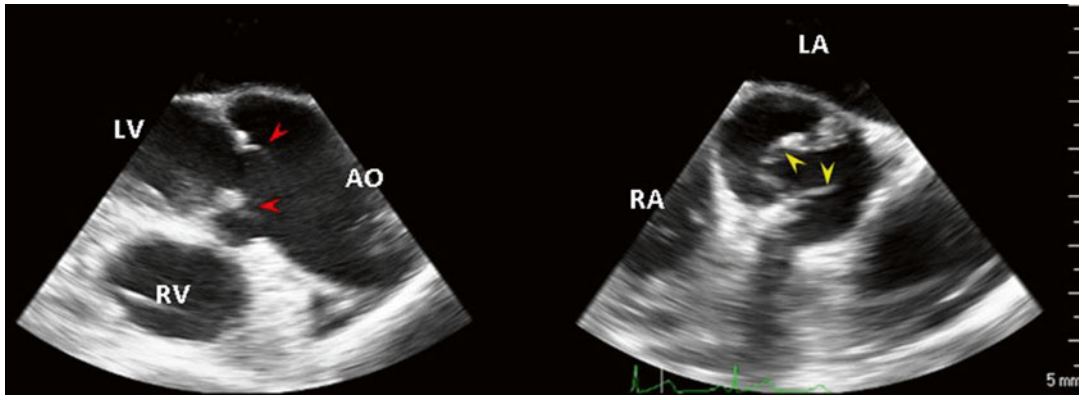

Fig. 2.26 Two-dimensional transesophageal echocardiography (2D TEE) image, x-plane view, showed aorta dilation and bicuspid AV (*yellow arrows*) with doming sign (*red arrows*) and small oval-shape orifice

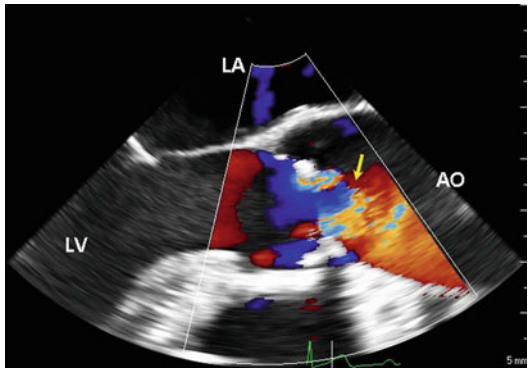

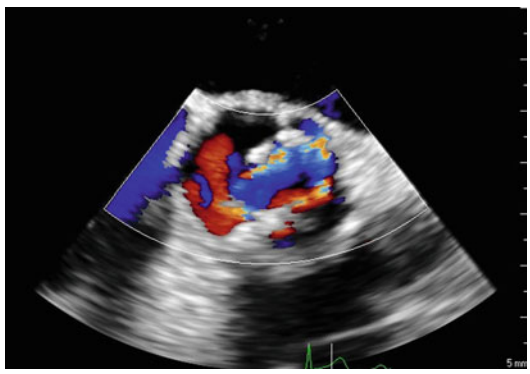

Figs. 2.27 and 2.28 2D TEE color Doppler, long-axis (*above*) and short-axis (*below*) view, showed bicuspid AV with aortic stenosis (*AS*) and high AV velocity (*arrow*)

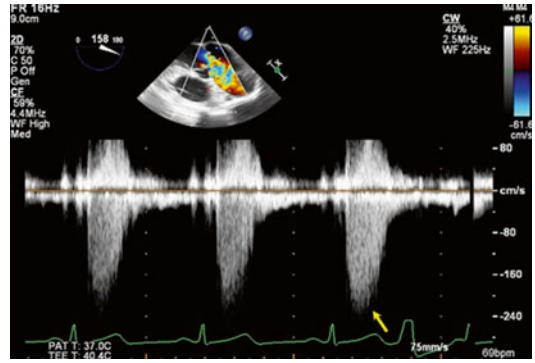

Fig. 2.29 2D TEE continuous-wave Doppler, AS with pressure gradient (peak gradient is about 20 mmHg) LV outflow (*arrow*) was present

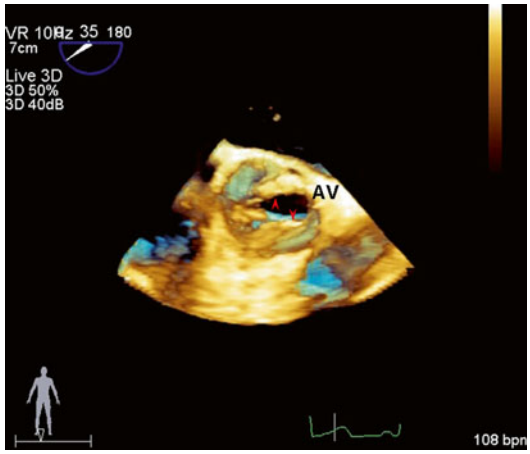

Fig. 2.30 3D TEE, short-axis view, showed bicuspid AV (*arrows*) with small oval-shape orifice

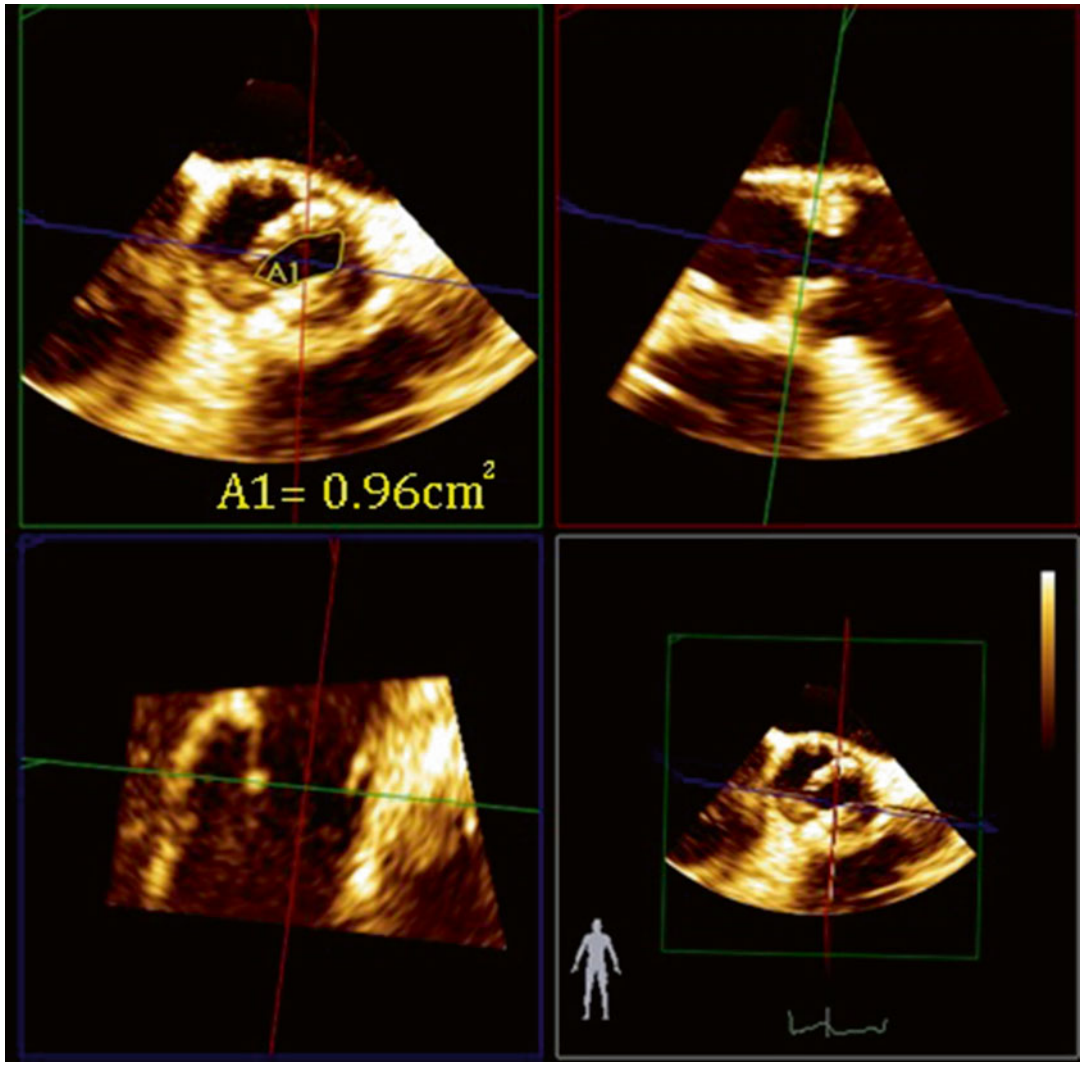

Fig. 2.31 Multi-planar reconstruction (MPR) of 3D TEE image, showed AV area is 0.96 cm^2

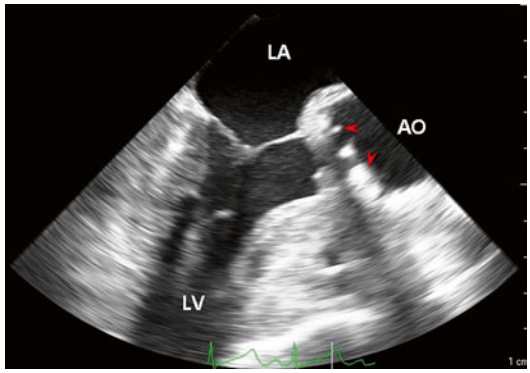

Fig. 2.32 2D TEE image, long-axis view, status post AV replacement with mechanical valve (*arrows*), showed good prosthesis function

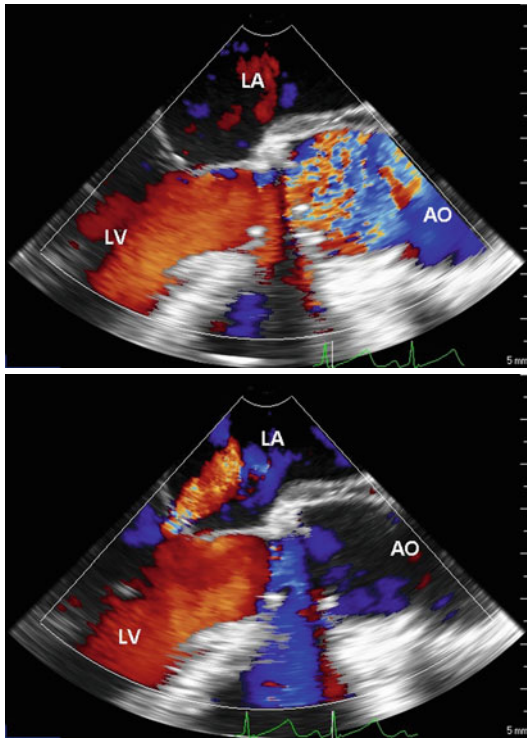

Figs. 2.33 and 2.34 2D color Doppler, showed AV post operation with slightly accelerated flow across the prosthesis in systole (*above*) and no AR in diastole (*below*), mild MR is present

Tips

The cusp size is often uneven with an eccentric orifice in bicuspid AV. The optimal visualization of prosthetic AV is achieved from short-axis and long-axis view at the mid-esophageal level, while upper-esophageal and trans-gastric views are not helpful due to poor image quality.

2.5 Rheumatic Heart Disease Having Aortic and Mitral Replacement

A 65-year-old woman had a long standing history of rheumatic heart disease with severe mitral, aortic stenosis and Af. She admitted for exertional dyspnea and dizziness off and on. Auscultation: irregular heart beat with a grade 2/6 systolic murmur over apex. ECG: Atrial fibrillation with moderate ventricular response. Chest X ray: Borderline heart size. Cardiac catheterization: mitral and aortic stenosis. Operation: AV and MV replacement, TV repair and Af ablation.

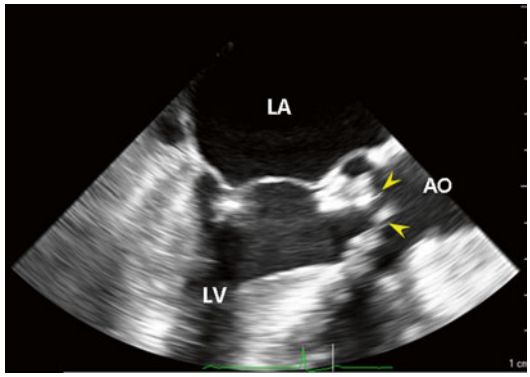

Fig. 2.35 Two-dimensional transesophageal echocardiogram (2D TEE) image, long-axis view, showed calcified aortic leaflets with systolic doming (*arrows*)

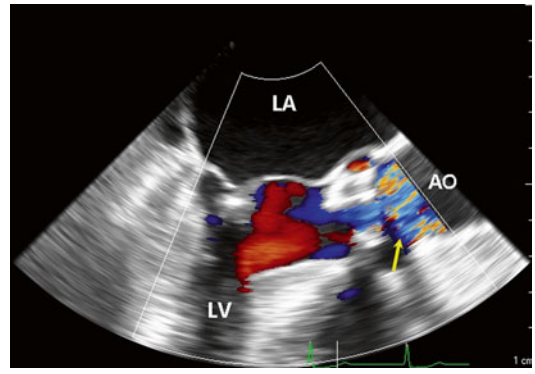

Fig. 2.37 2D TEE color Doppler, long-axis view in systole, showed accelerated flow across the calcified AV (*arrow*)

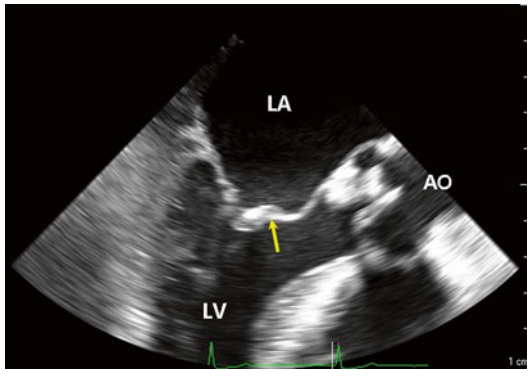

Fig. 2.36 2D TEE image, long-axis view in diastole, showed restricted motion of mitral leaflet tips with hockey-sign (*arrow*)

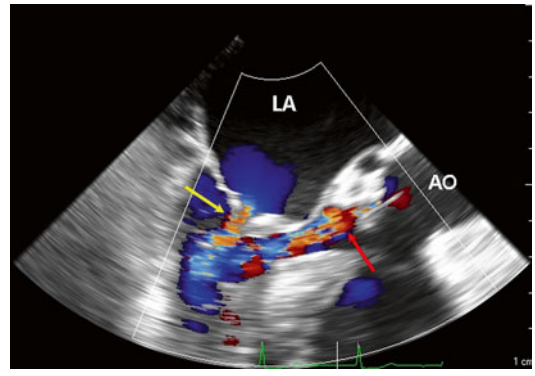

Fig. 2.38 2D TEE color Doppler, long-axis view in diastole, showed high-velocity mitral inflow (*yellow arrow*) and moderate AR (*red arrow*)

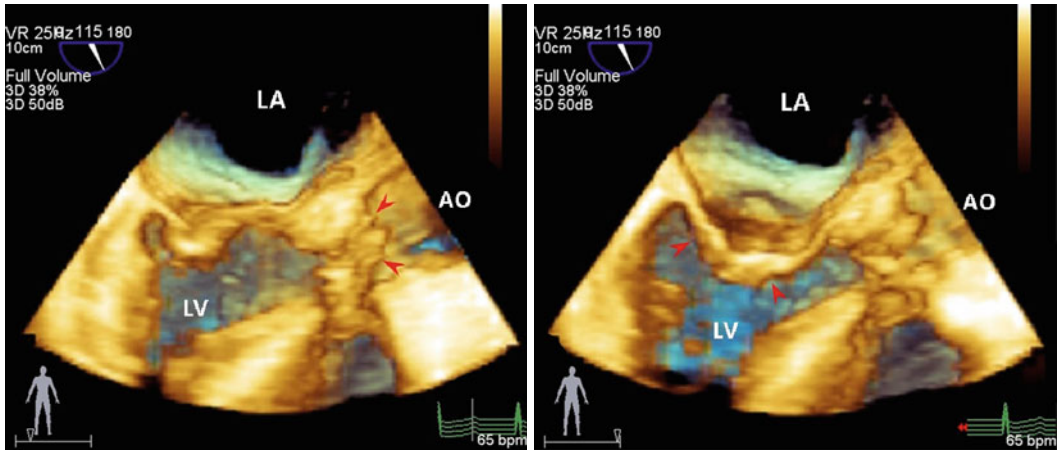

Figs. 2.39 and 2.40 3D TEE image, long-axis view in systole (*left*) and diastole (*right*), showed rheumatic aortic stenosis occurred concurrently with rheumatic mitral stenosis (*arrows*)

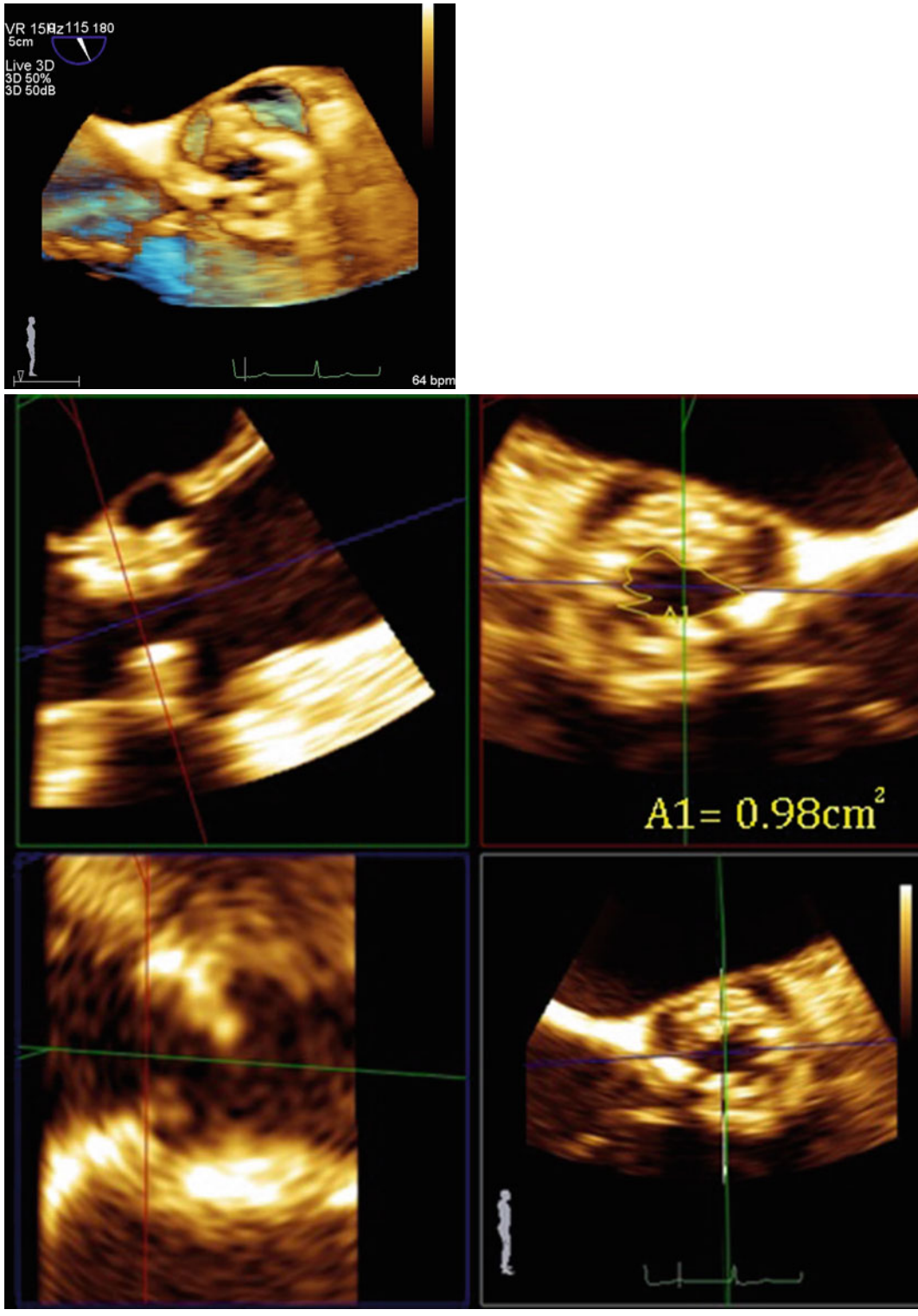

Figs. 2.41 and 2.42 3D TEE image, short-axis view (*above*) and MPR (*below*), showed fusion commissural of aortic leaflets with small AV area which is 0.98 cm^2

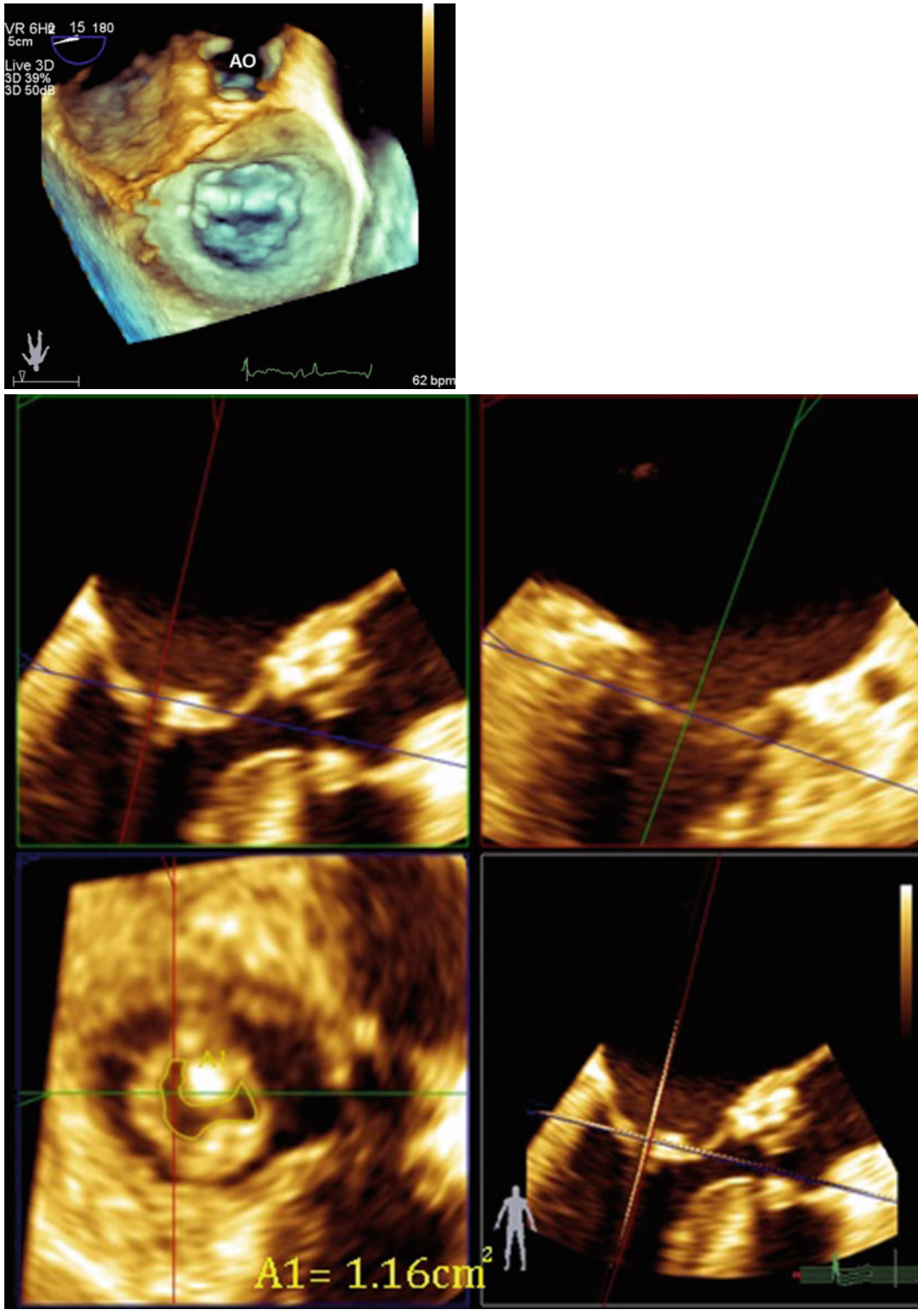

Figs. 2.43 and 2.44 3D TEE image, en face view (*above*) and MPR (*below*), showed small mitral orifice with the area is 1.16 cm^2

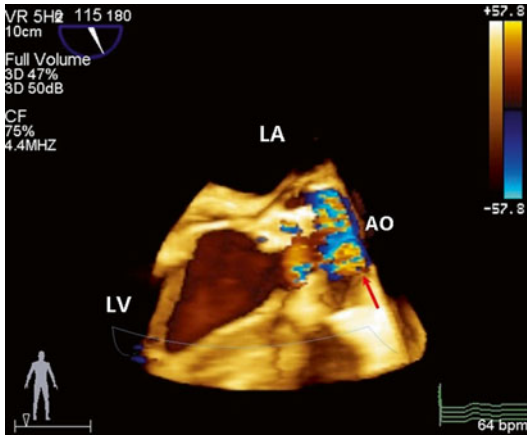

Fig. 2.45 3D TEE color Doppler, long- axis view in systole, showed accelerated flow across the calcified AV (*arrow*)

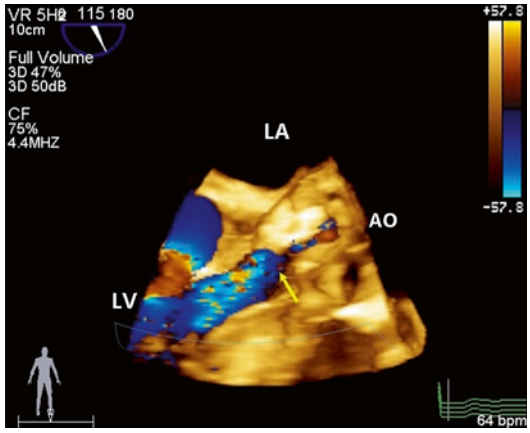

Fig. 2.46 3D TEE color Doppler, long-axis view in diastole, showed moderate AR (*arrow*)

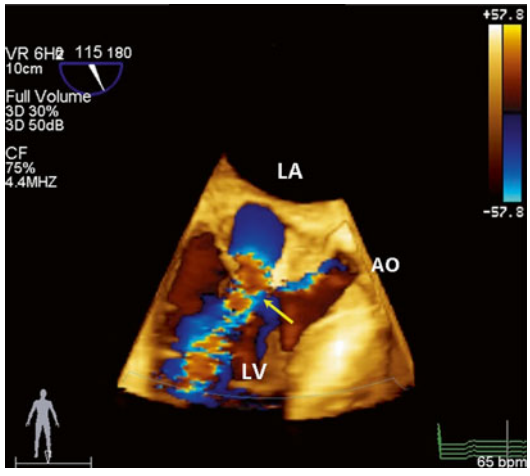

Fig. 2.47 3D TEE color Doppler, long-axis view in diastole, showed high-velocity mitral inflow (*arrow*)

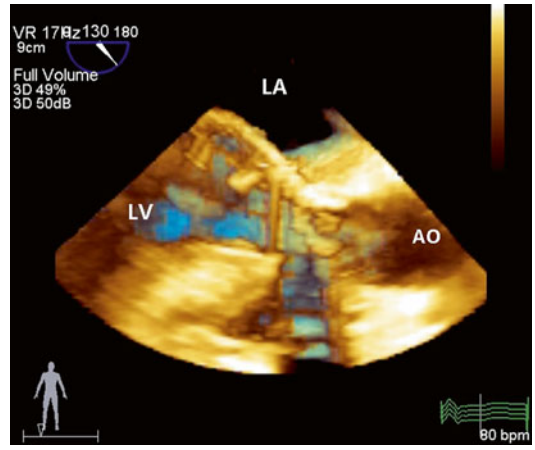

Fig. 2.48 3D TEE image, long-axis view, status post tissue aortic and mitral replacement, showed normal prosthetic function

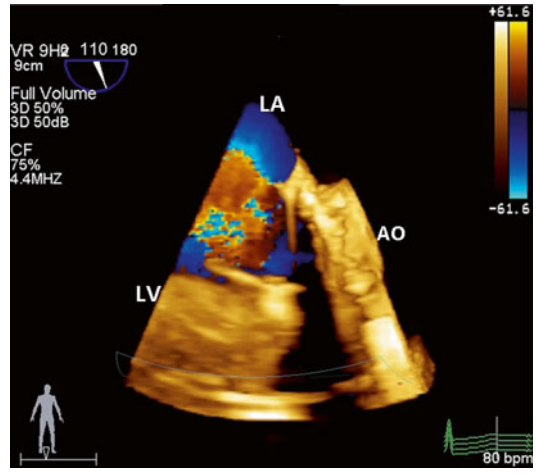

Fig. 2.49 3D TEE color Doppler, long-axis view, status post tissue aortic and mitral replacement, showed normal mitral inflow

Tips

Rheumatic heart disease preferentially involves the MV. Rheumatic AS may be diagnosed concurrently with rheumatic MV disease.

2.6 Aortic Stenosis Having Transcatheter Aortic Valve Implantation

A 73-year-old woman with a history of asthma and left side breast cancer status post mastectomy presented to our ER with complaints of chest pain, dyspnea and dizziness. Auscultation: regular heart beat with a grade 3/6 systolic murmur over apex. ECG: sinus tachycardia, left ventricular hypertrophy with repolarization abnormality, myocardial ischemia. Cardiac catheterization: three-vessel coronary artery disease, critical AS and severe MR. Chest CT: some mural thrombi at the orifice of right CCA, calcified plaques on the coronary arteries, calcified AV and left pleural effusion. Operation: CABG *x*2 (LAD and RCA), TV repair and emergency transcatheter aortic valve implantation (TAVI)

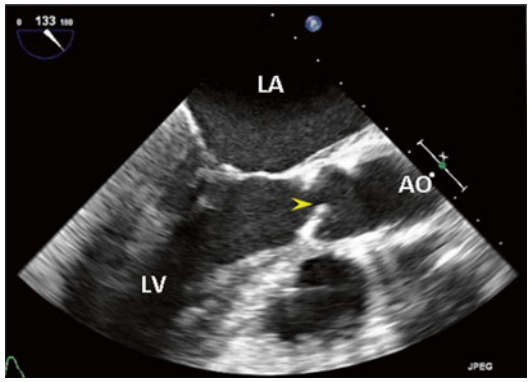

Fig. 2.50 Two-dimensional transesophageal echocardiography (2D TEE) image, long-axis view, showed calcified AV (*arrow*) with aortic stenosis (AS)

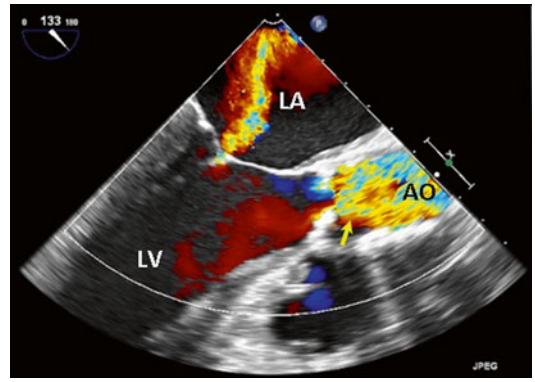

Fig. 2.52 2D TEE color Doppler, long-axis view, showed AS with high-velocity mosaic LV outflow (*arrow*)

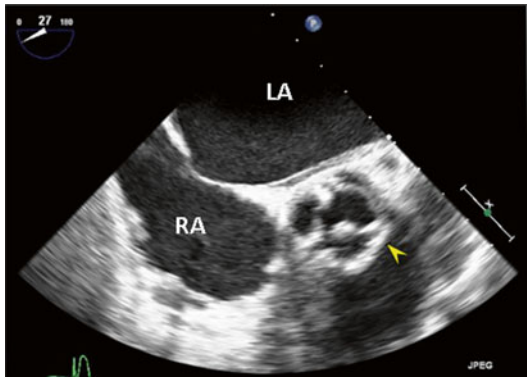

Fig. 2.51 2D TEE image, short-axis view, showed calcified AV (*arrow*) with AS

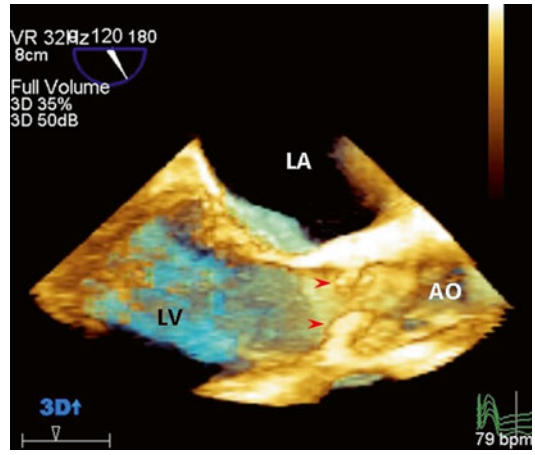

Fig. 2.53 3D TEE image, long-axis view, showed calcified AV (*arrows*) with AS

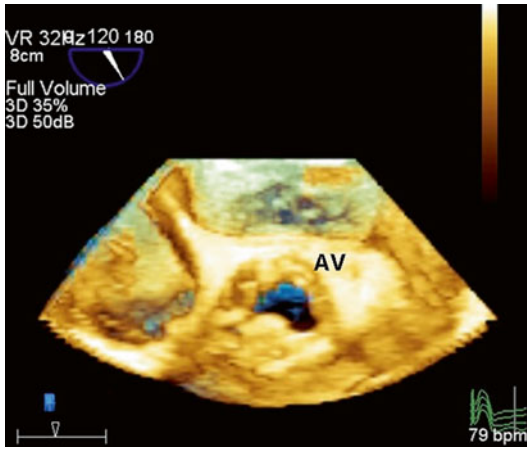

Fig. 2.54 3D TEE image, short-axis view, showed calcified AV with AS

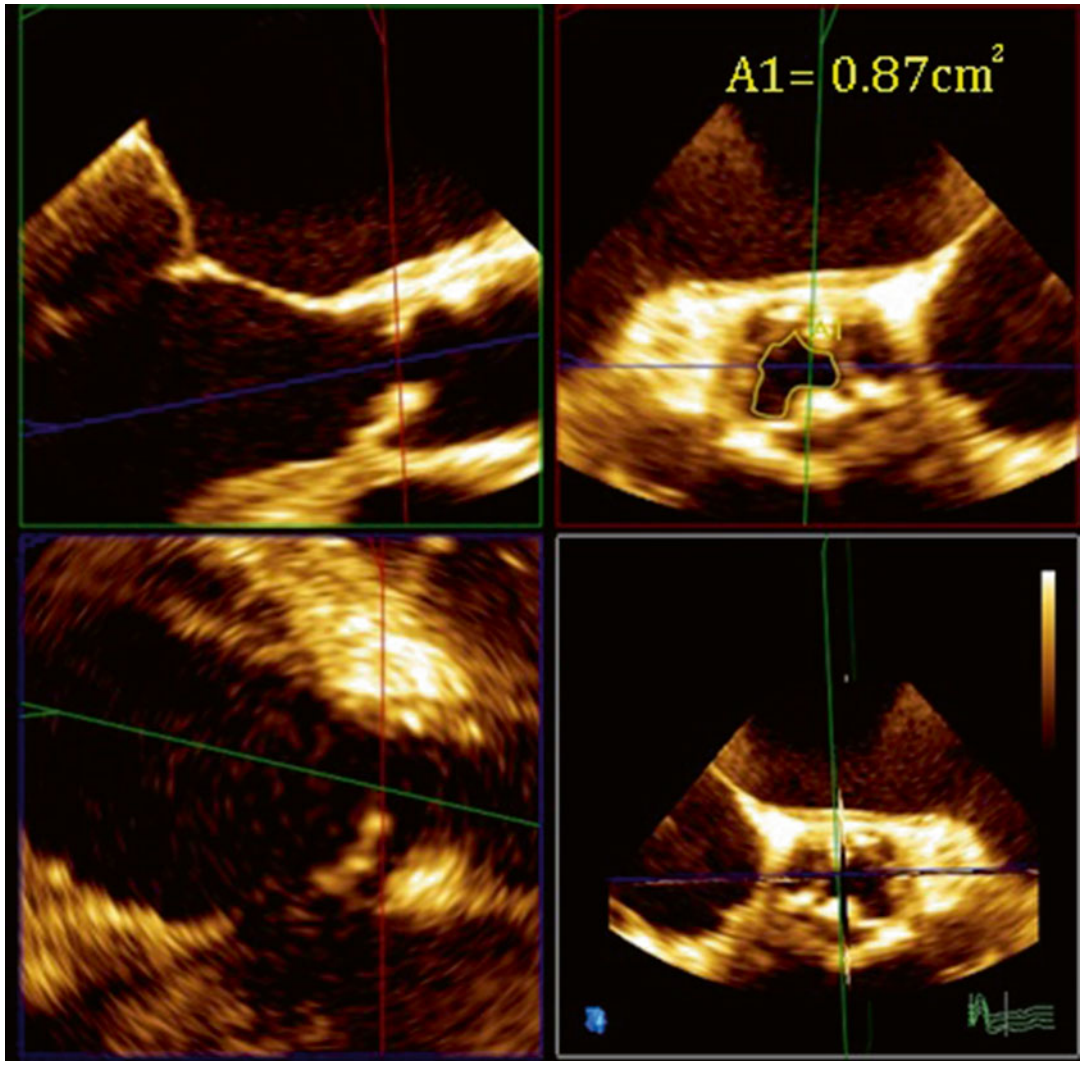

Fig. 2.55 Multi-planar reconstruction (MPR) of 3D TEE image, showed the aortic valve area is 0.87 cm^2

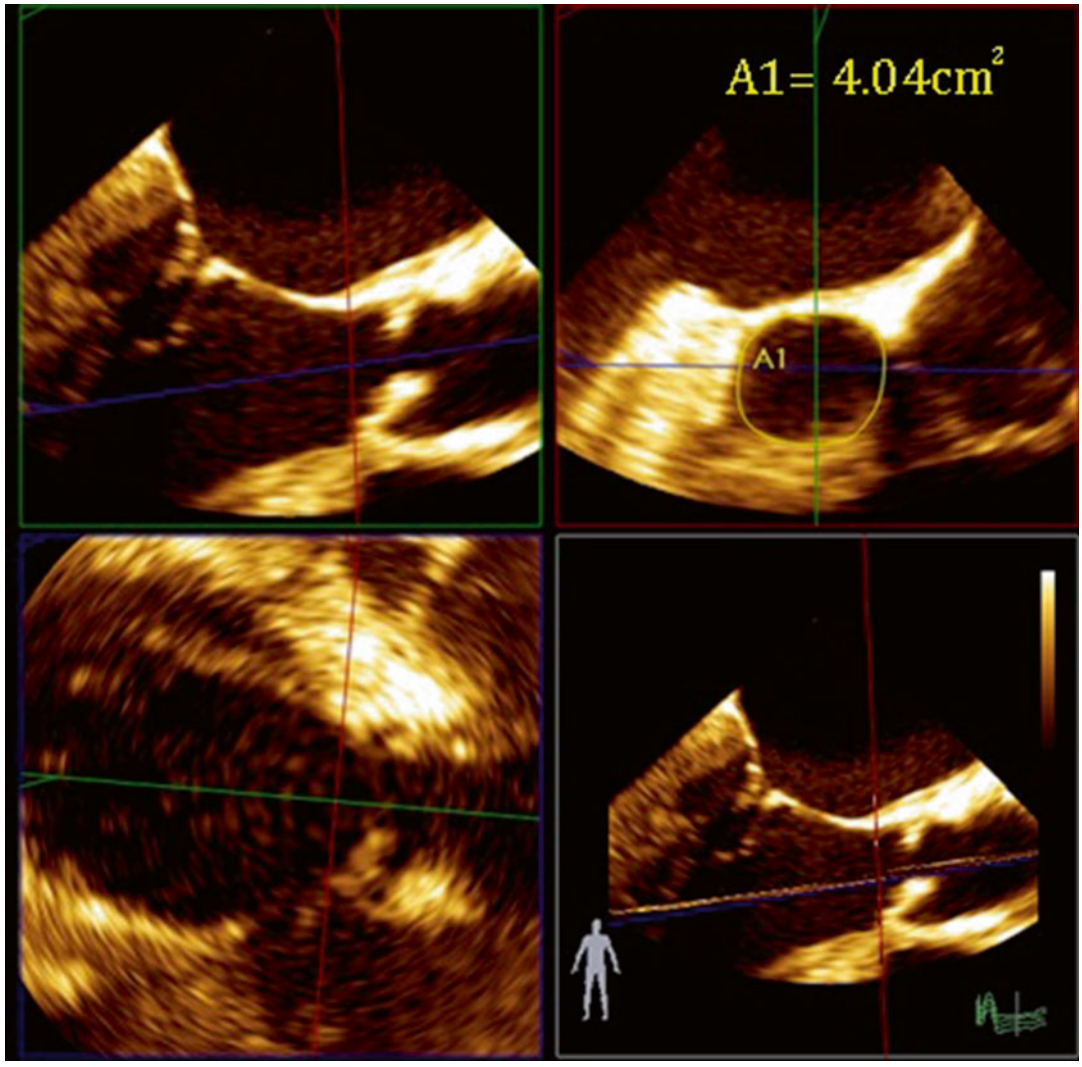

Fig. 2.56 MPR of 3D TEE image showed the aortic annular area is 4.04 cm^2

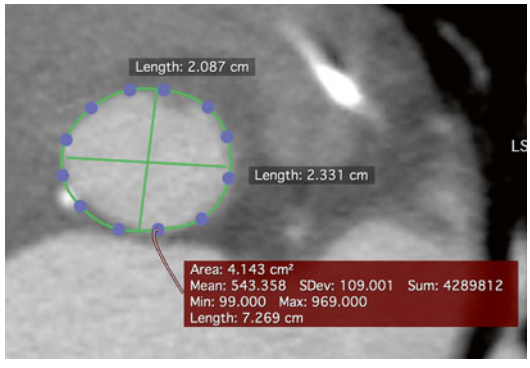

Fig. 2.57 CT angiogram showed the aortic annular area is 4.14 cm^2

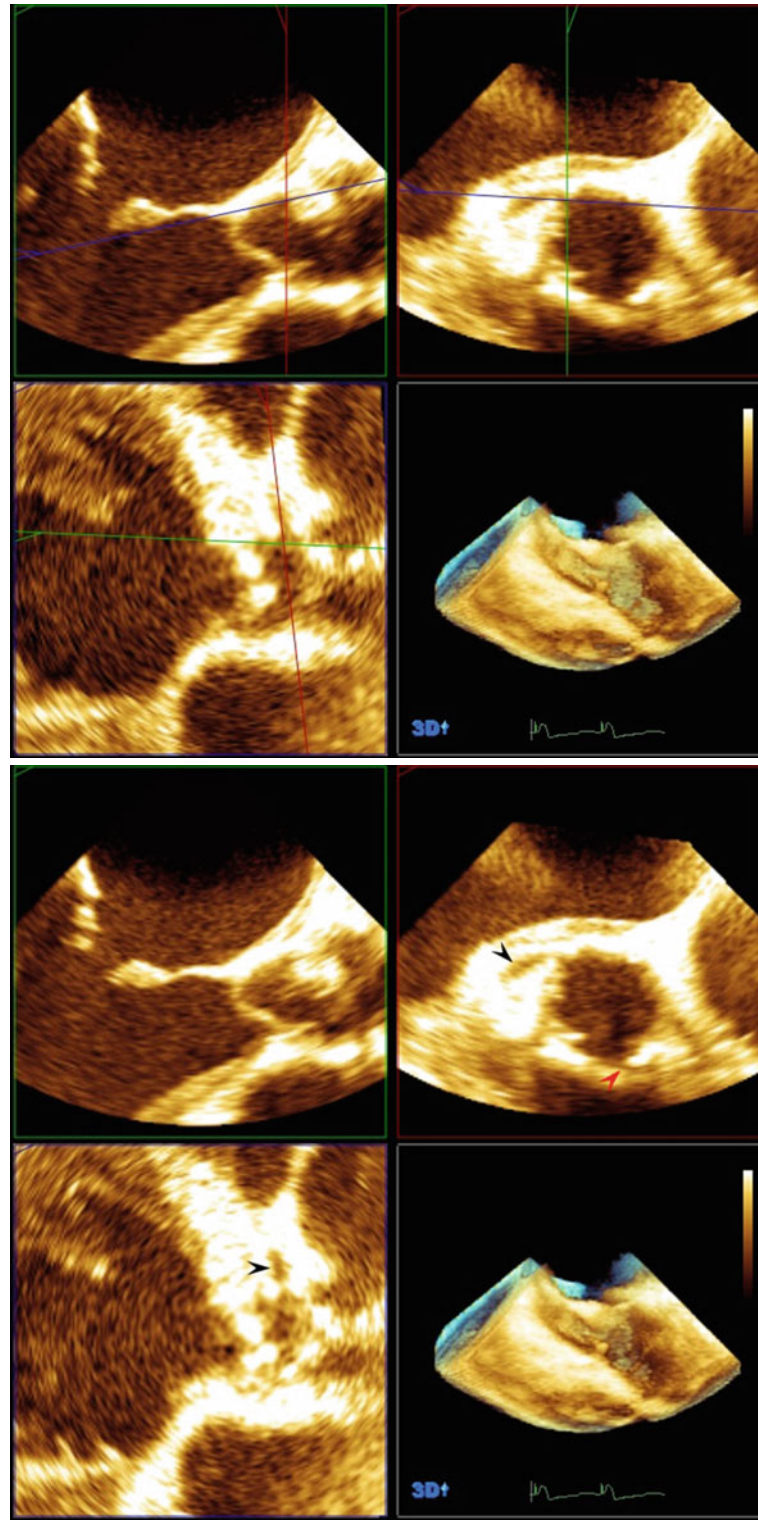

Figs. 2.58 and 2.59 MPR of 3D TEE image showed the anatomical relationship among sinus of valsalva, left coronary artery (*black arrows*) and right coronary artery (*red arrow*)

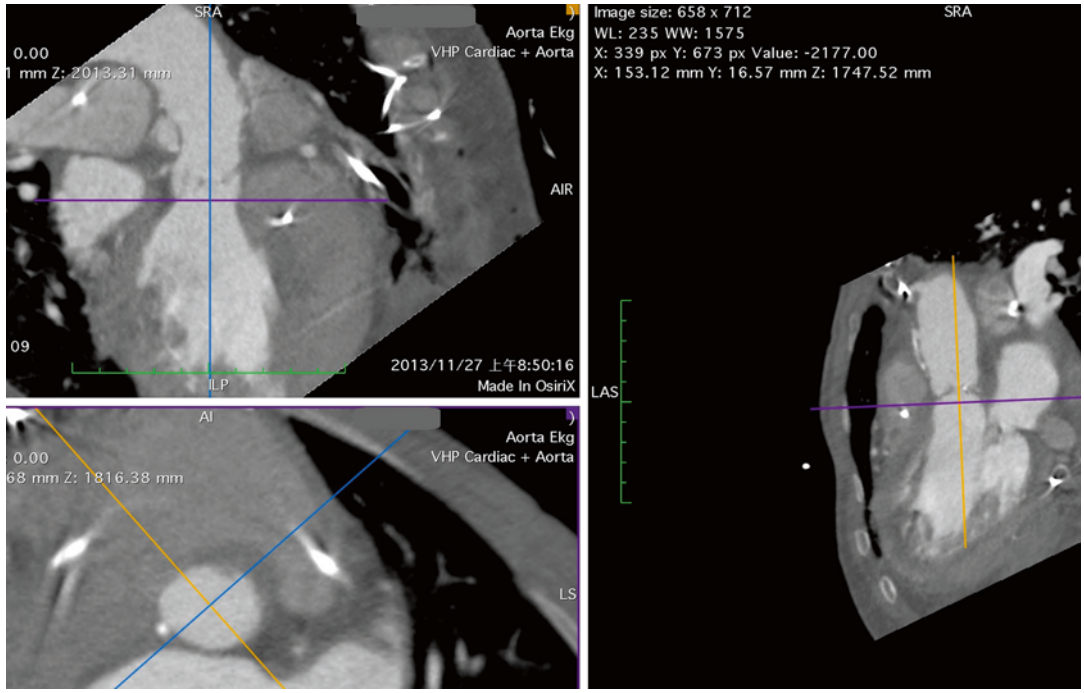

Fig. 2.60 CT angiogram showed the anatomical relationship between aortic annulus and its surroundings

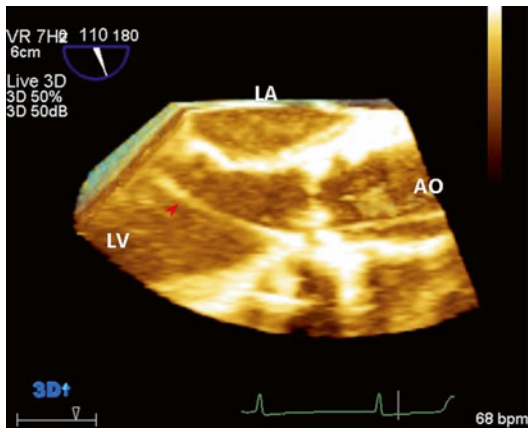

Fig. 2.61 3D TEE image, long-axis view, during the TAVI procedure, showed the guiding catheter (*arrow*) crossed AV from aorta to LV

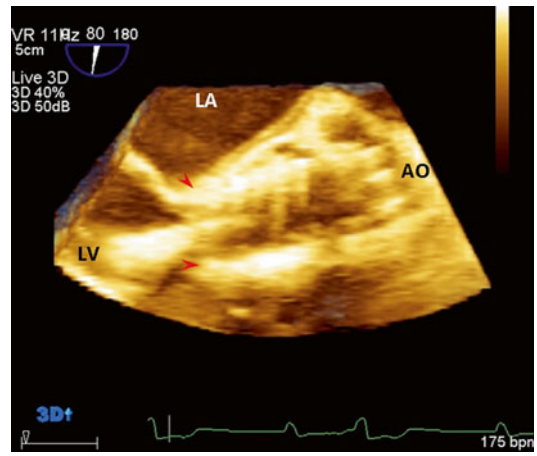

Fig. 2.62 3D TEE image, long-axis view, during the TAVI procedure, showed the open core valve (*arrows*)

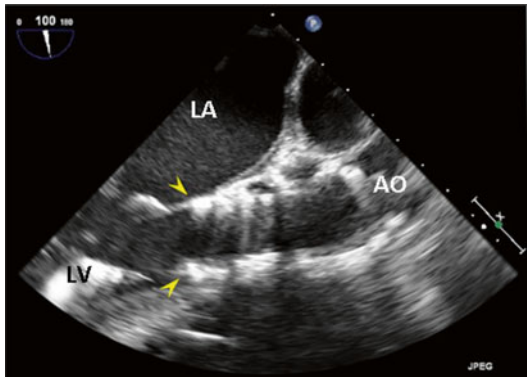

Fig. 2.63 2D TEE image, long-axis view, during the TAVI procedure, showed the open core valve (*arrows*)

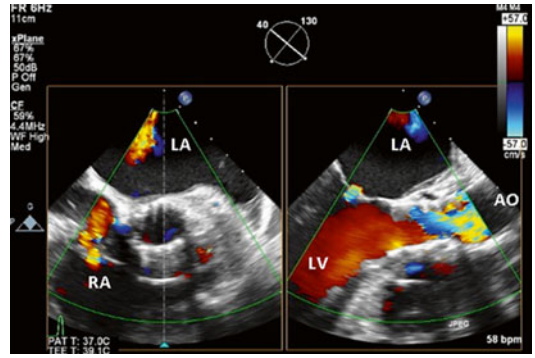

Fig. 2.66 2D TEE color Doppler, x-plane view, status post TAVI, showed normal LV outflow

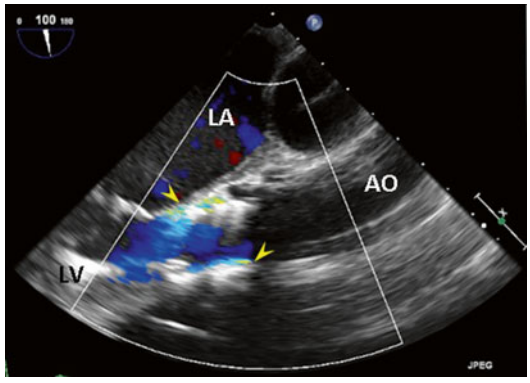

Fig. 2.64 2D TEE color Doppler, long-axis view, during the TAVI procedure, showed mild paravalvular leakage (*arrows*) when the valve was not fully opened

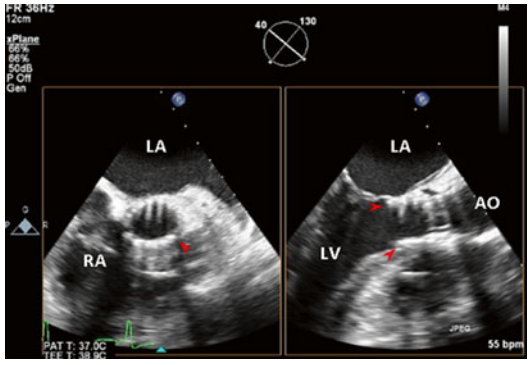

Fig. 2.65 2D TEE image, x-plane view, status post TAVI, showed the core valve (*arrows*)

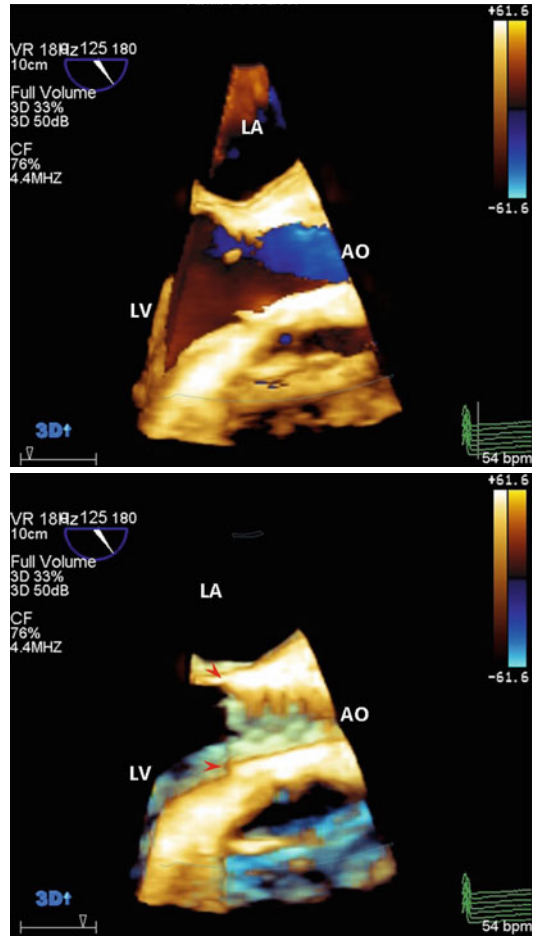

Figs. 2.67 and 2.68 3D TEE color Doppler (*above*) and color suppressed image (*below*), long-axis view, status post TAVI, showed the core valve (*arrows*) with normal LV outflow

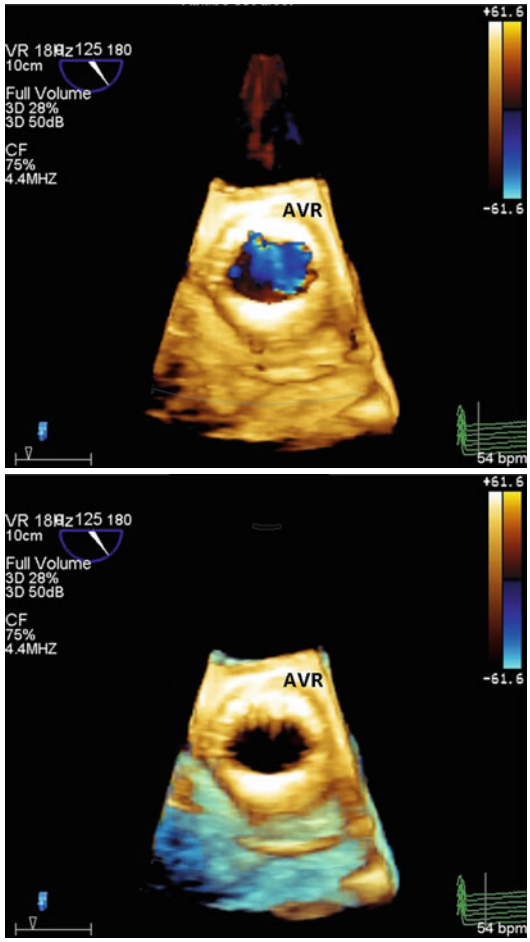

Figs. 2.69 and 2.70 3D TEE color Doppler (*above*) and color suppressed image (*below*), en face view of AV, status post TAVI, showed normal LV outflow and good prosthesis function

Tips

TAVI is an alternative to surgical AV replacement in patients who were at unacceptable risk for cardiac surgery requiring a sternotomy. Because TAVI is a relatively new procedure, it is important for both experienced and novice operators to be aware of the echocardiographic appearance of major complications.

Suggested Reading

Asano R, Nakano K, Kodera K, et al. Ascending-descending aortic bypass and aortic valve replacement for aortic coarctation with bicuspid aortic valve and an aberrant right subclavian artery;report of a case. Kyobu Geka. 2015;68(9):777–9. Japanese.

Chen GL, Li HT, Li HR, Zhang ZW. Transcatheter closure of ventricular septal defect in patients with aortic valve prolapse and mild aortic regurgitation: feasibility and preliminary outcome. Asian Pac J Trop Med. 2015;8(4):315–8.

Davarpasand T, Hosseinsabet A, Jalali A. Concomitant coronary artery bypass graft and aortic and mitral valve replacement for rheumatic heart disease: short- and mid-term outcomes. Interact Cardiovasc Thorac Surg. 2015;21(3):322–8.

Forteza A, Vera F, Centeno J, et al. Preservation of the bicuspid aortic valve associated with aneurysms of the aortic root and ascending aorta. Rev Esp Cardiol (Engl Ed). 2013;66(8):644–8.

Girdauskas E, Disha K, Rouman M, et al. Aortic events after isolated aortic valve replacement for bicuspid aortic valve root phenotype: echocardiographic follow-up study. Eur J Cardiothorac Surg. 2015;48(4):e71–6.

Günaydın ZY, Bektaş O, Karagöz A, Kaya A. Case images: a rare cause of severe aortic valve regurgitation: isolated aortic valve prolapse. Turk Kardiyol Dern Ars. 2015;43(2):208.

Khalique OK, Hamid NB, Kodali SK, et al. Improving the accuracy of effective orifice area assessment after transcatheter aortic valve replacement: validation of left ventricular outflow tract diameter and pulsed- wave doppler location and impact of three-dimensional measurements. J Am Soc Echocardiogr. 2015;28(11):1283–93.

Looi JL, Lee AP, Fang F, et al. Abnormal mitral-aortic intervalvular coupling in mitral valve diseases: a study using real-time three-dimensional transesophageal echocardiography. Clin Res Cardiol. 2015;104(10):831–42.

Mazzitelli D, Pfeiffer S, Rankin JS, et al. A regulated trial of bicuspid aortic valve repair supported by geometric ring annuloplasty. Ann Thorac Surg. 2015;99(6):2010–6.

Michelena HI, Corte AD, Prakash SK, et al. Bicuspid aortic valve aortopathy in adults: Incidence, etiology, and clinical significance. Int J Cardiol. 2015;201:400–7.

Rönnerfalk M, Tamás É. Structure and function of the tricuspid and bicuspid regurgitant aortic valve: an echocardiographic study. Interact Cardiovasc Thorac Surg. 2015;21(1):71–6.

Diseases of the Tricuspid and Pulmonary Valve

3

Abstract

Right-sided vlavular disorders are discussed in this chapter, including cases of TV prolapse, tricuspid prosthesis restenosis, subvalvular PS, and carcinoid syndrome.

The TV is the largest cardiac valve and the PV has thinner leaflets. 3D zoom mode is preferable for assessment for TV and PV leaflets whereas 3D full volume is better for regurgitation and valvular supporting structures.

3.1 Prolapse of Posterior Tricuspid Leaflet Having Tricuspid Repair

A 34-year-old man with previous VSD and TV repair suffered from chest tightness and palpitation off and on. Auscultation: irregular heart beat with a grade 2/6 systolic murmur over apex and left sternal border. ECG: atrial flutter and complete right bundle branch block. Chest X ray: cardiomegaly. Cardiac catheterization: severe TR and RV failure. Abdominal echo: engorged IVC and hepatic vein. Operation: re-do TV repair, partial pericardiectomy and Af ablation.

Electronic supplementary material The online version of this chapter (doi:10.1007/978-981-10-0587-9_3) contains supplementary material, which is available to authorized users.

W.-H. Yin, M.-C. Hsiung, *Atlas of Perioperative 3D Transesophageal Echocardiography*,
DOI 10.1007/978-981-10-0587-9_3

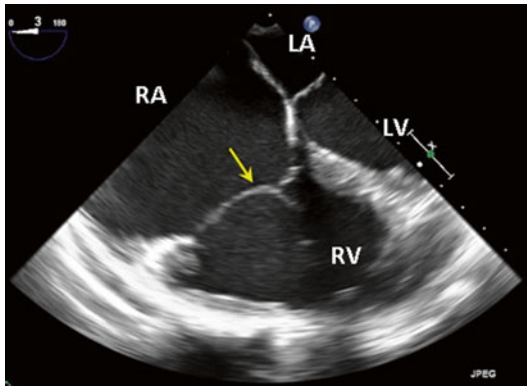

Fig. 3.1 Two-dimensional transesophageal echocardiography (2D TEE) image, four-chamber view, showed prolapse of posterior tricuspid leaflet (*arrow*), dilated RA and RV with RV dysfunction

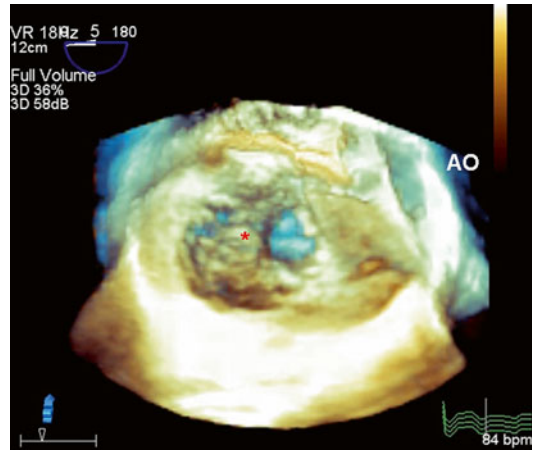

Fig. 3.3 3D TEE image, en face view of TV from atrial perspective in systole, showed prolapse of posterior tricuspid leaflet (*)

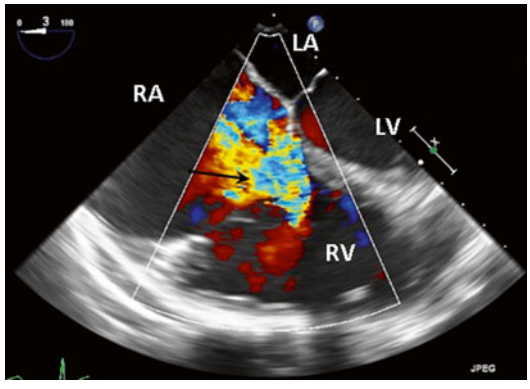

Fig. 3.2 2D TEE color Doppler, four-chamber view, showed severe eccentric TR (*arrow*) due to TV prolapse

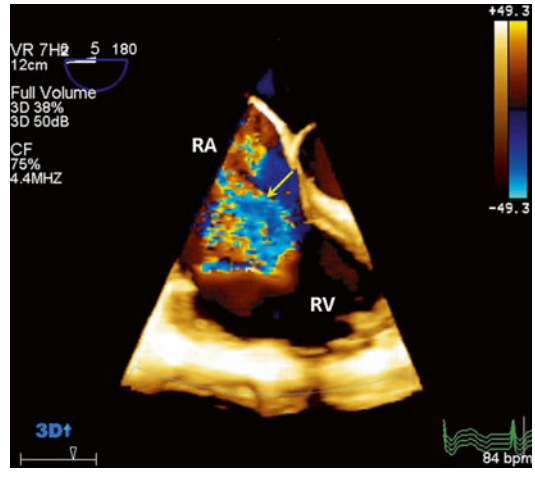

Fig. 3.4 3D TEE color Doppler, showed severe eccentric TR (*arrow*)

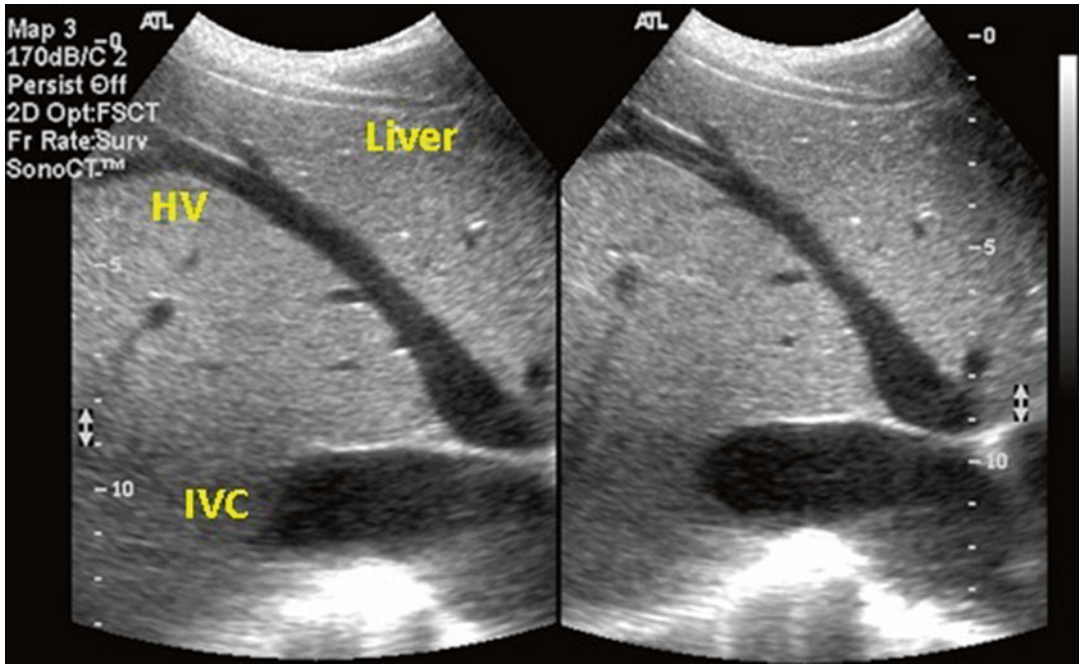

Fig. 3.5 2D abdominal echography showed engorged IVC and hepatic vein (*HV*)

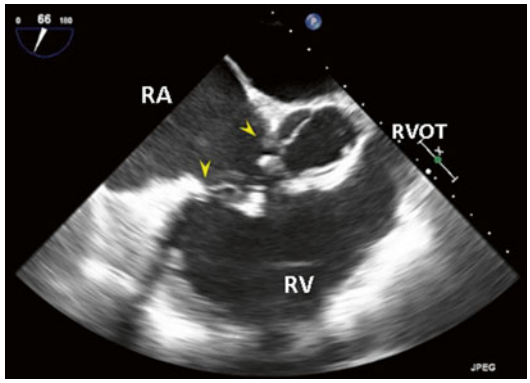

Fig. 3.6 2D TEE image, RV inflow-outflow view, status post TV repair with annuloplasty (*arrow*)

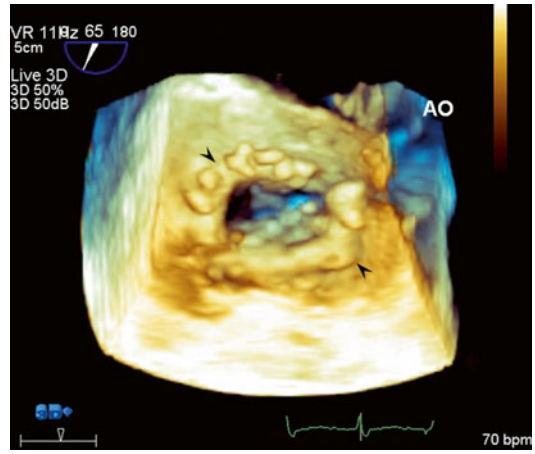

Fig. 3.7 3D TEE image, en face view of TV from atrial perspective, status post TV repair, showed the suture and ring (*arrows*)

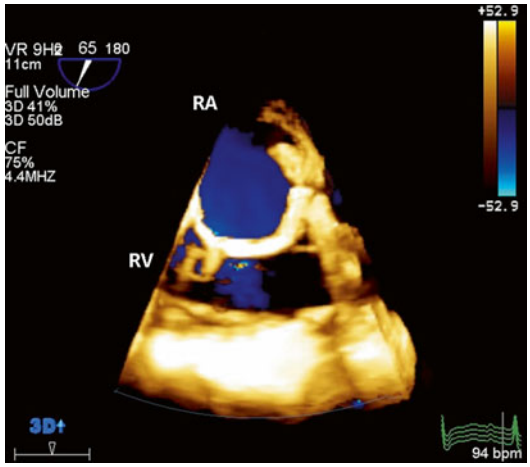

Fig. 3.8 3D TEE color Doppler, status post TV repair, showed repaired TV with normal RV inflow and mild TR

Tips

All kinds of TV repairs include an annuloplasty, which is a complete or partial ring placed around the opening of the valve to restore and retain its correct size and shape.

3.2 Prosthetic Tricuspid Valve Stenosis Having Redo Replacement

A 72-year-old woman had TV replacement 30 years ago. She experienced dyspnea on exertion, abdominal distention and poor appetite recently. Auscultation: regular heart beat without significant murmur. ECG: atrial fibrillation with rapid ventricular response, right axis deviation, counter clockwise rotation and complete right bundle branch block. Chest X ray: mild cardiomegaly and mild calcification of aortic arch. Operation: CABG x2 (SVG to LAD and RCA), TVR and permanent sutureless myocardial screw in lead placement of RV.

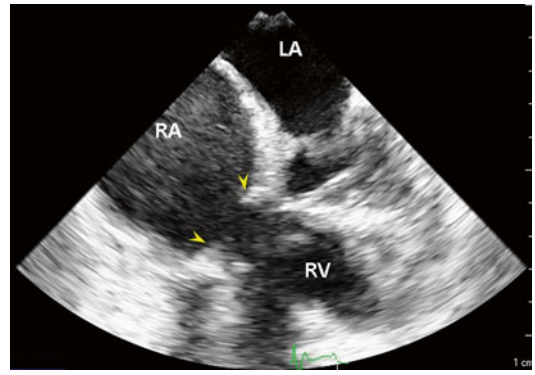

Fig. 3.9 Two-dimensional transesophageal echocardiography (2D TEE) image, status post tissue TV replacement (*arrows*), showed thickened tissue tricuspid prosthesis (*arrows*) with dilated RA

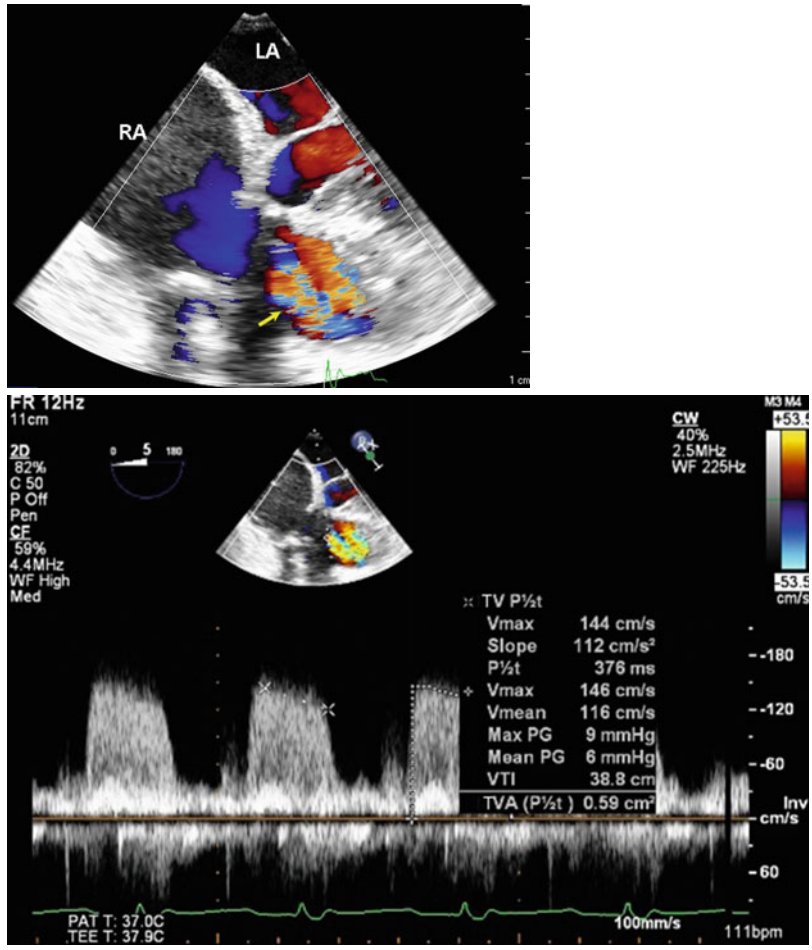

Figs. 3.10 and 3.11 2D TEE color Doppler (*above*) and continuous-wave Doppler (*below*), showed prosthetic tricuspid stenosis with narrow tricuspid orifice (calculated TV area is 0.59 cm^2) and high-velocity mosaic RV inflow (*arrow*) (peak gradient is 9 mmHg) in diastole

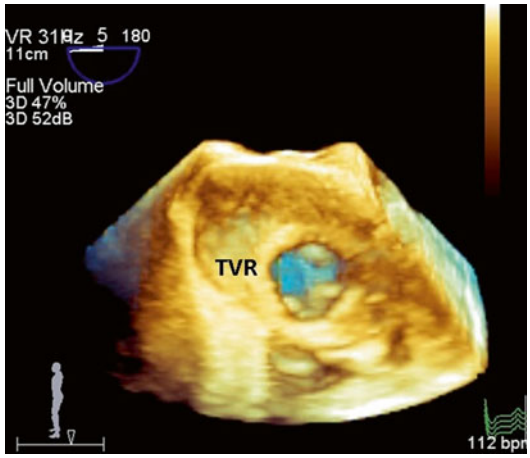

Fig. 3.12 3D TEE image, en face view of TV from atrial perspective in diastole, status post TV replacement (TVR), showed thickened tricuspid prosthesis with small TV area

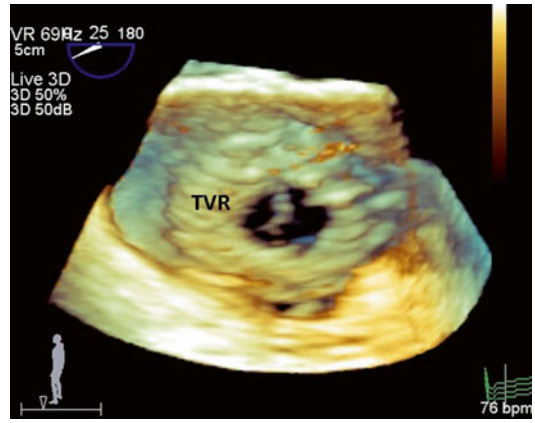

Fig. 3.14 3D TEE image, en face view of TV from atrial perspective, status post redo TV replacement (*TVR*)

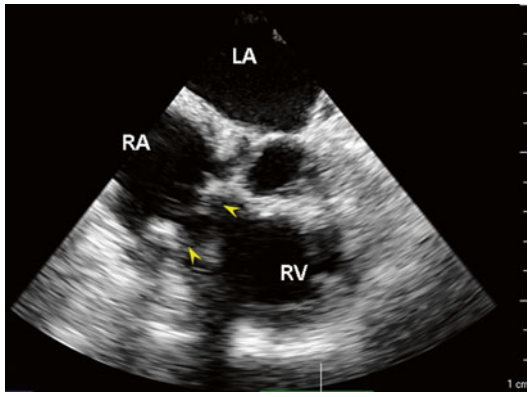

Fig. 3.13 2D TEE image, status post redo TV replacement with tissue valve (*arrows*)

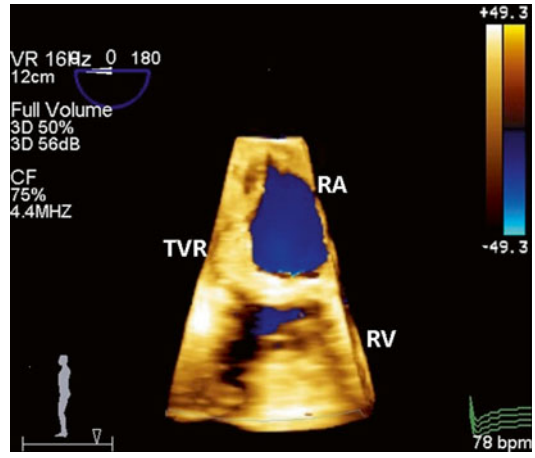

Fig. 3.15 3D TEE color Doppler, status post redo TV replacement (*TVR*), showed normal tricuspid prosthesis function without stenosis

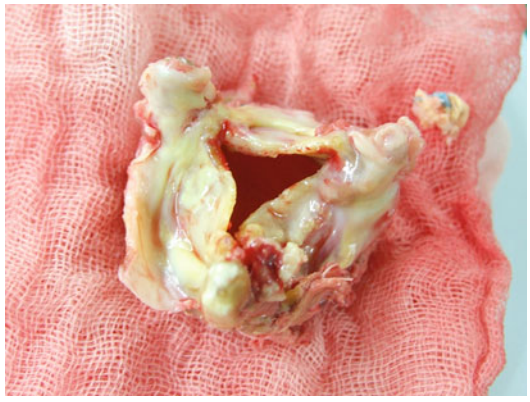

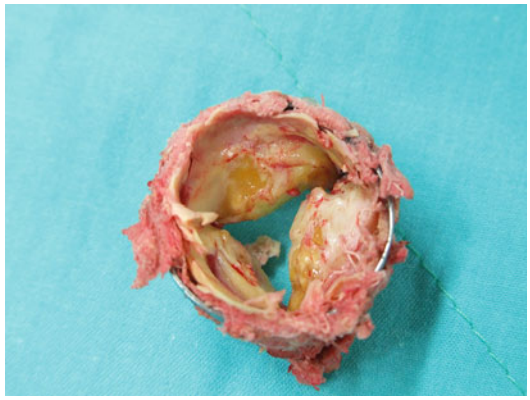

Figs. 3.16 and 3.17 Gross specimen of the calcified and stenotic tricuspid prosthesis

Tips

The prosthetic valve is difficult to image due to shadowing by the valvular graft sometimes, where the Doppler can deal with the situation.

3.3 Subvalvular Pulmonary Stenosis with Right Atrium Thrombus

A 61-year-old man had a history of congenital heart disease with severe pulmonic stenosis, single coronary artery disease and chronic atrial fibrillation. He suffered from sudden onset epigastralgia followed by syncope with generalized tonic-seizure like movement. Auscultation: irregular heart beat with a grade 2–6 systolic murmur over left upper sternal border and a grade 3/6systolic murmur over left lower sternal border and apex. Chest X ray: marked cardiomegaly. Operation: CABG x1 (LAD to SVG), carotid endarterectomy of ICA, removal of RA thrombus, myomectomy of RV outflow tract with resection of parietal band, atrial fibrillation ablation and LA & RA auricle obliteration.

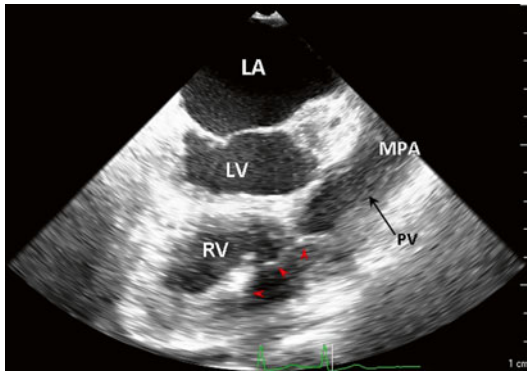

Fig. 3.18 Two-dimensional trsnseosphageal echocardiography (2D TEE) showed RV hypertrophy and a muscle band (*arrows*) at the junction of RV and infundibulum divided the cavity into two chambers. MPA, main pulmonary artery

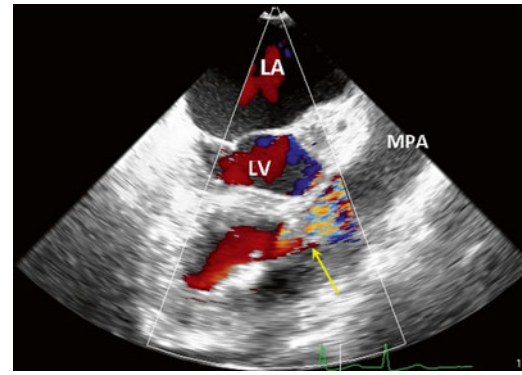

Fig. 3.19 2D TEE color Doppler showed infundibular pulmonic stenosis with accelerated flow (*arrow*) in RV outflow tract

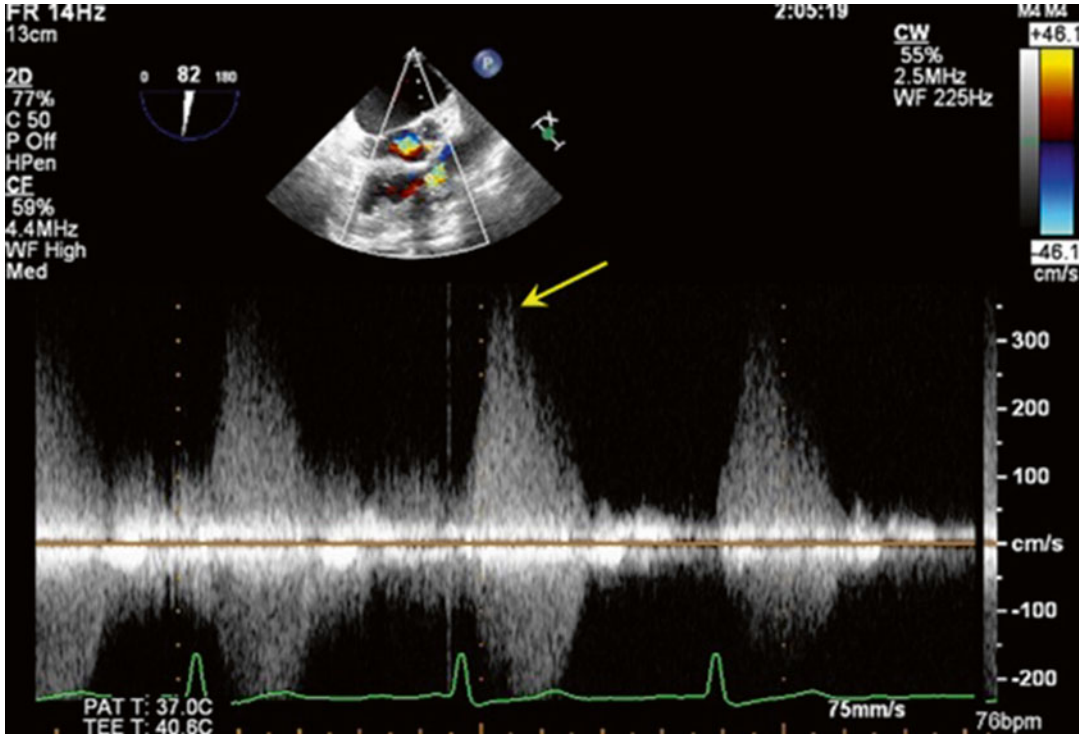

Fig. 3.20 2D TEE continuous-wave Doppler, showed high-velocity pressure (*arrow*) at RV outflow tract due to infundibular pulmonic stenosis

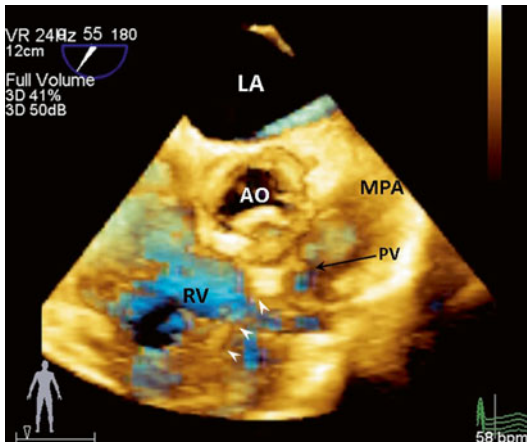

Fig. 3.21 3D TEE, short-axis view, showed infundibular pulmonic stenosis with a muscle band (*arrows*) at the junction of RV and infundibulum

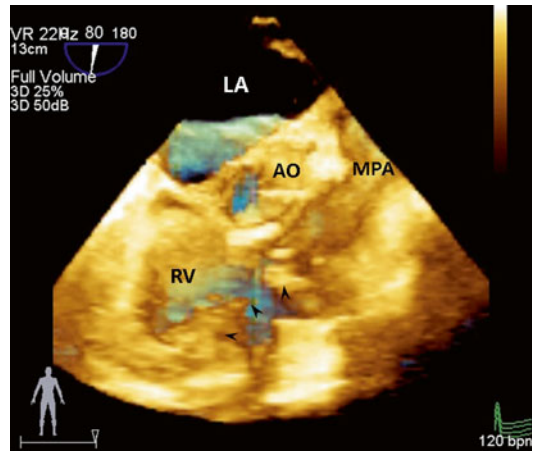

Fig. 3.22 3D TEE showed RV hypertrophy and a muscle band (*arrows*) at the junction of RV and infundibulum divided the cavity into two chambers

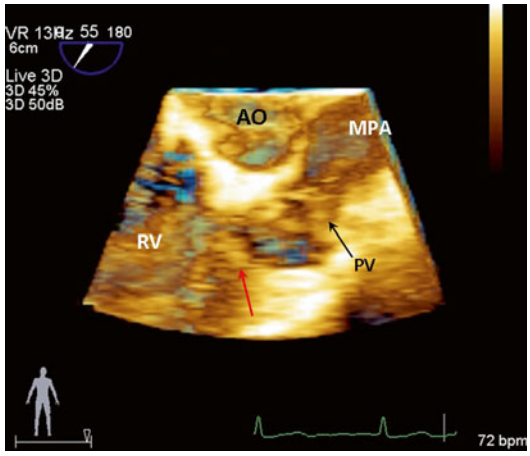

Fig. 3.23 3D TEE, zoom-mode of short- axis view, showed the stenosis position (*arrow*) at the infundibulum

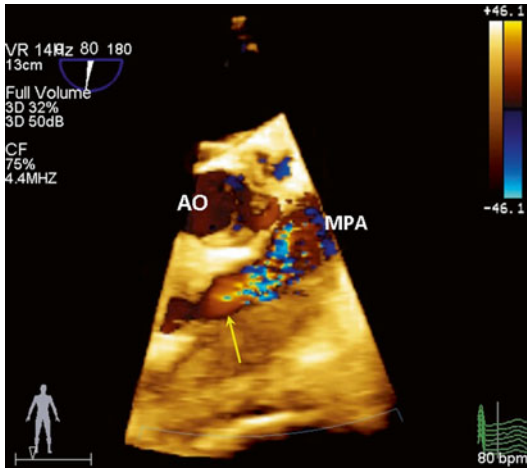

Fig. 3.24 3D TEE color Doppler showed infundibular pulmonic stenosis with accelerated flow (*arrow*) in RV outflow tract

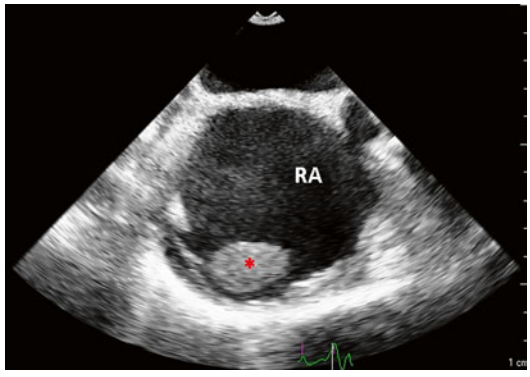

Fig. 3.25 2D TEE showed dilated RA with a thrombus (*) in it

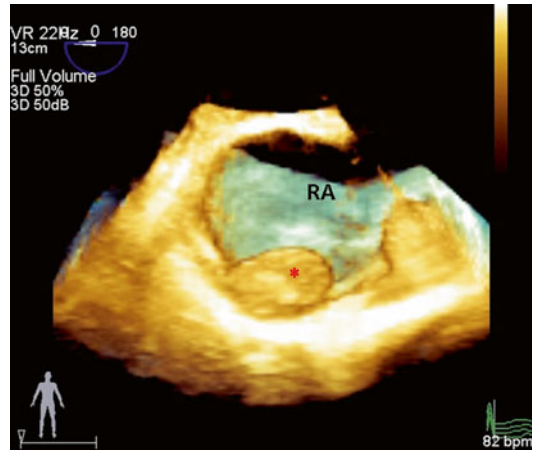

Fig. 3.26 3D TEE showed dilated RA with a thrombus (*) in it

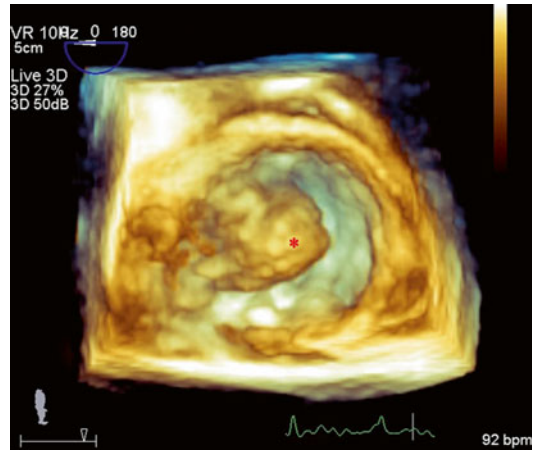

Fig. 3.27 3D TEE, view from RV perspective, showed a thrombus (*) in RA

Tips

TEE examination provides useful views to assess RV outflow tract and PV region to identify the pathology of subvalvular or supravalvular pulmonary stenosis.

3.4 Carcinoid Syndrome Having Aortic, Tricuspid and Pulmonary Replacement

A 65-year-old woman with left breast cancer and small intestine carcinoid tumor with liver metastasis status post operation 10 years ago suffered from exertional dyspnea. Auscultation: regular heart beat with a grade 3/6 pan-systolic murmur over xyphoid process and a grade 2/6 to and fro murmur over PA, left sternal border and aortic area. ECG: sinus rhythm, right axis deviation, clockwise rotation and non-specific ST-T change. Chest X ray: cardiomegaly. Cardiac catheterization: carcinoid heart disease with severe AR, TR and PR. Operation: AV, TV and PV replacement.

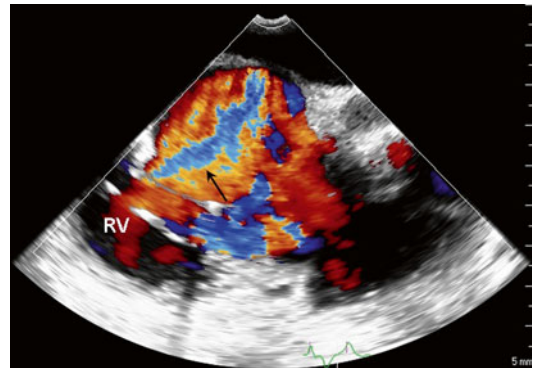

Fig. 3.30 2D TEE color Doppler showed severe TR (*arrow*) with the regurgitant jet nearly filling the RA

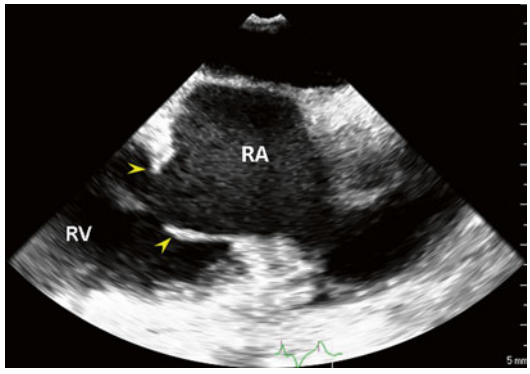

Fig. 3.28 Two-dimensional transesophageal echocardiogram (2D TEE) image, carcinoid involvement of the TV, showed retraction and thickening of the leaflets (*arrows*) that fail to coapt

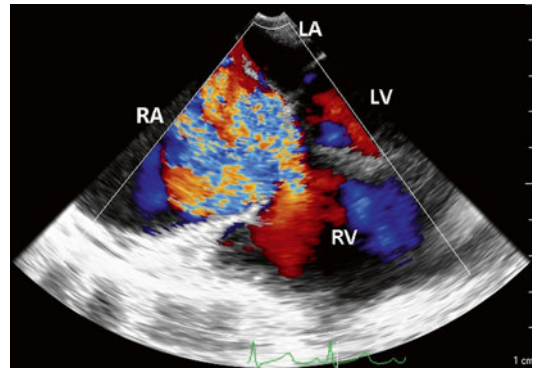

Fig. 3.31 2D TEE color Doppler, modified four-chamber view, showed severe TR through a wide regurgitant orifice

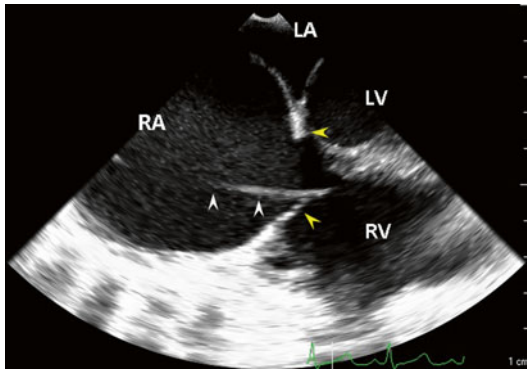

Fig. 3.29 2D TEE image, modified four-chamber view during operation, showed the central venous line across TV (*white arrows*) and carcinoid involvement of the TV with retraction and thickening of the leaflets (*yellow arrows*). Dilated RA and RV are also noted

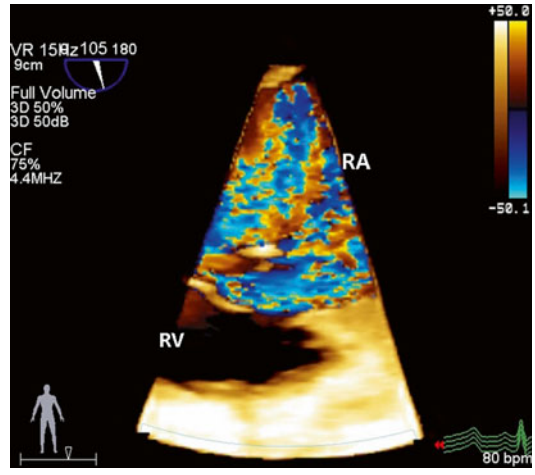

Fig. 3.32 3D TEE color Doppler showed severe TR with the regurgitant jet nearly filling the RA

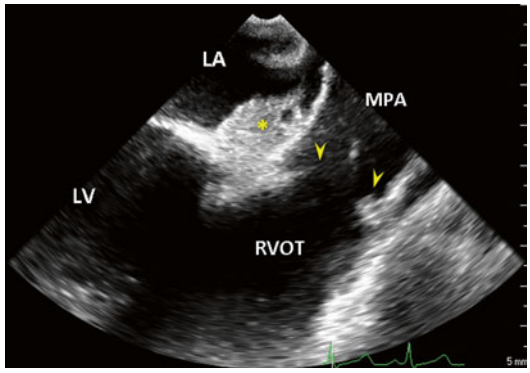

Fig. 3.33 2D TEE image showed carcinoid involvement of the PV with diminutive and rigid leaflets (*arrows*). A carcinoid neoplasm at LV outflow tract (*) was present

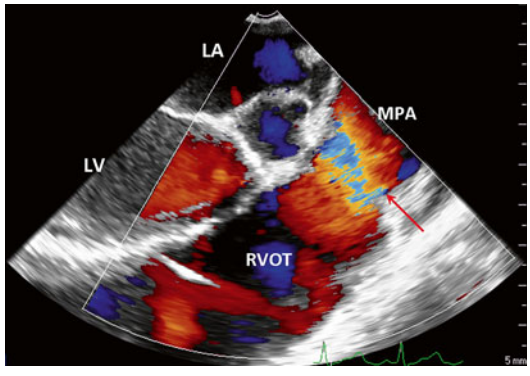

Fig. 3.34 2D TEE color Doppler showed pulmonic stenosis with high-velocity mosaic flow (*arrow*) across PV in systole

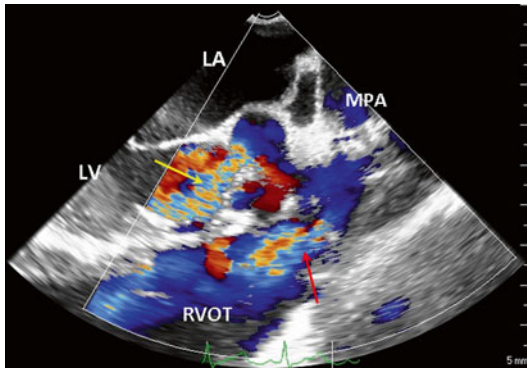

Fig. 3.35 2D TEE color Doppler showed severe PR (*red arrow*) and AR (*yellow arrow*) in diastole

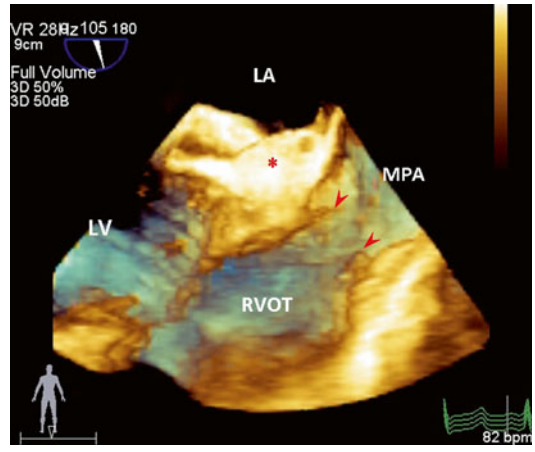

Fig. 3.36 3D TEE image showed carcinoid involvement of the PV with diminutive and rigid leaflets (*arrows*). A carcinoid neoplasm at LV outflow tract (*) was present

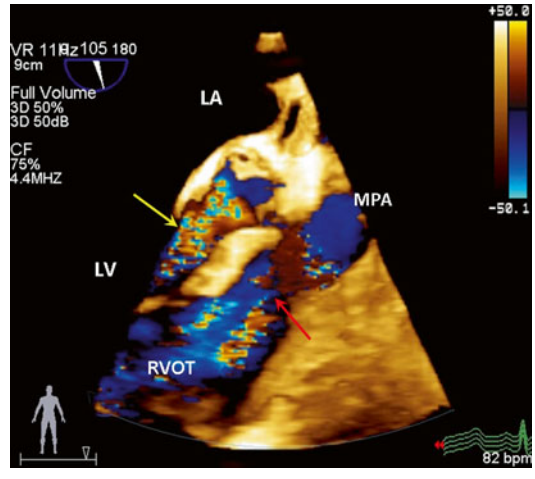

Fig. 3.37 3D TEE color Doppler showed severe PR (*red arrow*) and AR (*yellow arrow*)

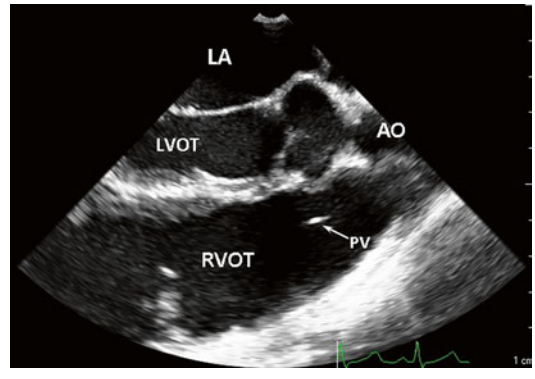

Fig. 3.38 2D TEE image, modified long-axis view, showed carcinoid involvement of the left heart with thickened AV

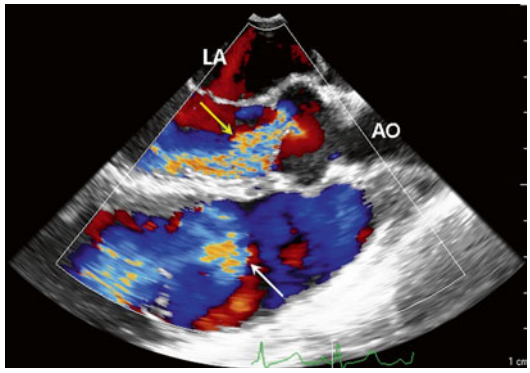

Fig. 3.39 2D TEE color Doppler, modified long-axis view, showed severe AR (*yellow arrow*) and PR (*white arrow*)

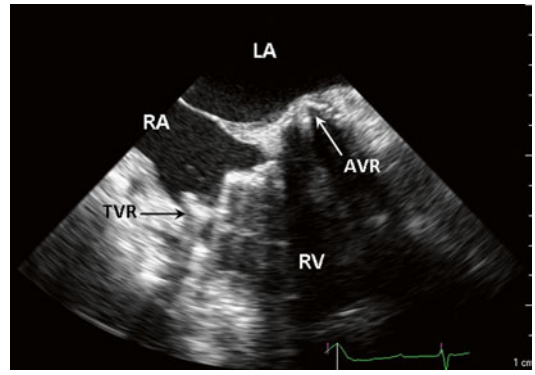

Fig. 3.42 2D TEE image, status post mechanical AV, TV and PV replacement (*AVR*, *TVR & PVR*), showed normal aortic and tricuspid prosthetic function

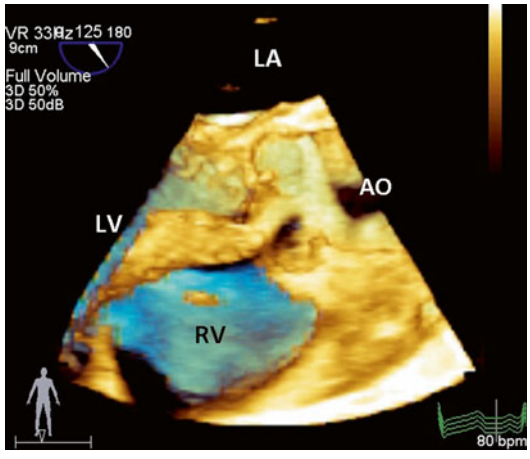

Fig. 3.40 3D TEE image, long-axis view, showed carcinoid involvement of the left heart with thickened AV

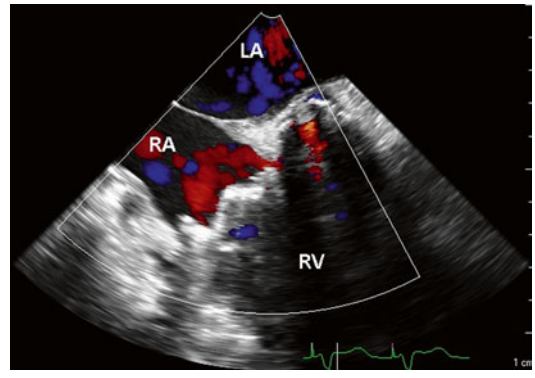

Fig. 3.43 2D TEE color Doppler, status post mechanical AV, TV and PV replacement, showed normal aortic and tricuspid prosthetic function with minimal AR and TR

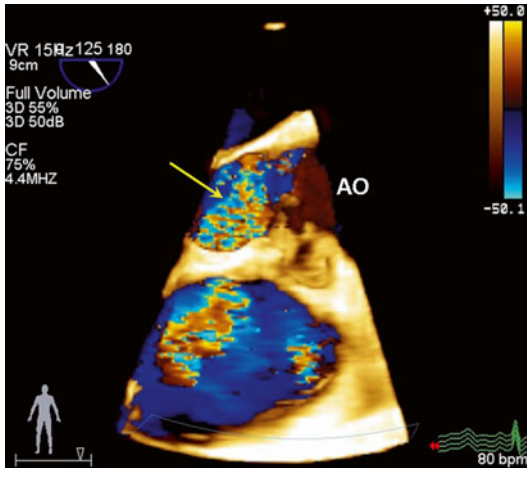

Fig. 3.41 3D TEE color Doppler, long-axis view, showed severe AR (*arrow*)

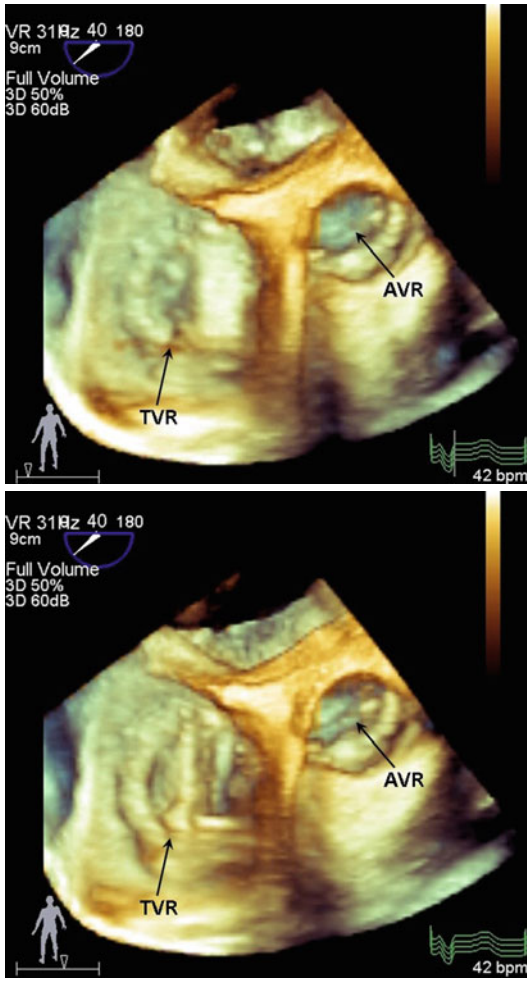

Figs. 3.44 and 3.45 3D TEE image, status post mechanical AV, TV and PV replacement (*AVR*, *TVR & PVR*), showed normal aortic and tricuspid prosthetic function with cardiac cycle

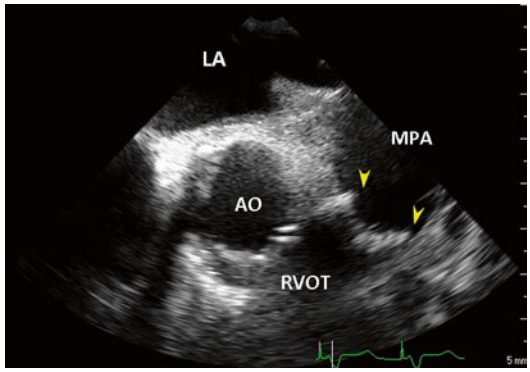

Fig. 3.46 2D TEE image, short-axis view, status post mechanical AV, TV and PV replacement, showed normal pulmonic prosthetic function (*arrows*)

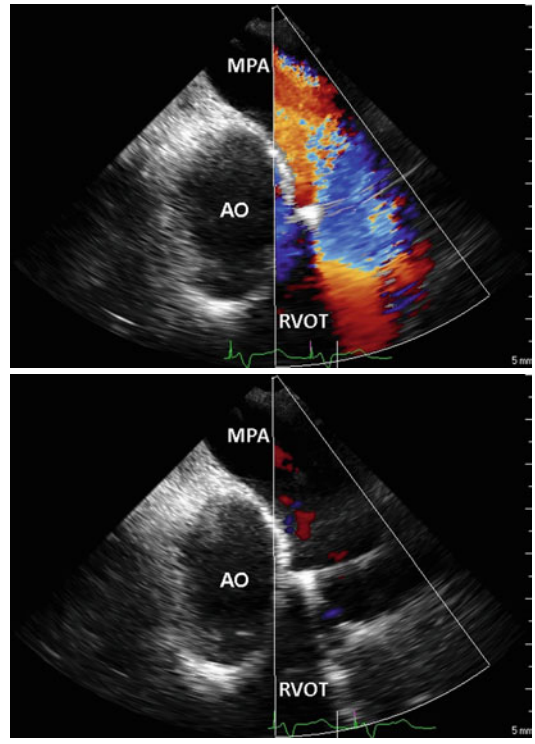

Figs. 3.47 and 3.48 2D TEE color Doppler, short-axis view, status post mechanical AV, TV and PV replacement, showed normal pulmonic prosthetic function without pulmonic stenosis or PR

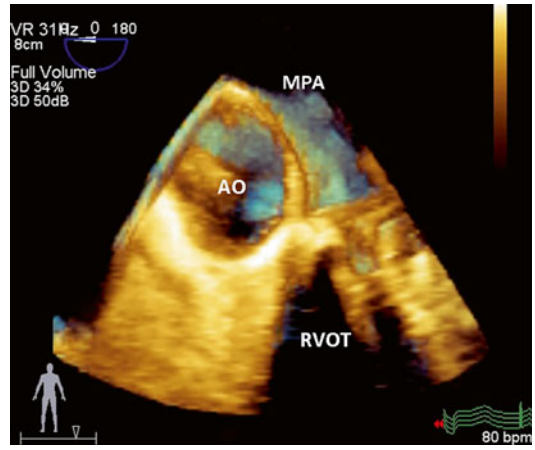

Fig. 3.49 3D TEE image, short-axis view, status post mechanical AV, TV and PV replacement, showed normal pulmonic prosthetic function

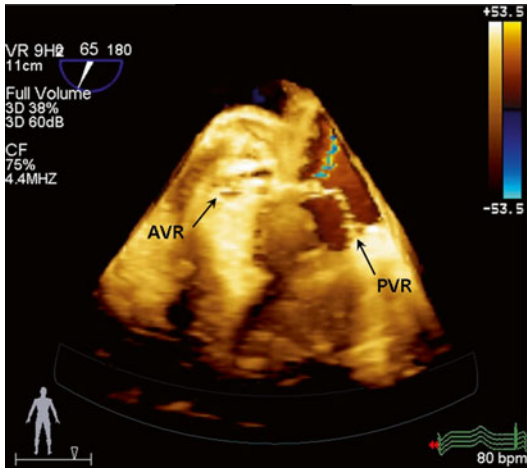

Fig. 3.50 3D TEE color Doppler, short-axis view, status post mechanical AV, TV and PV replacement (*AVR*, TVR & *PVR*), showed normal aortic and pulmonic prosthetic function

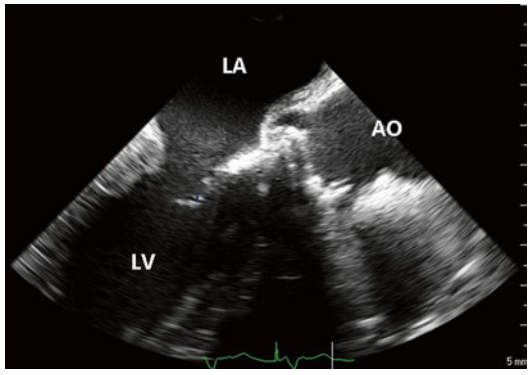

Fig. 3.51 2D TEE image, long-axis view, status post mechanical AV, TV and PV replacement, showed normal aortic prosthetic function

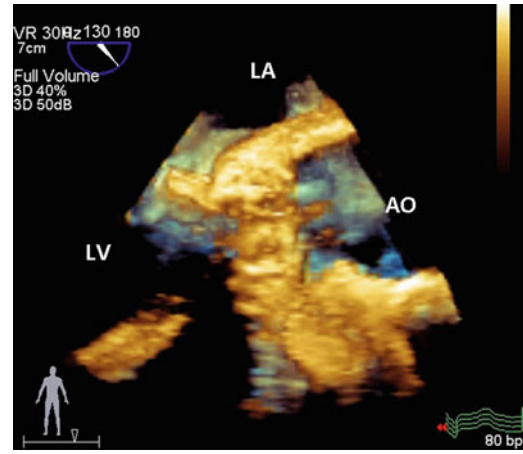

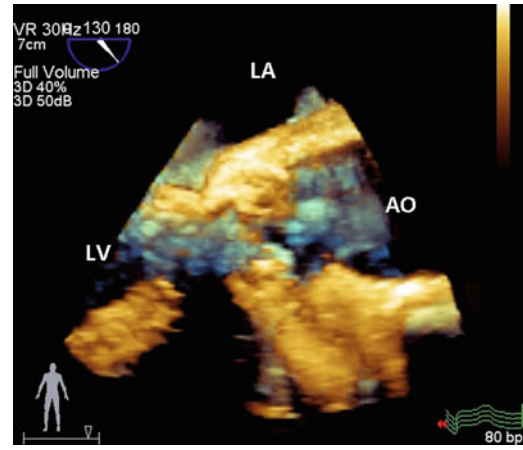

Figs. 3.52 and 3.53 3D TEE image, long-axis view, status post mechanical AV, TV and PV replacement, showed normal aortic prosthetic function

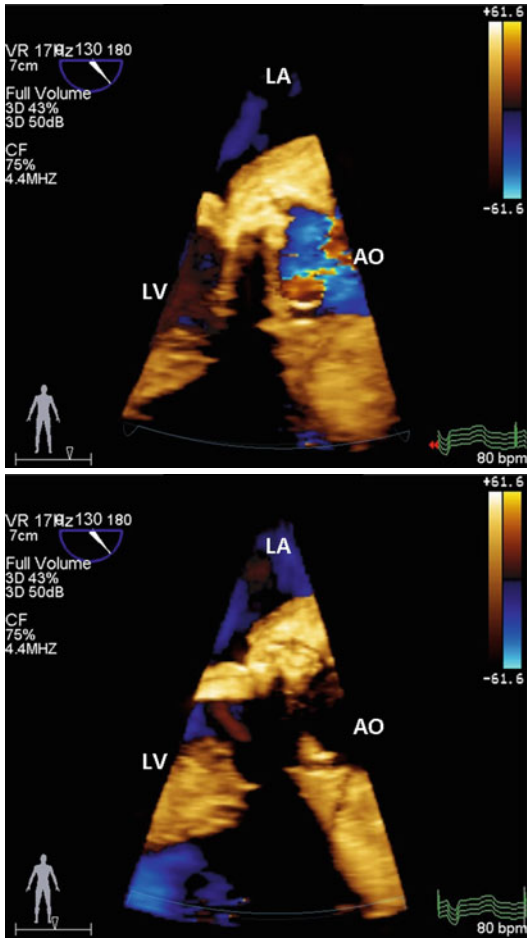

Figs. 3.54 and 3.55 3D TEE color Doppler, long-axis view, status post mechanical AV, TV and PV replacement, showed normal aortic prosthetic function

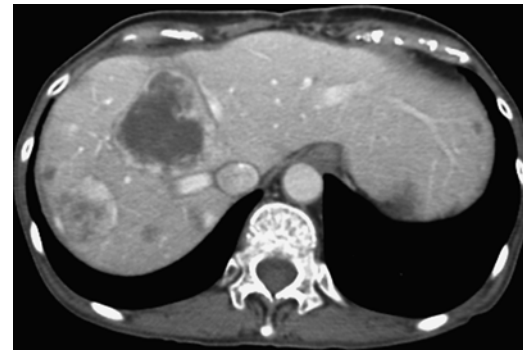

Fig. 3.56 Delay phase of contrast enhanced CT image showed multiple carcinoid metastatic lesions over liver

Tips

Carcinoid syndrome typically affects all right heart structures. If liver or lung metastasis was present, the symptoms may invade left heart.

Suggested Reading

Desai HM, Amonkar GP. Idiopathic mitral valve prolapse with tricuspid, aortic and pulmonary valve involvement: an autopsy case report. Indian J Pathol Microbiol. 2015;58(2):217–9.

Doğdu O, Baran O, Karaduman O, Yarlıoğlueş M. Subvalvular pulmonary stenosis, right ventricular hypertrophy and patent foramen ovale. Turk Kardiyol Dern Ars. 2011;39(7):626.

Elsayed M, Thind M, Nanda NC. Two- and three-dimensional transthoracic echocardiographic assessment of tricuspid valve prolapse with mid-to-late systolic tricuspid regurgitation. Echocardiography. 2015;32(6):1022–5.

Kocabay G, Sirma D, Mert M, Tigen K. Isolated tricuspid valve prolapsed: identification using two- and three- dimensionalechocardiography and transoesophageal echocardiography. Cardiovasc J Afr. 2011;22(5):272–3.

Miles LF, Leong T, McCall P, Weinberg L. Carcinoid heart disease: correlation of echocardiographic and histopathological findings. BMJ Case Rep. 2014;24:2014.

Muraru D, Badano LP, Sarais C, et al. Evaluation of tricuspid valve morphology and function by transthoracic three-dimensionalechocardiography. Curr Cardiol Rep. 2011;13(3):242–9.

Nalawadi SS, Siegel RJ, Wolin E, et al. Morphologic features of carcinoid heart disease as assessed by three-dimensional transesophageal echocardiography. Echocardiography. 2010;27(9):1098–105.

Reddy YN, Connolly HM, Ammash NM. Thrombotic obstruction of a melody valve-in-valve used for prosthetic tricuspid stenosis. World J Pediatr Congenit Heart Surg. 2015a;6(4):667–9.

Reddy G, Ahmed M, Alli O. Percutaneous valvuloplasty for severe bioprosthetic tricuspid valve stenosis in the setting of infective endocarditis. Catheter Cardiovasc Interv. 2015b;85(5):925–9.

Requilé A, Van De Bruaene A, Reenaers V, Dendale P. A case of carcinoid heart disease with desaturation and no liver metastases. Echocardiography. 2014;31(10):E307–9.

Roberts CC, Parmar RJ, Grayburn PA, et al. Clues to diagnosing carcinoid heart disease as the cause of isolated right-sided heart failure. Am J Cardiol. 2014;114(10):1623–6.

Tefera E, Bermudez-Cañete R, Rubio L. Discrete subpulmonic membrane in association with isolated severe pulmonary valvar stenosis. BMC Cardiovasc Disord. 2013;13:43.

Waller AH, Chatzizisis YS, Moslehi JJ, et al. Real-time three-dimensional transesophageal echocardiography enables preoperative pulmonary valvulopathy assessment. Eur Heart J Cardiovasc Imaging. 2014;15(6):713.

Yousif M, Elhassan NB, Ali SK, Ahmed Y. Isolated subpulmonic fibrous ring, mirror-image dextrocardia and situs solitus in a young lady unreported and a near miss. Interact Cardiovasc Thorac Surg. 2013;17(6):1043–4.

Prosthetic Valves

4

Abstract

Prosthetic valves are discussed in this chapter. Cases of paravalvular leakage, mitral prosthesis dysfunction having transcatheter valve in valve replacement, and aortic restenosis having transcatheter AV implantation are involved.

Bioprosthetic valve may be complicated by dehiscence or tissue degeneration. 3D TEE examination provides valuable information about the exact anatomic characteristics for further operative treatment.

4.1 Paravalvlular Leakage of Mitral Prosthesis

A 56-year-old woman status post MV replacement and TV repair 14 years ago suffered from severe shortness of breath and orthopnea. Auscultation: irregular heart beat with a grade 2 systolic murmur over apex. ECG: atrial fibrillation with moderate ventricular response, myocardial ischemia. Chest X ray: cardiomegaly and right pleural effusion. Coronary CT angiography: cardiomegaly and patency of three coronary arteries. Operation: redo MV replacement and TV repair.

Electronic supplementary material The online version of this chapter (doi:10.1007/978-981-10-0587-9_4) contains supplementary material, which is available to authorized users.

W.-H. Yin, M.-C. Hsiung, *Atlas of Perioperative 3D Transesophageal Echocardiography*,
DOI 10.1007/978-981-10-0587-9_4

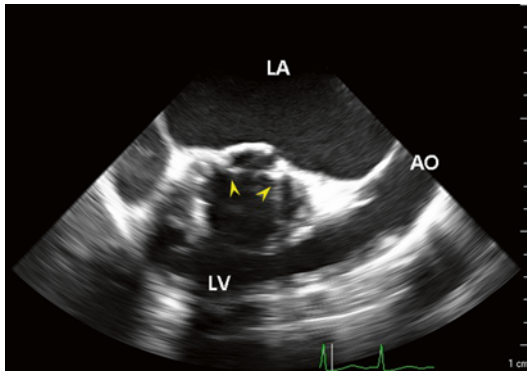

Fig. 4.1 Two-dimensional transesophageal echocardiography (2D TEE) image, long-axis view, status post mechanical MV replacement (*arrows*), showed dilated LA

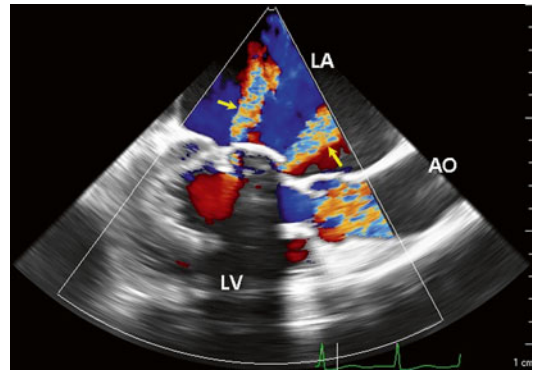

Fig. 4.2 2D TEE color Doppler, long-axis view, status post mechanical MV replacement, showed severe mitral paravalvular leakage (*arrows*)

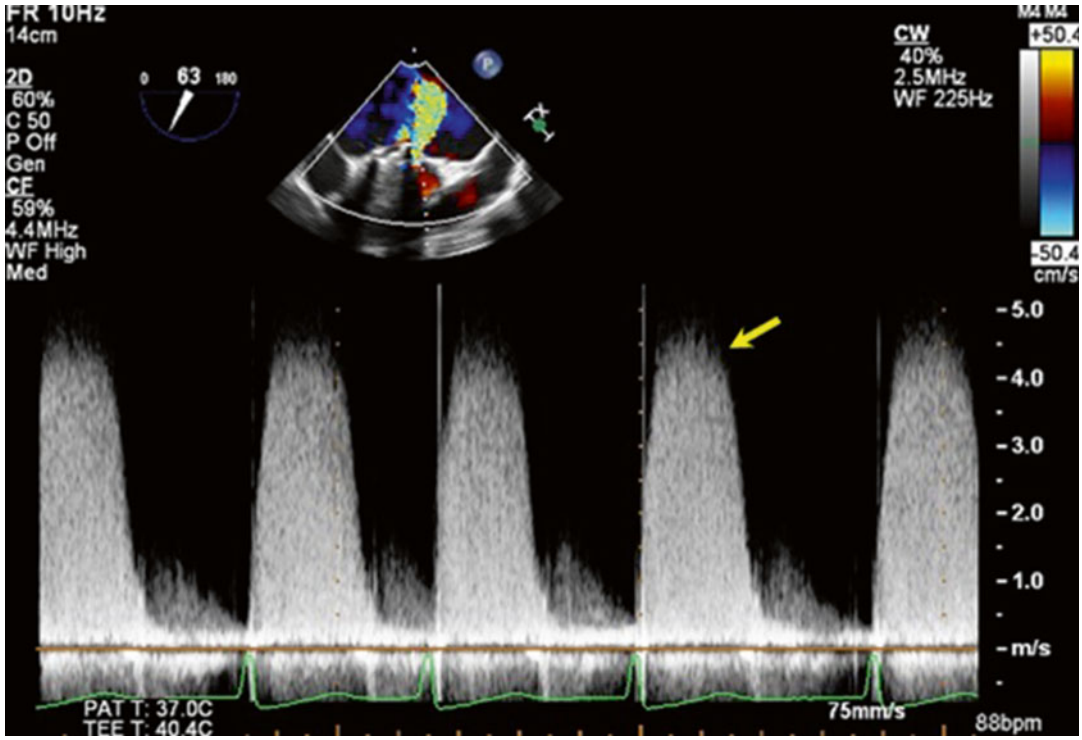

Fig. 4.3 2D TEE continuous-wave Doppler, status post MV replacement, high-pressure-gradient mitral paravalvular leakage (*arrow*) was present

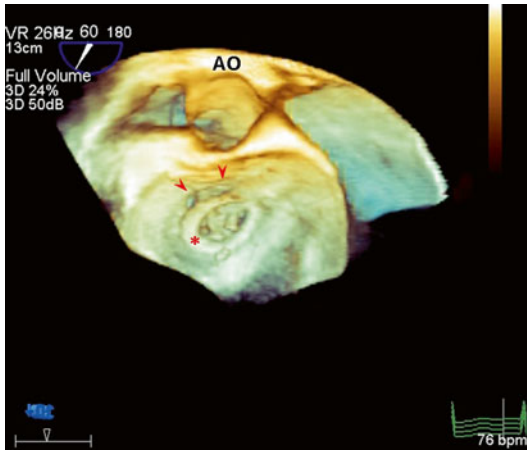

Fig. 4.4 3D TEE image, en face view, status post MV replacement, showed a tear (*arrows*) is around the mechanical prosthetic mitral annulus (*) from 9 o'clock position to 12 o'clock position

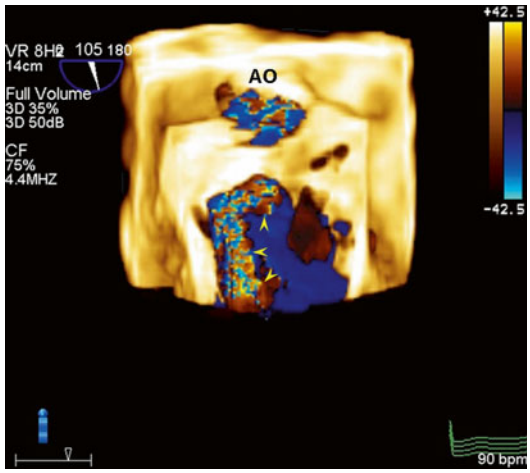

Fig. 4.5 3D TEE color Doppler, en face view, status post MV replacement, showed severe mitral paravalvular leakage jet (*arrows*)

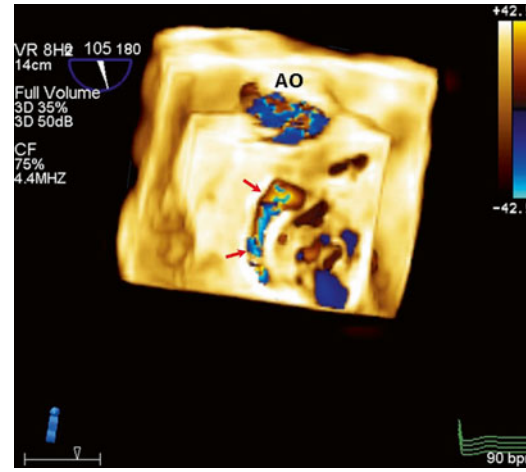

Fig. 4.6 3D TEE color Doppler image, en face view, after cropping down toward MV, showed the origin of the mitral paravalvular leakage (*arrows*)

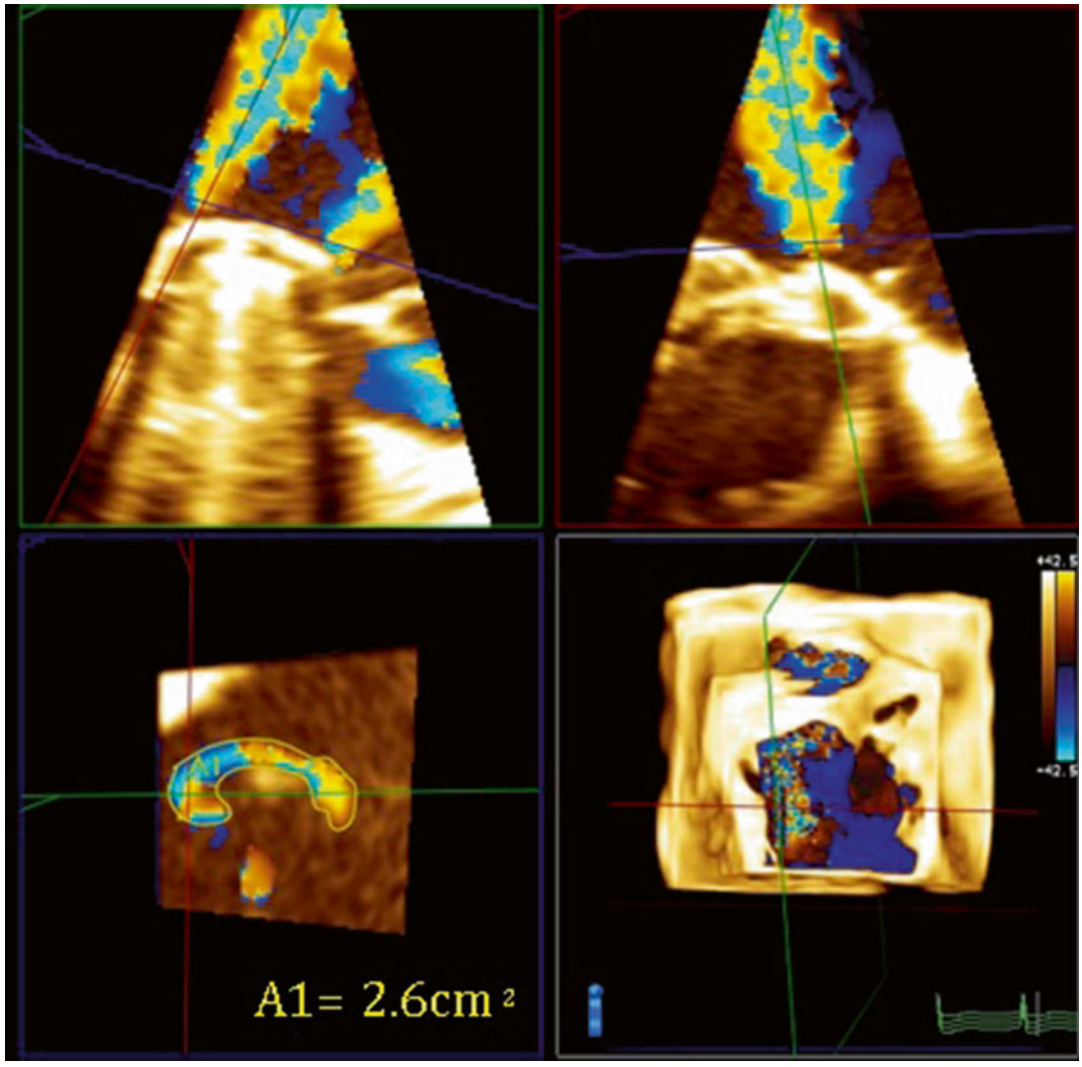

Fig. 4.7 Multi-planar reconstruction (MPR) of 3D TEE image, showed the origin of the paravalvular leakage is a crescent-shape orifice which area is 2.6 cm^2

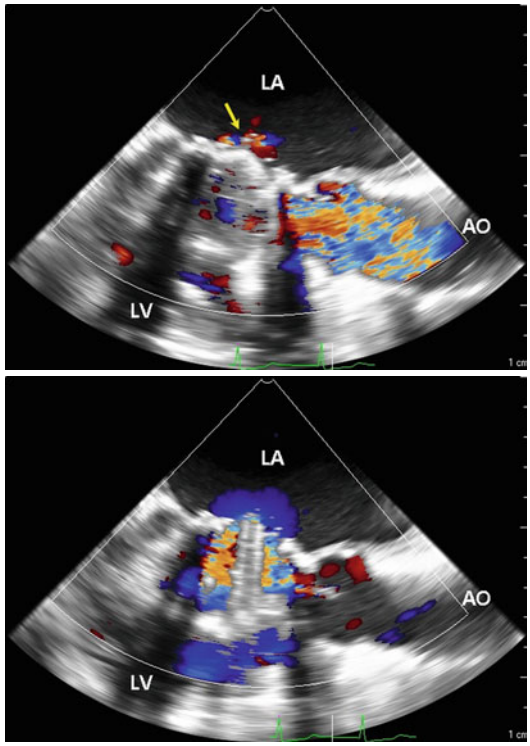

Figs. 4.8 and 4.9 2D TEE color Doppler, long-axis view, status post redo MV replacement with mechanical valve, showed mild MR (*arrow*) in systole (*above*) and normal mitral inflow in diastole (*below*)

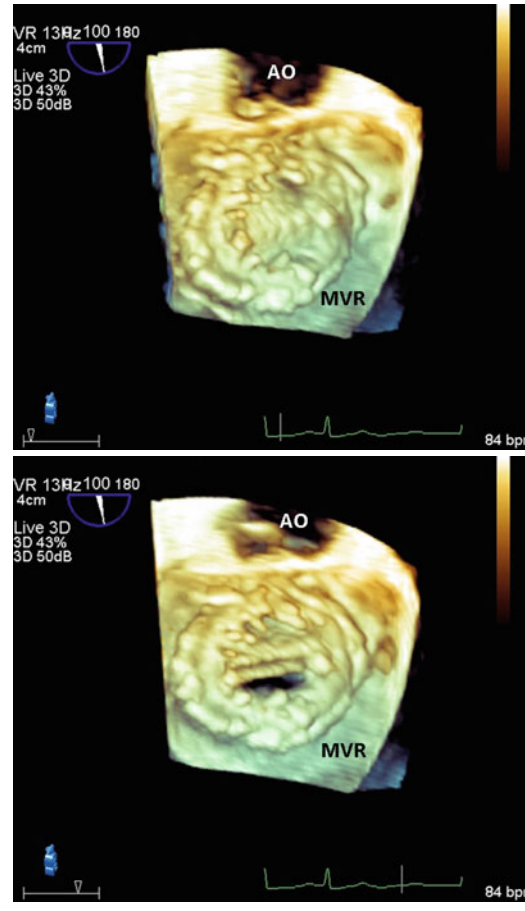

Figs. 4.10 and 4.11 3D TEE image, en face view, status post redo MV replacement (*MVR*) with mechanical valve, showed normal prosthesis function with cardiac cycle

Tips

MV replacement may be complicated by post-operative dehiscence of the valve or annuloplasty ring resulting in clinically significant MR or hemolysis. Real time 3D TEE provides valuable information about the exact anatomic characteristics of the dehiscence.

4.2 Mitral Prosthesis Dysfunction Having Valve in Valve Replacement

A 63-year-old woman had CABGx1 (LAD) and tissue MV replacement 2 years ago. But she suffered dyspnea on exertion and exercise intolerance recurrently. Auscultation: regular heart beat with a systolic murmur over apex and axillary area. ECG: 1 AV block, ST depression which possible indicated myocardial ischemia. Chest X ray: cardiomegaly. Cardiac catheterization: severe MR. Treatment: transcatheter mitral valve in valve replacement.

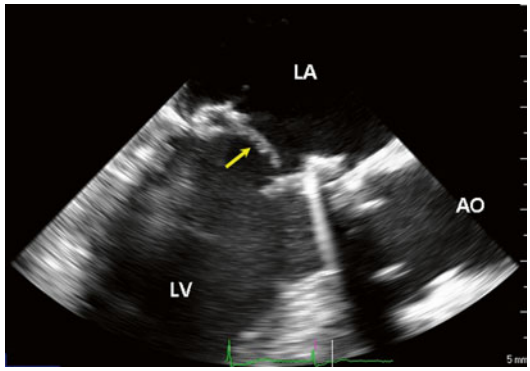

Fig. 4.12 Two-dimensional transesophageal echocardiography (2D TEE) image, long-axis view, status post tissue MV replacement, showed mitral prosthesis dysfunction (*arrow*) and dilated LA

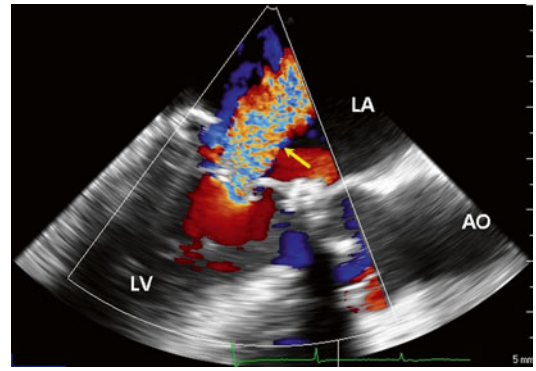

Fig. 4.13 2D TEE color Doppler, long-axis view, status post tissue MV replacement, showed severe MR (*arrow*) due to mitral prosthesis dysfunction

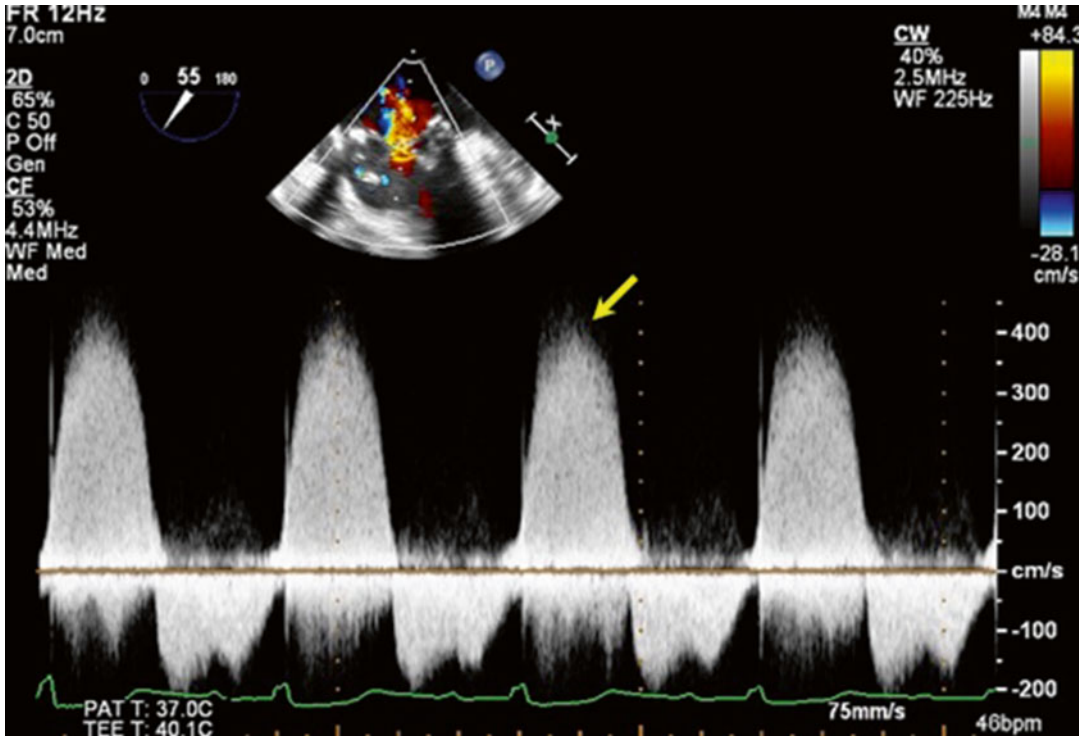

Fig. 4.14 2D TEE continuous-wave Doppler, status post tissue MV replacement, high pressure gradient MR (*arrow*) was present

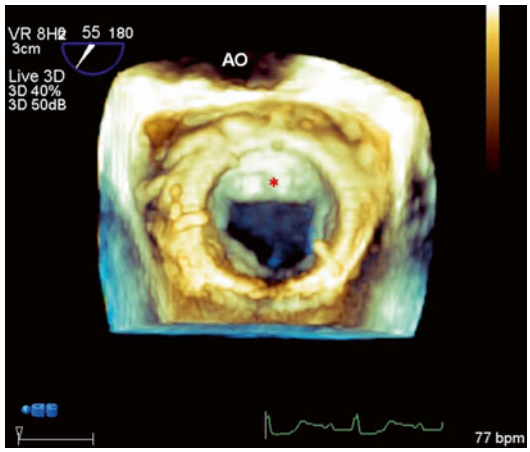

Fig. 4.15 3D TEE image, en face view, status post tissue MV replacement, showed one of the leaflets is fixed (*)

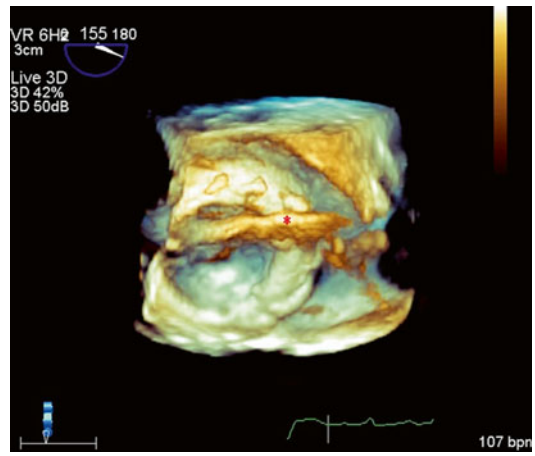

Fig. 4.17 3D TEE, zoom view, during the transcatheter mitral valve in valve replacement, showed the guiding catheter (*) crossed MV

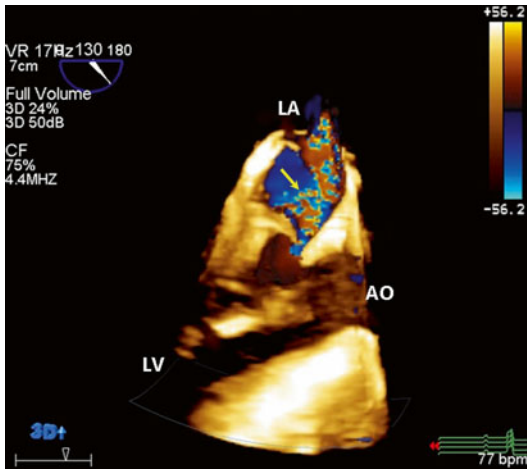

Fig. 4.16 3D TEE color Doppler, long-axis view, status post tissue MV replacement, showed severe MR (*arrow*) due to mitral prosthesis dysfunction

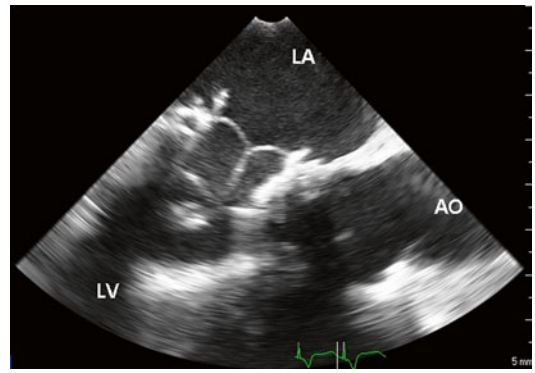

Fig. 4.18 2D TEE image, long-axis view, status post re-do tissue mitral valve in valve replacement, showed good mitral prosthesis function

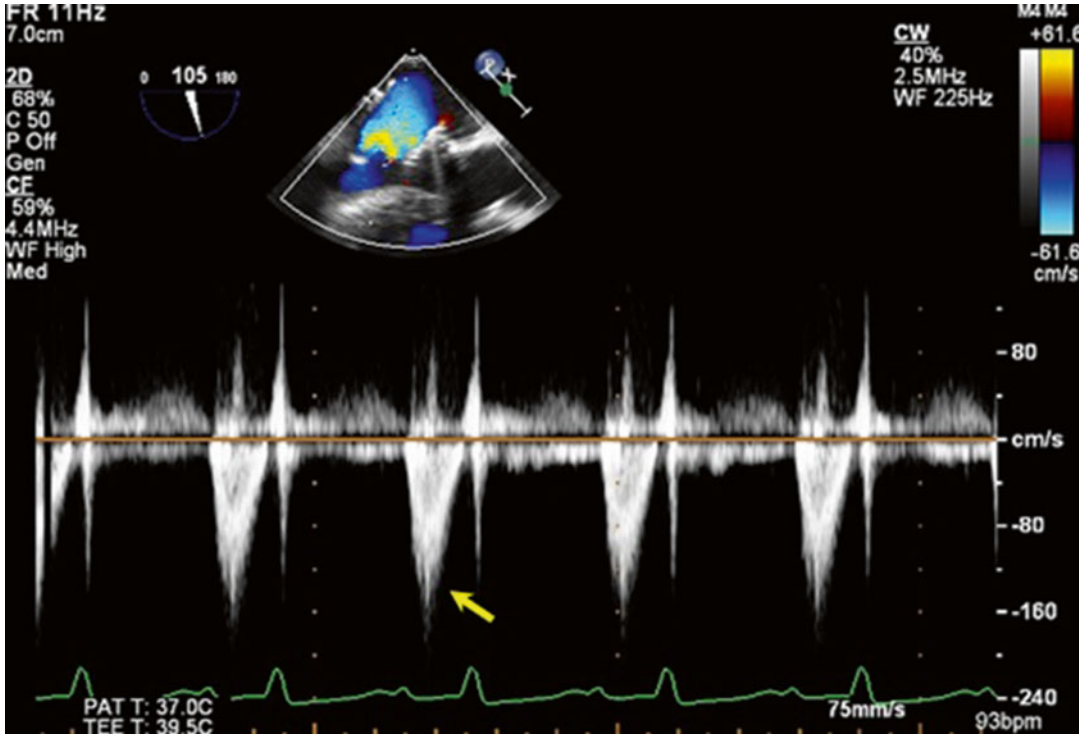

Fig. 4.19 2D TEE continuous-wave Doppler, status post mitral valve in valve replacement, showed normal mitral inflow pattern (*arrow*)

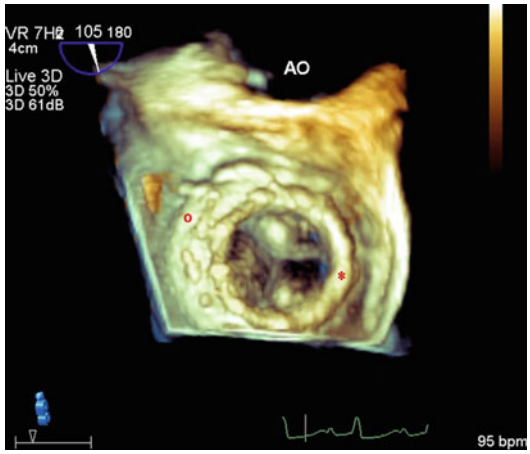

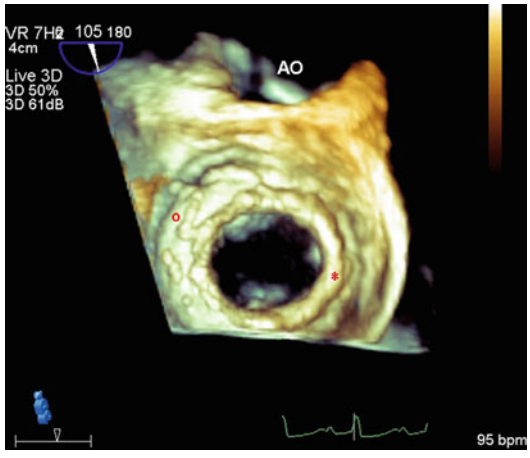

Figs. 4.20 and 4.21 3D TEE image, en face view, status post mitral valve in valve replacement, showed the new prosthetic mitral annulus (*) is within the old one (**o**), normal mitral prosthesis function with cardiac cycle

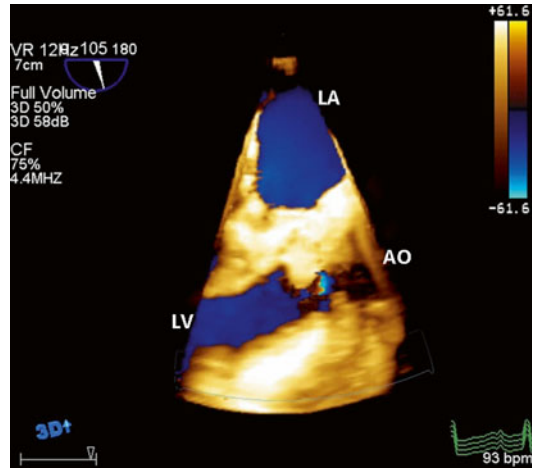

Fig. 4.22 3D TEE color Doppler, status post mitral valve in valve replacement, showed smooth mitral inflow

Tips

Patients need MV reoperations due to prosthetic dysfunction is a high-risk population. Transcatheter techniques may reduce the morbidity and mortality.

4.3 Aortic Prosthetic Stenosis Having Transcatheter Aortic Valve Implantation

A 61-year-old woman had bovine AV and MV replacement, TV repair and atrial fibrillation ablation 4 years ago. She suffered from exertional dyspnea recently. Auscultation: regular heart beat with a grade 2/6 systolic murmur over apex. ECG: atrial fibrillation with moderate ventricular response and right bundle branch block. Chest X ray: cardiomegaly. Contrast-enhanced chest CT: marked cardiomegaly, atherosclerosis of aorta and enlarged both thyroid glands. Treatment: transcatheter aortic valve implantation (TAVI) and temporal pacemaker implantation.

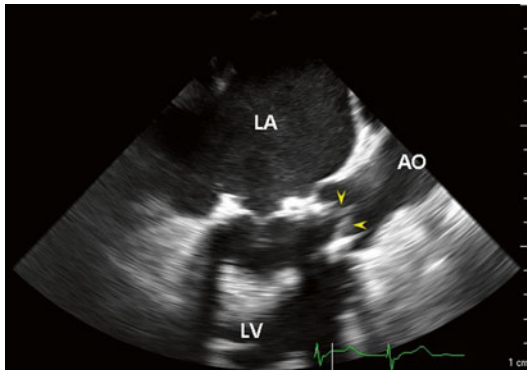

Fig. 4.23 Two-dimensional transesophageal echocardiography (2D TEE) image, long-axis view, status post tissue aortic and mitral valve replacement, showed aortic prosthesis failure with aortic stenosis (*arrows*) and dilated LA

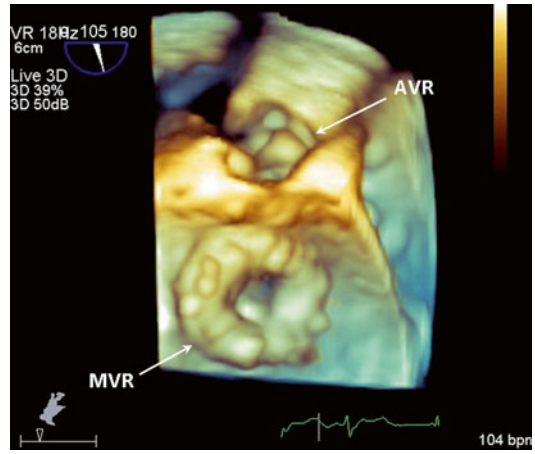

Fig. 4.25 3D TEE image, en face view, status post tissue aortic and mitral valve replacement, showed aortic prosthetic stenosis

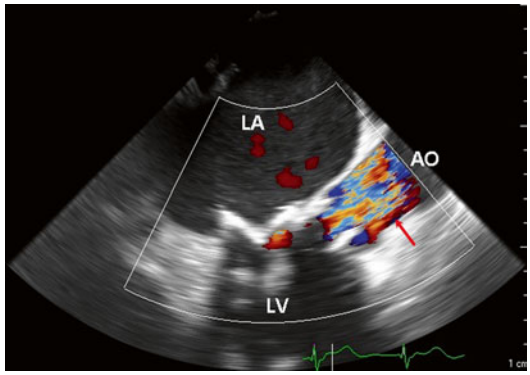

Fig. 4.24 2D TEE color Doppler, long-axis view, status post tissue aortic and mitral valve replacement, showed flow acceleration (*arrow*) across the aortic prosthesis

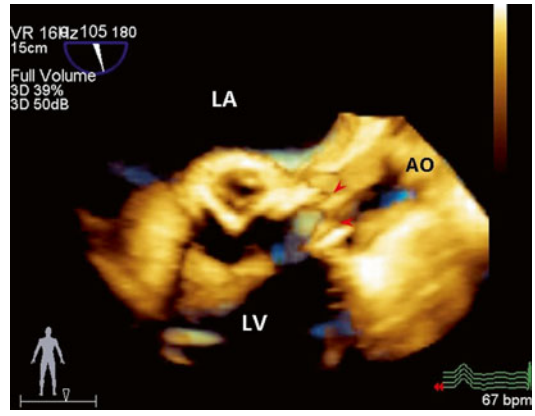

Fig. 4.26 3D TEE image, long-axis view, status post tissue aortic and mitral valve replacement, showed aortic prosthetic valve stenosis plus stent creep (*arrows*)

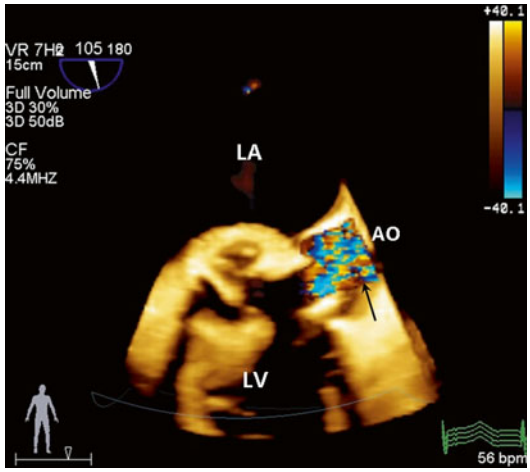

Fig. 4.27 3D TEE color Doppler, long-axis view, status post tissue aortic and mitral valve replacement, showed flow acceleration (*arrow*) across the aortic prosthesis

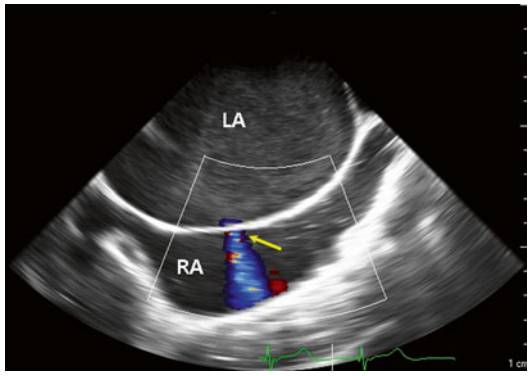

Fig. 4.28 2D TEE color Doppler showed a small PFO (*arrow*) with left to right shunt

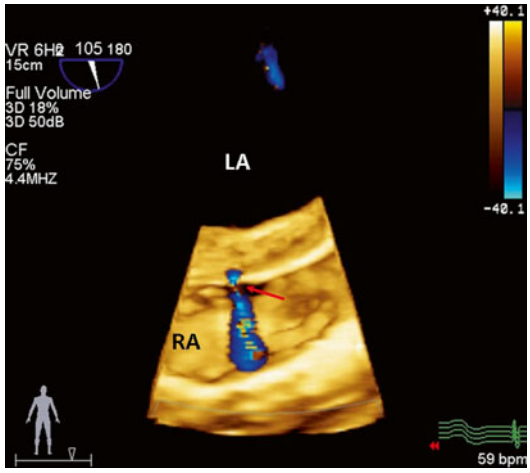

Fig. 4.29 3D TEE color Doppler showed a small PFO (*arrow*) with left to right shunt

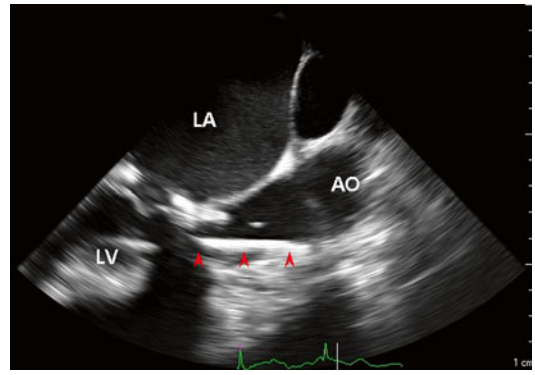

Fig. 4.30 2D TEE image, long-axis view, during the TAVI procedure, showed the guiding catheter (*arrows*) crossed the stenosis aortic prosthesis

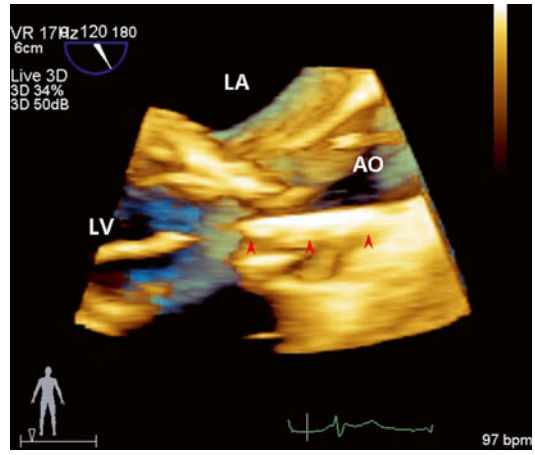

Fig. 4.31 3D TEE image, long-axis view, during the TAVI procedure, showed the guiding catheter (*arrows*) crossed the stenosis aortic prosthesis

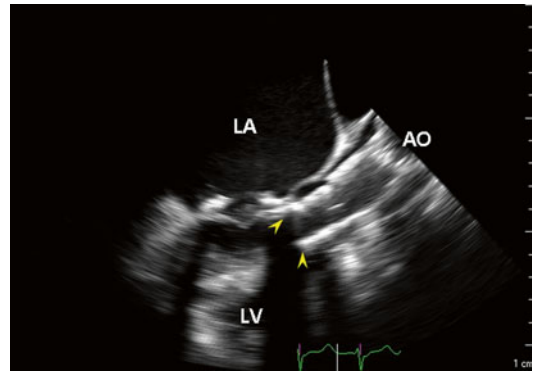

Fig. 4.32 2D TEE image, long-axis view, status post TAVI, showed the core valve (*arrows*) was opened to replace the stenosis one

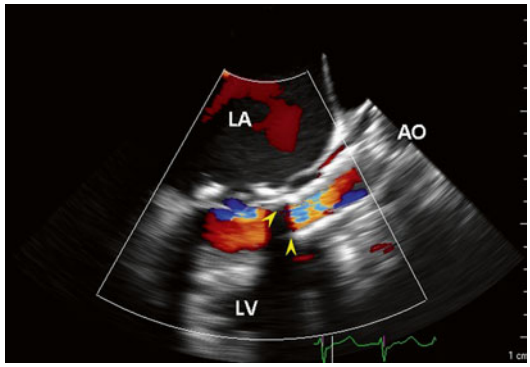

Fig. 4.33 2D TEE color Doppler, long- axis view, status post TAVI, showed normal flow within the core valve (*arrows*)

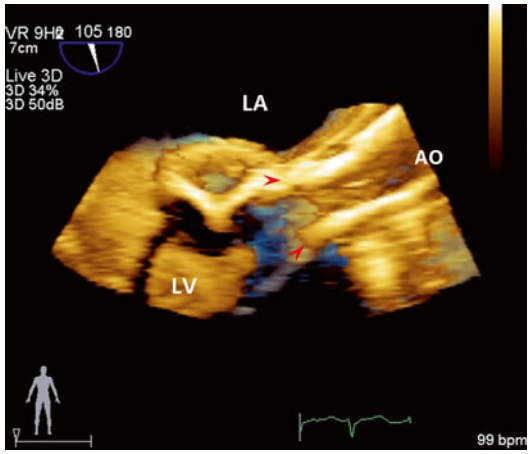

Fig. 4.34 3D TEE image, long-axis view, status post TAVI, showed the core valve (*arrows*) in ascending aorta

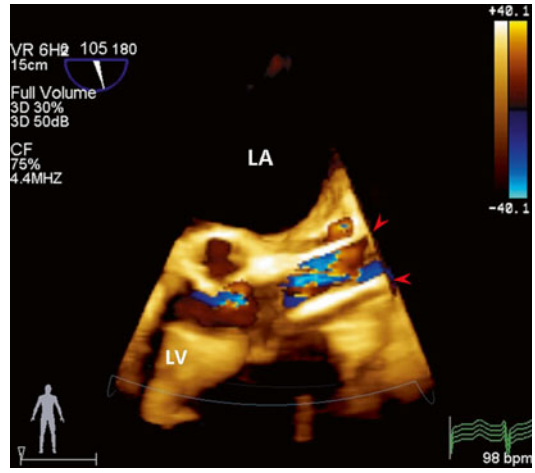

Fig. 4.35 3D TEE color Doppler, long- axis view, status post TAVI, showed normal flow within the core valve (*arrows*)

Tips

Failure of a bioprosthetic valve usually is a result of progressive tissue degeneration or stent creep. Fibrocalcific changes of the leaflets induce restrictive opening as prosthetic valve stenosis. Transcatheter valve in valve implantation is a reproducible option for the management of bioprothetic valve failure.

Suggested Reading

Attizzani GF, Ohno Y, Latib A, et al. Transcatheter aortic valve implantation under angiographic guidance with and without adjunctive transesophageal echocardiography. Am J Cardiol. 2015;116(4):604–11.

Bapat V, Asrress KN. Transcatheter valve-in-valve implantation for failing prosthetic valves. Eur Intervent. 2014;10(8):900–2.

Bruschi G, De Marco F, Botta L, et al. Right anterior minithoracotomy direct aortic self-expanding transcatheter aortic valve implantation: a single center experience. Int J Cardiol. 2015;181:437–42.

Gürsoy OM, Astarcıoğlu MA, Gökdeniz T, et al. Severe mitral paravalvular leakage: echo-morphologic description of 47 patients from real-time three-dimensional transesophageal echocardiography perspective. Anadolu Kardiyol Derg. 2013;13(7):633–40.

Oyama S, Ohuchi S, Okubo T, Kumagai K. Usefulness of echocardiography for detecting prosthesic valve dysfunction; report of a case. Kyobu Geka. 2014;67(11):1025–8. Japanese.

Ozkan M, Gürsoy OM, Astarcıoğlu MA, et al. Percutaneous closure of paravalvular mitral regurgitation with vascular plug III under the guidance of real-time three-dimensional transesophageal echocardiography. Turk Kardiyol Dern Ars. 2012;40(7):632–41.

Diseases of the Aorta

5

Abstract

Abnormalities of the aorta are details in this chapter, which contains aortic root fistula, ruptured sinus of Valsalva, and variants of aortic dissection.

The aorta begins at the AV and ends at the bifurcation in abdomen. It can be divided into the aortic root, ascending aorta, aortic arch, descending thoracic aorta, and abdominal aorta. In an aortic dissection patient, a CT angiography must be arranged to collaborate with the TEE assessment to confirm the range of the dissection.

5.1 Dilated Aortic Root Having David's Operation

A 62-year-old man has a longstanding history of gout and hypertension. He suffered orthopnea, progressive shortness of breath and palpitation. Auscultation: regular heart beat with a grade 3 systolic murmur over right sternal border. ECG: sinus rhythm, first degree AV block and early repolarization. Cardiac catheterization: two-vessel coronary artery disease and severe AR. Coronary CT angiography: coronary artery calcium score is 2091, ascending aorta dilatation and three-vessel coronary artery disease with obstructive atherosclerosis. Operation: David's operation, reconstruction of ascending aorta and CABG x2 (LAD, RCA).

Electronic supplementary material The online version of this chapter (doi:10.1007/978-981-10-0587-9_5) contains supplementary material, which is available to authorized users.

W.-H. Yin, M.-C. Hsiung, *Atlas of Perioperative 3D Transesophageal Echocardiography*,
DOI 10.1007/978-981-10-0587-9_5

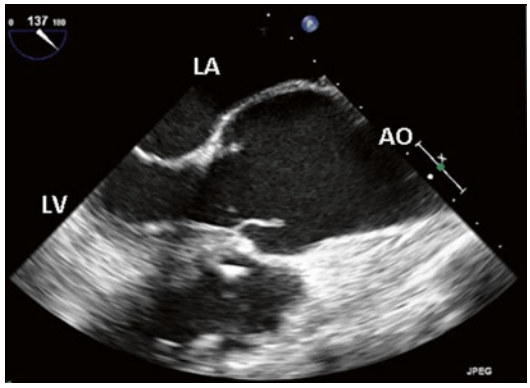

Fig. 5.1 Two-dimensional transesophageal echocardiography (2D TEE) image, long-axis view, showed dilated sinus of Valsalva and ascending aorta

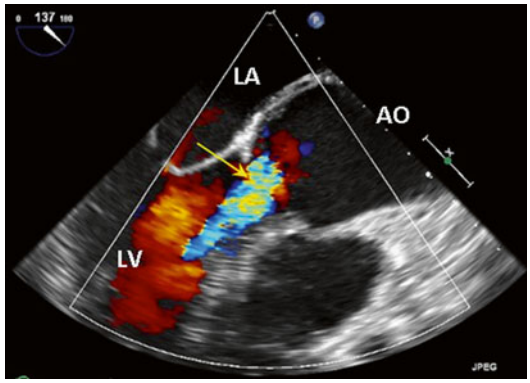

Fig. 5.2 2D TEE color Doppler, long-axis view, showed severe AR (*arrow*) due to sinus of Valsalva dilation

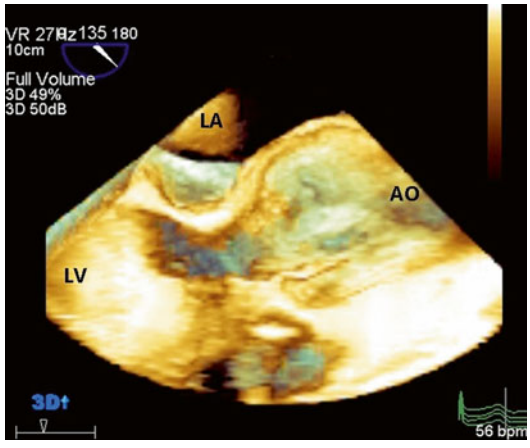

Fig. 5.3 3D TEE image, long-axis view, showed dilated sinus of Valsalva and ascending aorta

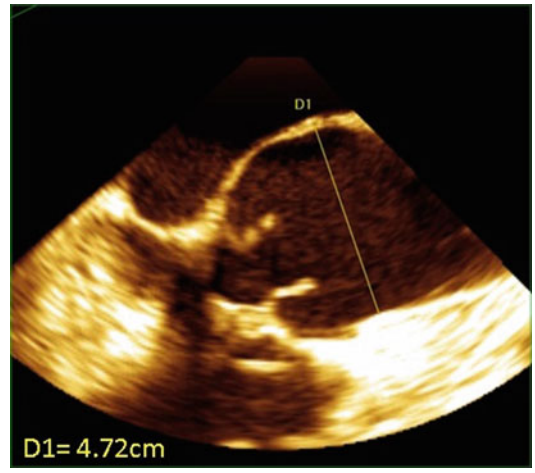

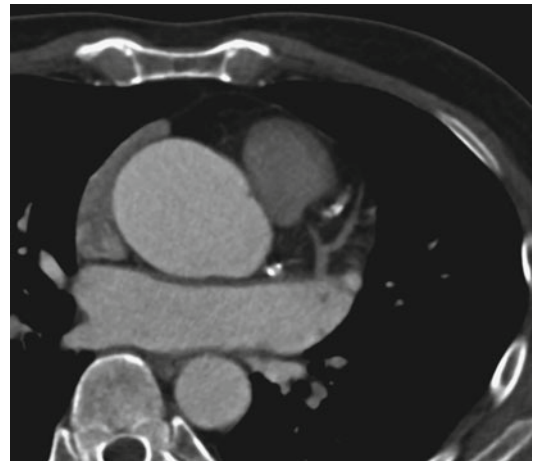

Figs. 5.4 and 5.5 Multi-planar reconstruction (MPR) of 3D TEE image (*above*) showed the ascending aorta dilated to 4.72 cm; contrast-enhanced CT image (*below*) also showed the dilated ascending aorta

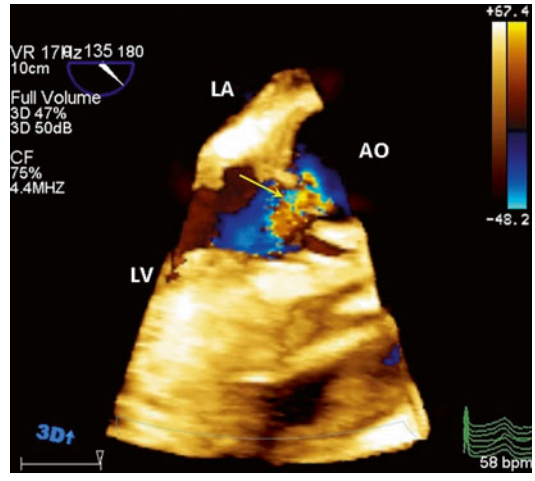

Fig. 5.6 3D TEE color Doppler, long-axis view, showed severe AR (*arrow*) due to sinus of valsalva dilation

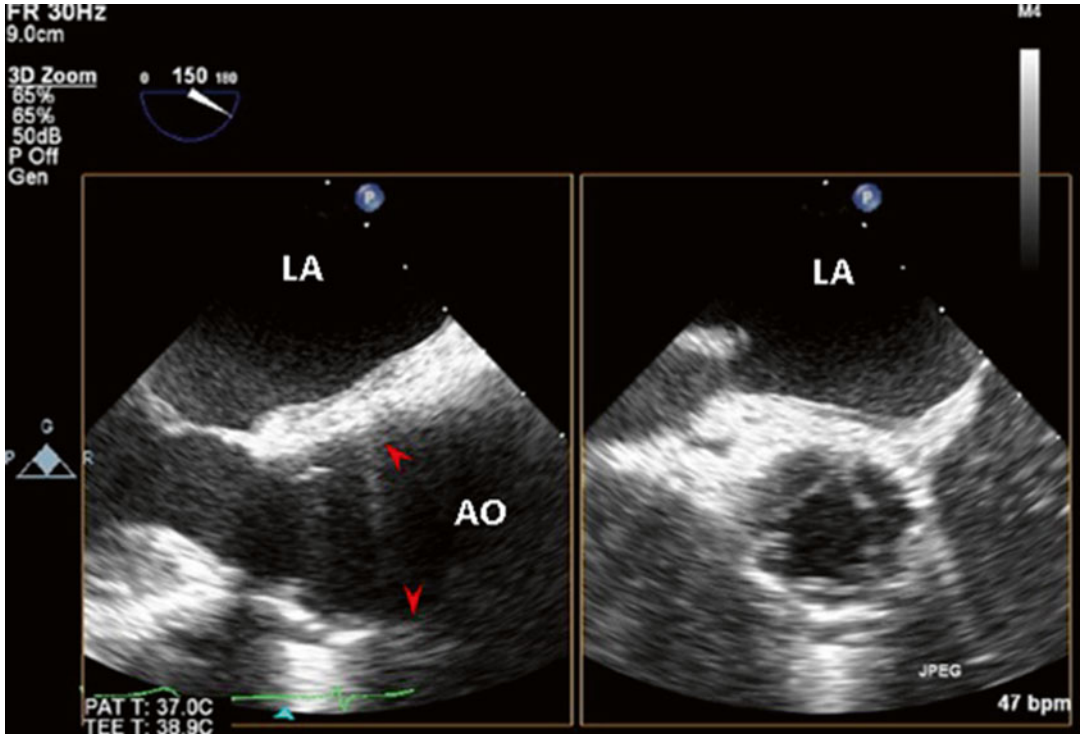

Fig. 5.7 2D TEE, x-plane view, status post David's operation, showed the artificial graft (*arrows*)

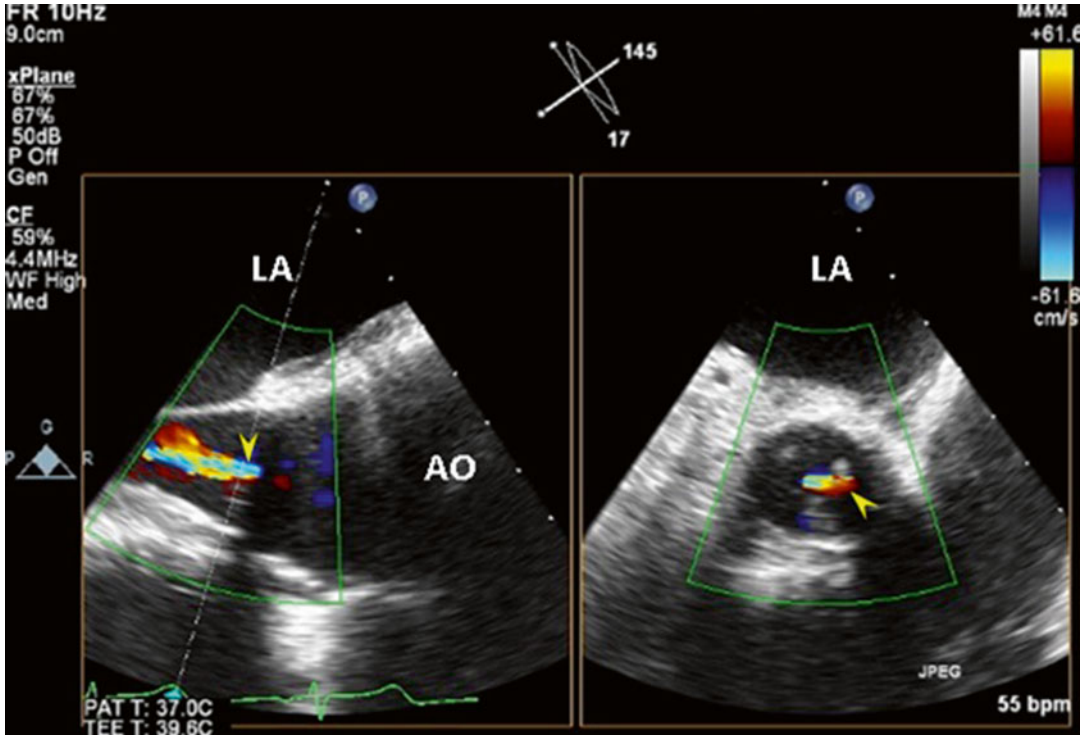

Fig. 5.8 2D TEE color Doppler, x-plane view, status post David's operation, showed mild AR (*arrows*)

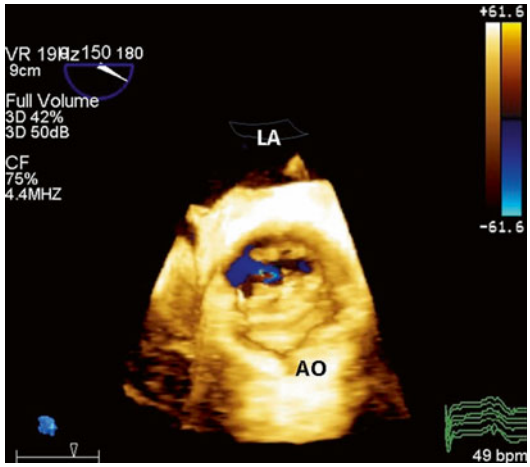

Fig. 5.9 3D TEE color Doppler, en face view of AV, status post David's operation, showed mild AR

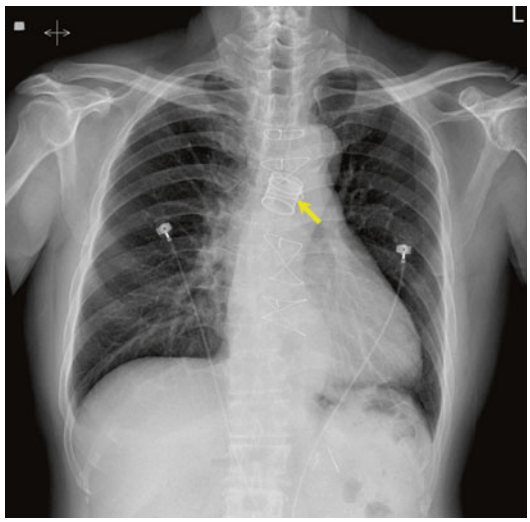

Fig. 5.10 Chest X ray, status post David's operation, showed the artificial graft (*arrow*) in ascending aorta

Tips

The type of surgical therapy of an aortic aneurysm depends on the presence of associated lesions of AV, sinus of Valsalva, and sinotubular junction. In brief, the David technique is performed as follows: after excision of the sinuses, the AV is implanted inside a straight Dacron tube in a manner similar to the implantation of an AV homograft.

5.2 Type A Aortic Dissection

A 58-year-old man with hypertension suffered sudden severe chest pain with radiation pain to abdomen and back. Acute type A aortic dissection was told by other hospital, then he was transfer to our hospital for surgical intervention. Auscultation: regular heart beat with a grade 2/6 systolic murmur over ascending aorta. ECG: counter clockwise rotation, non-specific ST-T change. Chest CT: type A aortic dissection from ascending aorta down to all the way extending, left renal artery originating from the false lumen. Operation: emergent reconstruction of ascending aorta, aortic arch and descending aorta, aorto-innominant artery and aorto-left CCA bypass.

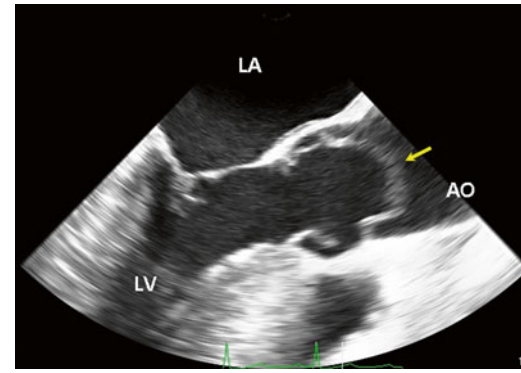

Fig. 5.11 Two-dimensional transesophageal echocardiography (2D TEE) image, long-axis view, showed dissection of ascending aorta with a highly mobile intimal flap (*arrow*) close above AV

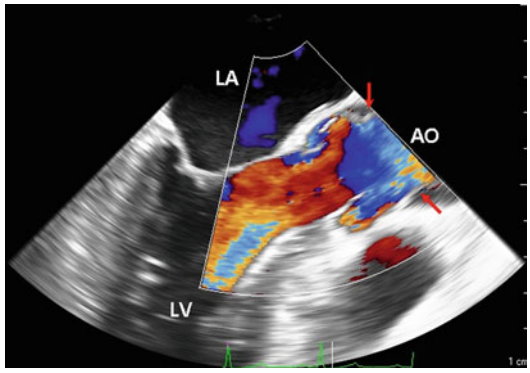

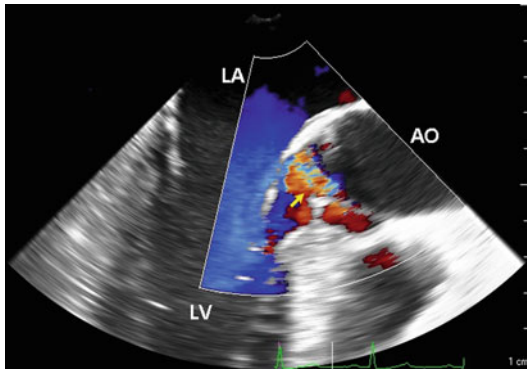

Figs. 5.12 and 5.13 2D TEE color Doppler, long-axis view, the intimal flap (*red arrows*) moved back and forth with cardiac cycle. It attached to the AV in diastole (*below*) causing eccentric AR (*yellow arrow*)

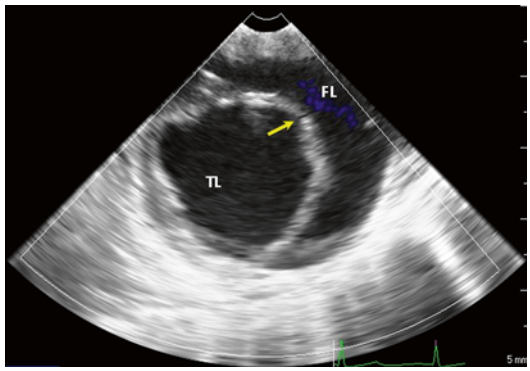

Fig. 5.14 2D TEE color Doppler of ascending aorta, short-axis view, showed the intimal flap (*arrow*) between the true lumen (*TL*) and the false lumen (*FL*)

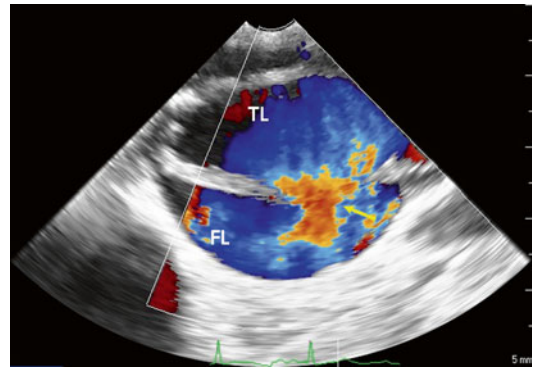

Fig. 5.15 2D TEE color Doppler of ascending aorta, short-axis view, showed blood flow (*arrow*) from the true lumen (*TL*) to the false lumen (*FL*) through the intimal flap tear

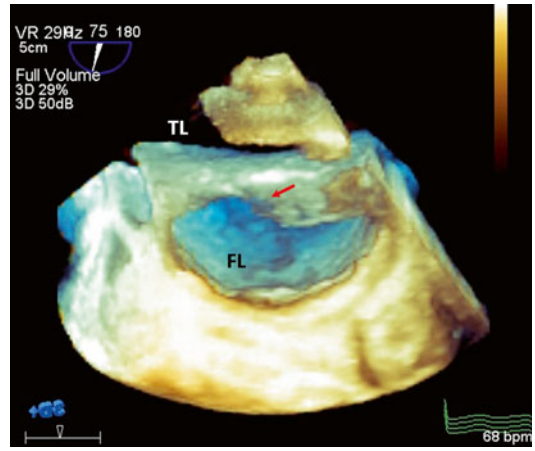

Fig. 5.16 3D TEE image showed the intimal flap with a huge irregular tear (*arrow*) between true lumen (*TL*) and false lumen (*FL*)

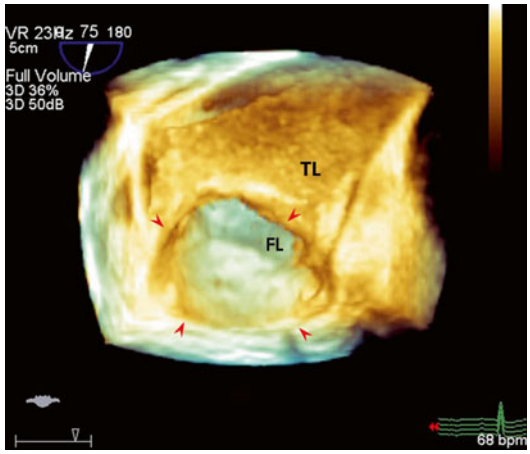

Fig. 5.17 3D TEE image showed the intimal flap with a huge irregular tear (*arrows*) between true lumen (*TL*) and false lumen (*FL*)

Tips

TEE is an appropriate diagnostic tool for aortic dissection to identify the intimal tear, true lumen, extension of dissection, and potential complications.

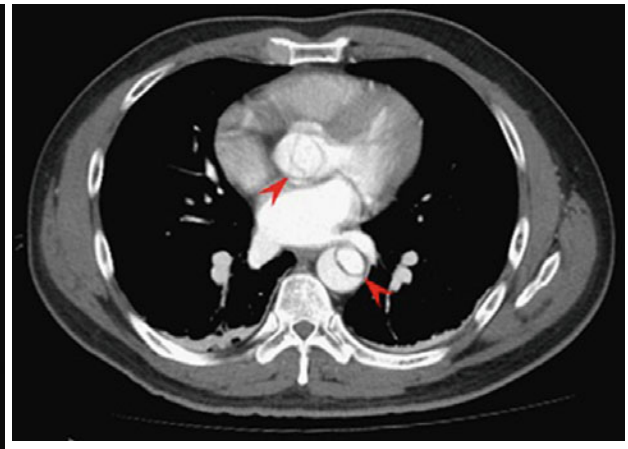

Figs. 5.18 and 5.19 Contrast-enhanced CT images showed type A aortic dissection from ascending aorta down to all the way extending (*arrows*)

5.3 Type A Aortic Dissection Having Bentall Operation

A 62-year-old woman has a history of hypertensive cardiovascular disease, hypothyroidism and type A aortic dissection. She experienced shortness of breath, dyspnea on exertion and chest distress. Auscultation: regular heart beat with a grade 4/6 pan-systolic murmur. ECG: sinus rhythm, left axis deviation and non- specific ST-T change. Chest CT: pericardial effusion and intramural hematoma seen in ascending aorta. Cardiac CT: type A aortic dissection from aortic root (5.7 cm) to distal ascending aorta with mural thrombi in the false lumen and mild pericardial effusion. Operation: Bentall operation.

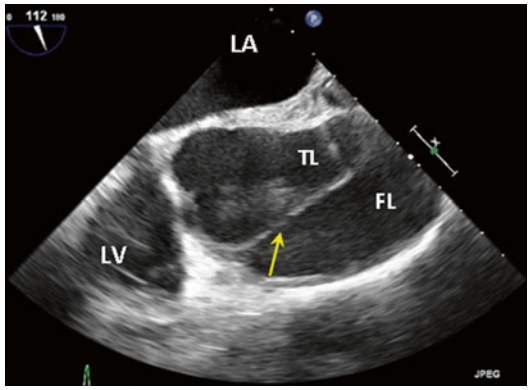

Fig. 5.20 Two-dimensional transesophageal echocardiography (2D TEE) image, long-axis view, showed dilated aortic root and a dissection flap with tear (*arrow*) between the true (*TL*) and false lumen (*FL*)

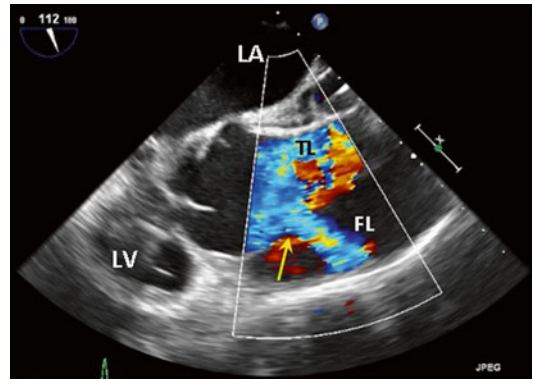

Fig. 5.21 2D TEE color Doppler, long-axis view, showed blood flow from the true lumen (*TL*) to the false lumen (*FL*) through the intimal flap tear (*arrow*)

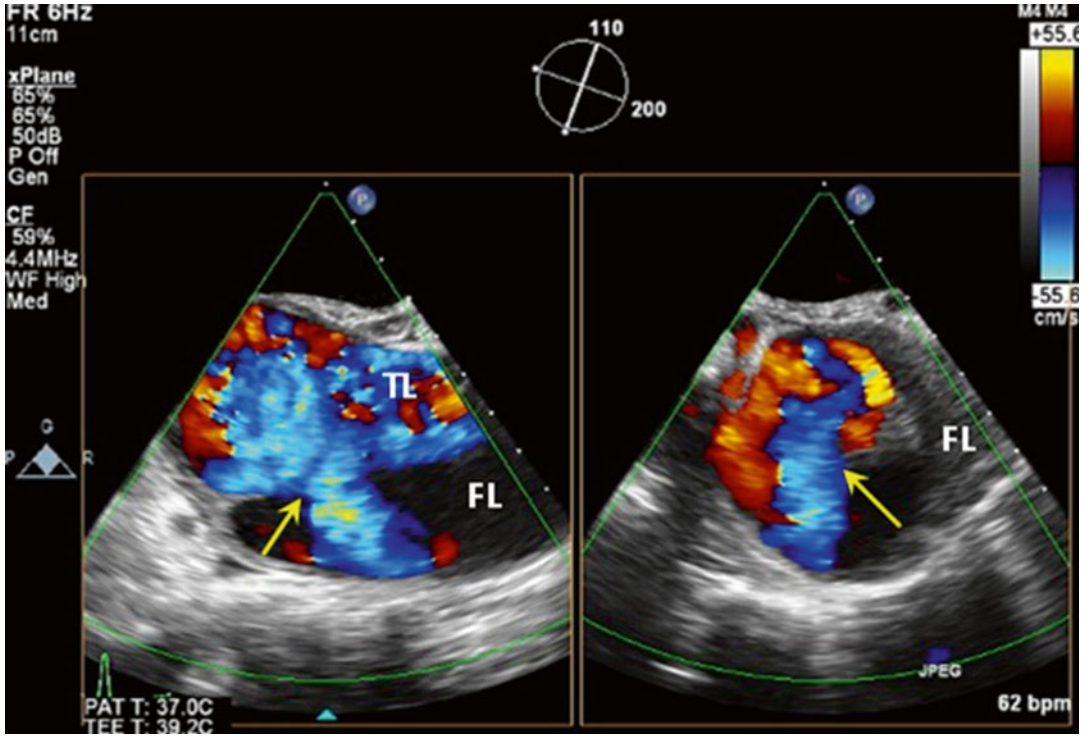

Fig. 5.22 2D TEE color Doppler, x-plane view, showed blood flow from the true lumen (*TL*) to the false lumen (*FL*) through the intimal flap tear (*arrow*)

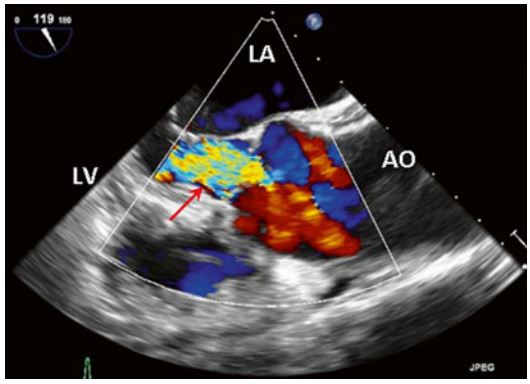

Fig. 5.23 2D TEE color Doppler, long-axis view, showed moderate to severe AR (*arrow*) due to dilated aortic annulus

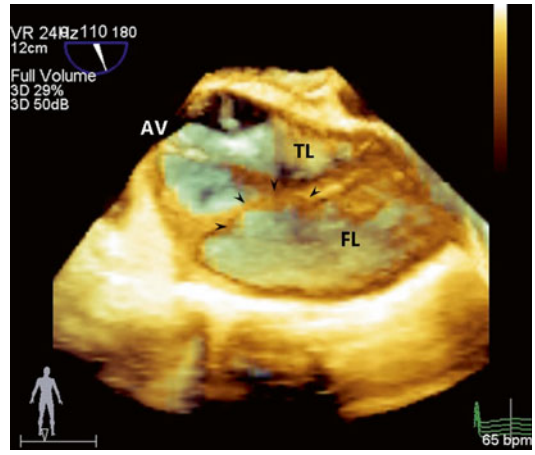

Fig. 5.24 3D TEE image, long-axis view, showed dilated aortic root and a dissection flap with tear (*arrows*)

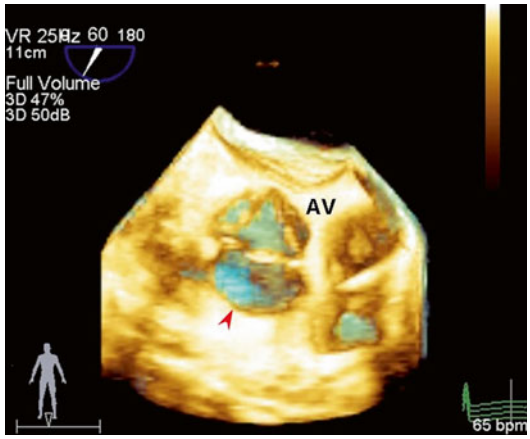

Fig. 5.25 3D TEE image, en-face view of AV, showed the prominent false lumen (*arrow*)

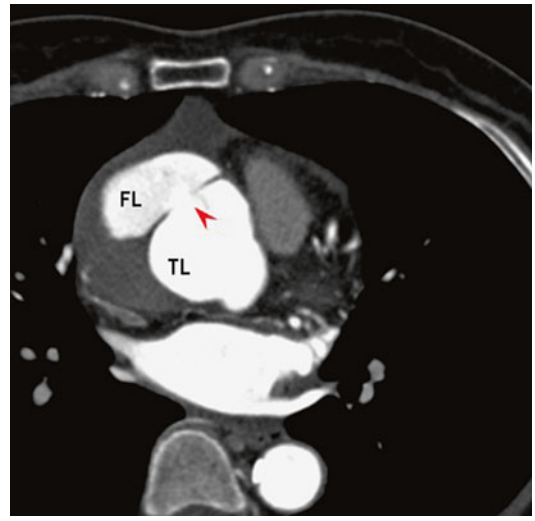

Fig. 5.27 Contrast-enhanced CT image showed type A aortic dissection with flap tear (*arrow*) in aortic root

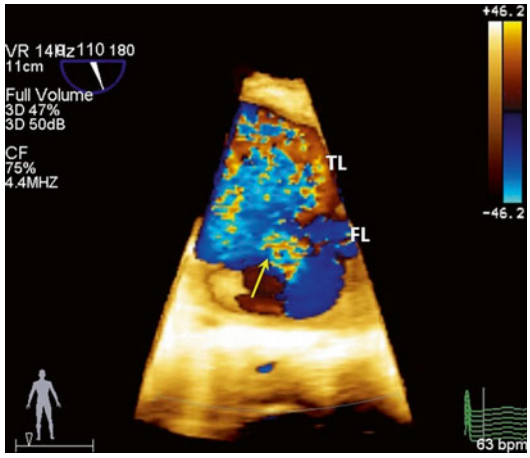

Fig. 5.26 3D TEE color Doppler, long-axis view, showed blood flow (*arrow*) from the true lumen (*TL*) to the false lumen (*FL*) through the intimal flap tear

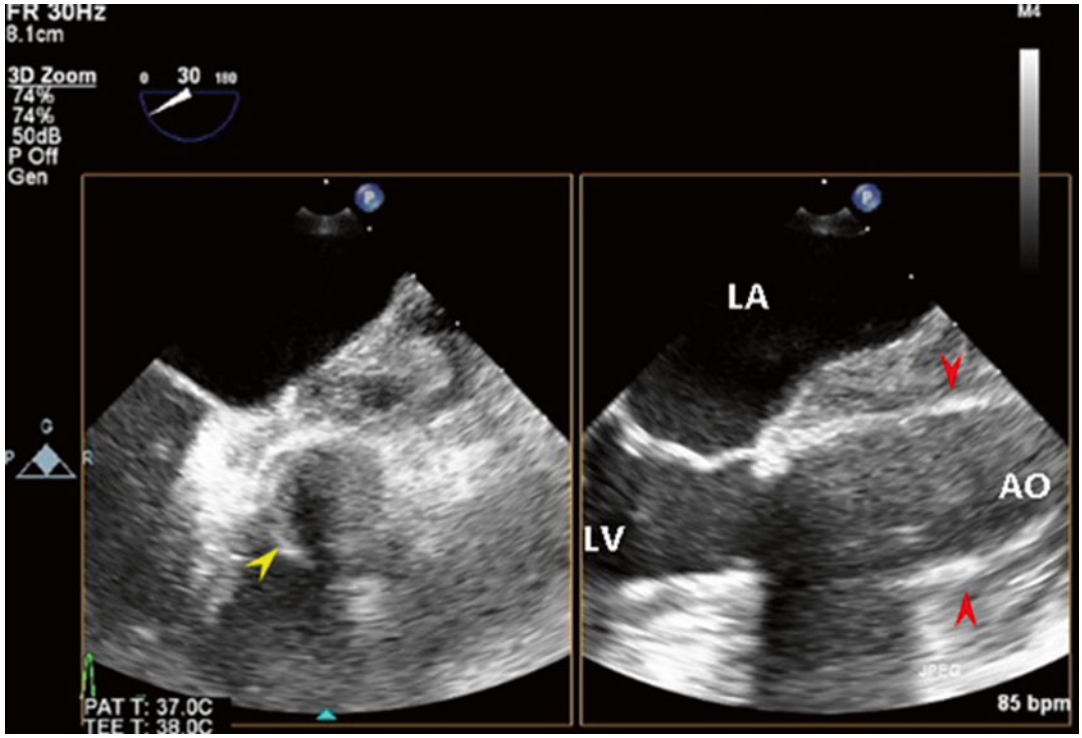

Fig. 5.28 2D TEE image, x-plane view, status post Bentall operation, showed the tissue AV prosthesis (*yellow arrow*) and the artificial graft (*red arrows*)

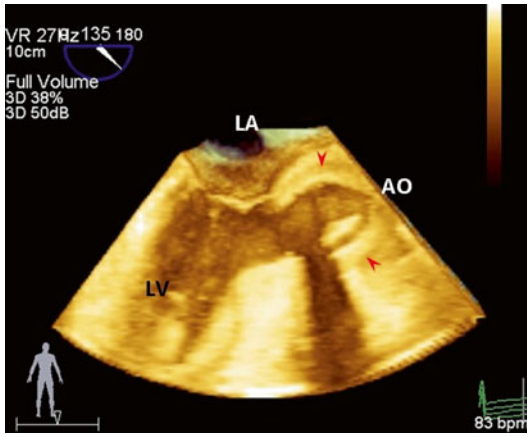

Fig. 5.29 3D TEE image, long-axis view, status post Bentall operation, showed the artificial graft (*arrows*)

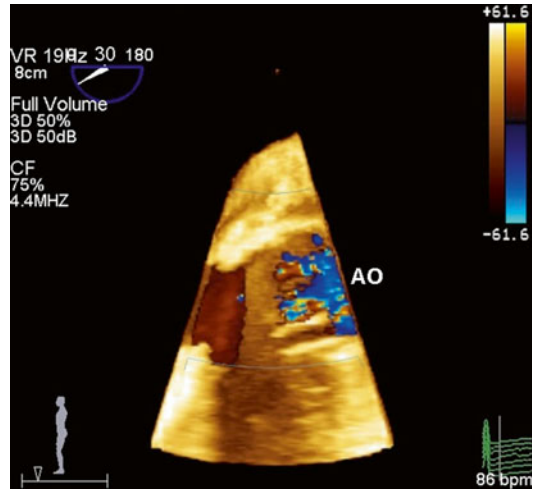

Fig. 5.30 3D TEE color Doppler, long- axis view, status post Bentall operation, showed normal LV outflow and no AR

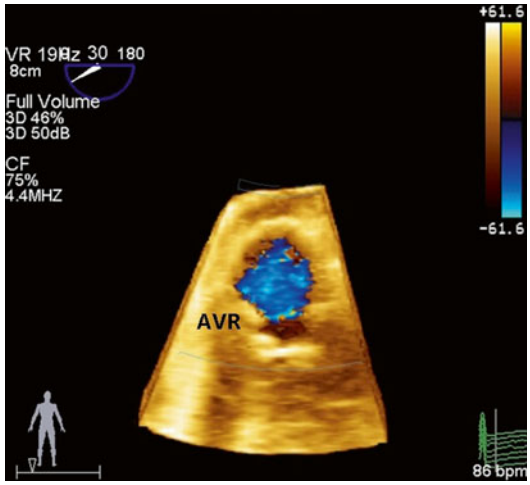

Fig. 5.31 3D TEE color Doppler, en face view of AV, status post Bentall operation, showed normal LV outflow and no AR

5.4 Type A Aortic Dissection with Intramural Hematoma

A 61-year-old man with medical-controlled hypertension suffered from chest pain and tightness. Auscultation: no significant murmur. ECG: sinus rhythm, LA enlargement and non-specific ST-T change. Chest CT angiography: type A aortic dissection from ascending aorta to aortic arch, atherosclerotic calcification of the thoracic aorta and coronary arteries, cardiomegaly, pericardial effusion and left pleural effusion. Operation: emergency aortic reconstruction.

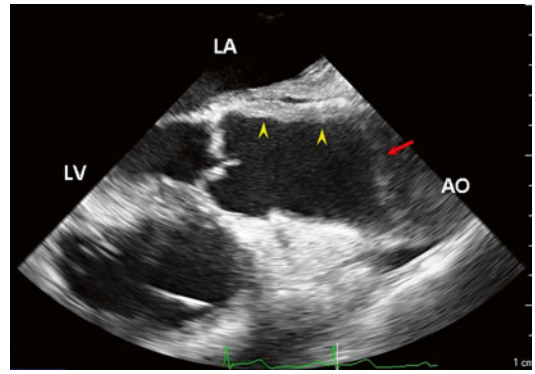

Fig. 5.32 Two-dimensional transesophageal echocardiography (2D TEE) image, long-axis view, showed a dissection flap (*red arrow*) and an intramural hematoma (*yellow arrows*) in ascending aorta

Tips

If an aortic dissection is associated with AV disease, which needs repair or replacement, Benetall operation is appropriate to replace the AV along with the ascending aorta. The indication of Bentall operation is the procedure of AV dysfunction severe enough to warrant AV replacement, the aortic root will be replaced if the ascending aorta exceeded by 4.0–4.5 cm in diameter, and the patients' life expectancy is anticipated to be greater than 10 years.

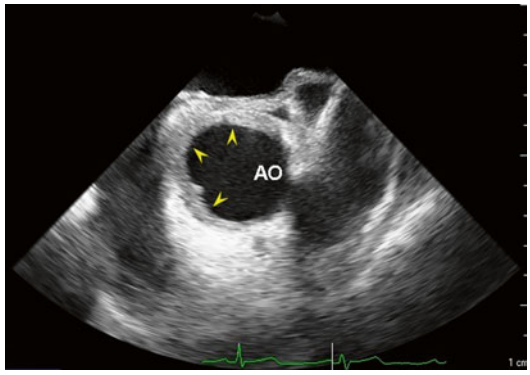

Fig. 5.33 2D TEE image, short-axis view, showed a crescent-shape intramural hematoma (*arrows*) in ascending aorta

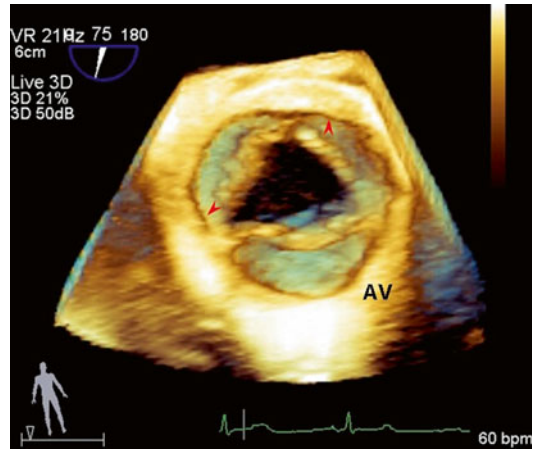

Fig. 5.36 3D TEE image, en face view of AV, showed an intramural hematoma (*arrows*) in ascending aorta

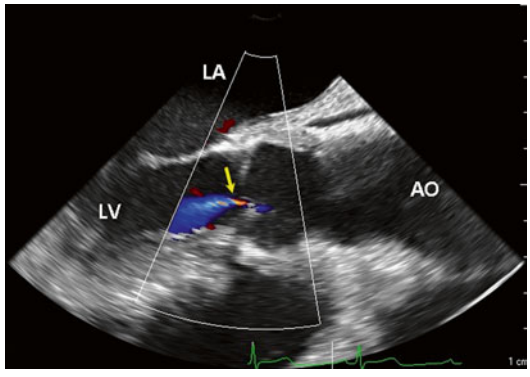

Fig. 5.34 2D TEE color Doppler, long-axis view, showed mild to moderate AR (*arrow*)

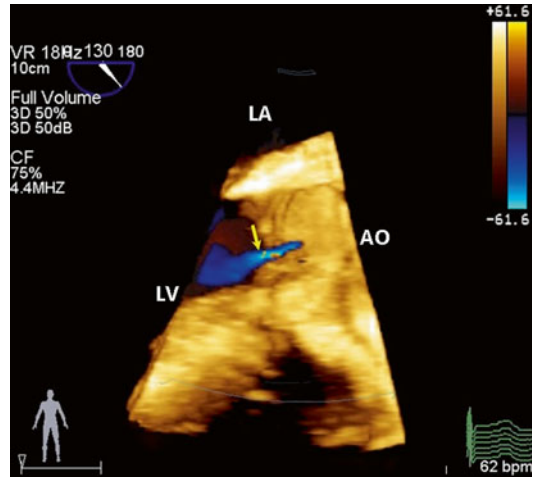

Fig. 5.37 3D TEE color Doppler, long-axis view, showed mild to moderate AR (*arrow*)

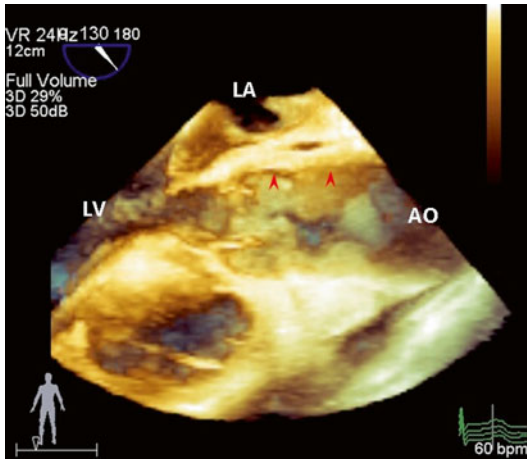

Fig. 5.35 3D TEE image, long-axis view, showed an intramural hematoma (*arrows*) in ascending aorta

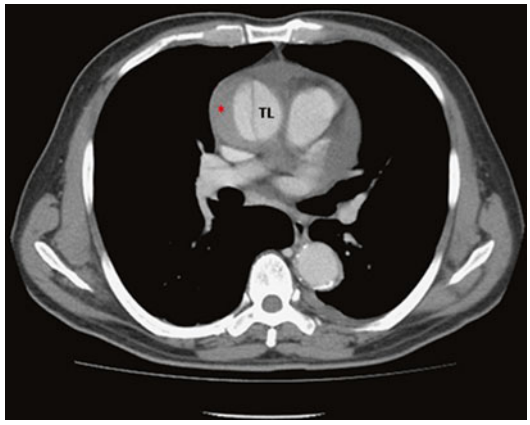

Fig. 5.38 Contrast-enhanced CT image showed type A aortic dissection with intimal flap between the true (*TL*) and false lumen and thrombus (*) in false lumen

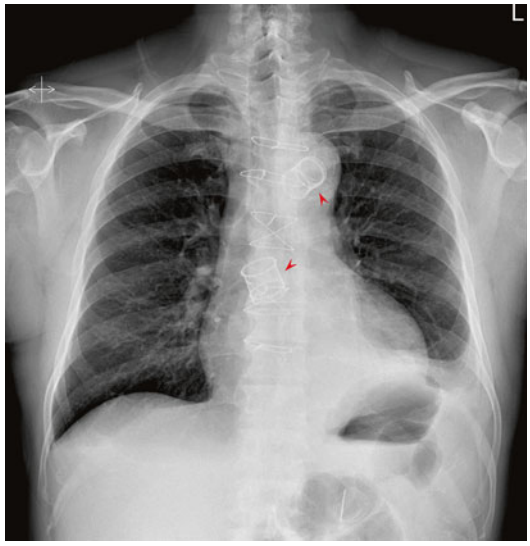

Fig. 5.39 Chest X ray, status post aortic reconstruction, showed the artificial grafts (*arrows*) in ascending aorta and aortic arch

Tips

Intramural hematoma is a variant of aortic dissection and appears as a circumferential or crescent-shape thickening of the aortic wall on ascending aorta short axis view.

5.5 Type B Aortic Dissection from Distal Aortic Arch

A 50-year-old man had a history of hypertension, type two diabetes mellitus and hyperlipidemia. He suffered from sudden onset lower back pain. Type B aortic dissection was found and medical treatment was given, but the symptoms worsen. Auscultation: regular heart beat without murmur. ECG: sinus rhythm and counter clockwise rotation. Thoracic and abdominal aorta CT angiography: type B aortic dissection from distal aortic arch, thoracic and abdominal aorta to bilateral common iliac arteries and SMA. Operation: reconstruction of distal aortic arch and upper thoracic aorta.

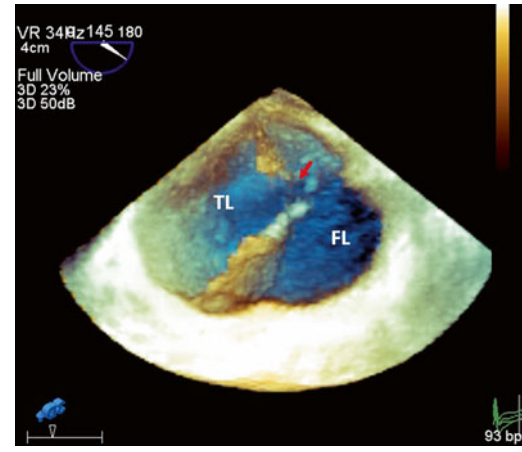

Fig. 5.40 Three-dimensional transesophageal echocardiography (3D TEE) of descending thoracic aorta, short-axis view, showed the intimal flap with tear (*arrow*) between the true lumen (*TL*) and the false lumen (*FL*)

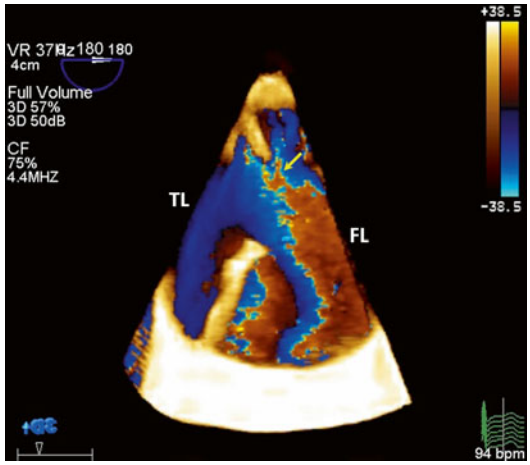

Fig. 5.41 3D TEE color Doppler of descending thoracic aorta, short-axis view, showed blood flow from the true lumen (*TL*) to the false lumen (*FL*) through the intimal flap tear (*arrow*)

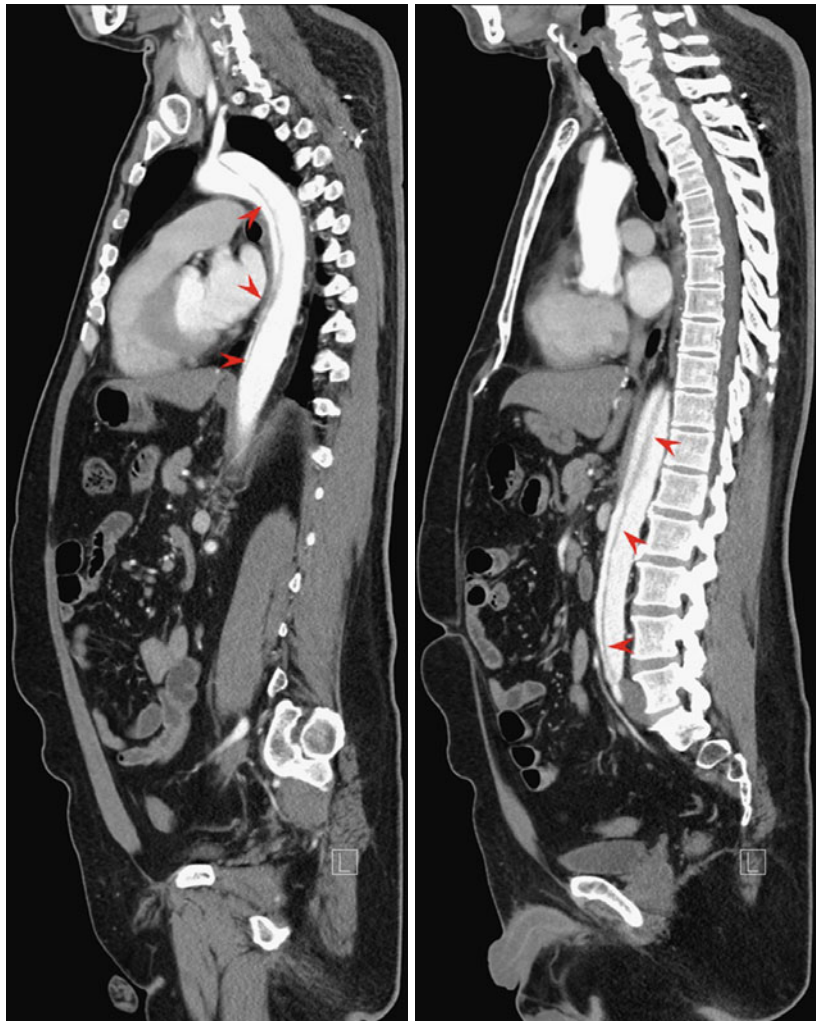

Figs. 5.42 and 5.43 Contrast-enhanced CT images showed type B aortic dissection (*arrows*) from distal aortic arch, thoracic and abdominal aorta to bilateral common iliac arteries and SMA

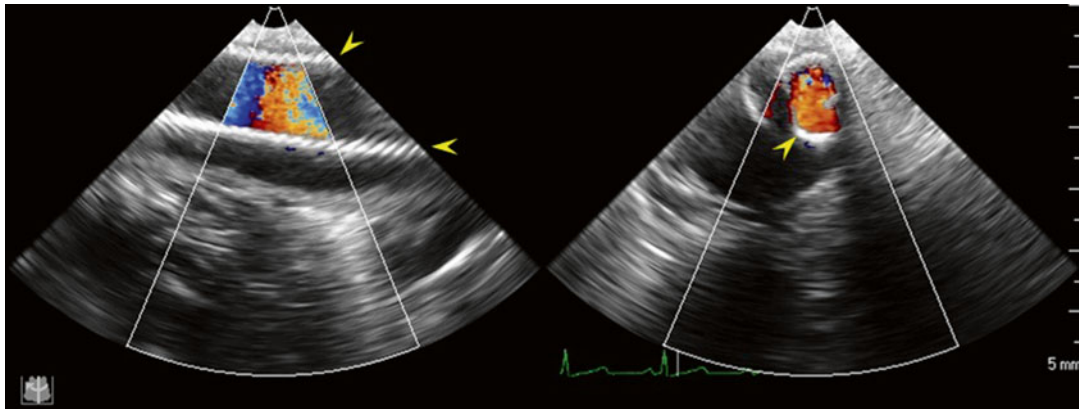

Fig. 5.44 2D TEE color Doppler of descending aorta, x-plane view, status post aortic reconstruction, showed flow within the artificial graft (*arrows*)

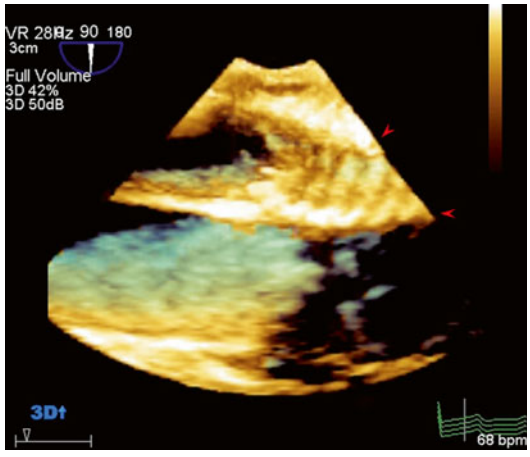

Fig. 5.45 3D TEE of descending aorta, long-axis view, status post aortic reconstruction, showed the artificial graft (*arrows*)

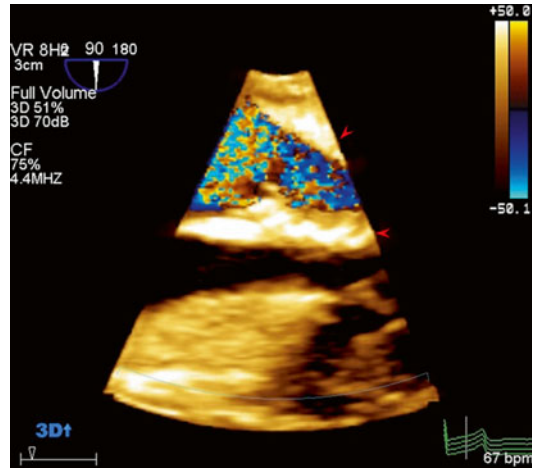

Fig. 5.46 3D TEE color Doppler of descending aorta, long-axis view, status post aortic reconstruction, showed flow within the artificial graft (*arrows*)

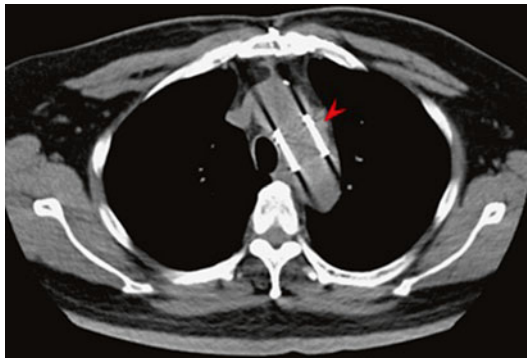

Fig. 5.47 Non-contrast-enhanced CT images, status post aortic reconstruction, showed artificial graft (*arrow*) in distal aortic arch

Tips

In the Stanford classification, type A aortic dissections refers to involvement of the ascending part of the aortic and any extension into other aortic sections, whereas type B refers to dissection involving the descending aorta with distal to the left subclavian artery.

5.6 Type B Aortic Dissection from Middle Descending Aorta

A 65-year-old man has a history of type B dissection status post right renal artery bypass graft, PAOD status post PTA, single-vessel coronary artery disease, type two diabetes mellitus, hyperlipidemia, hypertension and hyperuricemia. He suffered from sudden severe chest pain with radiation pain to the back, dizziness, general fatigue and cold sweating. Auscultation: RHB. EKG: sinus rhythm and left axis deviation. CT: type B aortic dissection, dissection extended from proximal portion of the descending aorta to lower abdominal aorta and right renal artery, lower abdominal aorta stenosis. Operation: reconstruction of middle descending thoracic aorta with intraluminal graft.

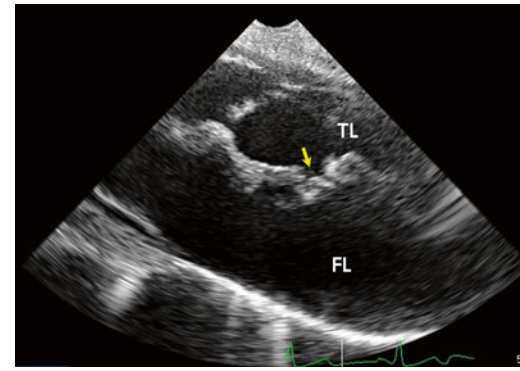

Fig. 5.48 Two-dimensional transesophageal echocardiography (2D TEE) image of descending aorta, long-axis view, showed the intimal flap with tear (*arrow*) between the true lumen (*TL*) and the false lumen (*FL*)

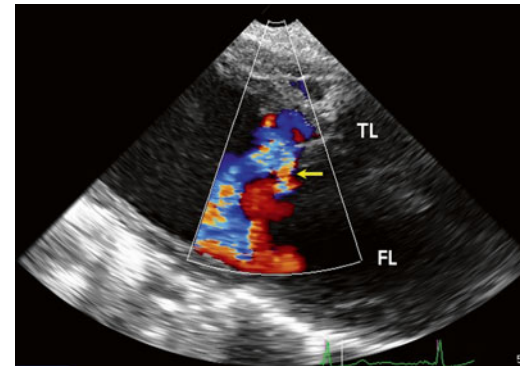

Fig. 5.49 2D TEE color Doppler of descending aorta, long-axis view, showed blood flow (*arrow*) from the true lumen (*TL*) to the false lumen (*FL*) through the intimal flap tear

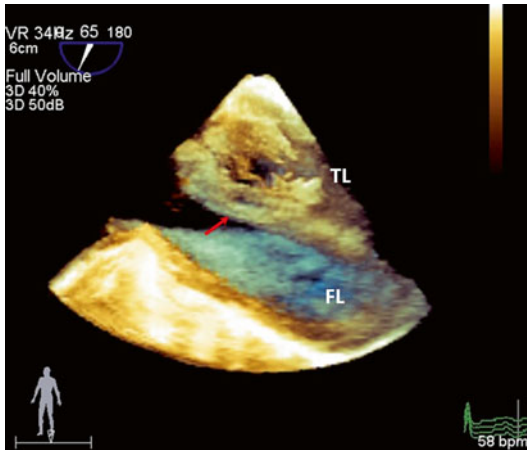

Fig. 5.50 3D TEE image of descending aorta, long-axis view, showed the intimal flap with tear (*arrow*) between the true lumen (*TL*) and the false lumen (*FL*)

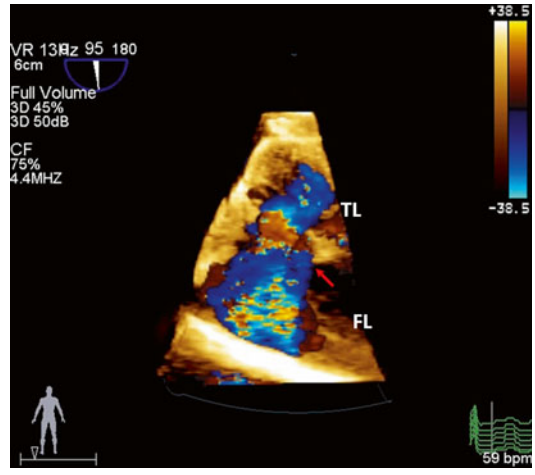

Fig. 5.51 3D TEE color Doppler of descending aorta, long-axis view, showed blood flow from the true lumen (*TL*) to the false lumen (*FL*) through the intimal flap tear (*arrow*)

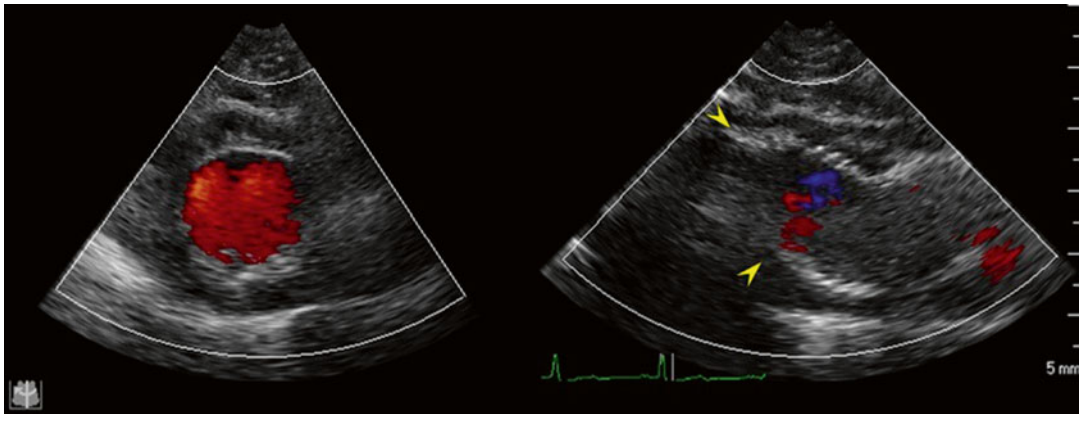

Fig. 5.52 2D TEE color Doppler of descending aorta, x-plane view, status post aortic reconstruction, showed flow within the artificial graft (*arrows*)

Fig. 5.53 Preoperative contrast-enhanced CT image showed type B aortic dissection from proximal portion of the descending aorta to lower abdominal aorta and intimal flap tear at descending aorta (*arrow*)

Fig. 5.54 Contrast-enhanced CT image, status post aortic reconstruction, showed artificial grafts (*arrows*) in descending aorta

Tips

In aortic dissection, the great vessel is divided into true lumen and false lumen by intimal flap. The false lumen is typically larger than the true lumen.

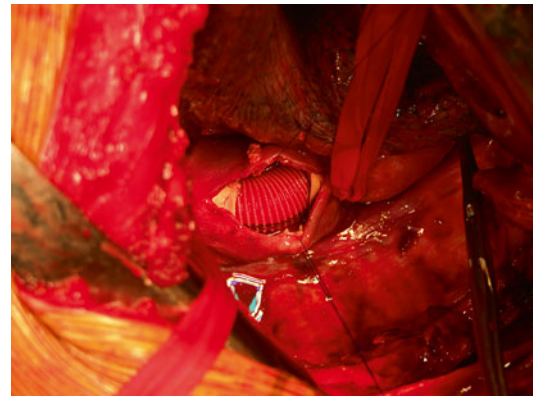

Fig. 5.55 Picture during operation showed an artificial graft in descending aorta

5.7 Aorta-to-Left Ventricular Fistula Having Occluder Implantation

A 54-year-old man had a history of bicuspid AV with infective endocarditis status post AV replacement. He presented with a residual shunt from aorta to LV and symptoms of shortness of breath and dyspnea on exertion. Auscultation: regular heart beat with a grade 2/6 low-pitched continuous murmur over left sternal border. ECG: first degree AV block. Cardiac catheterization: sinus of Valsalva aneurysm with an aorta to LV fistula and moderate amount shunt. Treatment: occluder implantation.

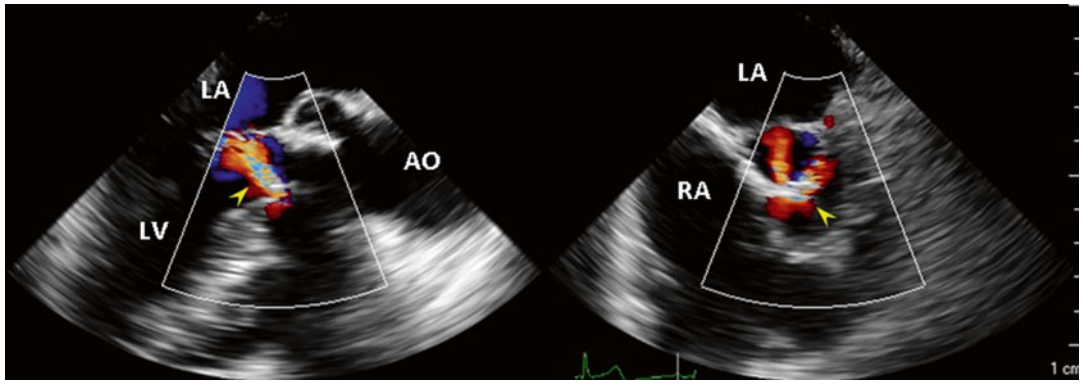

Fig. 5.56 Two-dimensional transesophageal echocardiography (2D TEE) color Doppler, x-plane view, status post tissue AV replacement, showed an aorta-to-LV fistula with moderate amount shunts (*arrows*)

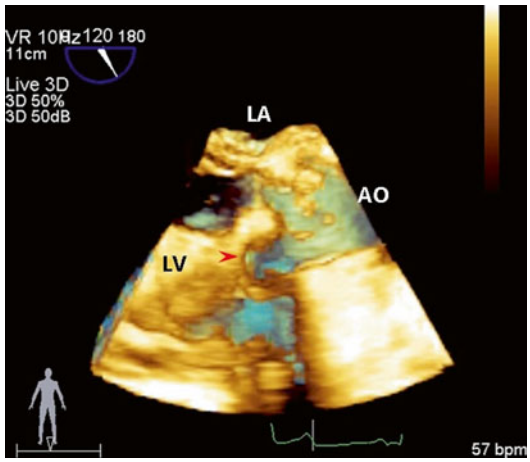

Fig. 5.57 3D TEE image, long-axis view, showed dehiscence of the AV replacement. An echolucent space (*arrow*) was seen posterior to the prosthetic aortic annulus

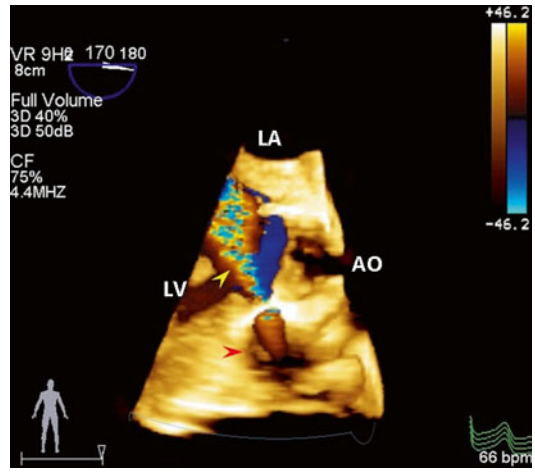

Fig. 5.58 3D TEE color Doppler, long-axis view, showed dehiscence of the AV replacement. An echolucent space (*red arrow*) was seen posterior to the prosthetic aortic annulus with continuous flow (*yellow arrow*) from aorta to LV

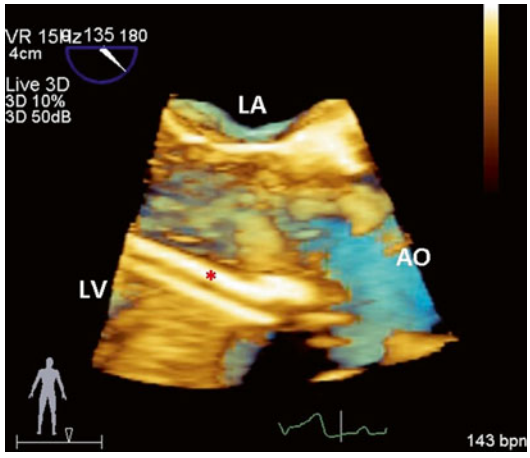

Fig. 5.59 3D TEE image, long-axis view, during occluder implantation, showed the guiding catheter (*) crossed the fistula from aorta to LV

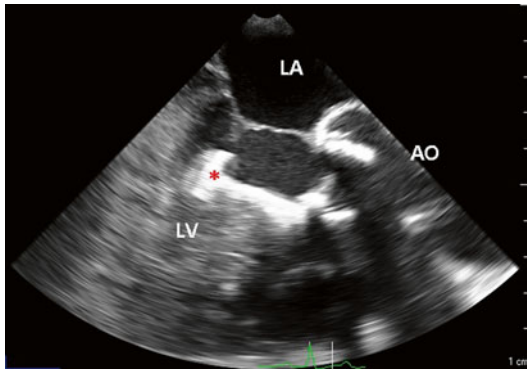

Fig. 5.60 2D TEE image, long-axis view, during the procedure, showed the occluder (*) was deployed to occlude the fistula

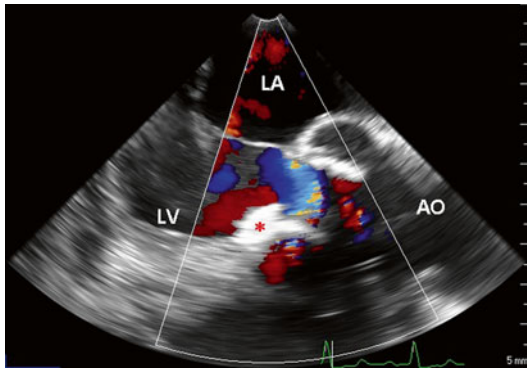

Fig. 5.61 2D TEE color Doppler, long-axis view, status post occluder (*) implantation, showed only trivial residual shunt

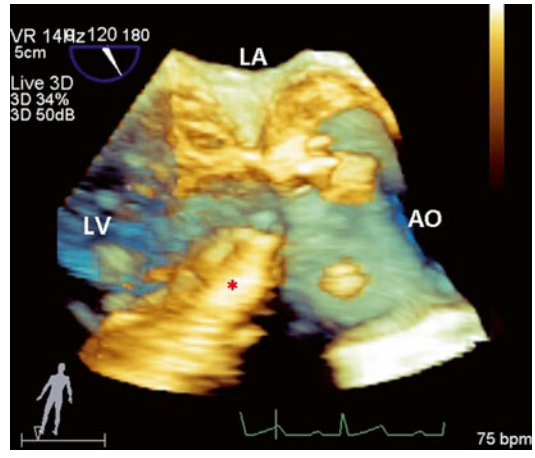

Fig. 5.62 3D TEE image, long-axis view, status post occluder (*) implantation

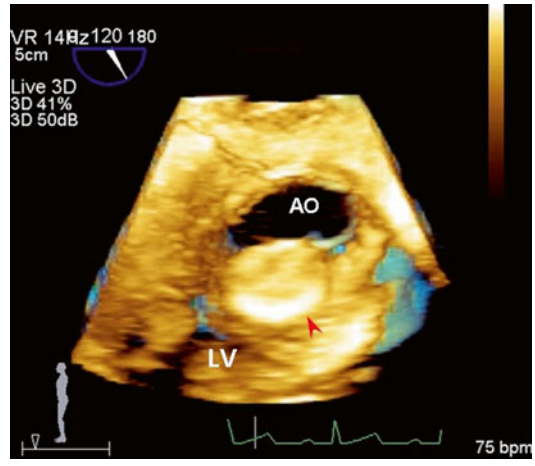

Fig. 5.63 3D TEE image, viewed from LV perspective, status post occluder (*arrow*) implantation

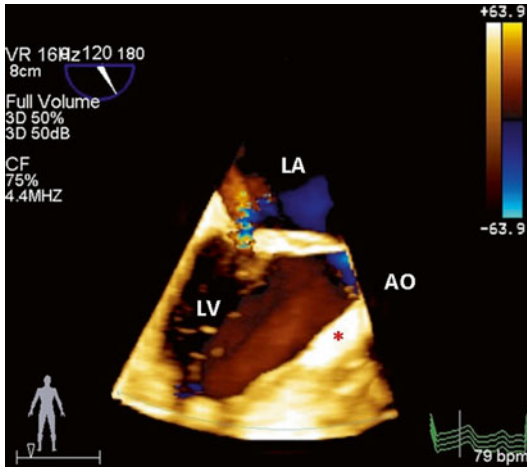

Fig. 5.64 3D TEE color Doppler, long-axis view, status post occluder (*) implantation, showed only trivial residual shunt

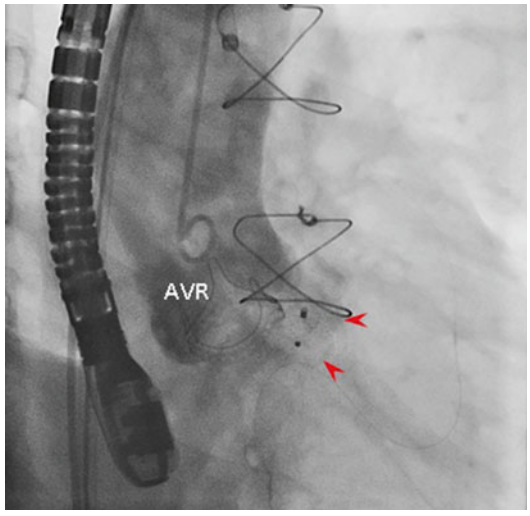

Fig. 5.65 Fluoroscopy status post occluder implantation, showed the deployed occluder (*arrows*)

Tips

The patient had received a bioprosthetic AV followed by a formation of an aorta-to-LV fistula. It may be caused by an episode of endocarditis, but the blood culture test of this patient is negative.

5.8 Aortic Pseudoaneurysm Having Occluder Implantation

A 58-year-old man had a past history of coronary artery disease status post coronary artery bypass graft, valvular disease status post AV replacement and MV repair, chronic atrial fibrillation status post ablation, PFO status post closure and hypertension under medical treatment. He suffered from shortness of breath for a month then a giant ascending aortic pseudoaneurysm was diagnosed. Auscultation: regular heart beat without murmur. ECG: normal sinus rhythm and left axis deviation. Chest X ray: cardiomegaly and enlarged ascending aorta. Cardiac CT angiography: giant ascending aortic aneurysm (7.23 cm × 9.77 cm) and pseudoaneurysm formation with a small hole about 1 cm connected between the true lumen and the false lumen. Treatment: occluder implantation.

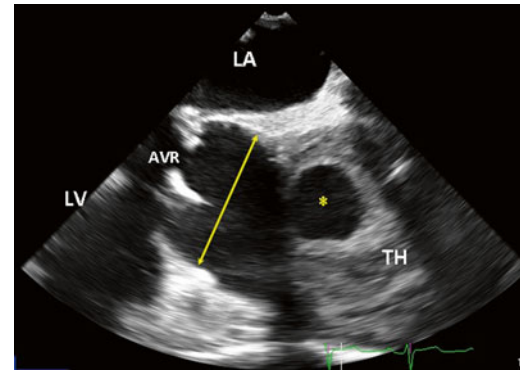

Fig. 5.66 Two-dimensional transesophageal echocardiography (2D TEE), long-axis view, status post tissue AV replacement (*AVR*), showed dilated ascending aorta (*arrow*) with a thrombus (*TH*) wrapped pseudoaneurysm (*)

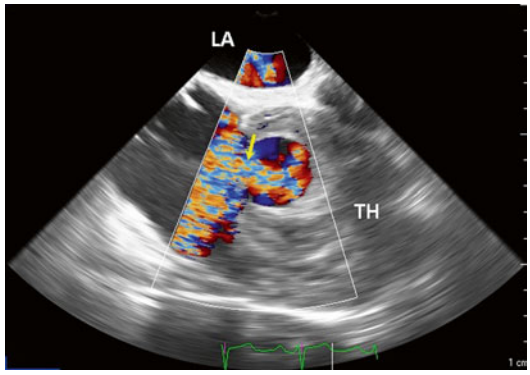

Fig. 5.67 2D TEE color Doppler, long-axis view, status post tissue AV replacement, showed a flow (*arrow*) from aorta to the pseudoaneurysm

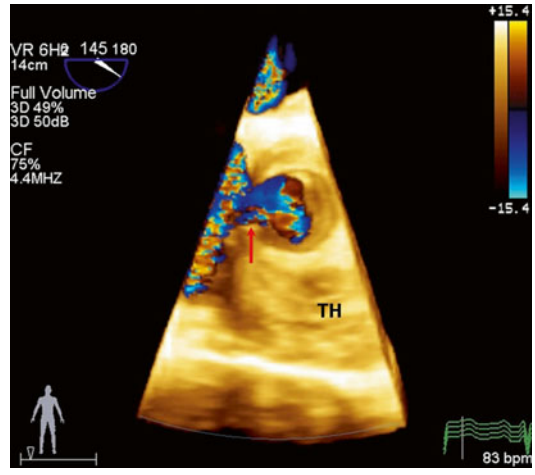

Fig. 5.69 3D TEE color Doppler, long-axis view, status post tissue AV replacement, showed a thrombus (*TH*) wrapped pseudoaneurysmat in proximal ascending aorta with flow (*arrow*) across the communication

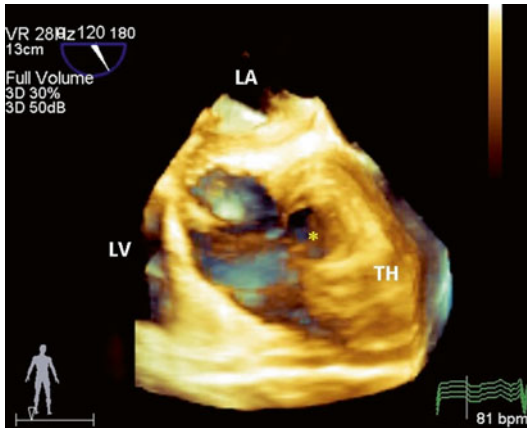

Fig. 5.68 3D TEE, long-axis view, status post tissue AV replacement, showed a thrombus (*TH*) wrapped pseudoaneurysm (*) at proximal ascending aorta

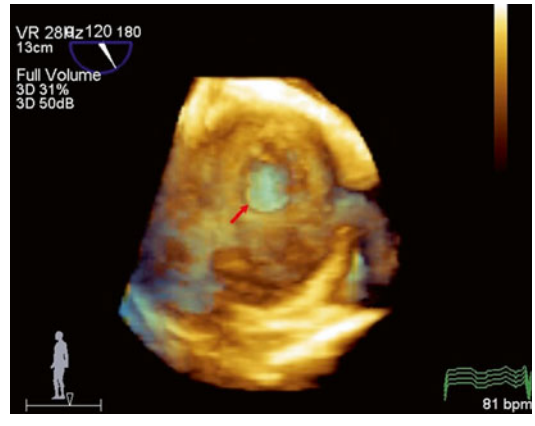

Fig. 5.70 3D TEE, viewed from ascending aorta perspective, showed the communication (*arrow*) between ascending and the pseudoaneurysm

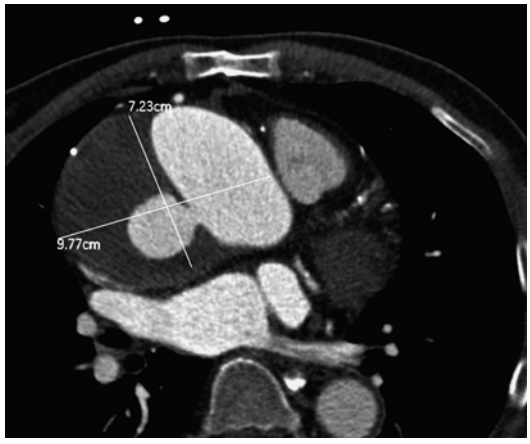

Fig. 5.71 Contrast-enhanced CT image showed a giant ascending aortic aneurysm (7.23 cm × 9.77 cm) and pseudoaneurysm formation with a small hole about 1 cm connected between the true lumen and the false lumen

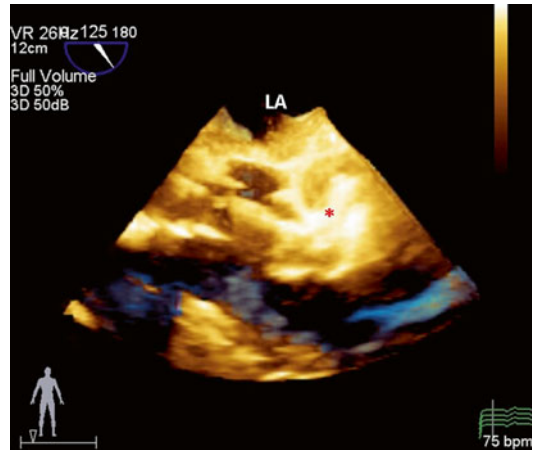

Fig. 5.73 3D TEE, long-axis view, during the procedure, showed the occluder (*) was deployed to occlude the communication between ascending aorta and the pseudoaneurysm

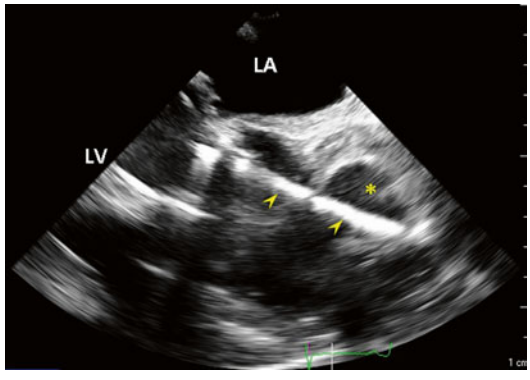

Fig. 5.72 2D TEE, long-axis view, during occluder implantation, showed the guiding catheter (*arrows*) crossed the communication from aorta to pseudoaneurysm (*)

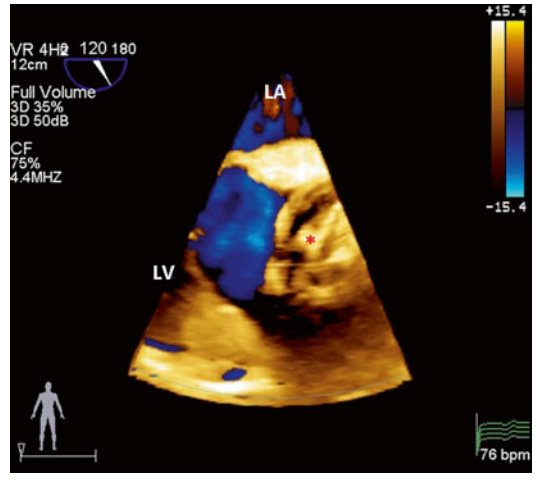

Fig. 5.74 3D TEE color Doppler, long-axis view, status post occluder (*) implantation, showed only trivial residual shunt

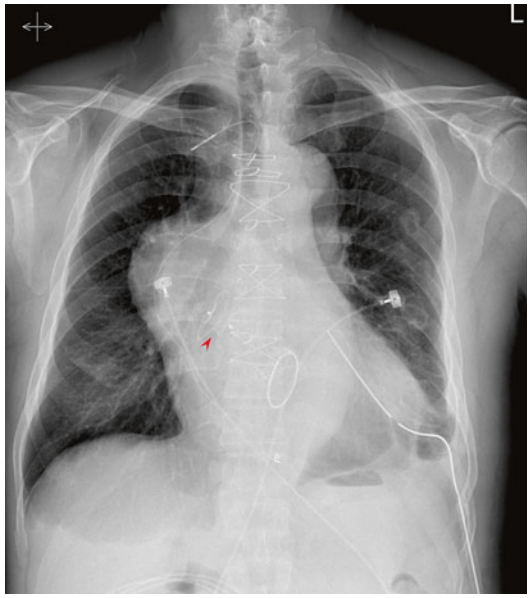

Fig. 5.75 Chest X ray, status post occluder implantation, showed the deployed occluder (*arrows*)

Tips

An aortic pseudoaneurysm is different from an aneurysm. The previous contains rupture of aortic wall that involves all the layers.

5.9 Ruptured Sinus of Valsalva Aneurysm Having Occluder Implantation

A 29-year-old woman was in good health before. She suffered from chest tightness and exertional dyspnea. Auscultation: regular heart beat a with grade 3/6 systolic murmur over left sternal border. ECG: normal sinus rhythm. Treatment: occluder to block the shunt.

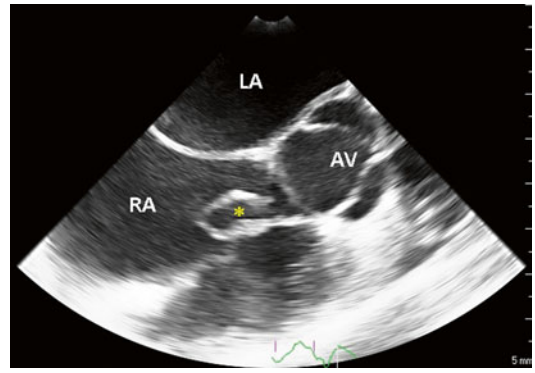

Fig. 5.76 Two-dimensional transesophageal echocardiogram (2D TEE) image, short-axis view, showed a sinus of Valsalva aneurysm (*), which is a "wind sock"-like membranous outpouching of NCC protruded into RA

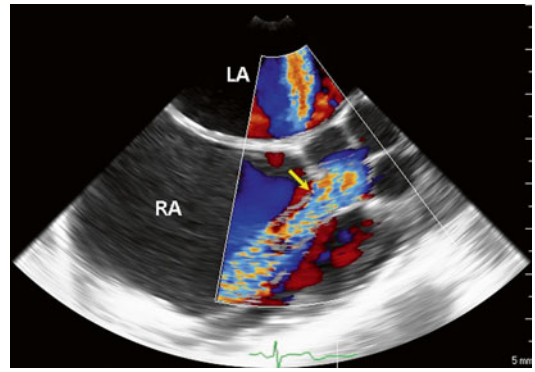

Fig. 5.77 2D TEE color Doppler, short-axis view, showed mosaic-pattern flow (*arrow*) crossed the ruptured sinus of Valsalva aneurysm

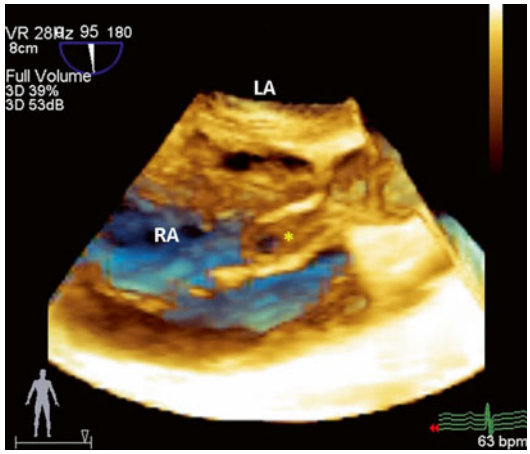

Fig. 5.78 3D TEE image, short-axis view, showed a sinus of Valsalva aneurysm (*) of NCC protruded into RA

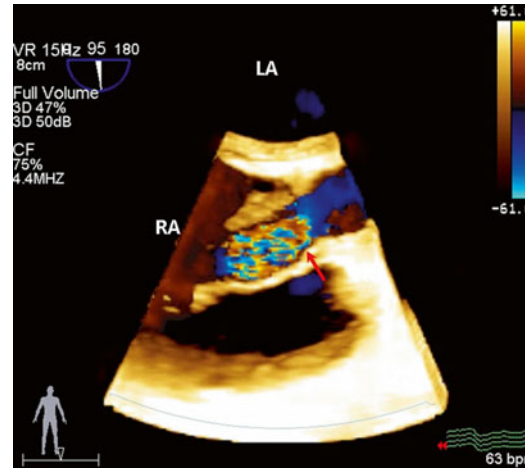

Fig. 5.80 3D TEE color Doppler, short-axis view, showed an aorta-to-RA shunt (*arrow*) through the ruptured sinus of Valsalva aneurysm

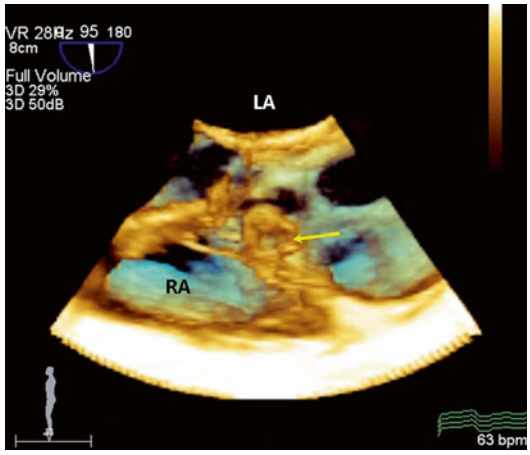

Fig. 5.79 3D TEE image, viewed from RA perspective, showed a rupture (*arrow*) of sinus Valsalva aneurysm

Fig. 5.81 Fluoroscopy showed ruptured sinus Valsalva aneurysm with an insignificant shunt (*arrow*)

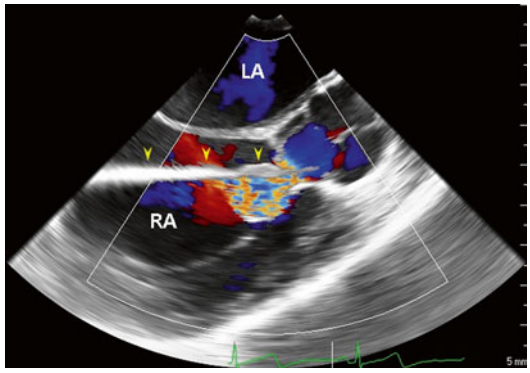

Fig. 5.82 2D TEE color Doppler, short-axis view, during occluder implantation, showed the guiding catheter (*arrows*) crossed the rupture of sinus Valsalva aneurysm from aorta to RA

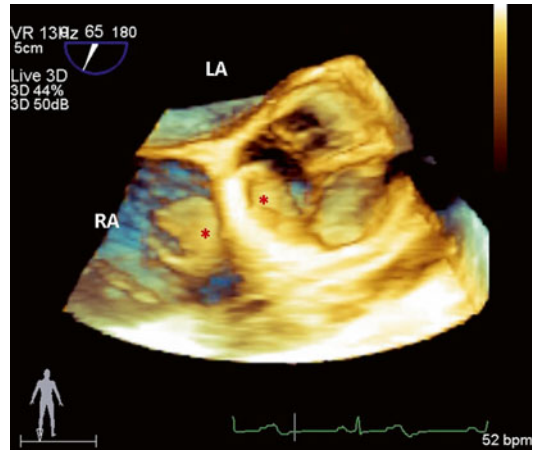

Fig. 5.84 3D TEE image, short-axis view, status post occluder implantation, showed the occluder (*) block the aorta-to-RA fistula

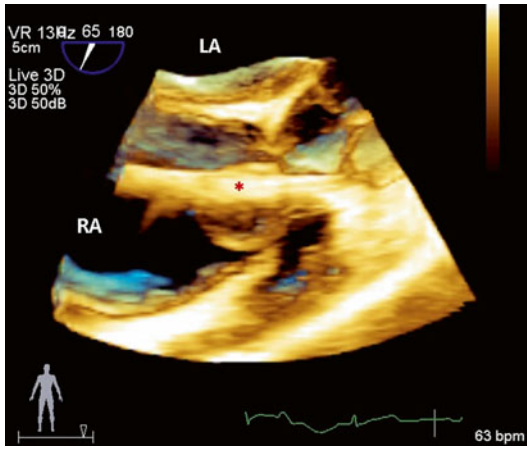

Fig. 5.83 3D TEE image, short-axis view, during the procedure, showed the guiding catheter (*) crossed the rupture of sinus Valsalva aneurysm from aorta to RA

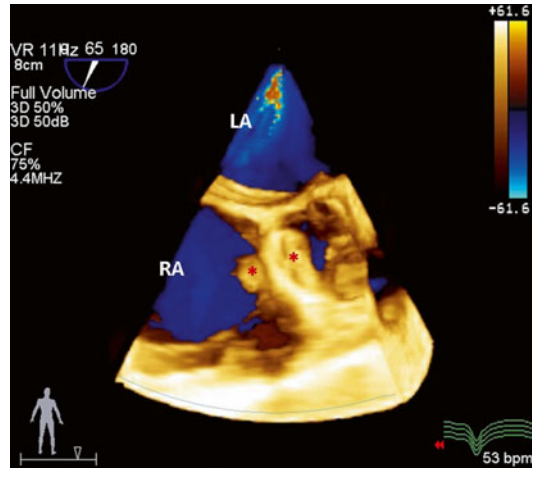

Fig. 5.85 3D TEE image, short-axis view, status post occluder (*) implantation, showed no residual shunt

Tips

Isolated sinus of Valsalvs aneurysm may be congenital or from trauma, endocarditis, Marfan syndrome, or syphilis. A percutaneous approach to repair sinus of Valsalva rupture may be an alternative strategy.

Suggested Reading

Ashoub A, Tang A, Shaktawat S. Extensive aneurysms of sinuses of Valsalva precluding valve sparing aortic root reimplantation (David procedure). Interact Cardiovasc Thorac Surg. 2011;12(3):500–1.

Benedik J, Wendt D, Perrey M, et al. Adjustment of aortic annulus size during David re-implantation (how to do it). Scand Cardiovasc J. 2013;47(4):245–6.

Brinster DR, Parrish DW, Meyers KS, et al. Central aortic cannulation for Stanford type A aortic dissection with the use of three-dimensional and two-dimensional transesophageal echocardiography. J Card Surg. 2014;29(5):729–32.

Cao X, Zhang F, Wang L, Jing H, Li N. Transthoracic minimally invasive closure for the treatment of ruptured sinus of Valsalva Aneurysm: a case report. J Cardiothorac Surg. 2014;9:27.

Červenka L, Melenovský V, Husková Z, et al. Inhibition of soluble epoxide hydrolase does not improve the course of congestive heart failure and the development of renal dysfunction in rats with volume overload induced by aorto-caval fistula. Physiol Res. 2015;64:857–73.

Fujita A, Kurazumi H, Suzuki R, et al. Aortic arch-descending aorta bypass for intraoperative lower body malperfusion during chronic type A aortic dissection repair. Kyobu Geka. 2015;68(6):435–8. Japanese.

Gomero-Cure W, Lowery RC, O'Donnell S. Stent graft-induced new entry tear after endoluminal grafting for aortic dissection repaired with open interposition graft. J Vasc Surg. 2013;58(6):1652–6.

Hashimoto K, Itoh S, Tajima Y, et al. Distal aortic arch aneurysm, acute type B aortic dissection, and acute bilateral limb ischemia treated by two-stage total arch replacement;report of a case. Kyobu Geka. 2015;68(5):371–4. Japanese.

İlkay E, Çelebi ÖÖ, Kaçmaz F, Pampal K. Retrograde approach for percutaneous closure in a patient with ruptured sinus of Valsalva. Turk Kardiyol Dern Ars. 2014;42(8):759–62.

Itoga NK, Kakazu CZ, White RA. Enhanced visual clarity of intimal tear using real-time 3D transesophageal echocardiography during TEVAR of a type B dissection. J Endovasc Ther. 2013;20(2):221–2.

Kassaian SE, Abbasi K, Mousavi M, Sahebjam M. Endovascular treatment of acute type B dissection complicating aortic coarctation. Tex Heart Inst J. 2013;40(2):176–81.

Kieser TM, Spence FP, Kowalewski R. Iatrogenic aortic root and left main dissection during non-emergency coronary surgery: a solution applicable to heavily calcified coronary arteries. Interact Cardiovasc Thorac Surg. 2015;22:246–8.

Lin CH, Murphy J, Balzer DT. Case report: percutaneous closure of an ascending aortic pseudoaneurysm by 3D angiography guidance. Methodist Debakey Cardiovasc J. 2015;11(2):137–9.

Marjanović I, Sarac M, Tomić A, et al. Visceral hybrid reconstruction of thoracoabdominal aortic aneurysm after open repair of type A aortic dissection by the Bentall procedure with the elephant trunk technique--a case report. Vojnosanit Pregl. 2014;71(9):879–83.

Michel S, Hagl C, Juchem G, Sodian R. Type A intramural hematoma often turns out to be a type A dissection. Heart Surg Forum. 2013;16(6):E351–2.

Rajan S, Sonny A, Sale S. Retrograde type A aortic dissection after thoracoabdominal aneurysm repair: early diagnosis with intraoperative transesophageal echocardiography. A A Case Rep. 2015;4(5):58–60.

Rossokha OA, Shelestova IA, Boldyrev SI, et al. Detection of determinants of functional aortic regurgitation in patients with ascending aorta aneurism by transesophagea1 echocardioscopy. Kardiologiia. 2015;55(3):61–6. Russian.

Sabzi F, Khosravi D. Huge dissected ascending aorta associated with pseudo aneurysm and aortic coarctation feridoun. Acta Med Iran. 2015;53(7):444–7.

Stiver K, Bayram M, Orsinelli D. Aortic root bentall graft disarticulation following repair of type a aortic dissection. Echocardiography. 2010;27(2):E27–9.

Thorsgard ME, Morrissette GJ, Sun B, et al. Impact of intraoperative transesophageal echocardiography on acute type A aortic dissection. J Cardiothorac Vasc Anesth. 2014;28(5):1203–7.

Tourmousoglou C, Meineri M, Feindel C, Brister S. Repair of aorto-left ventricular and aorto-right ventricular fistulas following prosthetic valve endocarditis. J Card Surg. 2013;28(6):654–9.

Coronary Artery Diseases

6

Abstract

This chapter, Coronary Artery Disease, covers ischemic MR, LV apex akinesis having Dor's procedure, and a post myocardial infarction VSD.

Complications of myocardial infarction must be aware of besides the wall motion. When evaluating ventricular function in the perioperative period, changes in preload, pacing, respiration, and performance are dynamic and are affected significantly by the physiologic changes.

6.1 Ischemic Mitral Regurgitation Having Mitral Repair

A 61-year-old man suffered from chest tightness. Triple coronary artery disease with recent myocardial infarction was diagnosed at another hospital. Auscultation: regular heart beat with a grade 3 murmur over apex. ECG: sinus rhythm, first degree AV block, clockwise rotation and non-specific ST-T change. Chest X ray: cardiomegaly with LV enlargement. Operation: CABG x4 (LIMA to diagonal branch, SVG to LAD, SVG to OM and SVG to RCA) and MV repair.

Electronic supplementary material The online version of this chapter (doi:10.1007/978-981-10-0587-9_6) contains supplementary material, which is available to authorized users.

W.-H. Yin, M.-C. Hsiung, *Atlas of Perioperative 3D Transesophageal Echocardiography*,
DOI 10.1007/978-981-10-0587-9_6

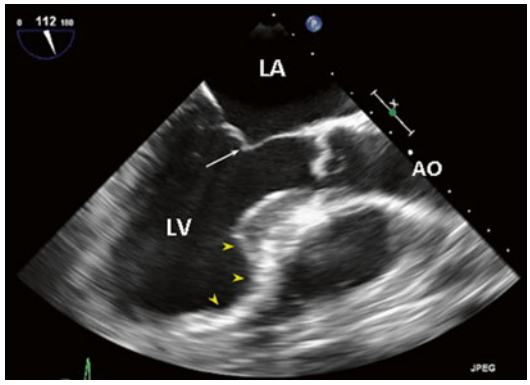

Fig. 6.1 Two-dimensional transesophageal echocardiography (2D TEE), long-axis view, showed a small apical anterior septal aneurysm (*yellow arrows*) and "sea gull" sign of anterior mitral leaflet (*white arrow*) which caused by ischemic tethering of leaflet with chordae

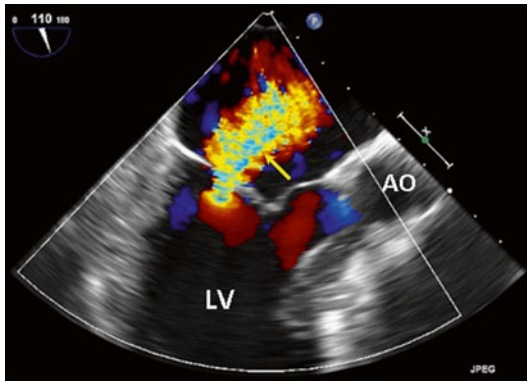

Fig. 6.2 2D TEE color Doppler, long-axis view, showed severe ischemic MR (*arrow*)

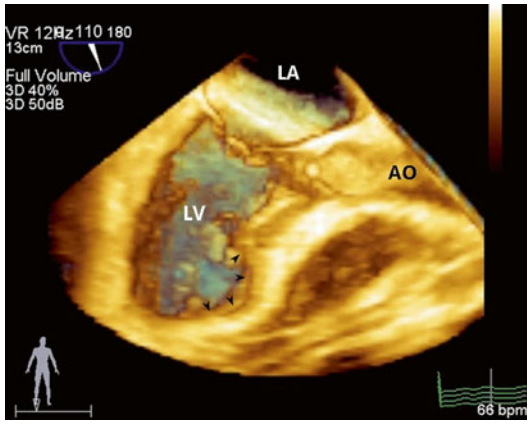

Fig. 6.3 3D TEE, long-axis view, showed a small apical anterior septal aneurysm (*arrows*)

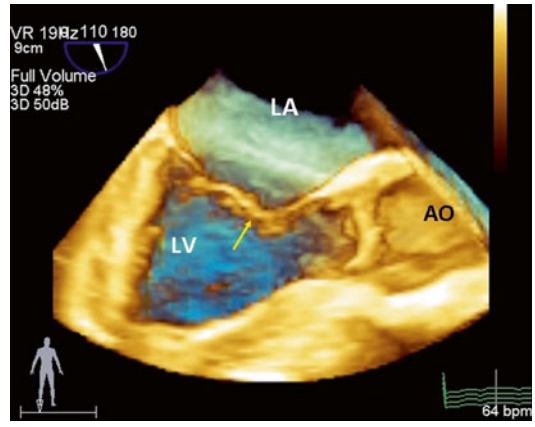

Fig. 6.4 3D TEE, long-axis view, showed "sea gull" sign of anterior mitral leaflet (*arrow*) which caused by ischemic tethering of leaflet with chordae

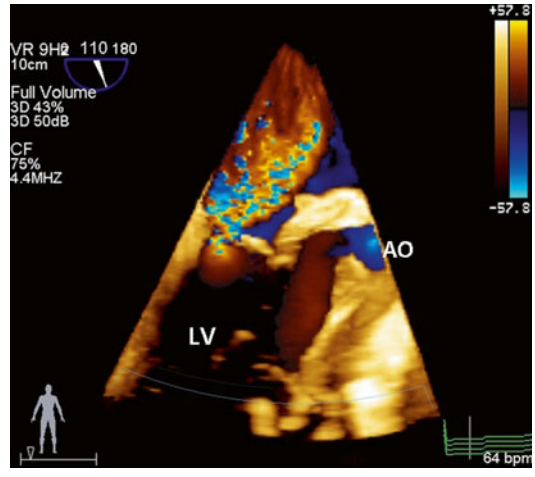

Fig. 6.5 3D TEE color Doppler, long-axis view, showed severe ischemic MR

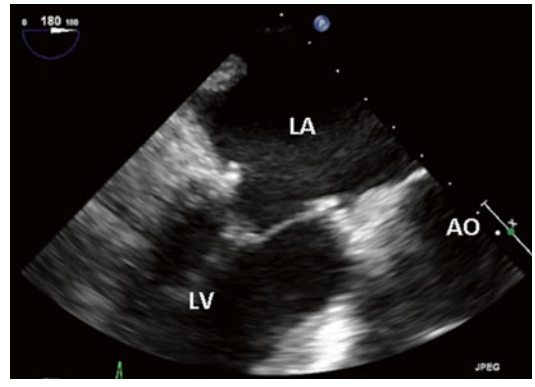

Fig. 6.6 2D TEE, long-axis view, status post CABG and MV repair, showed normal MV function

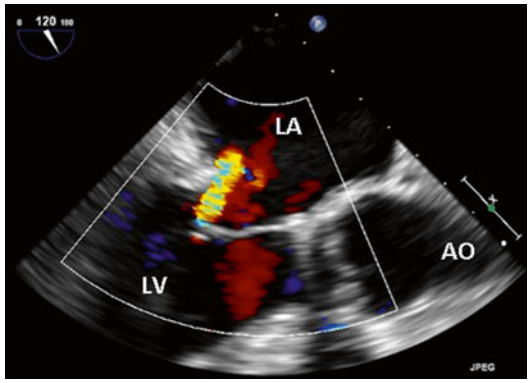

Fig. 6.7 2D TEE color Doppler, long-axis view, status post CABG and MV repair, showed mild MR

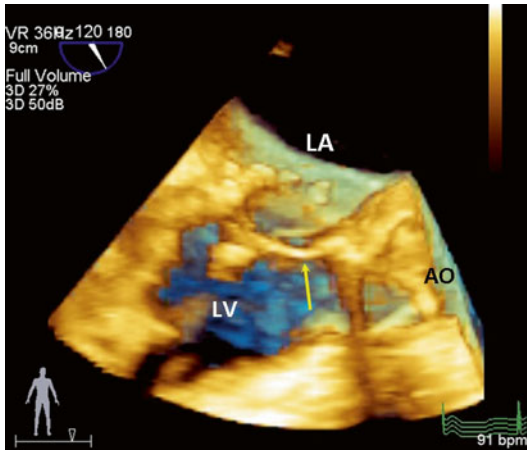

Fig. 6.8 3D TEE, long-axis view, status post CABG and MV repair, the physic ring (*arrow*) was seen

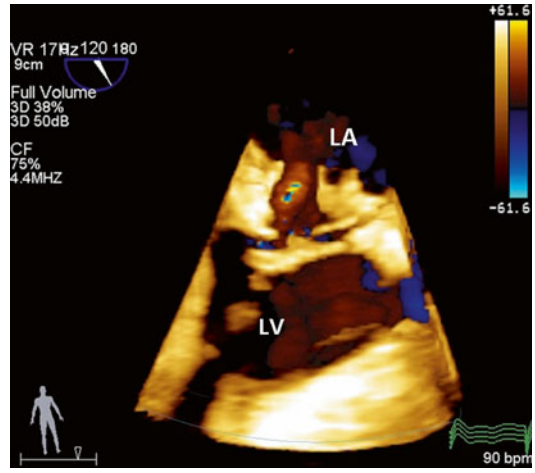

Fig. 6.9 3D TEE color Doppler, long-axis view, status post CABG and MV repair, showed mild MR

Tips

Examination of mitral leaflet, subvalvular apparatus, and ventricular function are all essential to evaluate the etiology of MR.

6.2 Left Ventricular Apex Akinesis with Thrombus Having Dor Procedure

A 24-year-old man with gout suffered from severe chest pain, cold sweating, vomiting and mild dyspnea. Emergent cardiac catheterization showed LAD coronary aneurysm and thrombus impaction. But PTCA and thrombus suction failed. Auscultation: regular heart beat without significant murmur. ECG: sinus rhythm and old anterior wall myocardial infarction with aneurysm formation. Chest CT: dilated cardiac apex and prominent left coronary artery. Operation: CABG x1 (SVG to LAD), Dor procedure and removal of LV thrombus.

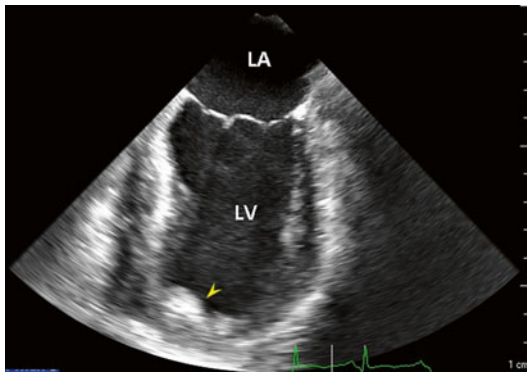

Fig. 6.10 Two-dimensional transesophageal echocardiography (2D TEE), two-chamber view, showed LV apex akinesis with thrombus (*arrow*) seen

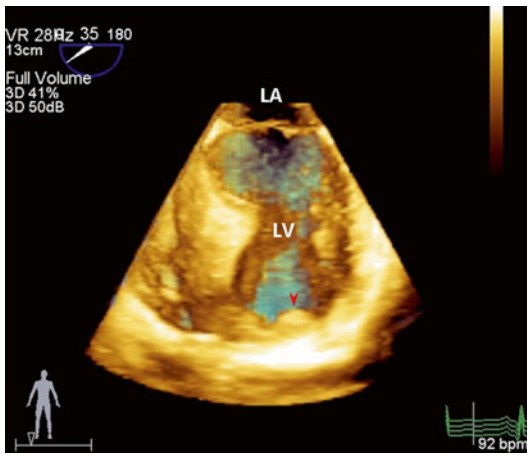

Fig. 6.11 3D TEE, two-chamber view, showed LV apex akinesis with thrombus (*arrow*) seen

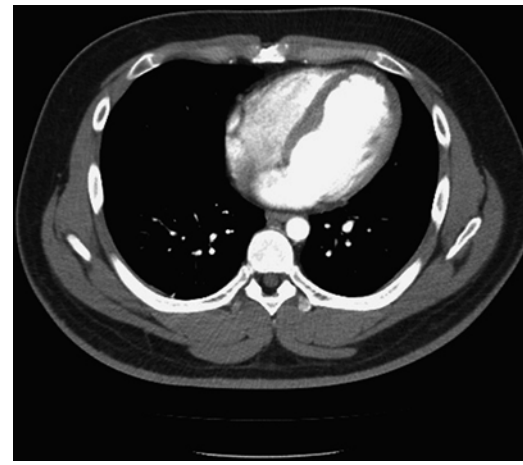

Fig. 6.12 Contrast-enhanced CT, showed dilated LV apex

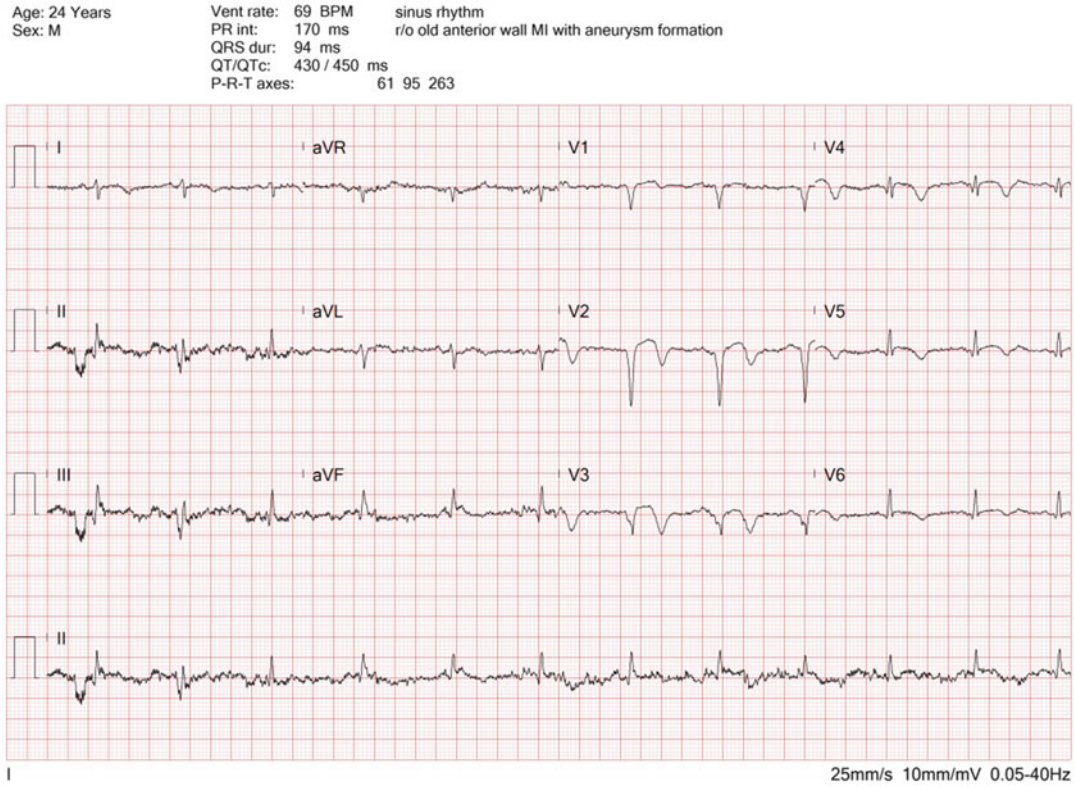

Fig. 6.13 ECG showed old anterior wall myocardial infarction with aneurysm formation

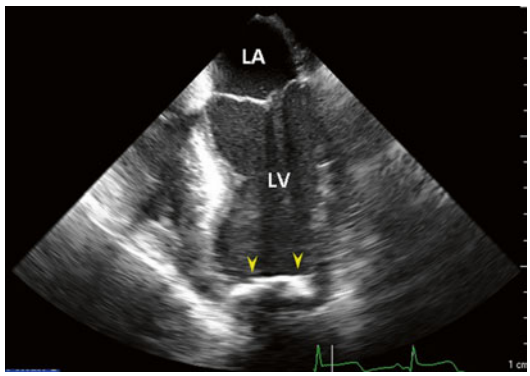

Fig. 6.14 2D TEE, two-chamber view, status post Dor's procedure, showed patch repair of LV apex (*arrows*) to reduce the akinetic region therefore increase the ejection fraction

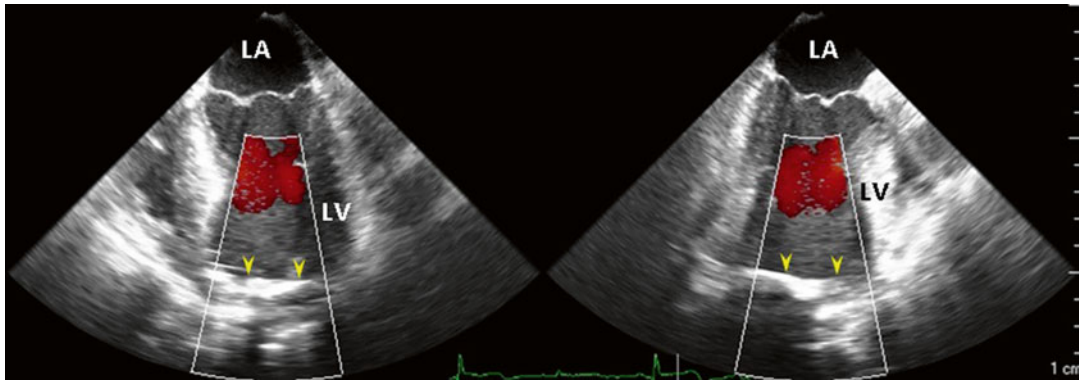

Fig. 6.15 2D TEE color Doppler, x-plane view, status post Dor's procedure, showed patch repair of LV apex (*arrows*) to separate the akinetic apex from normal region and increase the stroke volume

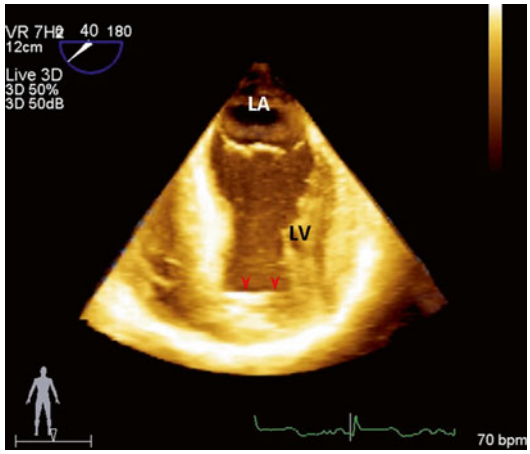

Fig. 6.16 3D TEE, two-chamber view, status post Dor's procedure, showed patch repair at LV apex (*arrows*)

Tips

Poor cardiac function will cause blood deposition and increase the possibility of thrombus formation. Understanding of cardiacmuscular segment model helps determine associated coronary abnormalities.

6.3 A Post Myocardial Infarction Ventricular Septal Defect Having Occluder Implantation

The 49-year-old woman denied any systemic history. She suffered from chest tightness, chest distress, shortness of breath and exertional dyspnea recently. Auscultation: irregular heart beat with a holosystolic murmur over apex. ECG: sinus tachycardia, complete right bundle branch block and anterior wall ST elevation myocardial infarction. Chest X ray: cardiomegaly. Cardiac catheterization: dyskinesis of LV apex and hypokinesis of LV anterior wall, moderate to severe LV systolic dysfunction and a ventricular septal defect (VSD). Treatment: VSD occluder implantation and PCI of LAD.

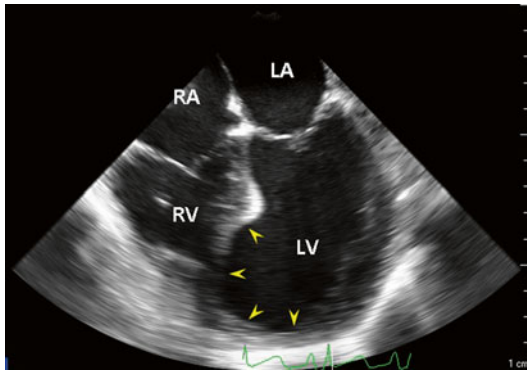

Fig. 6.17 Two-dimensional transesophageal echocardiography (2D TEE), four-chamber view, showed myocardial infarction with LV apical septum akinesis (*arrows*)

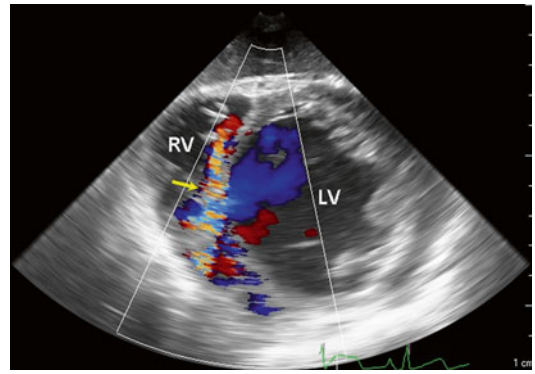

Fig. 6.19 2D TEE color Doppler, transgastric short-axis view, showed a post myocardial infarction VSD with a left to right shunt (*arrow*)

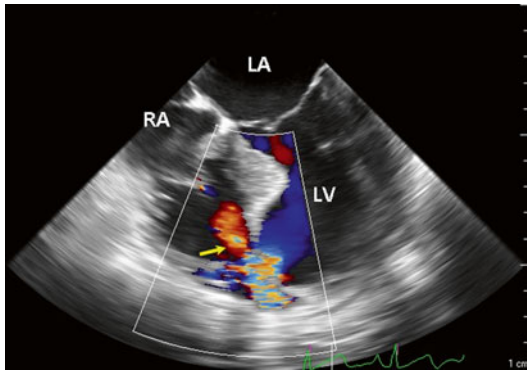

Fig. 6.18 2D TEE color Doppler, four-chamber view, showed a post myocardial infarction apical VSD with a left to right shunt (*arrow*)

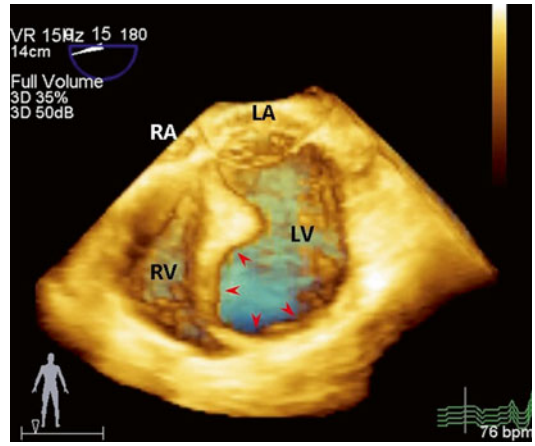

Fig. 6.20 3D TEE, four-chamber view, showed myocardial infarction with LV apical septum akinesis (*arrows*)

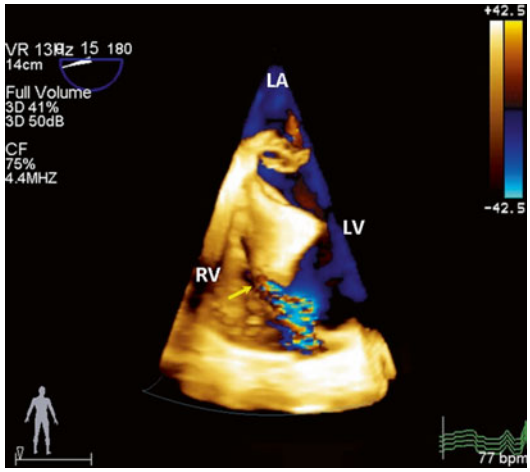

Fig. 6.21 3D TEE color Doppler, four-chamber view, showed a post myocardial infarction apical VSD with a left to right shunt (*arrow*)

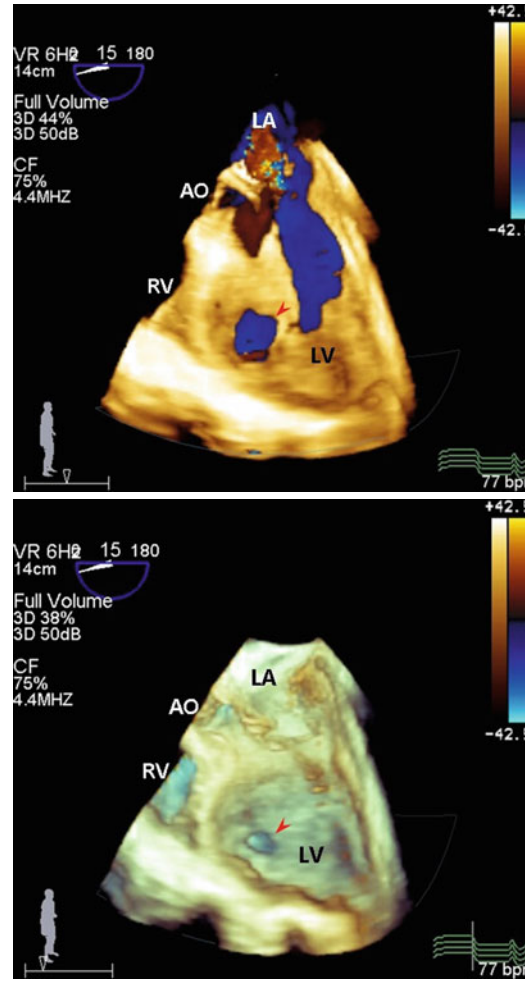

Figs. 6.22 and 6.23 3D TEE color Doppler (*above*) and color suppressed image (*below*), viewed from LV perspective, showed the VSD (*arrows*) at apex

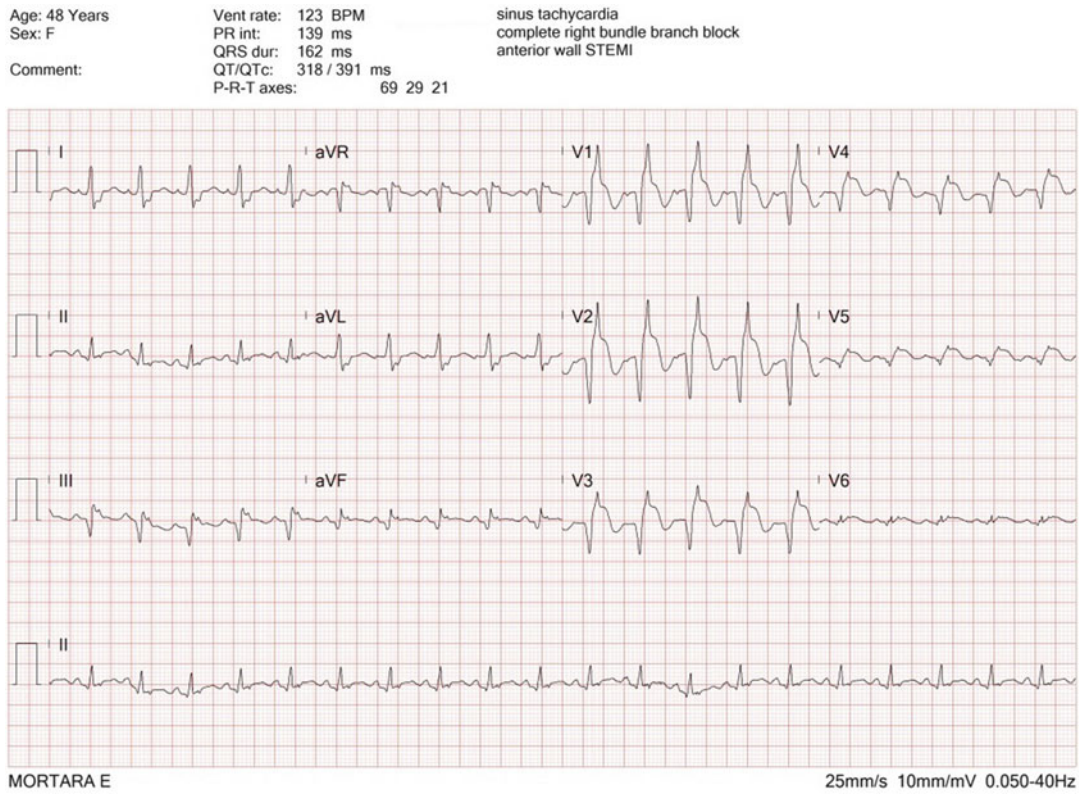

Fig. 6.24 ECG showed anterior wall ST elevation myocardial infarction

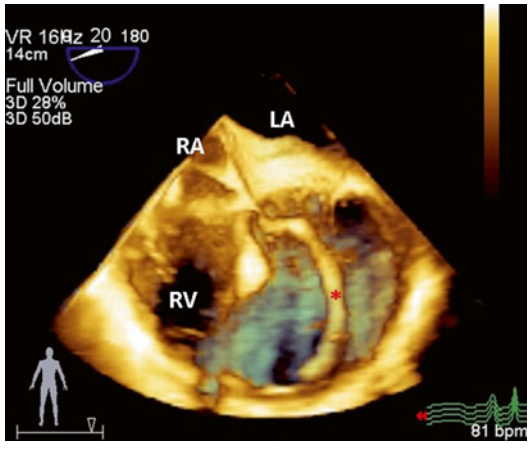

Fig. 6.25 3D TEE, four-chamber view, during occluder implantation, showed the guiding catheter (*) in LV

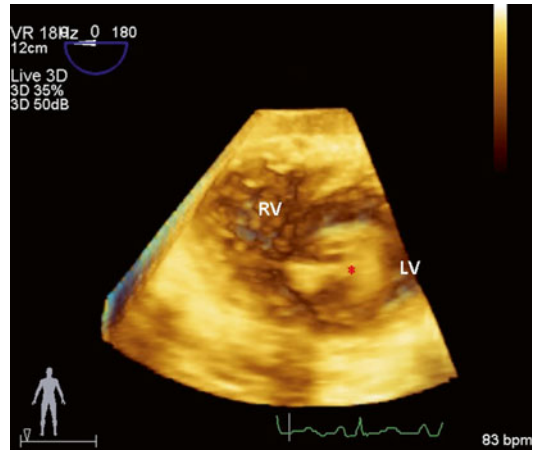

Fig. 6.26 3D TEE, transgastric short-axis view, during the procedure, showed the occluder (*) was deployed to occlude the apical VSD

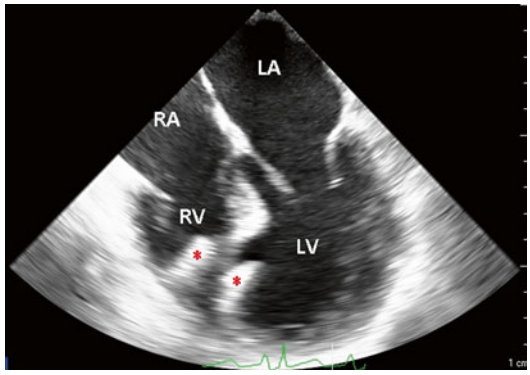

Fig. 6.27 2D TEE, four-chamber view, status post occluder (*) implantation

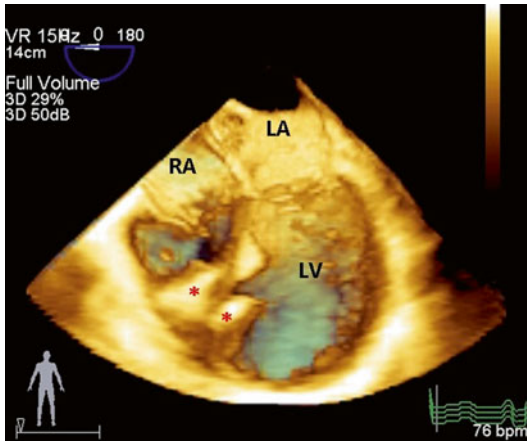

Fig. 6.28 3D TEE, four-chamber view, status post occluder (*) implantation

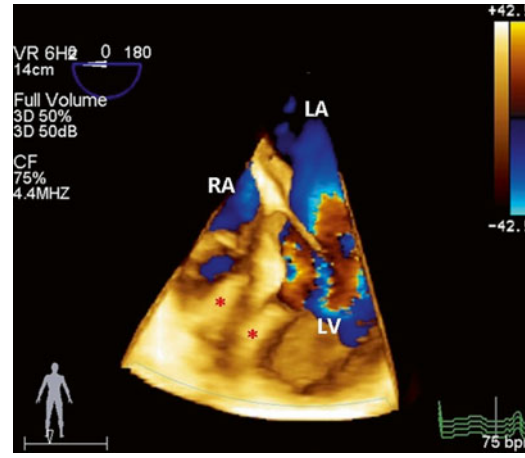

Fig. 6.29 3D TEE color Doppler, four-chamber view, status post occluder (*) implantation, showed only trivial residual shunt

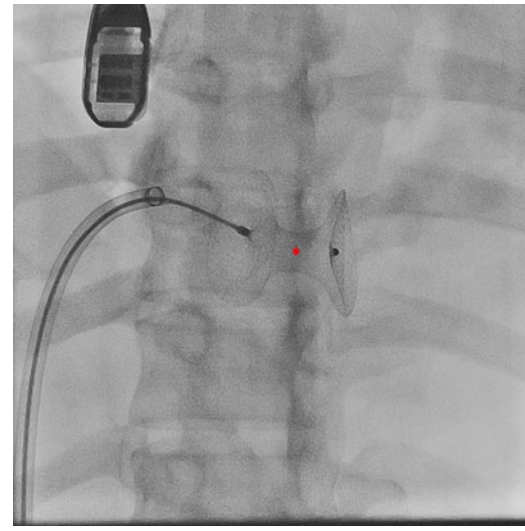

Fig. 6.30 Fluoroscopy, status post occluder implantation, showed the deployed occluder (*)

Tips

VSD in this case is a complication of myocardial infarction. Transgastric view can show the VSD directly assisted by 3-D TEE in determination of the VSD number, size, location, and associated lesions.

Suggested Reading

Baldasare MD, Polyakov M, Laub GW, et al. Percutaneous repair of post-myocardial infarction ventricular septal defect: current approaches and future perspectives. Tex Heart Inst J. 2014;41(6):613–9.

Egbe AC, Poterucha JT, Rihal CS, et al. Transcatheter closure of postmyocardial infarction, iatrogenic, and postoperative ventricular septal defects: The Mayo Clinic experience. Catheter Cardiovasc Interv. 2015;86:1264–70.

Fattouch K, Castrovinci S, Murana G, et al. Relocation of papillary muscles for ischemic mitral valve regurgitation: the role of three-dimensional transesophageal echocardiography. Innovations (Phila). 2014;9(1):54–9.

Gianstefani S, Douiri A, Delithanasis I, et al. Incidence and predictors of early left ventricular thrombus after ST-elevation myocardial infarction in the contemporary era of primary percutaneous coronary intervention. Am J Cardiol. 2014;113(7):1111–6.

Grayburn PA, She L, Roberts BJ, et al. Comparison of transesophageal and transthoracic echocardiographic measurements of mechanism and severity of mitral regurgitation in ischemic cardiomyopathy (from the surgical treatment of ischemic heart failure trial). Am J Cardiol. 2015;116(6):913–8.

Osaki S, Edwards NM, Kohmoto T. Strategies for left ventricular assist device insertion after the Dor procedure. J Heart Lung Transplant. 2009;28(5):520–2.

Shabestari MM, Ghaderi F, Hamedanchi A. Transcatheter closure of postinfarction ventricular septal defect: a case report and review of literature. J Cardiovasc Thorac Res. 2015;7(2):75–7.

Trivedi KR, Aldebert P, Riberi A, et al. Sequential management of post-myocardial infarction ventricular septal defects. Arch Cardiovasc Dis. 2015;108(5):321–30.

Zeng X, Nunes MC, Dent J, et al. Asymmetric versus symmetric tethering patterns in ischemic mitral regurgitation: geometric differences from three-dimensional transesophageal echocardiography. J Am Soc Echocardiogr. 2014;27(4):367–75.

Zou H, Zhang Y, Tong J, Liu Z. Multidetector computed tomography for detecting left atrial/left atrial appendage thrombus: a meta-analysis. Intern Med J. 2015;45(10):1044–53.

Congenital Heart Diseases 7

Abstract

Congenital heart diseases are discussed in this chapter, which covers case with subaortic stenosis, and cases with ASDs or VSDs received occluder implantation or patch repair.

3D TEE can carefully measure the morphology and pathology of the ASDs and VSDs from varies perspectives, detect any intraprocedure accidental event which should be solved immediately, and evaluate the result of the treatment to confirm that no residual remains

7.1 Patent Foramen Ovale Having Occluder Implantation

A 22-year-old man with funnel chest status post operation had a patent foramen ovale (PFO). He admitted for chest discomfort and dizziness. Auscultation: regular heart beat without significant murmur. ECG: sinus bradycardia. Treatment: PFO occluder.

Electronic supplementary material The online version of this chapter (doi:10.1007/978-981-10-0587-9_7) contains supplementary material, which is available to authorized users.

W.-H. Yin, M.-C. Hsiung, *Atlas of Perioperative 3D Transesophageal Echocardiography*,
DOI 10.1007/978-981-10-0587-9_7

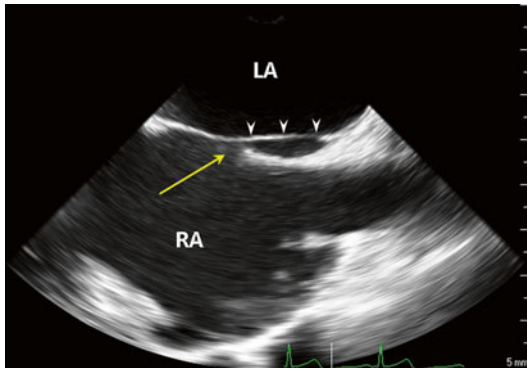

Fig. 7.1 Two-dimensional transesophageal (2D TEE), bicaval view, showed a PFO (*yellow arrow*) covered by a flaplike structure (*white arrows*)

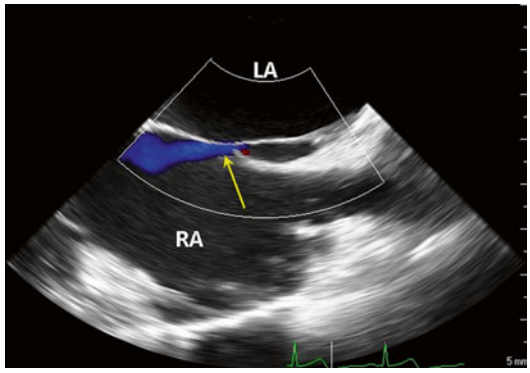

Fig. 7.2 2D TEE color Doppler, bicaval view, showed a left-to-right shunt (*arrow*) across the PFO

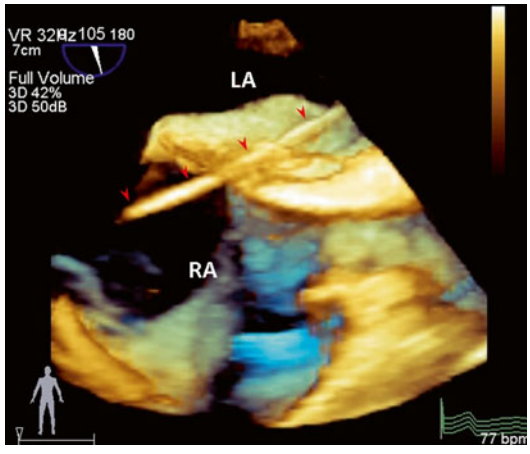

Fig. 7.3 3D TEE, bicaval view, during the occluder implantation, showed a guiding catheter (*arrows*) across the PFO

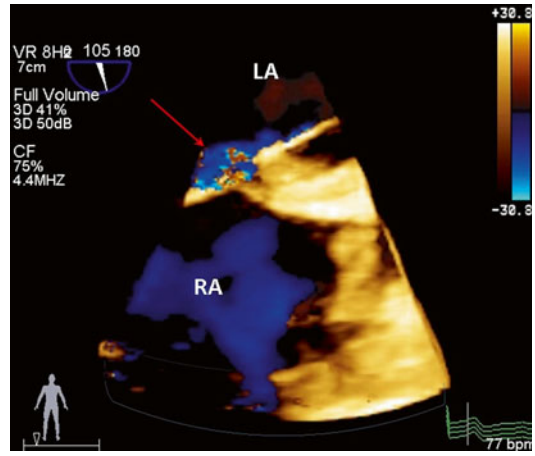

Fig. 7.4 3D TEE color Doppler, bicaval view, during the occluder implantation, showed a guiding catheter across the PFO with a left- to-right shunt (*arrow*)

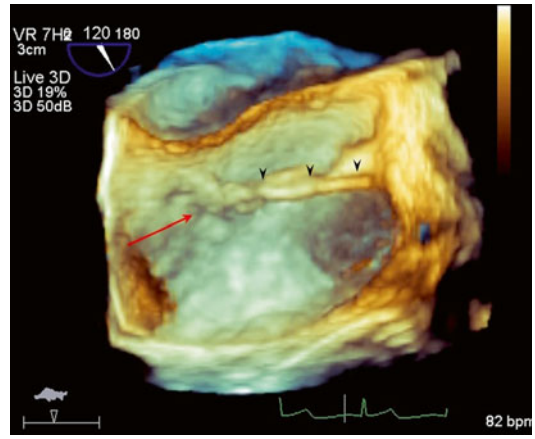

Fig. 7.5 3D TEE, view from LA perspective, during the occluder implantation, showed a guiding catheter (*black arrows*) across the PFO (*red arrow*)

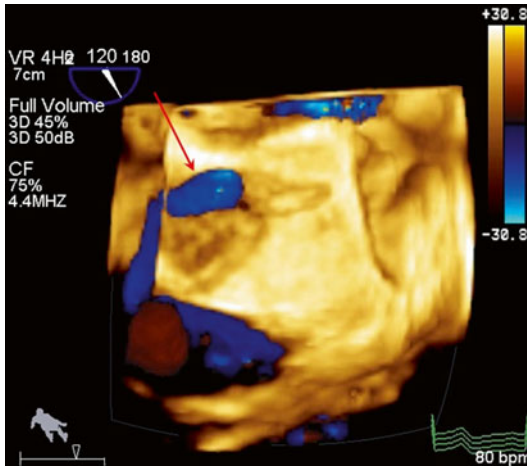

Fig. 7.6 3D TEE color Doppler, view from LA perspective, during the occluder implantation, showed a left-to-right shunt across the PFO (*arrow*)

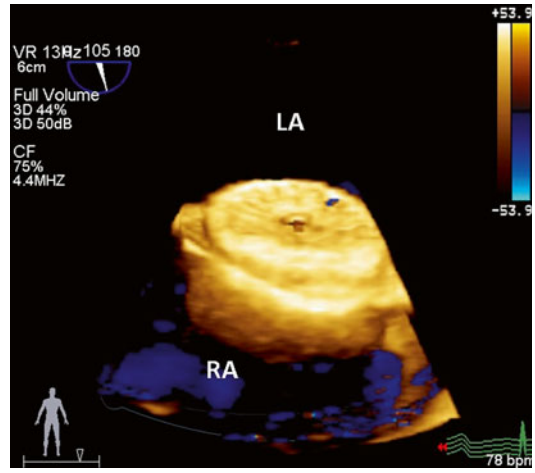

Fig. 7.9 3D TEE color Doppler, bicaval view, status post occluder implantation, showed the PFO was blocked by the occluder without residual

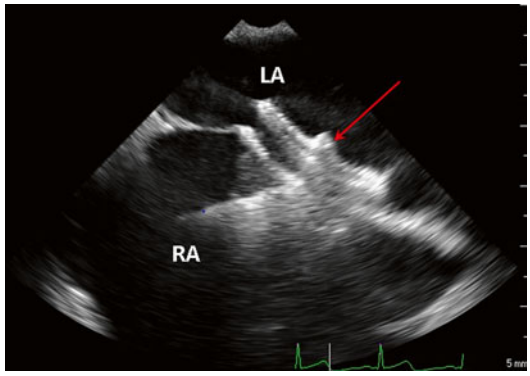

Fig. 7.7 2D TEE, bicaval view, status post occluder implantation, showed the PFO was blocked by the occluder (*arrow*)

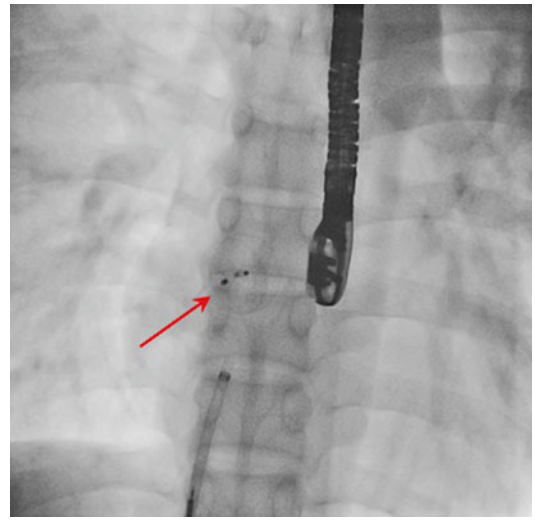

Fig. 7.10 Fluoroscopy, status post occluder implantation, showed the occluder (*arrow*) was successfully deployed

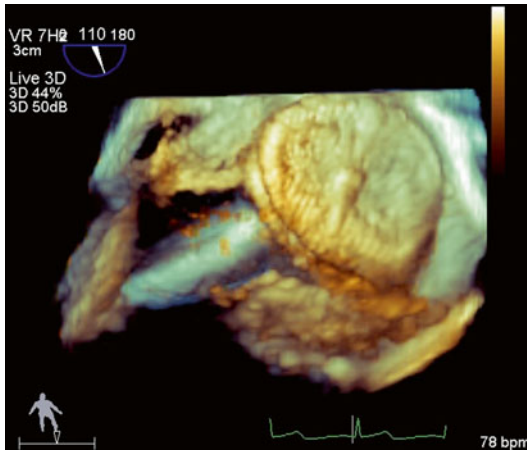

Fig. 7.8 3D TEE, view from LA perspective, status post occluder implantation, showed the occluder was successfully deployed

Tips

Bicaval view has the advantage of providing high quality image of the interatrial septum as the ultrasound beam is perpendicular to the septum. Transcatheter treatment of PFO is safe, whereas patients with PFO are at high risk of stroke.

7.2 Primum Atrial Septal Defect

A 48-year-old woman admitted for exertional dyspnea and chest pain. Auscultation: regular heart beat with a grade 3/6 systolic murmur over apex. ECG: sinus rhythm and incomplete right bundle branch block. Chest X ray: mild cardiomegaly. Cardiac catheterization: atrial septal defect (ASD) and moderate to severe MR. Operation: ASD patch repair, MV and TV repair.

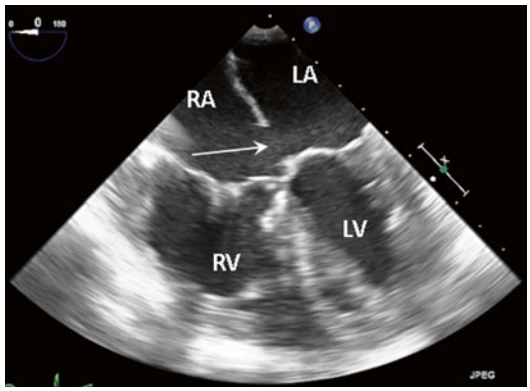

Fig. 7.11 Two-dimensional transesophageal echocardiography (2D TEE), four-chamber view, showed a primum ASD (*arrow*) with the defect adjacent to the central fibrous body. Dilated RA and RV were also present

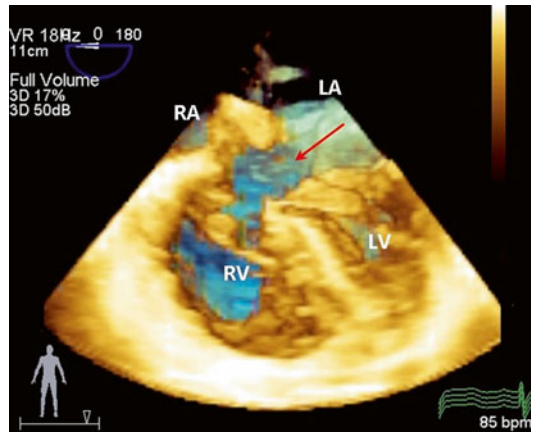

Fig. 7.13 3D TEE, four-chamber view, showed a primum ASD (*arrow*) with the defect adjacent to the central fibrous body

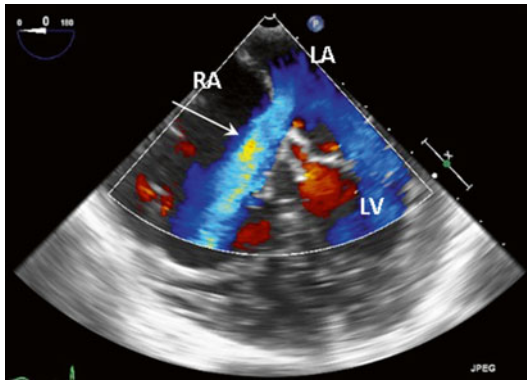

Fig. 7.12 2D TEE color Doppler, four-chamber view, showed a primum ASD with a left-to-right shunt (*arrow*) across it into enlarged RA and RV

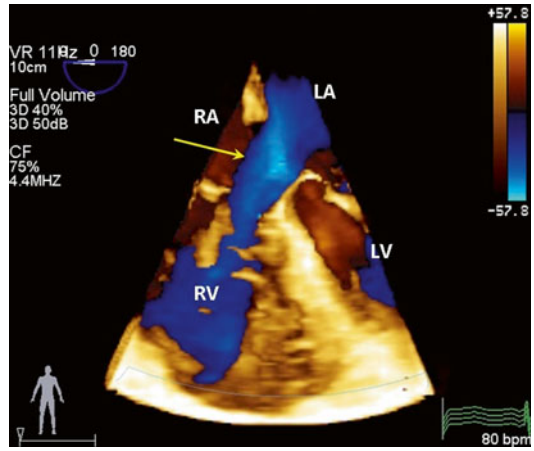

Fig. 7.14 3D TEE color Doppler, four-chamber view, showed a primum ASD with a left-to-right shunt (*arrow*) across it into enlarged RA and RV

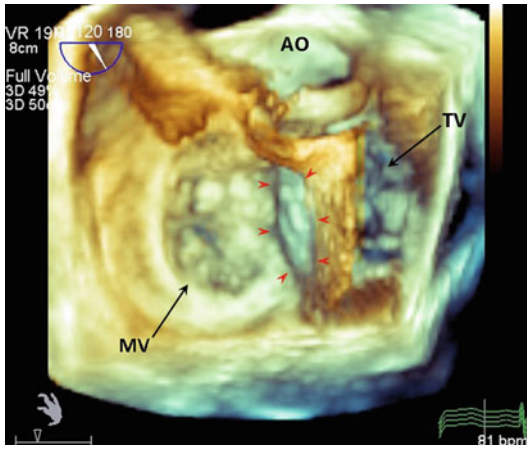

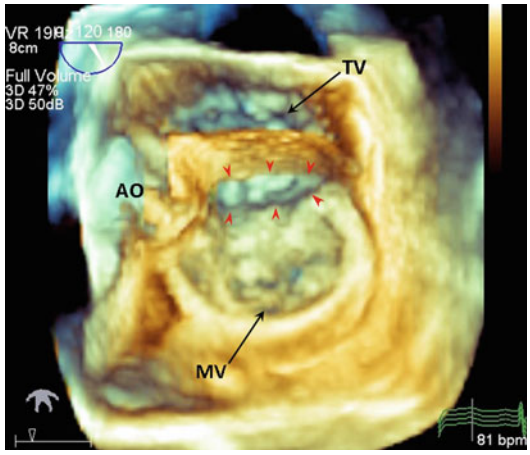

Figs. 7.15 and 7.16 3D TEE, view from atrial perspective, showed a primum ASD (*arrows*) near atrioventricular connection

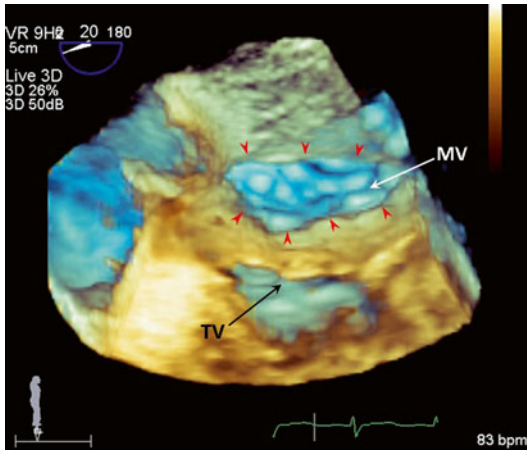

Fig. 7.17 3D TEE, view from right side perspective, showed a primum ASD (*arrows*) near atrioventricular connection

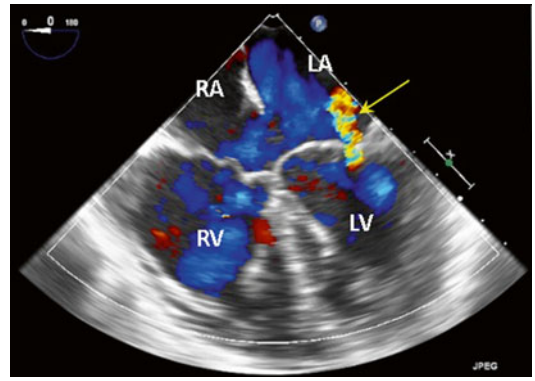

Fig. 7.18 2D TEE color Doppler, four-chamber view, showed moderate to severe MR (*arrow*) caused by valve abnormity associated with primum ASD

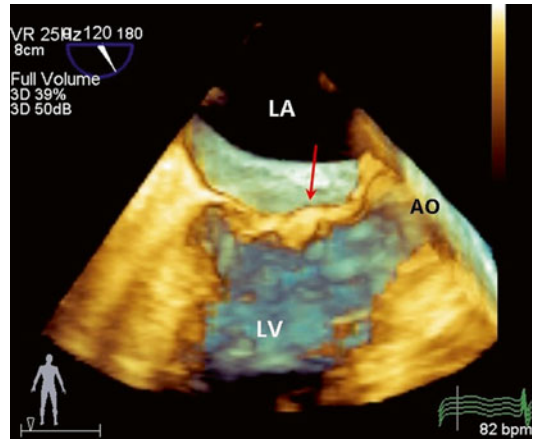

Fig. 7.19 3D TEE, long-axis view, showed MV abnormity (*arrow*) associated with primum ASD

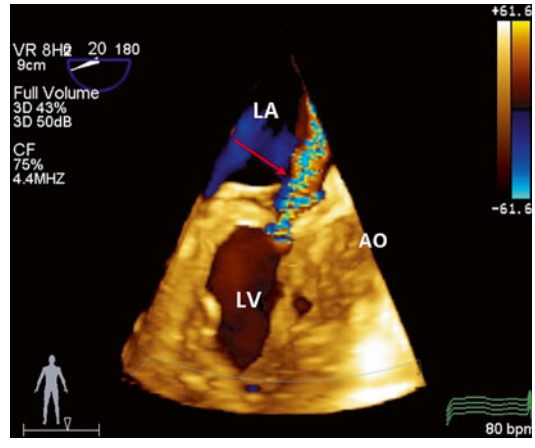

Fig. 7.20 3D TEE color Doppler, long-axis view, showed moderate to severe MR (*arrow*) caused by valve abnormity associated with primum ASD

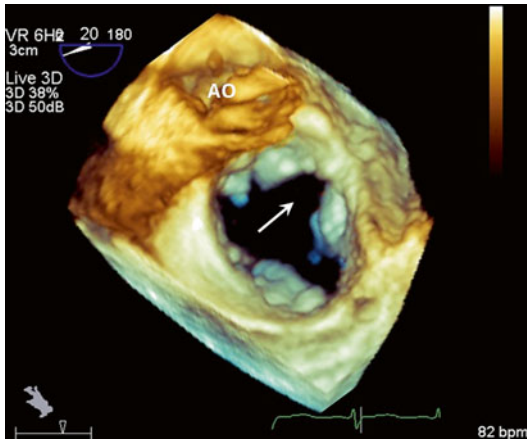

Fig. 7.21 3D TEE, en face view, showed cleft MV with discontinuity of the anterior mitral leaflet (*arrow*)

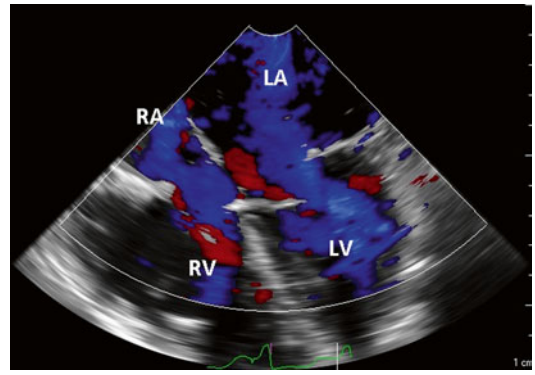

Fig. 7.24 2D TEE color Doppler, four-chamber view, status post ASD patch repair, MV and TV repair, showed minimal ASD residual and MR

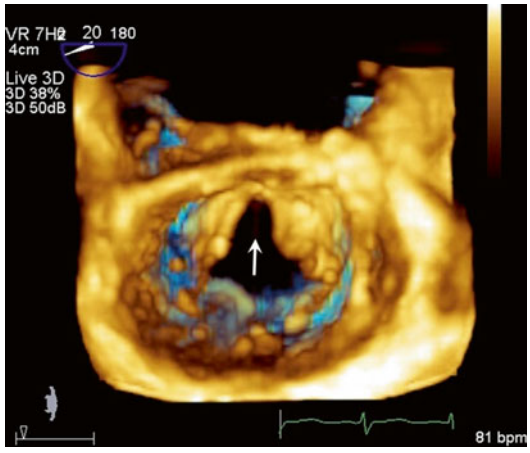

Fig. 7.22 3D TEE, view from ventricular perspective, showed cleft MV with discontinuity of the anterior mitral leaflet (*arrow*)

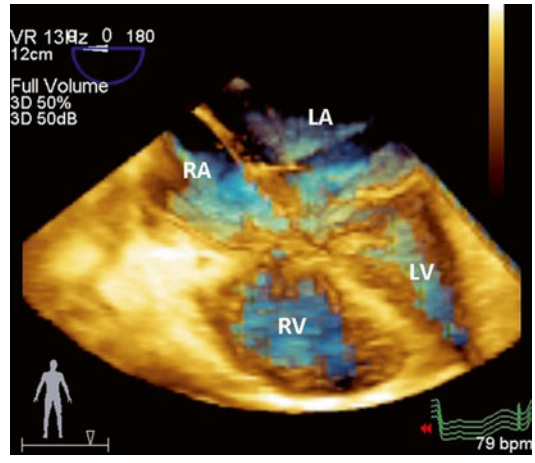

Fig. 7.25 3D TEE, four-chamber view, status post ASD patch repair, MV and TV repair, showed intact interatrial septum and normal MV function

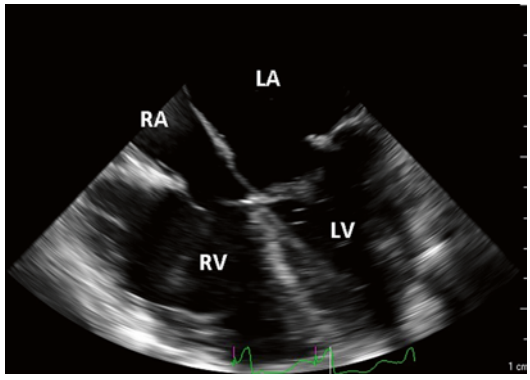

Fig. 7.23 2D TEE, four-chamber view, status post ASD patch repair, MV and TV repair, showed intact interatrial septum and normal MV function

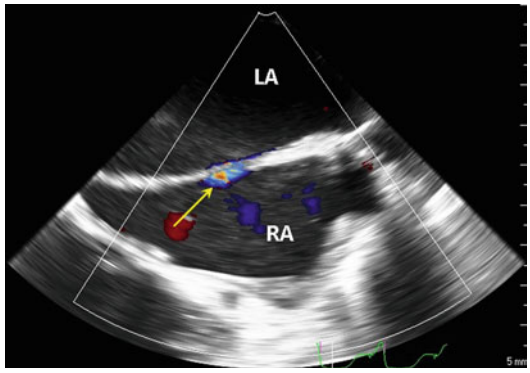

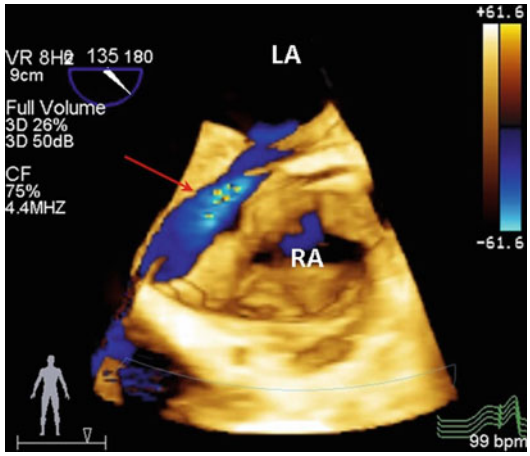

Figs. 7.26 and 7.27 2D (*above*) and 3D (*below*) TEE color Doppler, status post ASD patch repair, MV and TV repair, showed minimal ASD residual (*arrow*)

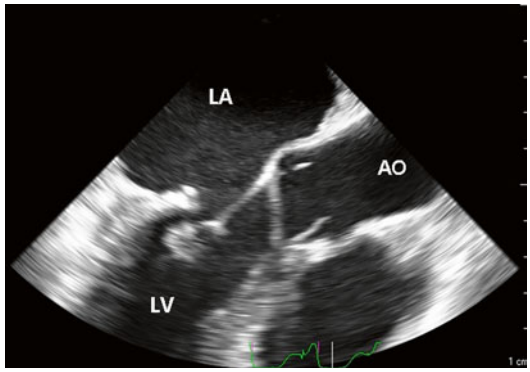

Fig. 7.28 2D TEE long-axis view, status post ASD patch repair, MV and TV repair, showed normal MV function

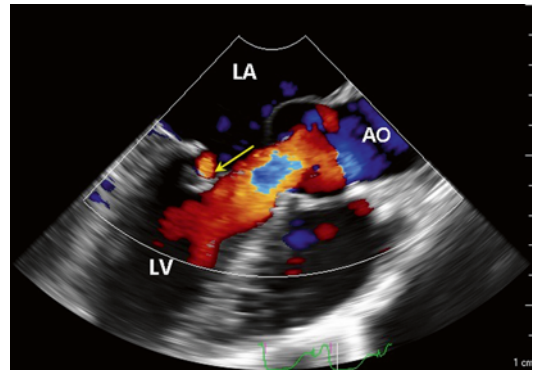

Fig. 7.29 2D TEE color Doppler, long- axis view, status post ASD patch repair, MV and TV repair, showed minimal MR (*arrow*)

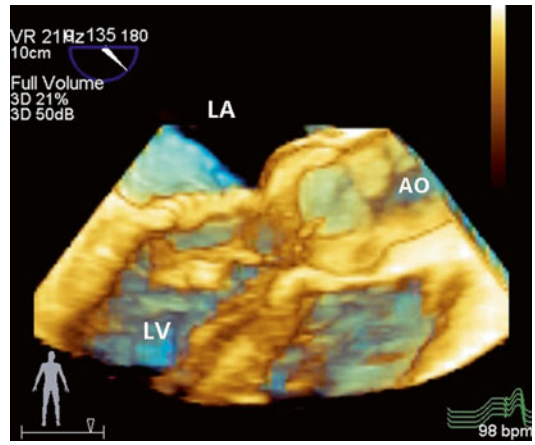

Fig. 7.30 3D TEE, long-axis view, status post ASD patch repair, MV and TV repair, showed normal MV function

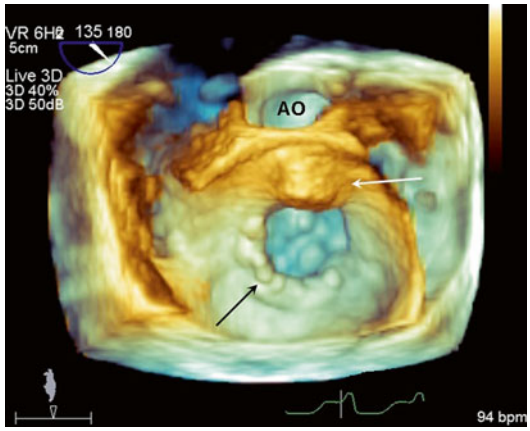

Fig. 7.31 3D TEE, en face view, status post ASD patch repair (*white arrow*) and MV repair (*black arrow*)

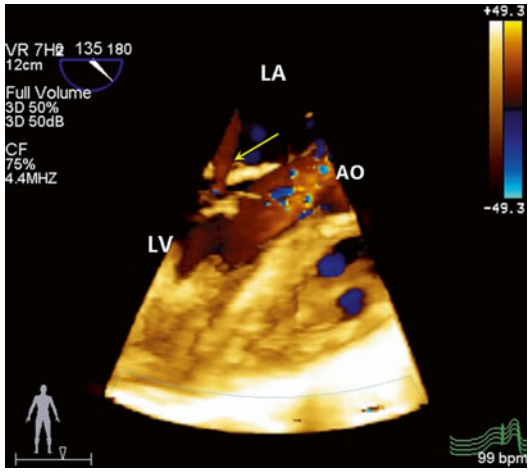

Fig. 7.32 2D TEE color Doppler, long- axis view, status post ASD patch repair, MV and TV repair, showed minimal MR (*arrow*)

Tips

A cleft MV can be seen carefully in 3D TEE from ventricular perspective. There is significant thickening and fibrosis along the edges of the cleft.

7.3 Secundum Atrial Septal Defect Having Occluder Implantation

An 89-year-old woman with a history of atrial septal defect (ASD) and hypertension suffered from shortness of breath and chest discomfort. Auscultation: regular heart beat with a grade 2/6 systolic murmur over second interspace. ECG: sinus bradycardia, first degree AV block, clock rotation and myocardial ischemia. Chest X ray: cardiomegaly and engorgement of pulmonary trunk and bilateral pulmonary arteries. Cardiac catheterization: single vessel coronary artery disease. Treatment: ASD occluder.

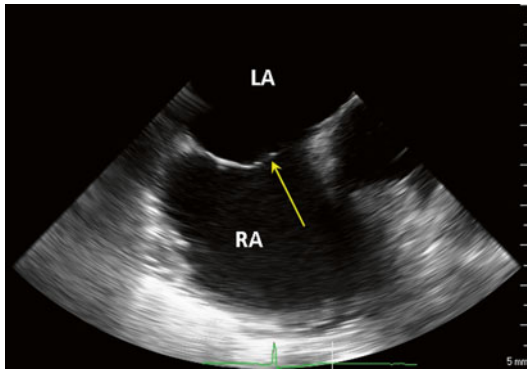

Fig. 7.33 Two-dimensional transesophageal echocardiography (2D TEE), short-axis view, showed dilated RA and a secundum ASD (*arrow*) in midsection of the atrial septum

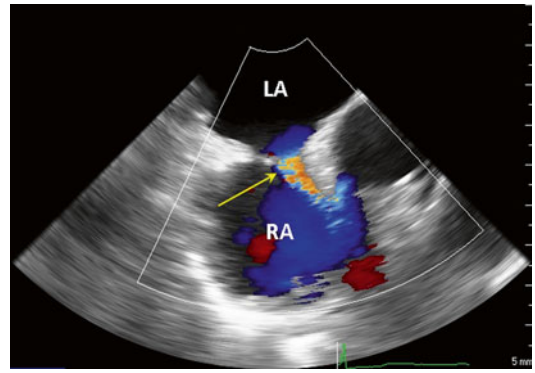

Fig. 7.35 2D TEE color Doppler, short- axis view, showed a left-to-right shunt (*arrow*) across the ASD

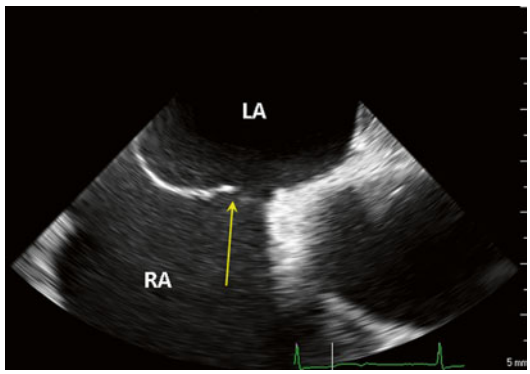

Fig. 7.34 2D TEE, short-axis view, showed a secundum ASD (*arrow*) in midsection of the atrial septum

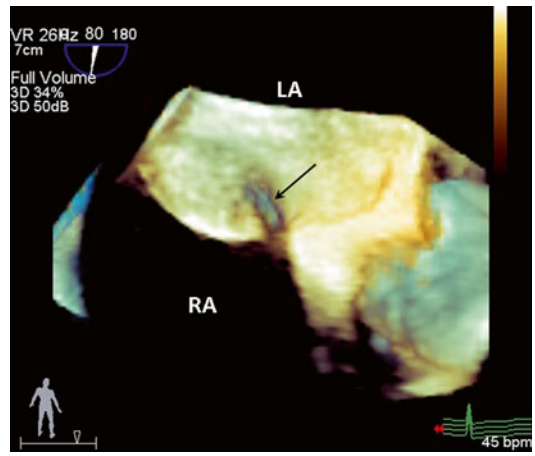

Fig. 7.36 3D TEE showed a secundum ASD (*arrow*) in midsection of the atrial septum

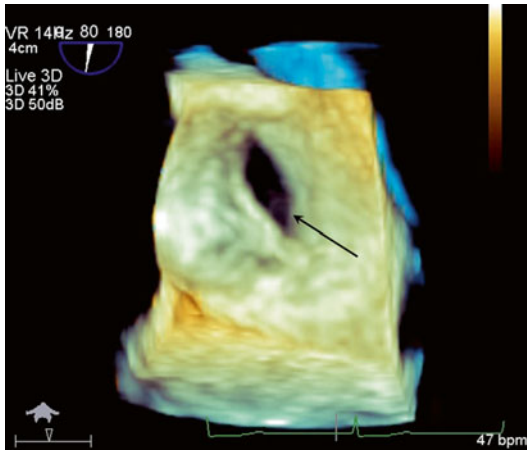

Fig. 7.37 3D TEE, view from LA perspective, showed a secundum ASD (*arrow*) in midsection of the atrial septum

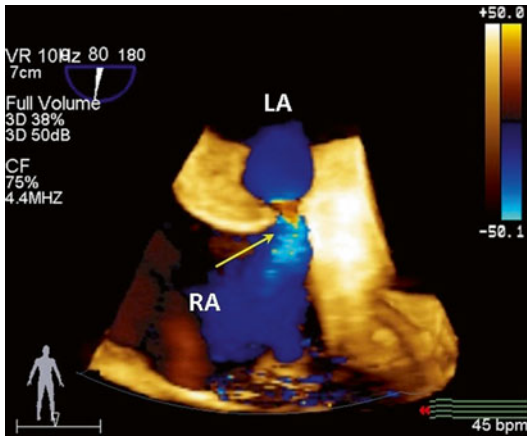

Fig. 7.38 3D TEE color Doppler showed a left-to-right shunt (*arrow*) across the ASD

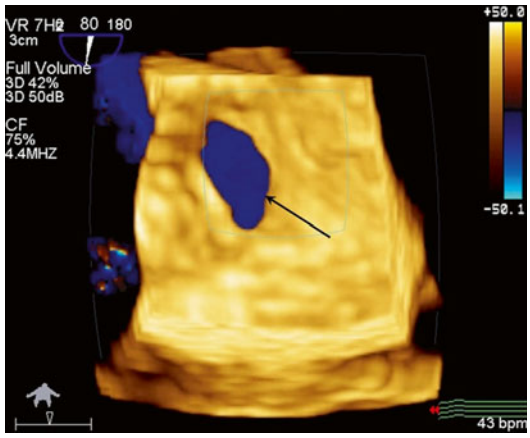

Fig. 7.39 3D TEE color Doppler, view from LA perspective, showed a continuous flow (*arrow*) across the ASD

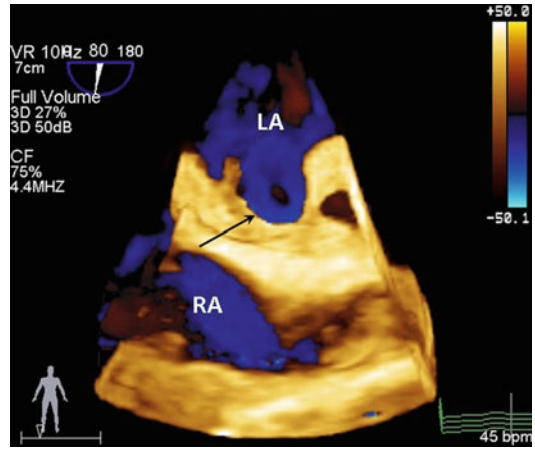

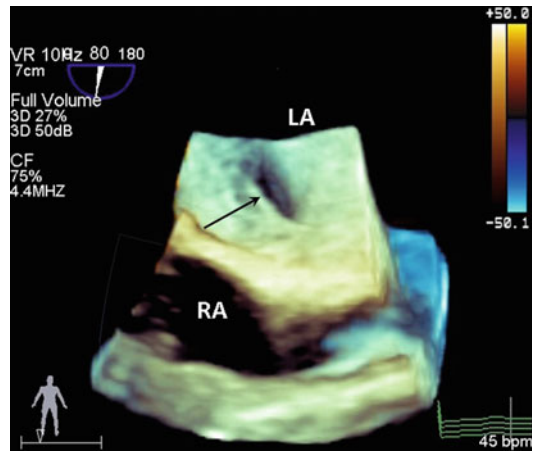

Figs. 7.40 and 7.41 3D TEE color Doppler (*above*) and color-suppressed (*below*) showed a continuous flow across the ASD (*arrow*)

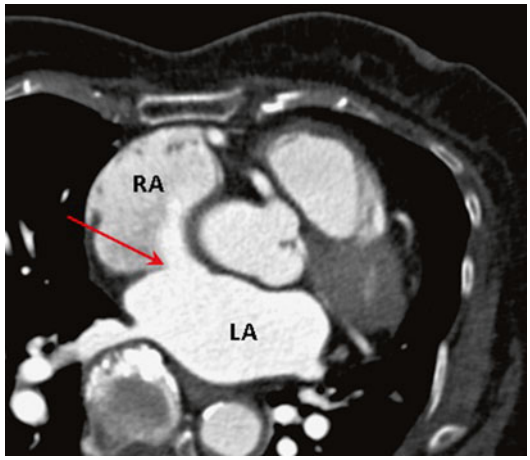

Fig. 7.42 Contrast-enhanced CT showed a secundum ASD (*arrow*) in midsection of the atrial septum

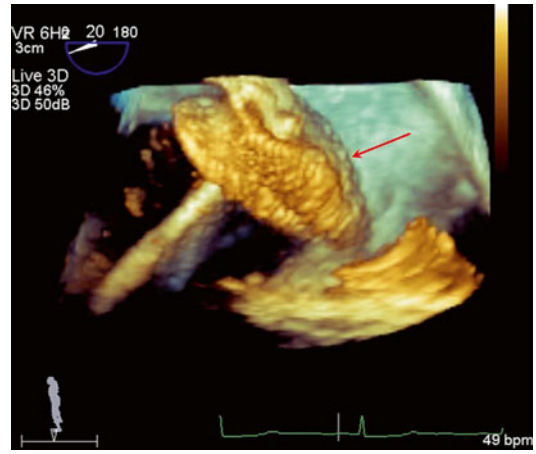

Fig. 7.44 3D TEE, view from LA perspective, during the procedure, showed the occluder (*arrow*) was deployed to occlude the secundum ASD

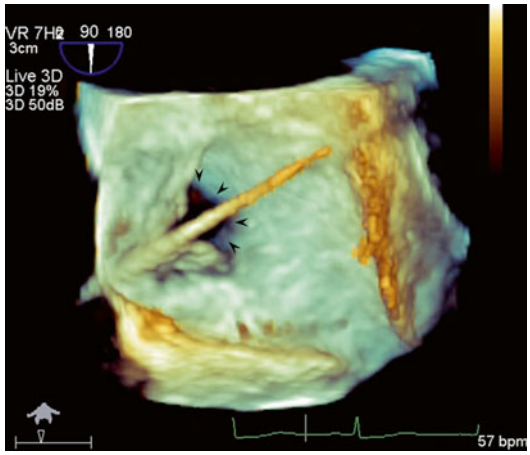

Fig. 7.43 3D TEE, view from LA perspective, during the occluder implantation procedure, showed a guiding catheter across the ASD (*arrows*)

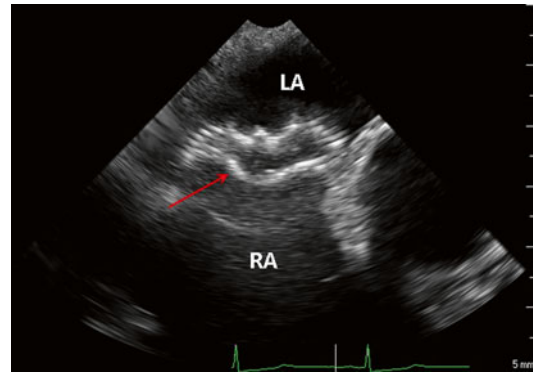

Fig. 7.45 2D TEE, status post occluder implantation, showed the secundum ASD was blocked by the occluder (*arrow*)

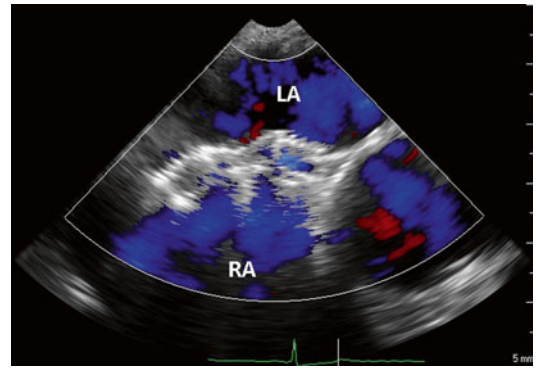

Fig. 7.46 2-D TEE color Doppler, status post occluder implantation, showed a trivial residual shunt

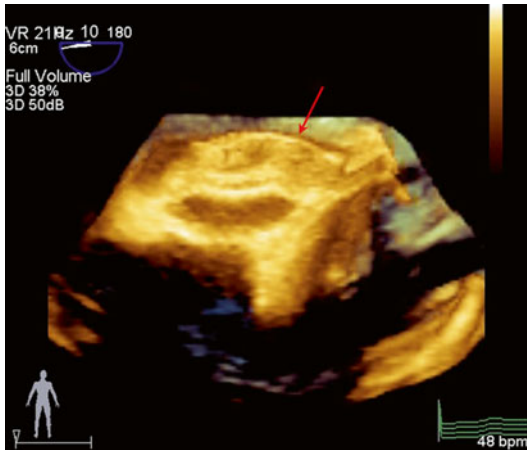

Fig. 7.47 3D TEE, status post occluder implantation, showed the secundum ASD was blocked by the occluder (*arrow*)

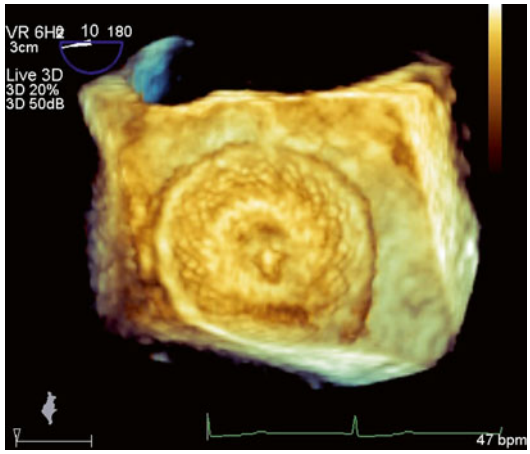

Fig. 7.48 3D TEE, view from LA perspective, status post occluder implantation, showed the secundum ASD was blocked by the occluder

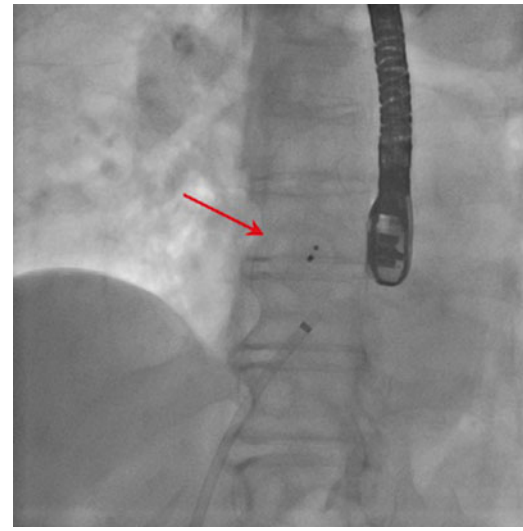

Fig. 7.49 Fluoroscopy status post occluder implantation showed the deployed occluder (*arrow*)

Tips

Secundum ASDs are located in the central portion of the interatrial septum, which are the most amendable to implant an occluder. A preprocedure TEE examination is essential to evaluate the presence of a rim to ensure that the patient is appropriate for occluder implantation.

7.4 Atrial Septal Defect Occluder Device Embolization

A 43-year-old man who was incidentally diagnosed with secundum atrial septal defects (ASDs) ("Swiss cheese" like multiple defects) presented for further evaluation. Auscultation: regular heart beat with a grade 2/4 continuous murmur over sternal border. Chest X ray: borderline cardiomegaly. Contrast-enhanced cardiac CT: coronary artery calcium score is 0 and small defects over interarterial septum. The patient refused surgical repair, percutaneous closure by occluders was arranged. During the procedure, after implantation of two devices, residual defect with significant shunting persisted. When the third device was attempted, the first one dropped into LA, rapidly migrated to the right iliac artery and caused embolization. The device was pushed back to proximal descending aorta intravascularly. Emergency sternotomy was done to remove the device and to accomplish ASD patch repair.

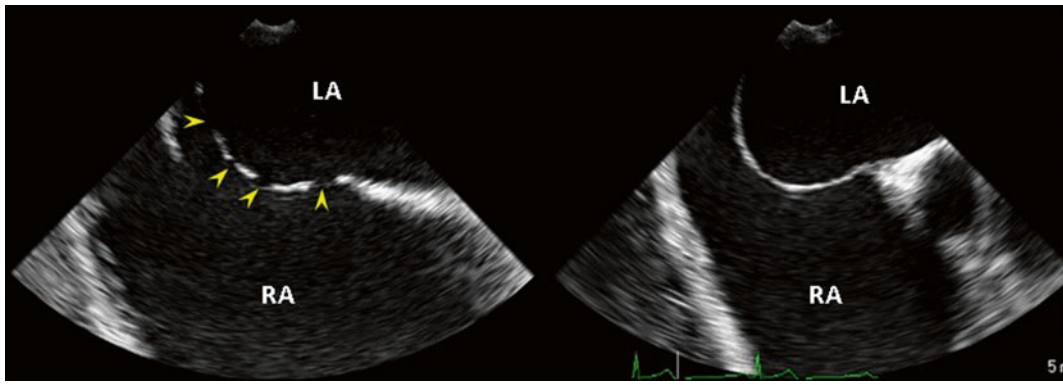

Fig. 7.50 Two-dimensional transesophageal echocardiography (2D TEE) image, x-plane view, showed four defects (*arrows*) over interarterial septum

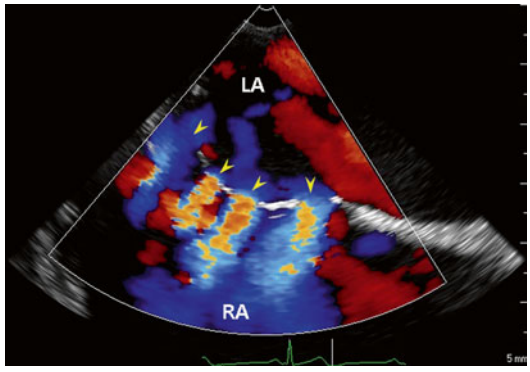

Fig. 7.51 2D TEE color Doppler, short- axis view, showed four shunts (*arrows*) from LA to RA through the ASDs

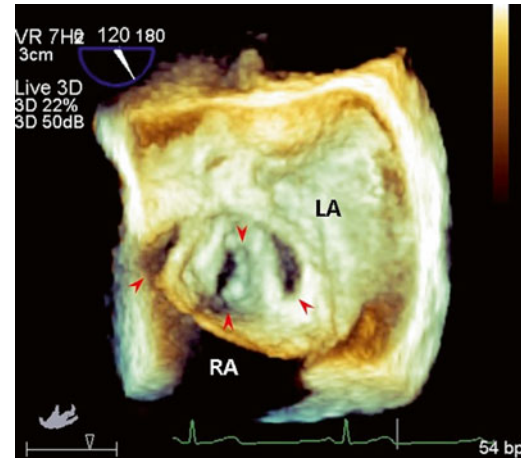

Fig. 7.52 3D TEE image, viewed from LA perspective to RA, showed four defects (*arrows*) over interarterial septum

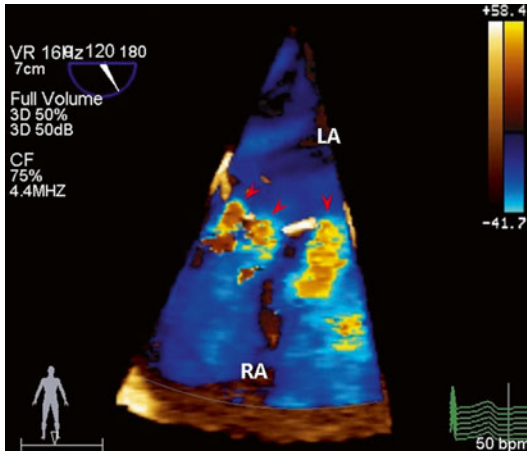

Fig. 7.53 3D TEE color Doppler, short-axis view, showed flows (*arrows*) from LA to RA through the ASDs

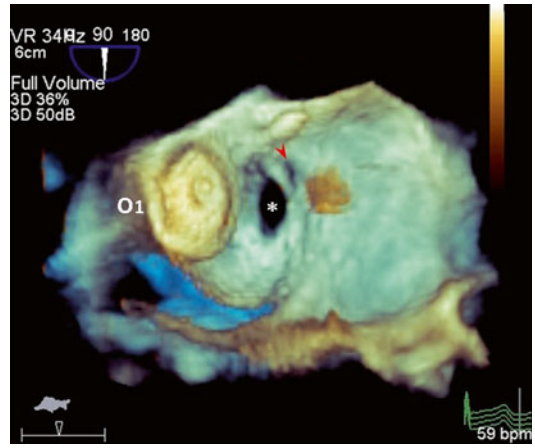

Fig. 7.55 3D TEE image, during occluder implantation procedure, after the first implantation of occluder (O_1), defects (* and *arrow*) persisted

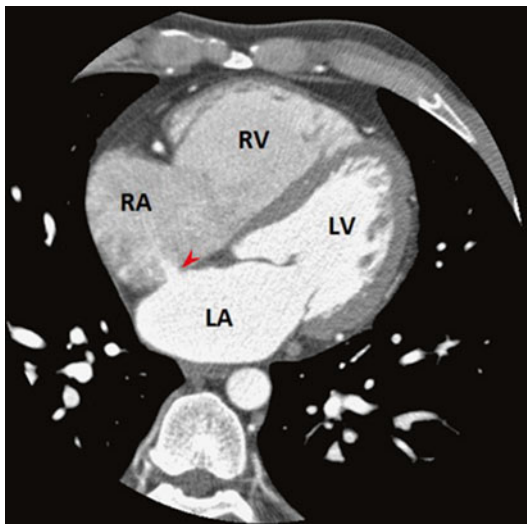

Fig. 7.54 Contrast-enhanced cardiac CT showed dilated RA and RV with a small defect (*arrow*) over interarterial septum

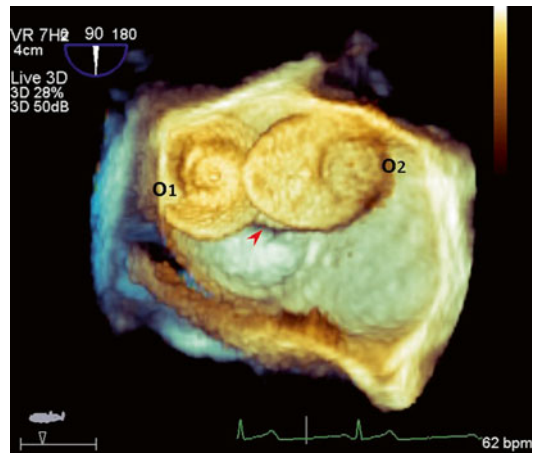

Fig. 7.56 3D TEE image, during the procedure, after implantation of the first (O_1) and the second (O_2) occluders, residual defects (*arrow*) were seen

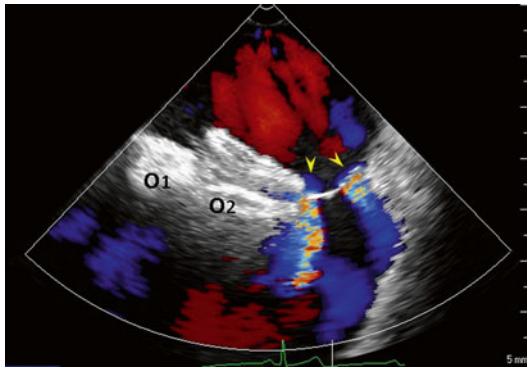

Fig. 7.57 2D TEE color Doppler, during the procedure, after implantation of the first (O_1) and the second (O_2) occluders, there were still flows (*arrows*) through the defects

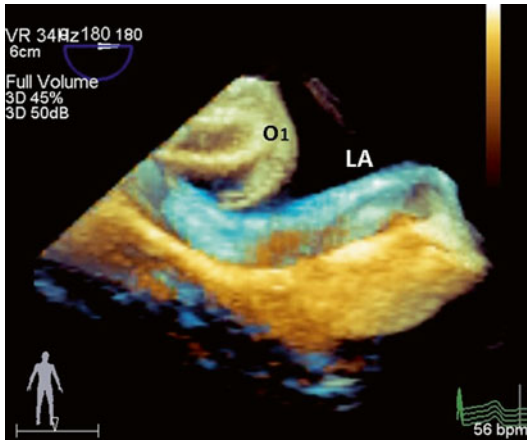

Fig. 7.58 3D TEE image showed the first occluders (O_1) dropped into LA when the third device was attempted

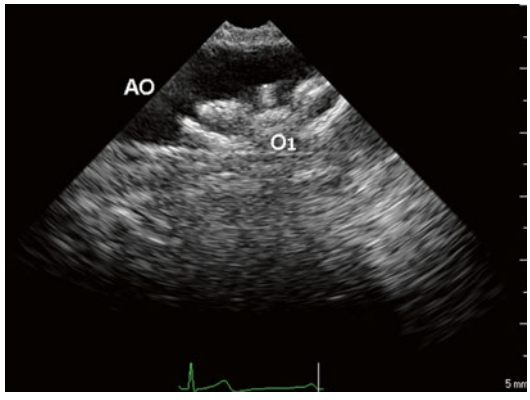

Fig. 7.59 2D TEE showed occluder (O_1) in descending aorta

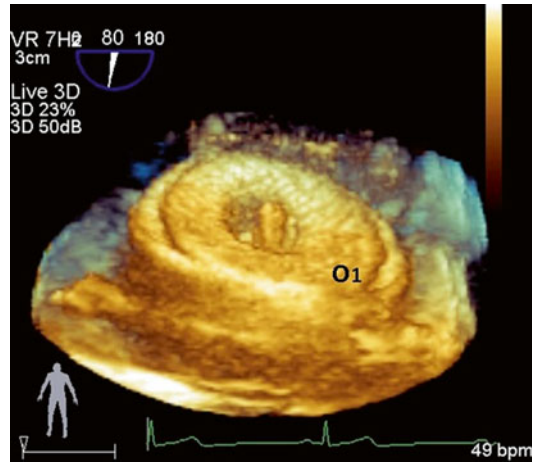

Fig. 7.60 3D TEE showed occluder (O_1) in descending aorta

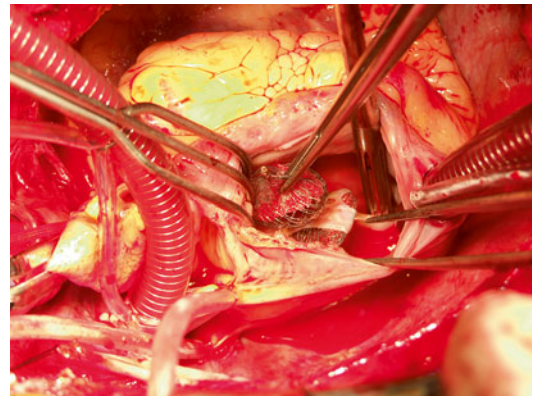

Fig. 7.61 Picture during removal of the occluder from proximal descending aorta

Tips

Occluders can be used to closed ASDs, but the ASDs cannot be too large, too many, and there must be an adequate rim to seat the occluder.

7.5 Supracristal Ventricular Septal Defect Having Patch Repair

A 45-year-old man with heart murmur presented with exertional chest tightness, shortness of breath and dyspnea on exertion. Auscultation: regular heart beat with a grade 3/6 pan-systolic murmur over left lower sternal border and pulmonary area. ECG: sinus rhythm and complete right bundle branch block. Cardiac catheterization: ventricular septal defect (VSD) and LAD myocardial bridge. Operation: patch repair of VSD.

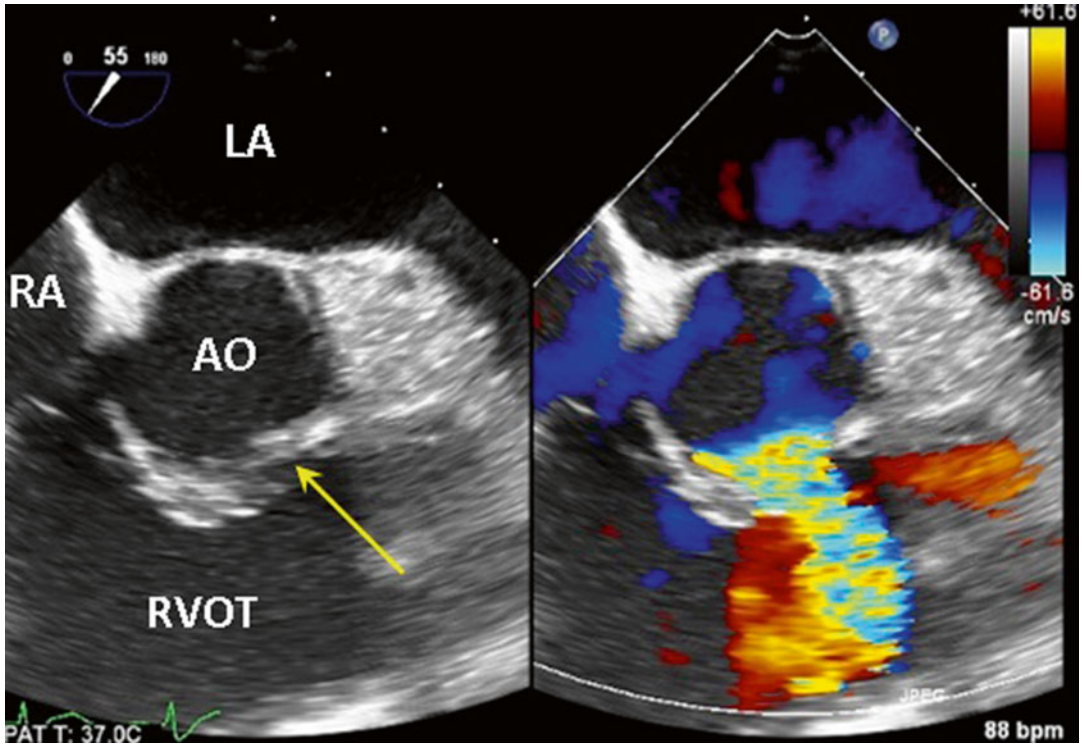

Fig. 7.62 Two-dimensional transesophageal echocardiography (2D TEE) color compare, short-axis view, showed a supracristal VSD (*arrow*) located at the 5 o'clock position and adjacent to the PV with flow from LV outflow tract to RV outflow tract

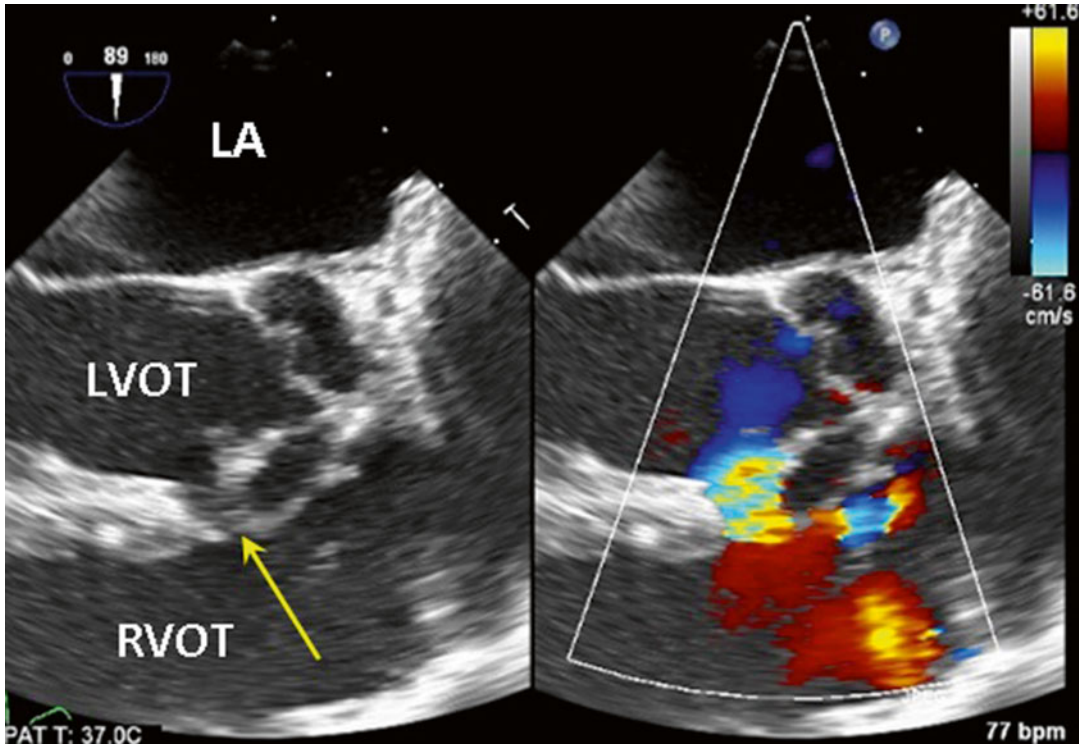

Fig. 7.63 2D TEE color compare, modified long-axis view, showed a supracristal VSD (*arrow*) located just below the AV with flow from LV outflow tract to RV outflow tract

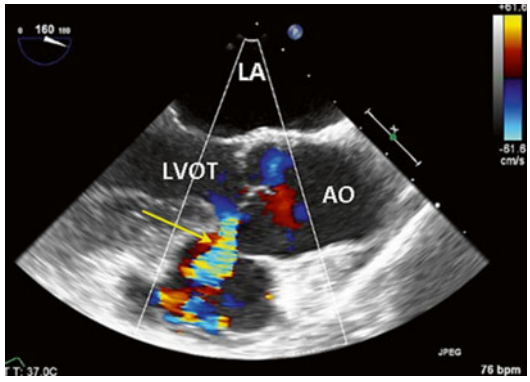

Fig. 7.64 2D TEE color Doppler, modified long-axis view, showed a supracristal VSD located just below the AV with flow (*arrow*) from LV outflow tract to RV

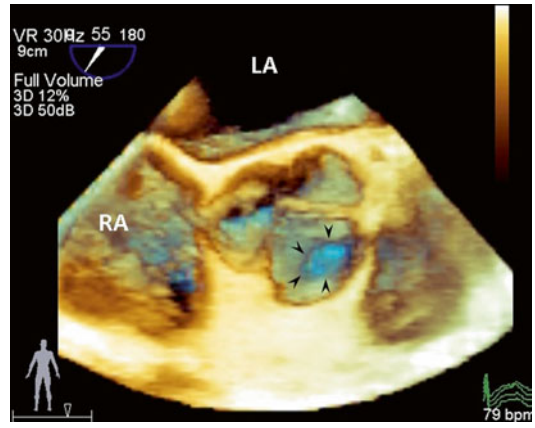

Fig. 7.65 3D TEE, short-axis view, showed a supracristal VSD (*arrows*) located inferior to the AV and above the crista ventricularis

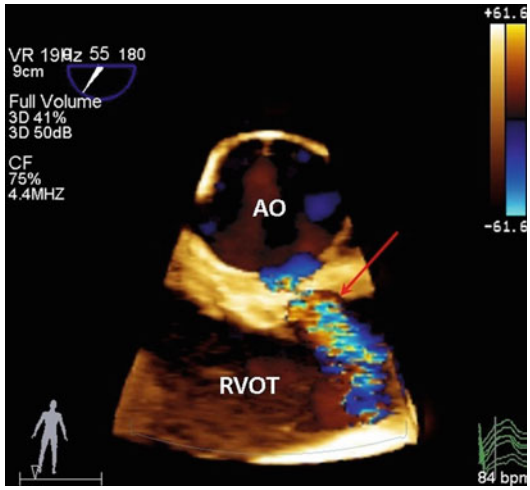

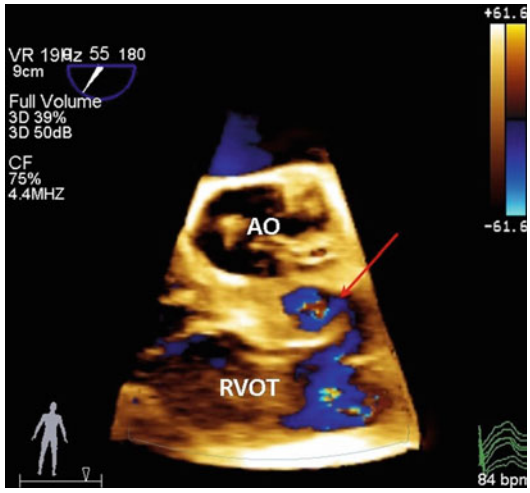

Figs. 7.66 and 7.67 3D TEE color Doppler, short-axis view in systole (*above*) and diastole (*below*), showed a continuous left-to-right shunt (*arrow*) across the supracristal VSD

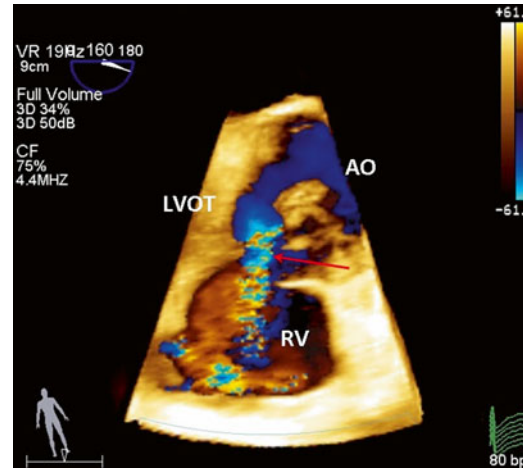

Fig. 7.68 2D TEE color Doppler, modified long-axis view, showed a left-to-right shunt (*arrow*) across the supracristal VSD

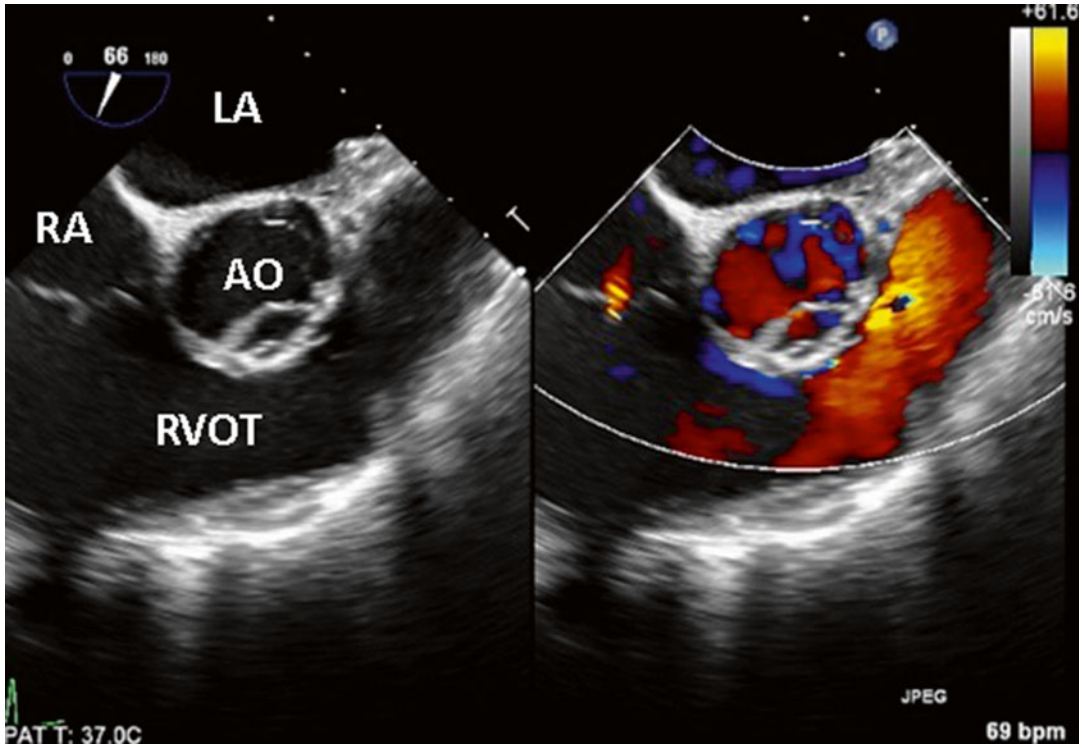

Fig. 7.69 2D TEE color compare, short-axis view, status post VSD patch repair, no abnormal intracardiac shunt was present

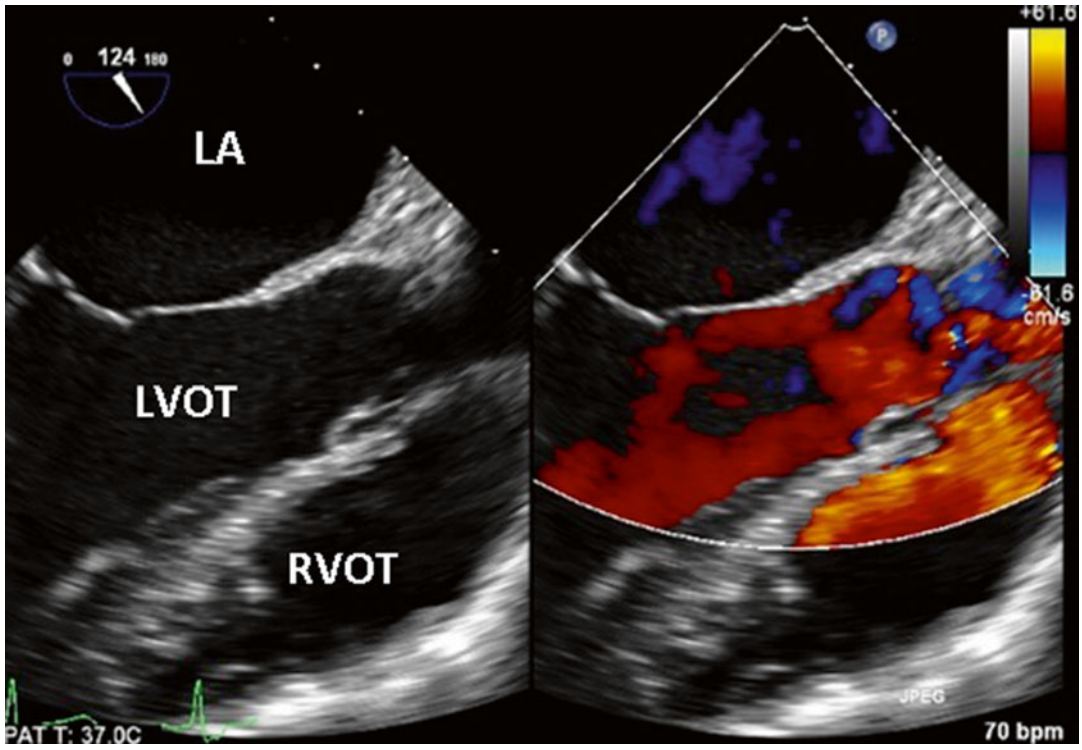

Fig. 7.70 2D TEE color compare, long-axis view, status post VSD patch repair, no abnormal intracardiac shunt was present

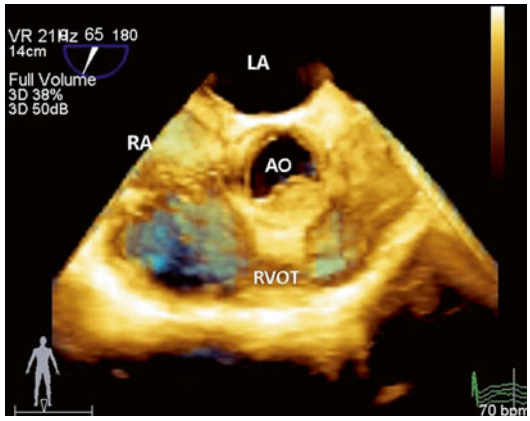

Fig. 7.71 3D TEE, short-axis view, status post VSD patch repair

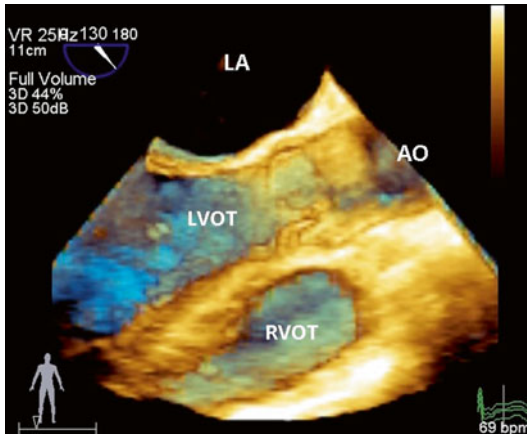

Fig. 7.72 3D TEE, long-axis view, status post VSD patch repair

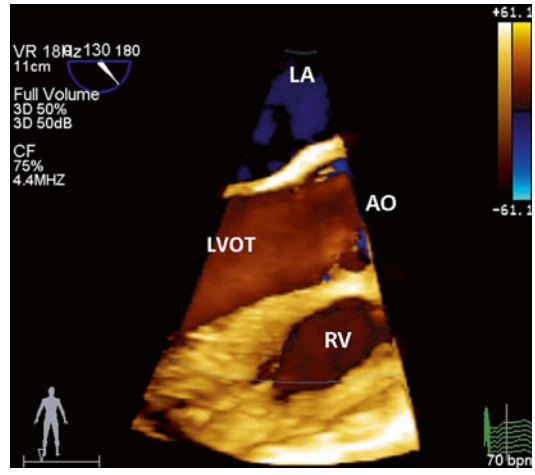

Fig. 7.73 3D TEE color Doppler, long-axis view, status post VSD patch repair, no abnormal intracardiac shunt was present

Tips

A supracristal VSD, so called outlet VSD or subatrial VSD, is located in the RVOT portion of septum, above the crista ventricularis, inferior to the AV and below the PV.

7.6 Subaortic Stenosis Having Resection

A 23-year-old woman is a known case of congenital heart disease with discrete subaortic membranous stenosis since she was born. She suffered from exertional dyspnea and chest tightness for months. Auscultation: a 3/6 systolic murmur over apex with transmission to neck and gallop. ECG: sinus rhythm and non- specific ST-T change. Operation: resection of subaortic membranous tissue.

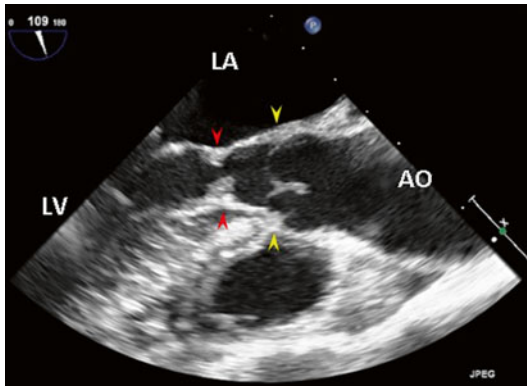

Fig. 7.74 Two-dimensional transesophageal echocardiography (2D TEE), long-axis view, showed a subaortic membrane (*red arrows*) locate 1.5 cm apically to the AV (*yellow arrow*s)

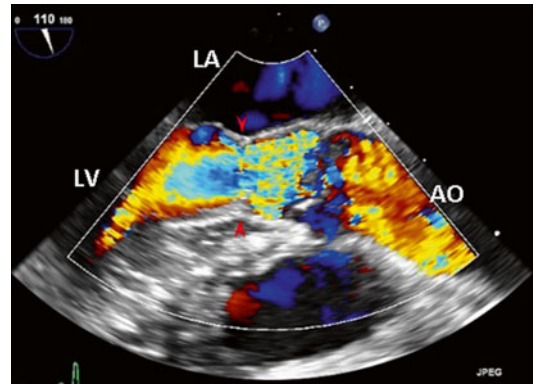

Fig. 7.75 2D TEE color Doppler, long-axis view, showed high-velocity flow in the LV outflow track (LVOT) caused by discrete subaortic membranous stenosis (*arrows*)

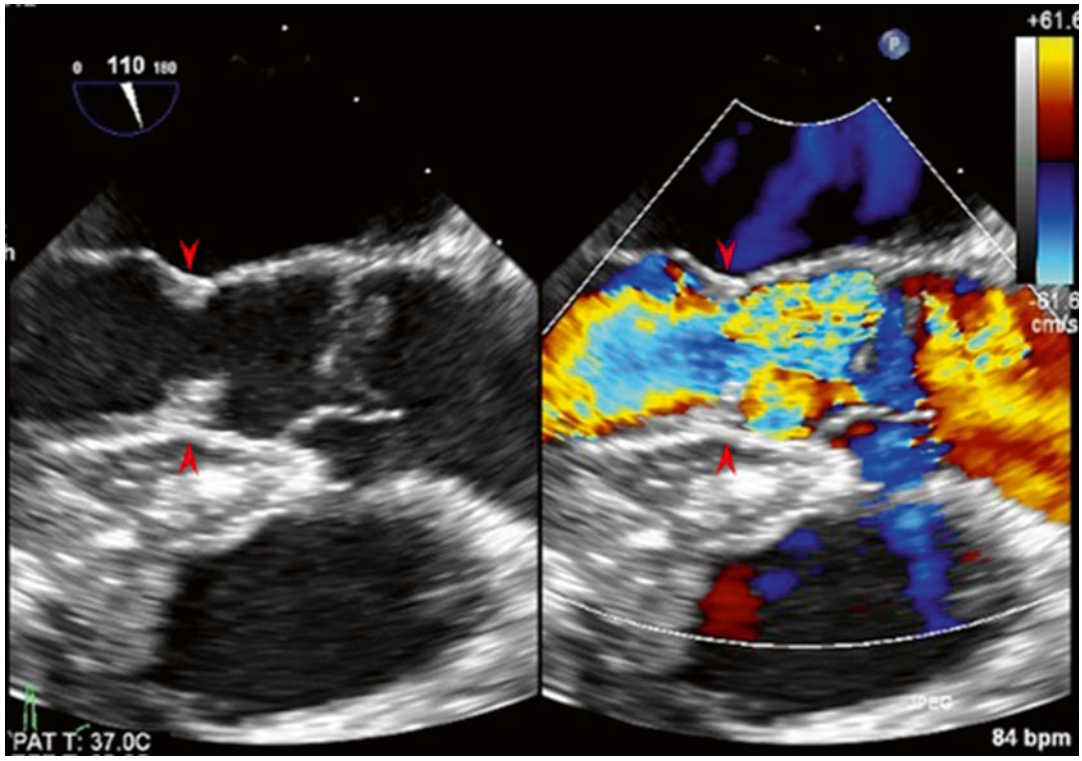

Fig. 7.76 2D TEE color compare, long-axis view, showed flow disturbance on the LV side of the AV with the AV leaflets appear normal, which indicated subaortic stenosis (*arrows*)

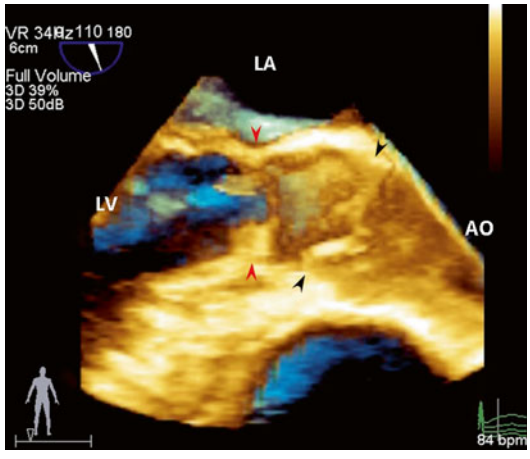

Fig. 7.77 3D TEE, long-axis view, showed a subaortic membrane (*red arrows*) locate 1.5 cm apically to the AV (*black arrows*)

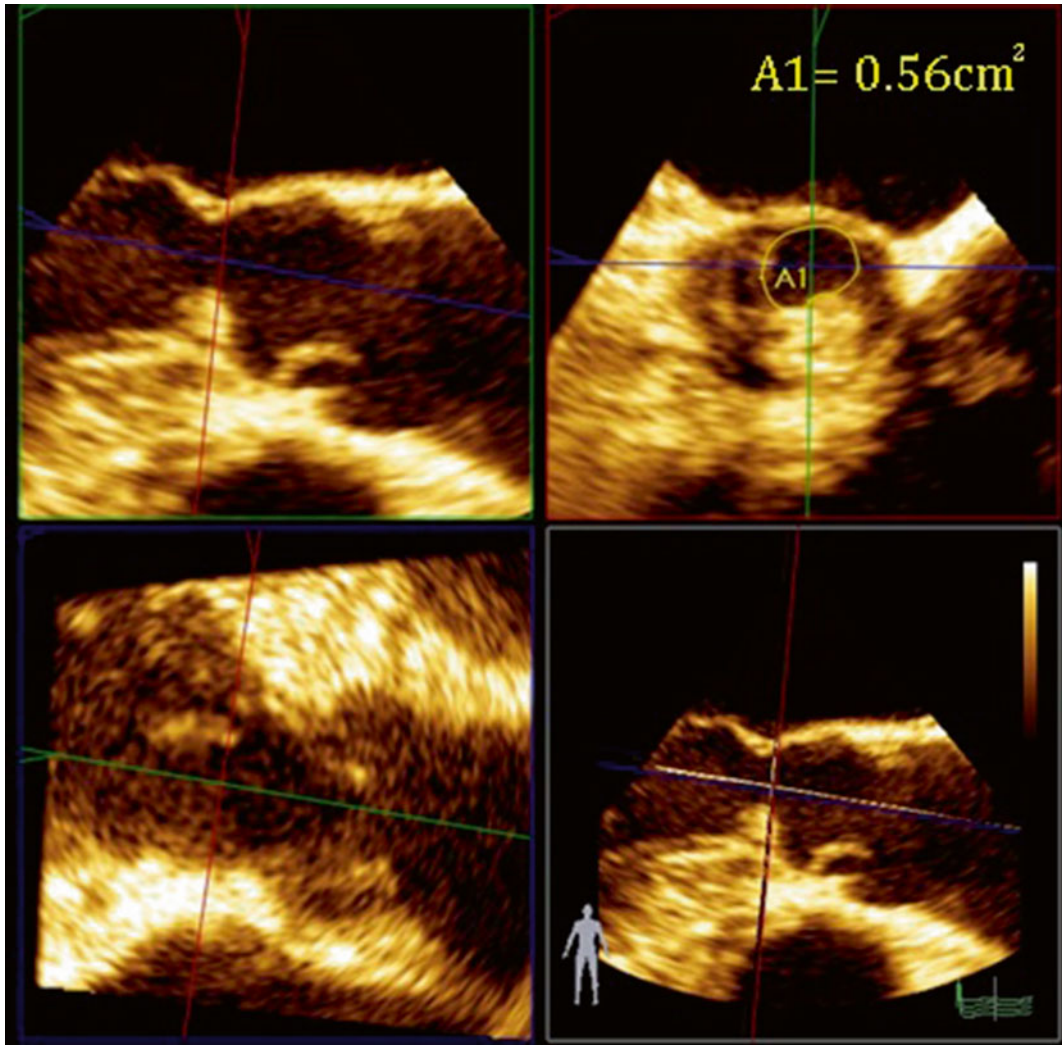

Fig. 7.78 Multi-planer reconstruction (MPR) of 3D TEE, showed subaortic stenosis area is 0.56 cm^2

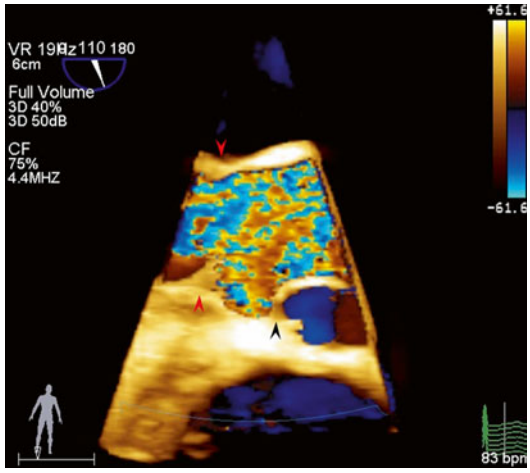

Fig. 7.79 3D TEE color Doppler, long-axis view, showed flow disturbance between the subaortic membrane (*red arrows*) and AV (*black arrow*)

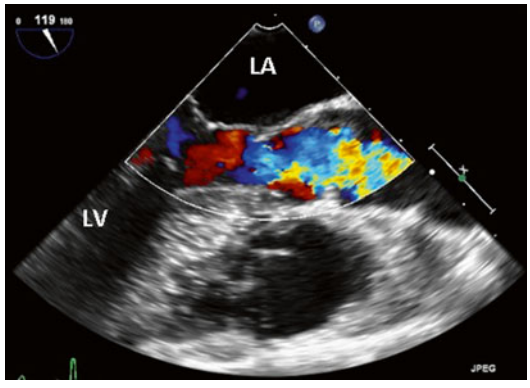

Fig. 7.80 2D TEE color Doppler, long-axis view, status post resection of the subaortic membranous tissue, showed normal flow in the LVOT

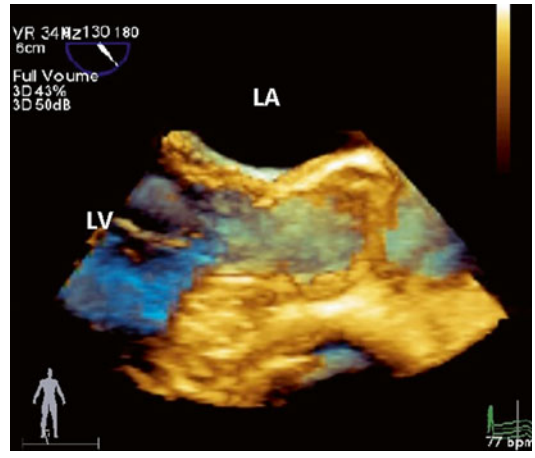

Fig. 7.81 3D TEE, long-axis view, status post resection of the subaortic membranous tissue, no more subaortic stenosis was present

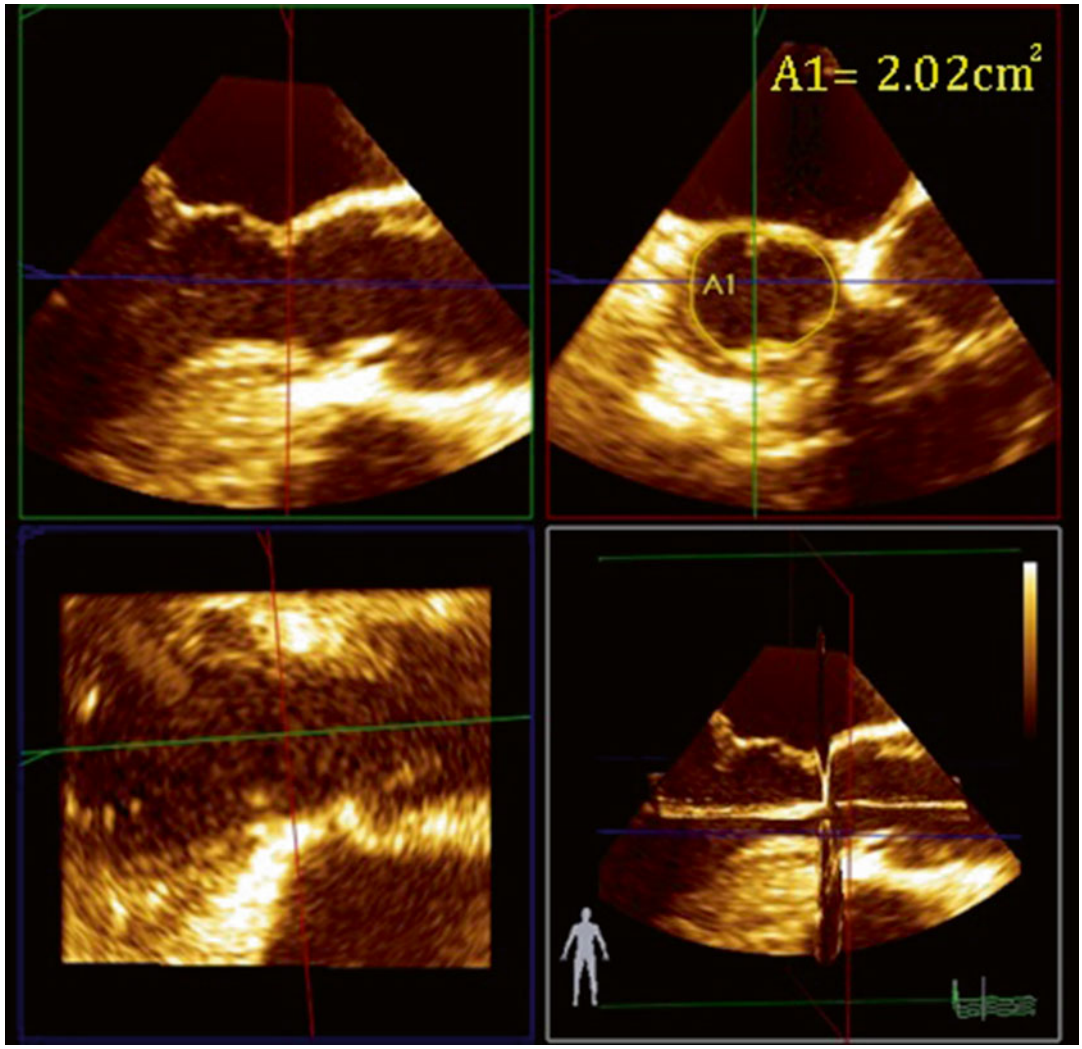

Fig. 7.82 MPR of 3D TEE, status post resection, showed LVOT area is 2.02 cm^2

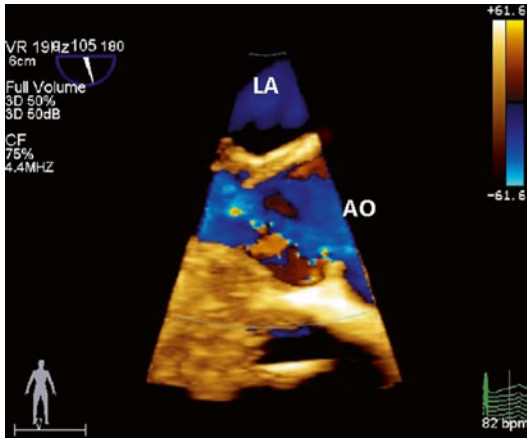

Fig. 7.83 3-D TEE color Doppler, long-axis view, status post resection, showed normal flow in the LVOT

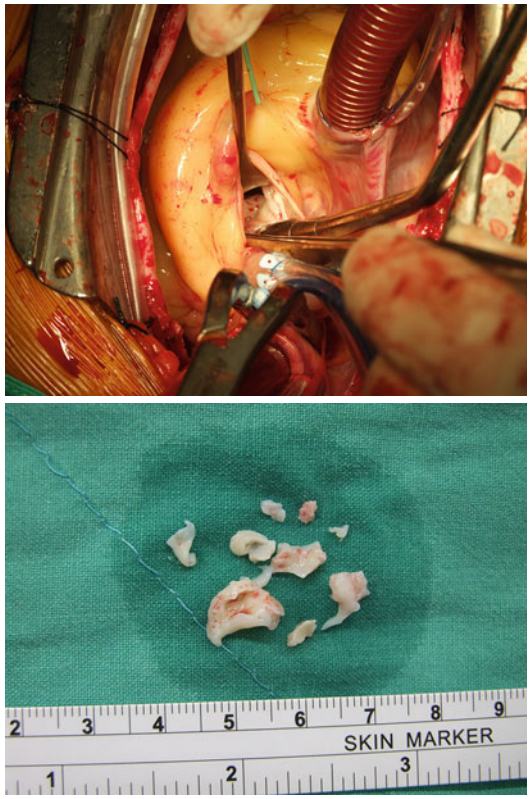

Figs. 7.84 and 7.85 Picture during operation (*above*) and gross specimen of the excised tissue (*below*)

Tips

If aortic acceleration was present with normal AV appearance, subaortic stenosis and dynamic obstruction must be suspected.

Suggested Reading

Assaidi A, Sumian M, Mauri L, et al. Transcatheter closure of complex atrial septal defects is efficient under intracardiac echocardiographic guidance. Arch Cardiovasc Dis. 2014;107(12):646–53.

Baruteau AE, Petit J, Lambert V, et al. Transcatheter closure of large atrial septal defects: feasibility and safety in a large adult and pediatric population. Circ Cardiovasc Interv. 2014;7(6):837–43.

Bayar N, Arslan Ş, Çağırcı G, et al. Assessment of morphology of patent foramen ovale with transesophageal echocardiography in symptomatic and asymptomatic patients. J Stroke Cerebrovasc Dis. 2015;24(6):1282–6.

Chen HY, Pan CZ, Shu XH. Partially unroofed coronary sinus diagnosed by real-time dimensional transesophageal echocardiagraphy after operation of secundum atrial septal defect. Int J Cardiovasc Imaging. 2015;31(1):45–6.

Choi AD, Ahmad S, Mathias M, et al. Diagnosis and surgical management of subaortic stenosis and mitral valve systolic anterior motion. J Heart Valve Dis. 2013;22(4):599–602.

Demirkol S, Barçın C, et al. Percutaneous closure of second secundum atrial septal defect under guidance of three-dimensional transesophageal echocardiography guidance. Anadolu Kardiyol Derg. 2013;13(4):E22–3.

Hartlage GR, Consolini MA, Pernetz MA, et al. Bad company: supracristal VSD presenting with ruptured sinus of valsalva aneurysm. a case presentation with echocardiographic depiction and an analysis of contemporary literature. Echocardiography. 2015;32(3):575–83.

Jeng W, Ming CH, Shen KT, et al. Atrial septal occluder device embolization to an iliac artery: a case highlighting the utility of three-dimensional transesophageal echocardiography during percutaneous closure. Echocardiography. 2012;29:1128–31.

Jung P, Sohn HY. 35-year-old woman with unclear cardiac surgery in infancy. Operation of atrial septal defect type 1 (ostium primum defect) with mitral valve involvement. Dtsch Med Wochenschr. 2012;137(14):713–4.

Kuroda M, Kumakura M, Sato T, Saito S. The usefulness of three-dimensional transesophageal echocardiography for a primum atrial septal defect. Anesth Analg. 2015;121(5):1151–4.

Mihara H, Shibayama K, Harada K, et al. LV outflow tract area in discrete subaortic stenosis and hypertrophic obstructive cardiomyopathy: a real-time 3-dimensional transesophageal echocardiography study. JACC Cardiovasc Imaging. 2014;7(4):425–8.

Sugasawa Y, Hayashida M, Inada E. Discrete subaortic stenosis diagnosed intraoperatively. J Anesth. 2014;28(2):311.

Zhang S, Zhu D, An Q, et al. Minimally invasive perventricular device closure of doubly committed subarterial ventricular septaldefects: single center long-term follow-up results. J Cardiothorac Surg. 2015;10(1):119.

Cardiomyopathies

8

Abstract

This chapter provides cardiomyopathies. Hypertrophic cardiomyopathies are common genetic cardiac disease with properties of LV hypertrophy most asymmetric.

Patients with hypertrophic cardiomyopathy usually generate systemic hypertension or MV systolic anterior motion which should be corrected by surgical therapy.

8.1 Apical Hypertroph Cardiomyopathy with Severe Mitral Regurgitation Having Mitral Repair

A 60-year-old man with a history of atrial fibrillation and hyperthyroidism status post partial thyroidectomy suffered dyspnea after exercise with worsening symptom. Auscultation: irregular heart beat with a grade 2/6 systolic murmur over apex. ECG: atrial fibrillation, LV hypertrophy with strain and counter clockwise rotation. Cardiac catheterization: LV apical hypertrophy with normal contractility and severe MR. Operation: MV and TV repaired and atrial fibrillation ablation.

Electronic supplementary material The online version of this chapter (doi:10.1007/978-981-10-0587-9_8) contains supplementary material, which is available to authorized users.

W.-H. Yin, M.-C. Hsiung, *Atlas of Perioperative 3D Transesophageal Echocardiography*,
DOI 10.1007/978-981-10-0587-9_8

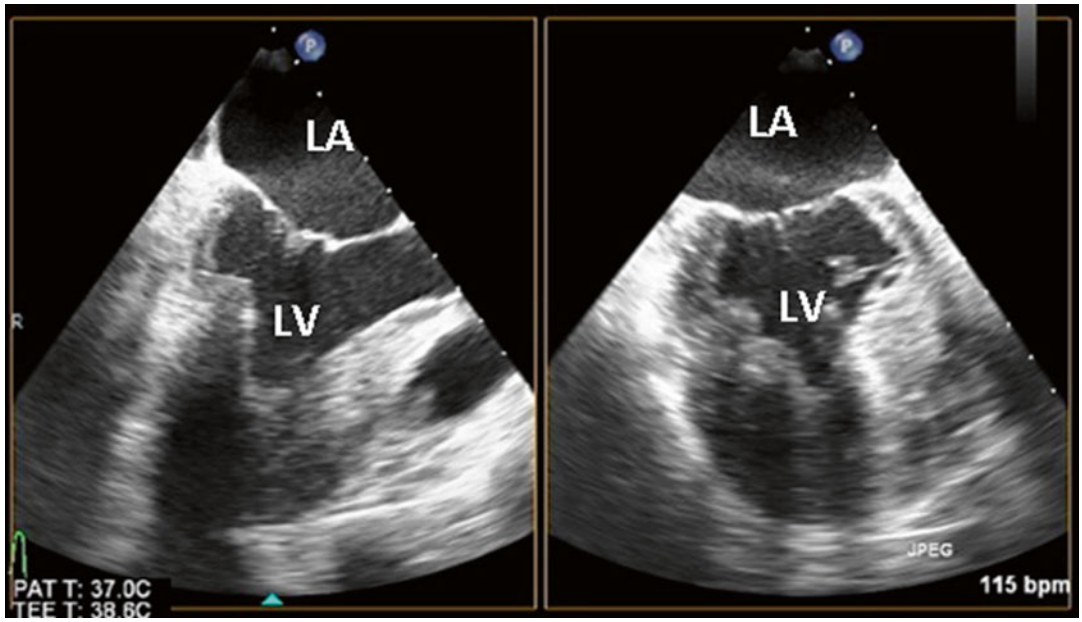

Fig. 8.1 Two-dimensional transesophageal echocardiography (2D TEE), x-plane view, showed LV apical hypertrophic cardiomyopathy with normal function

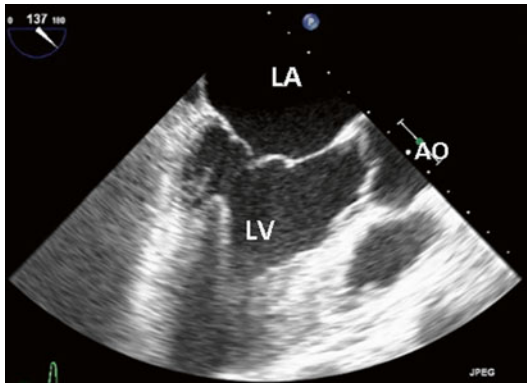

Fig. 8.2 2D TEE, long-axis view, showed localized apical hypertrophy with a spade-like shape LV cavity in the whole cardiac cycle

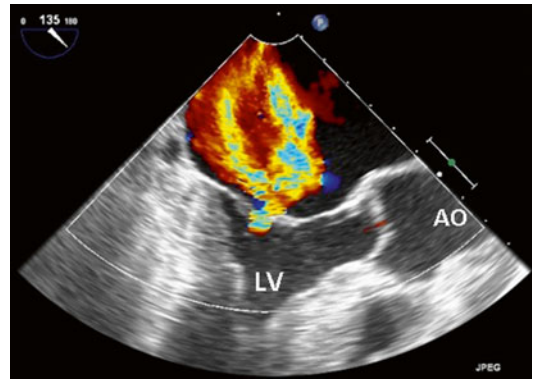

Fig. 8.3 2D TEE color Doppler, long-axis view, showed severe MR

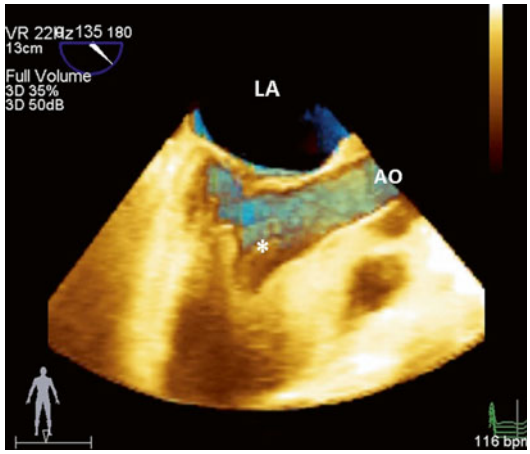

Fig. 8.4 3D TEE, long-axis view, showed localized apical hypertrophy with a spade-like shape LV cavity (*)

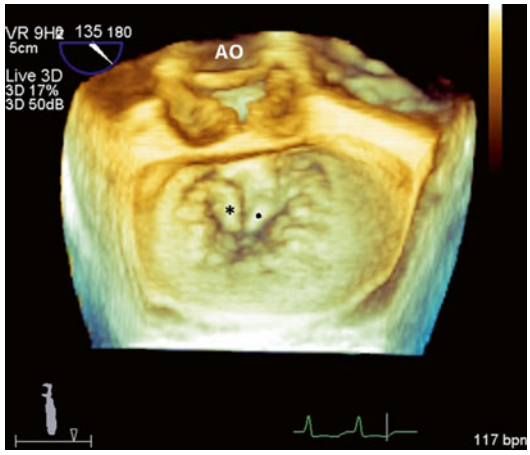

Fig. 8.5 3D TEE, en face view, showed prolapse of A1 (*) and A2 (.)

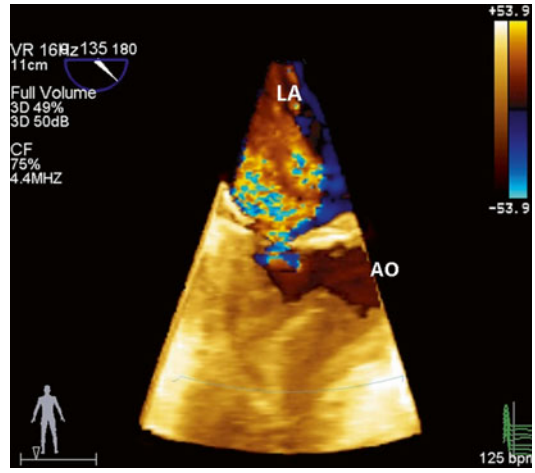

Fig. 8.6 3D TEE color Doppler, long-axis view, showed severe MR due to prolapse of anterior mitral leaflet

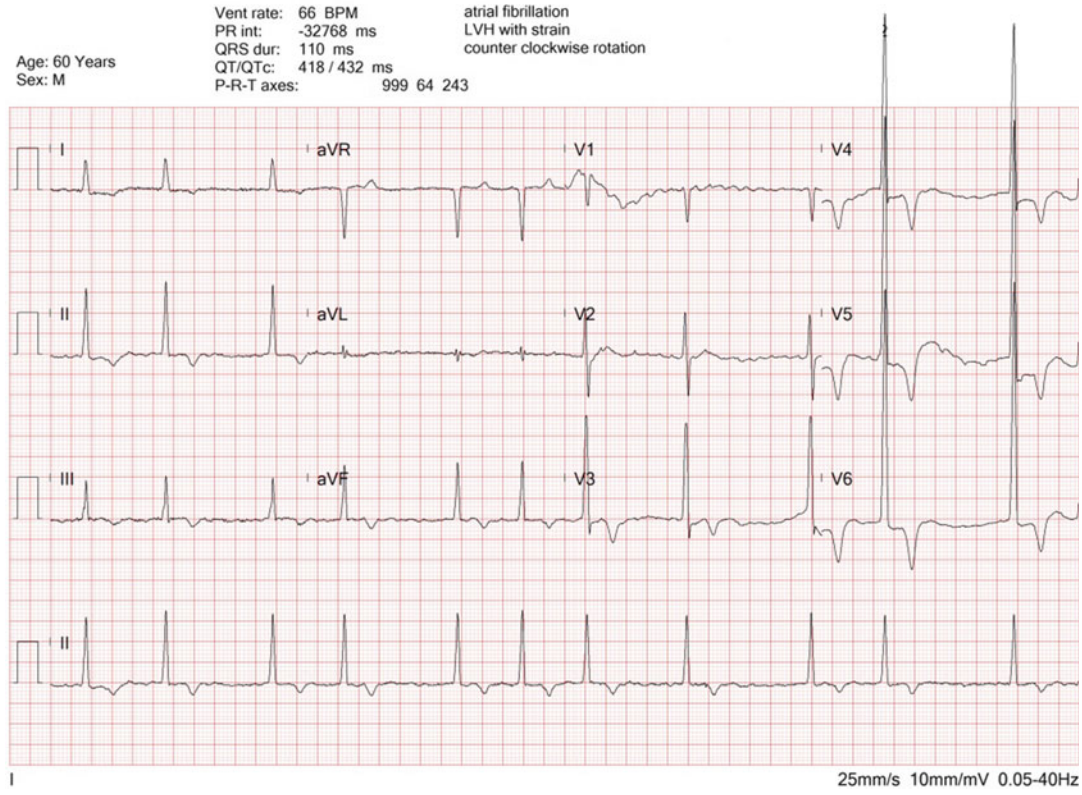

Fig. 8.7 ECG showed atrial fibrillation, LV hypertrophy with strain and counter clockwise rotation

Fig. 8.8 Fluoroscopy showed a spade-like LV demonstrating apical hypertrophic cardiomyopathy

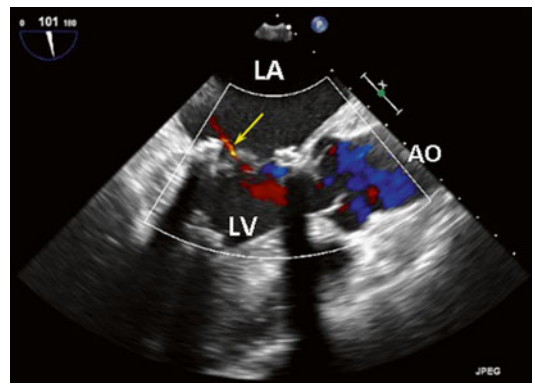

Fig. 8.9 2D TEE color Doppler, long-axis view, status post MV repair, showed mild MR (*arrow*)

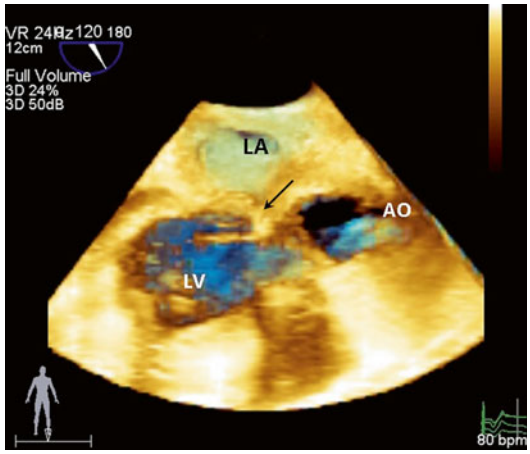

Fig. 8.10 3D TEE, long-axis view, showed repaired MV with suture (*arrow*)

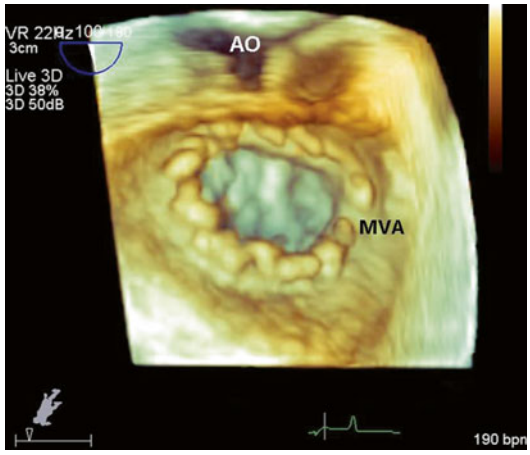

Fig. 8.11 3D TEE, en face view, status post MV repair (*MVA*)

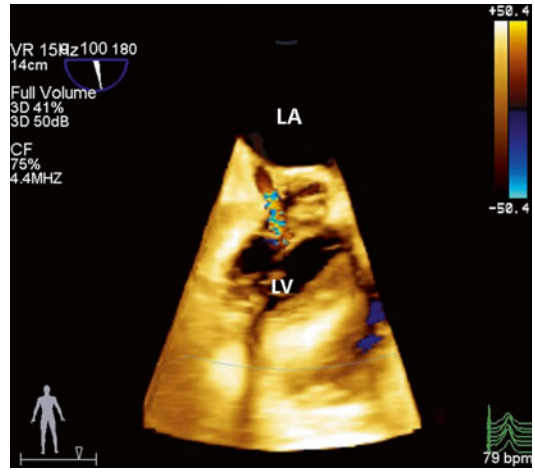

Fig. 8.12 3D TEE color Doppler, long-axis view, status post MV repair, showed mild MR

Tips

Apical hypertrophic cardiomyopathy is a rare form of hypertrophic cardiomyopathy which usually involves the apex of the LV and develops cardiac arrhythmias.

8.2 Hypertrophic Obstructive Cardiomyopathy Having Myectomy and Mitral Replacement

A 42-year-old man with medical-controlled hypertension and type two diabetes mellitus suffered from intermittent chest pain and dyspnea on exertion. Auscultation: regular heart beat with a grade 2/6 systolic murmur over apex. ECG: biatrial enlargement, LV hypertrophy with strain and old septal wall myocardial infarction. Cardiac catheterization: hypertrophic cardiomyopathy with dynamic LV outflow tract obstruction and severe MR, double vessel coronary artery disease. Operation: MV replacement, myectomy of IVS and CABG x2 (SVG to LAD and D2).

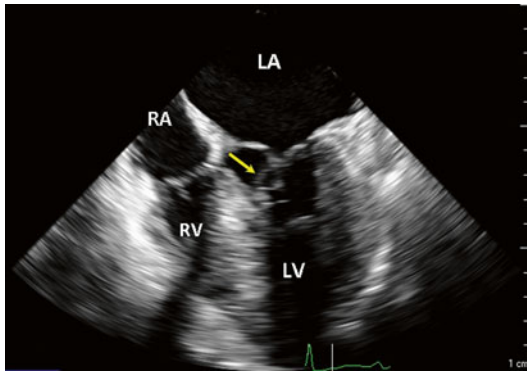

Fig. 8.13 2D TEE, four-chamber view, showed systolic anterior motion of the MV (*arrow*) at end-systole

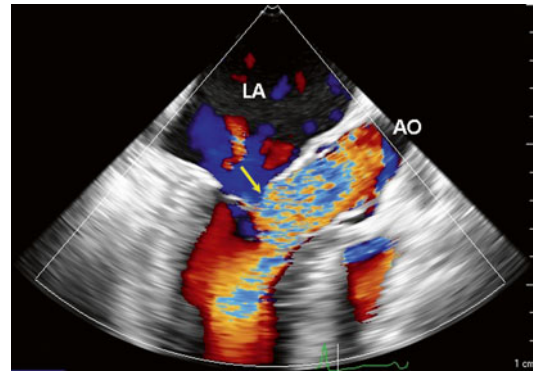

Fig. 8.15 2D TEE color Doppler, long-axis view, showed turbulence in LV outflow tract (*arrow*) due to subaortic dynamic obstruction

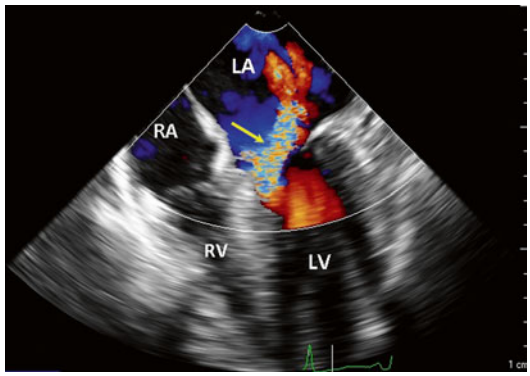

Fig. 8.14 2D TEE color Doppler, four-chamber view, showed severe eccentric MR (*arrow*) due to systolic anterior motion of the MV

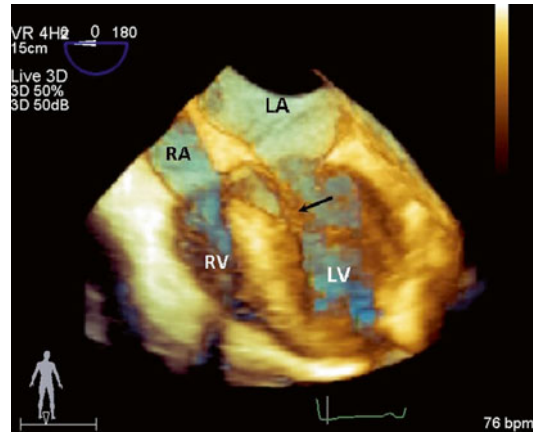

Fig. 8.16 3D TEE, four-chamber view, showed systolic anterior motion of the MV (*arrow*) at end-systole

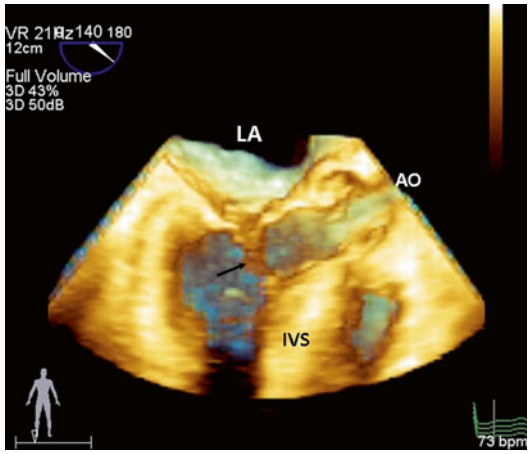

Fig. 8.17 3D TEE image, long-axis view, showed systolic anterior motion of the MV (*arrow*) and dynamic outflow tract obstruction. IVS, interventricular septum

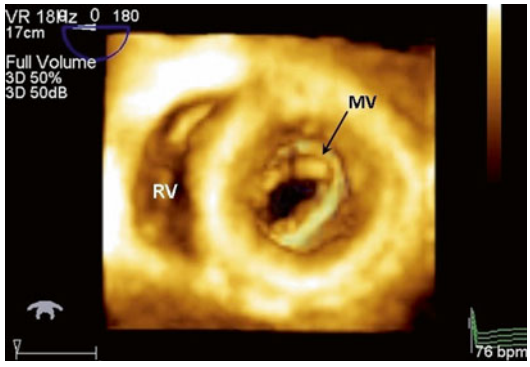

Fig. 8.18 3D TEE, short-axis view from ventricular perspective, showed LV hypertrophic cardiomyopathy

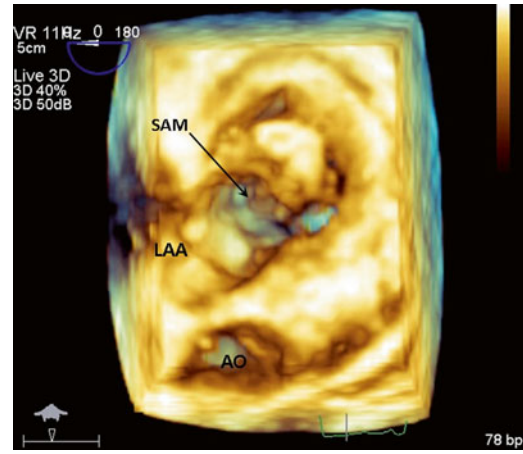

Fig. 8.19 3D TEE, view from LA perspective, showed systolic anterior motion (*SAM*) of the MV indicating LV outflow tract obstruction. *LAA* left atrial appendage

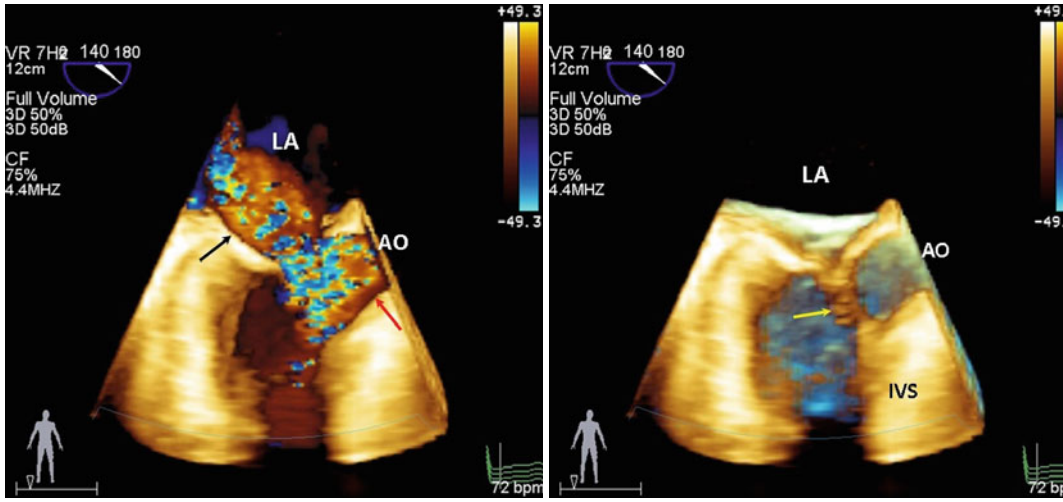

Figs. 8.20 and 8.21 3D TEE color Doppler (*left*) and color suppressed (*right*), long-axis view, showed severe eccentric MR (*black arrow*) and turbulence in LV outflow tract (*red arrow*) caused by systolic anterior motion of the MV (*yellow arrow*)

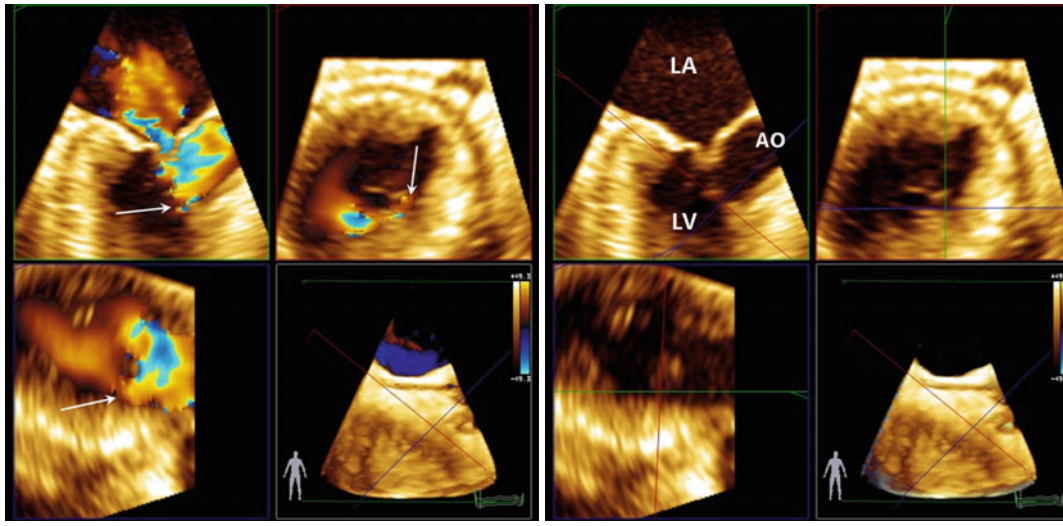

Figs. 8.22 and 8.23 Multi-planer reconstruction of 3D TEE color Doppler (*left*) and color suppressed (*right*) showed severe eccentric MR and LV outflow tract obstruction with a flow convergence area (*arrows*)

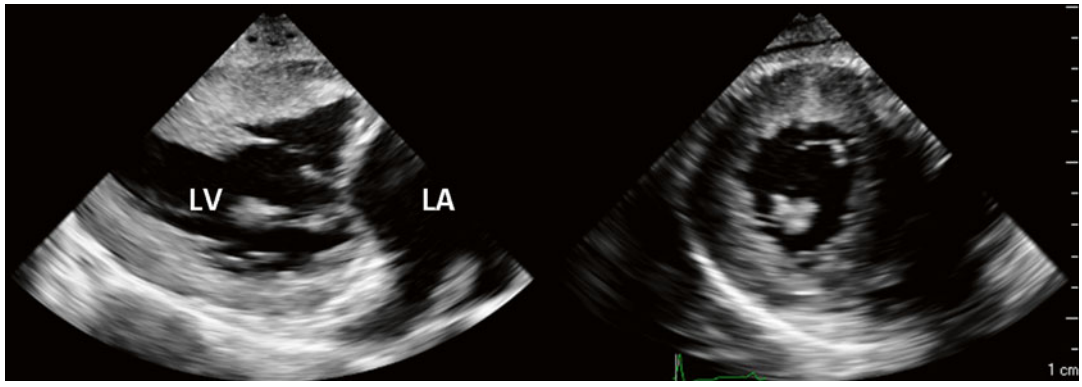

Fig. 8.24 Two-dimensional transesophageal echocardiography (2D TEE), transgastric x-plane view, showed LV hypertrophic cardiomyopathy with normal function

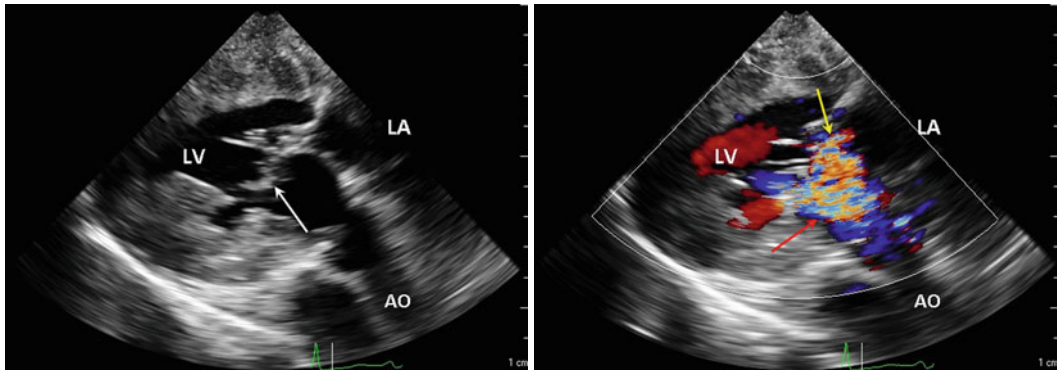

Figs. 8.25 and 8.26 2D TEE (*left*) and color Doppler (*right*), transgastric long-axis view, showed systolic anterior motion of MV (*white arrow*) in association with severe MR (*yellow arrow*). Turbulence in outflow tract (*red arrow*) was seen due to subaortic dynamic obstruction

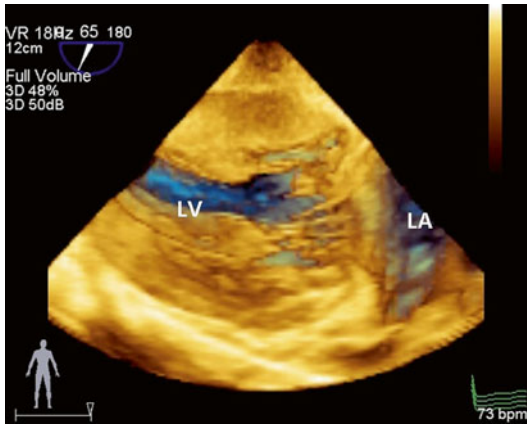

Fig. 8.27 3D TEE, transgastric two-chamber view, showed LV hypertrophic cardiomyopathy

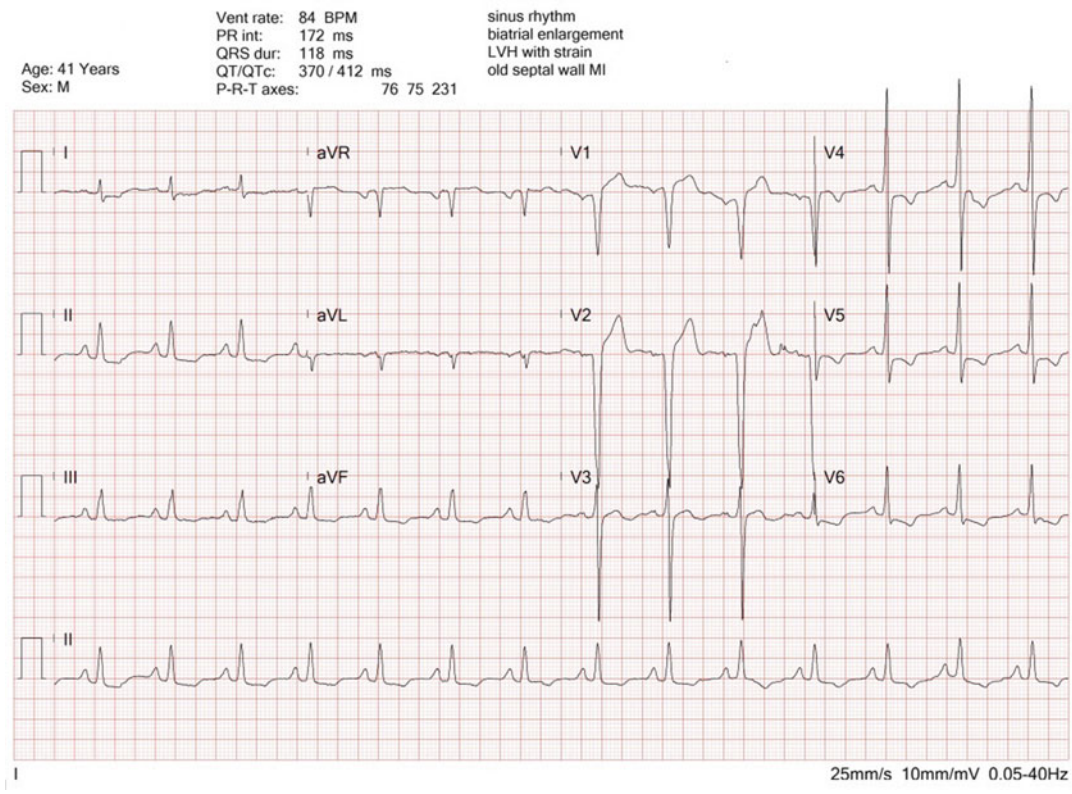

Fig. 8.28 ECG showed sinus rhythm, biatrial enlargement, LV hypertrophy with strain and old septal wall myocardial infarction

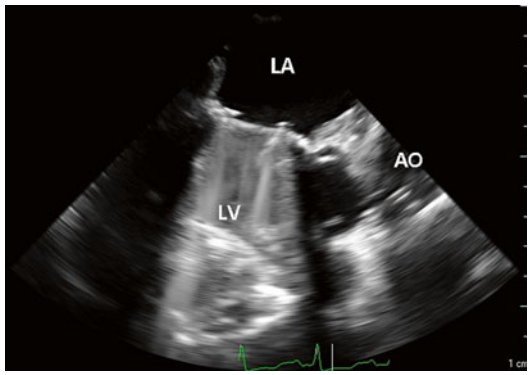

Fig. 8.29 2D TEE, long axis view, status post mechanical MV replacement and myectomy of IVS, showed normal prosthesis function without systolic anterior motion

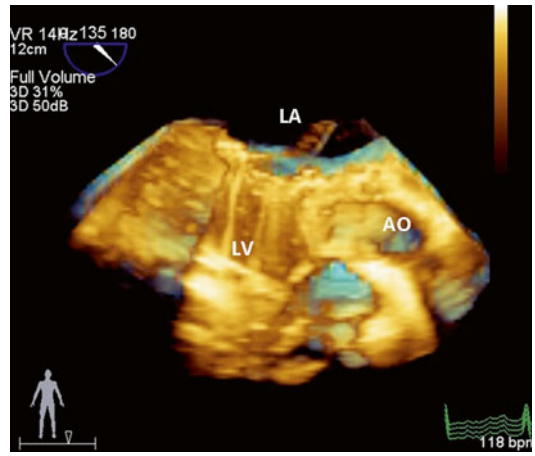

Fig. 8.30 3D TEE, long-axis view, status post mechanical MV replacement and myectomy of IVS, showed normal prosthesis function without systolic anterior motion

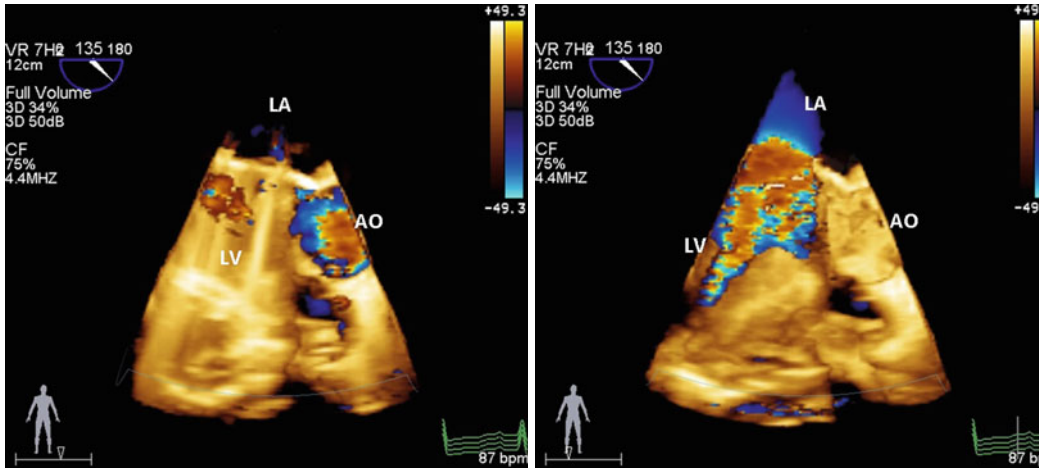

Figs. 8.31 and 8.32 3D TEE color Doppler, long-axis view, status post mechanical MV replacement and myectomy of IVS, showed normal prosthesis function without MR or LV outflow tract obstruction

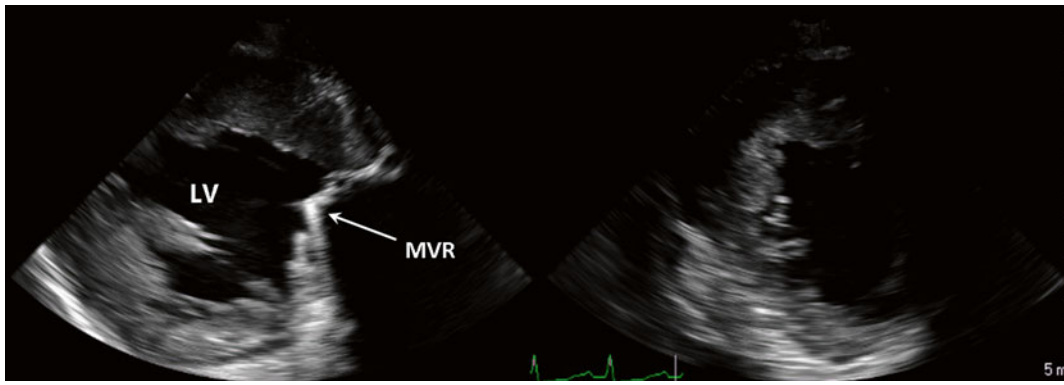

Fig. 8.33 2D TEE, transgastric x-plane view, status post mechanical MV replacement (*MVR*) and myectomy of IVS, showed normal prosthesis function

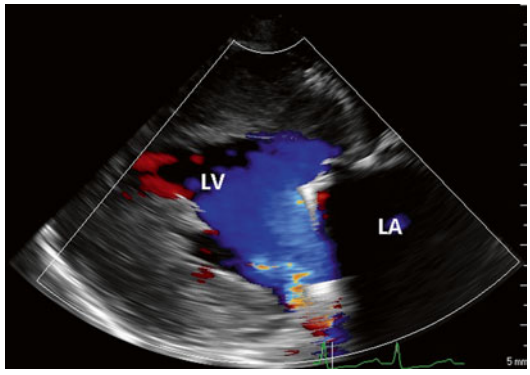

Fig. 8.34 2D TEE color Doppler, transgastric long-axis view, status post mechanical MV replacement and myectomy of IVS, showed normal prosthesis function without MR or LV outflow tract obstruction

Tips

Systolic anterior motion occurs only in mid to late systole. The severity of obstruction can be altered by loading conditions.

8.3 Hypertrophic Obstructive Cardiomyopathy Having Aortic, Mitral Replacement and Myectomy

A 74-year-old man had a past history of hyperlipidemia, hypertension, carotid stenosis and valvular heart disease with moderate to severe AR and MR. he suffered from progressive effort angina and chest distress with shortness of breath. Auscultation: regular heart beat without significant murmur. ECG: sinus bradycardia (52BPM), first degree AV block and LV hypertrophy. Chest X ray: cardiomegaly. Cardiac catheterization: valvular heart disease with moderate to severe AR and MR, insignificant coronary artery disease. Operation: myectomy, AV and MV replacement and CABG x1 (SVG to LAD).

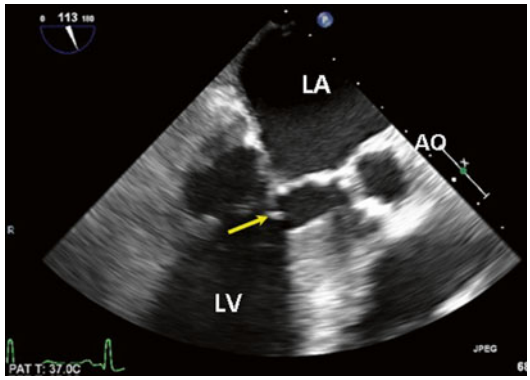

Fig. 8.35 Two-dimensional transesophageal echocardiography (2D TEE), long-axis view, showed asymmetric septal hypertrophy with systolic anterior motion of mitral leaflet (*arrow*)

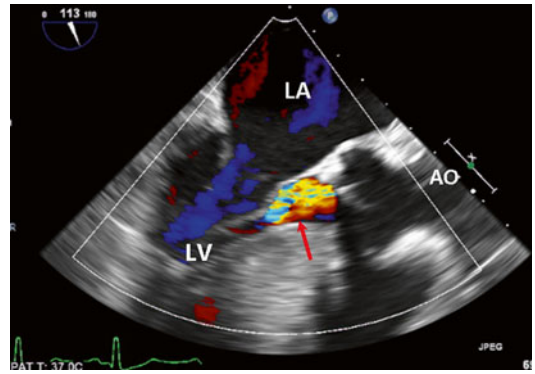

Fig. 8.37 2D TEE color Doppler, long-axis view, showed moderate to severe AR (*arrow*) in diastole

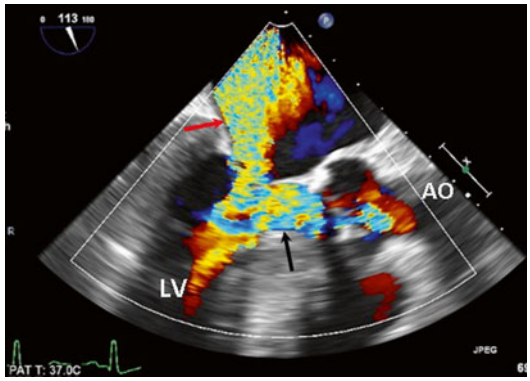

Fig. 8.36 2D TEE color Doppler, long-axis view in systole, showed moderate to severe eccentric MR (*red arrow*) in associated with systolic anterior motion of mitral leaflet; turbulent flow in LV outflow tract (*black arrow*) was seen due to subaortic dynamic obstruction

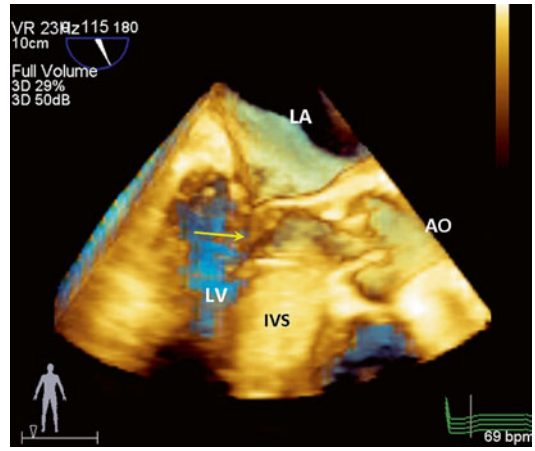

Fig. 8.38 3D TEE, long-axis view, showed asymmetric septal hypertrophy with systolic anterior motion of mitral leaflet (*arrow*). IVS, interventricular septum

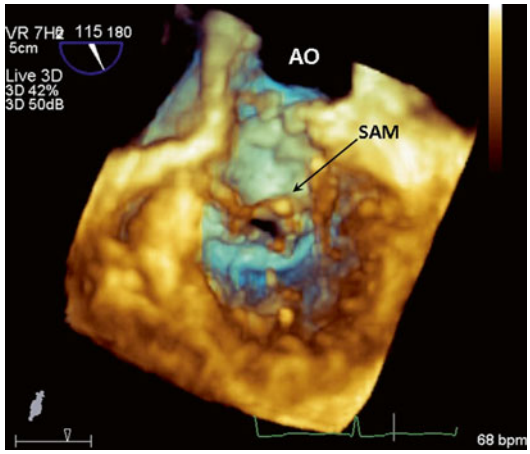

Fig. 8.39 3D TEE, view from LV perspective, showed mitral leaflet systolic anterior motion (*SAM*) indicating LV outflow tract obstruction

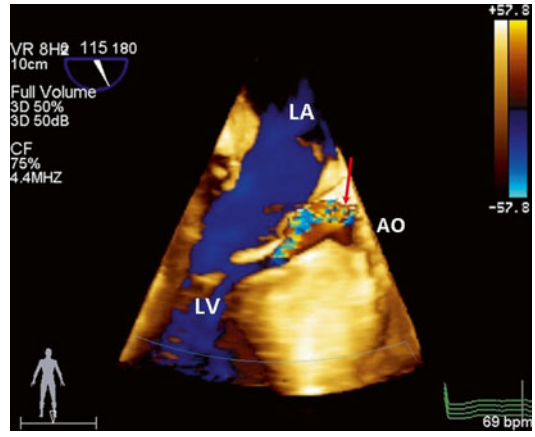

Fig. 8.42 3D TEE color Doppler, long-axis view, showed moderate to severe AR (*arrow*) in diastole

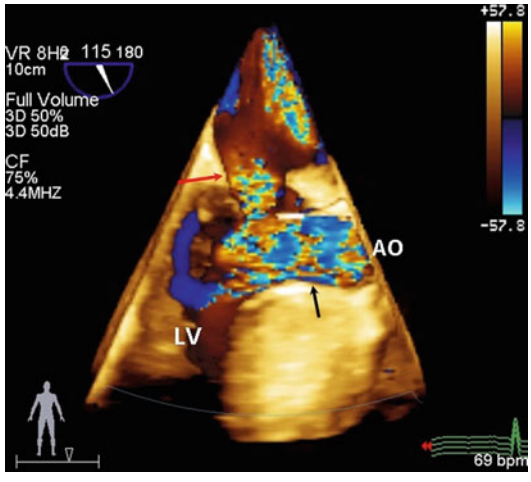

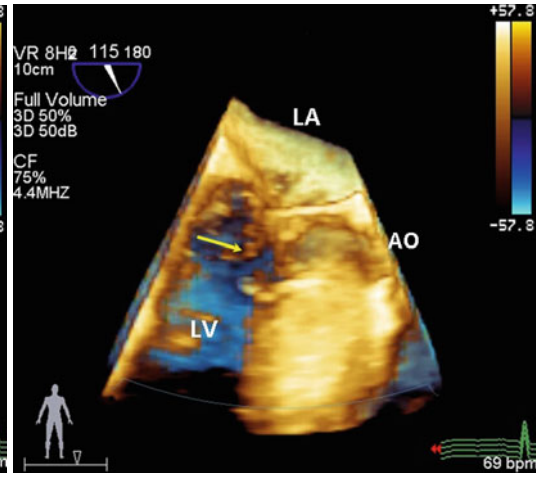

Figs. 8.40 and 8.41 2D TEE color Doppler (*left*) and color suppressed (*right*), long-axis view, showed moderate to severe MR (*red arrow*) and turbulent flow in LV outflow tract (*black arrow*) due to systolic anterior motion of the mitral leaflet (*yellow arrow*)

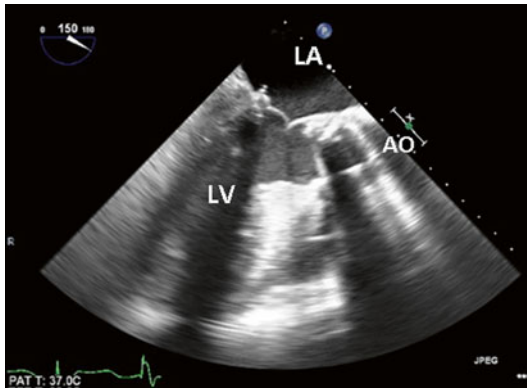

Fig. 8.43 2D TEE, long-axis view, status post myectomy, tissue AV and MV replacement, showed normal prosthetic function without systolic anterior motion

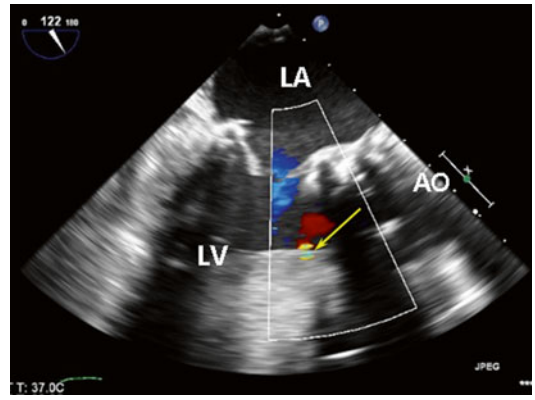

Fig. 8.44 2D TEE color Doppler, long-axis view, status post myectomy, tissue AV and MV replacement, coronary flow seen drained to LVOT due to myectomy (*arrow*)

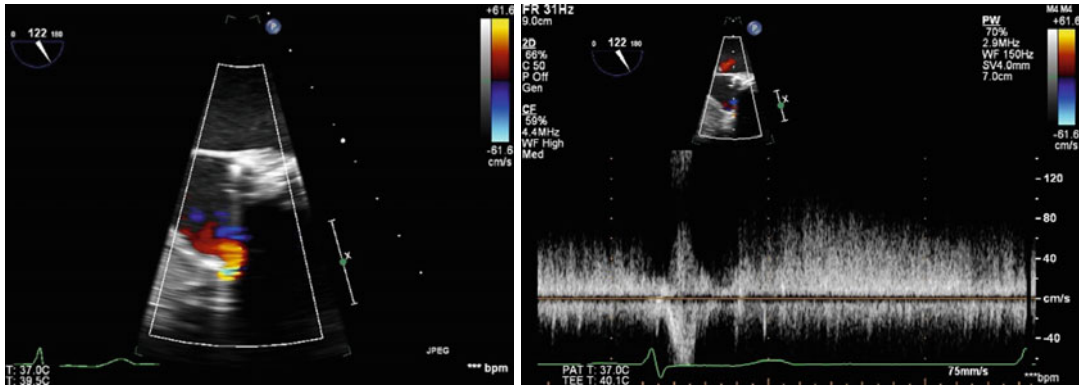

Figs. 8.45 and 8.46 2D TEE color (*left*) and pulsed Doppler (*right*), status post myectomy, showed a small coronary flow drained to LVOT with continuous flow

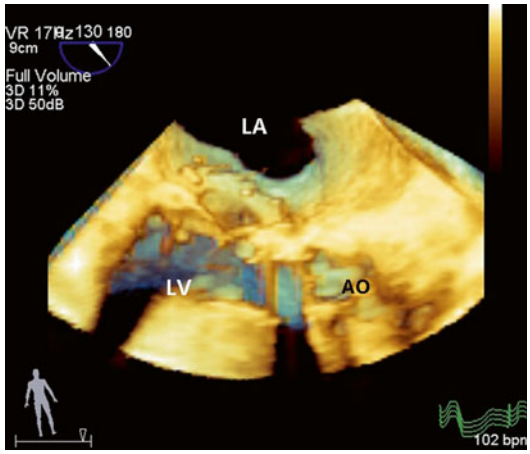

Fig. 8.47 3D TEE, long-axis view, status post myectomy, tissue AV and MV replacement, showed normal prosthetic function without systolic anterior motion

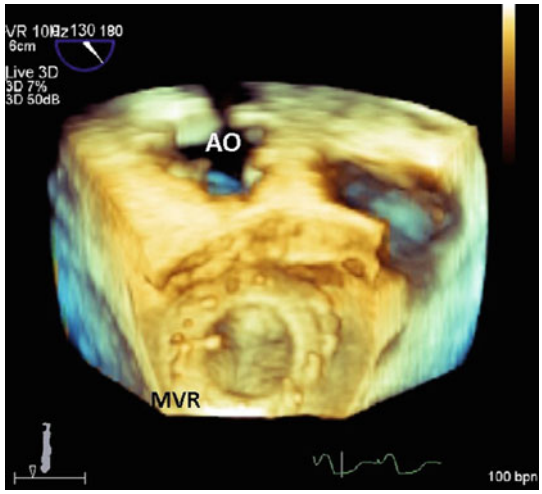

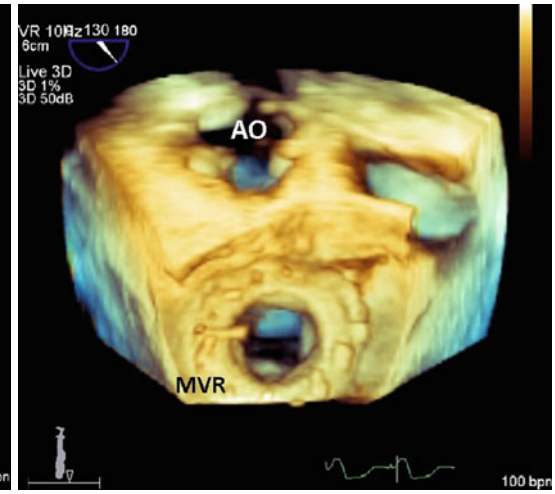

Figs. 8.48 and 8.49 3D TEE, en face view, status post tissue AV and MV replacement, showed normal prosthetic function

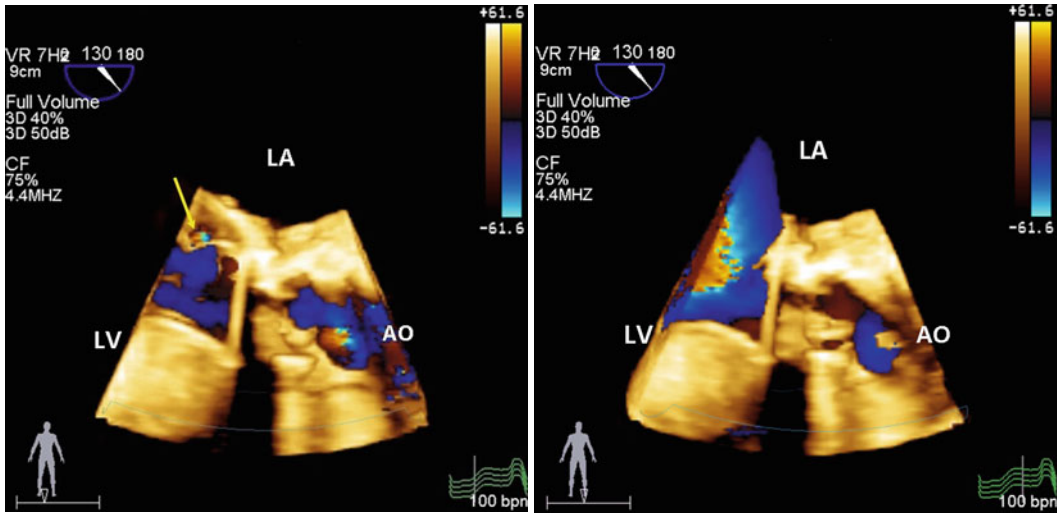

Figs. 8.50 and 8.51 3D TEE color Doppler, long-axis view, status post myectomy, tissue AV and MV replacement, showed minimal MR (*arrow*) and AR

Tips

Following septal myectomy, it is important to check the complication of the procedure which includes iatrogenic fistula and valvular damage.

Suggested Reading

Karataş MB, Güngör B, Mutluer FO, et al. Incremental utility of live/real time three-dimensional transesophageal echocardiography in a case with ventricular septal aneurysm and hypertrophic obstructive cardiomyopathy: a case report. Anadolu Kardiyol Derg. 2014;14(5):478–80.

Numata S, Yaku H, Doi K, et al. Excess anterior mitral leaflet in a patient with hypertrophic obstructive cardiomyopathy and systolic anterior motion. Circulation. 2015;131(18):1605–7.

Roy RR, Hakim FA, Hurst RT, et al. Two cases of apical ballooning syndrome masking apical hypertrophic cardiomyopathy. Tex Heart Inst J. 2014;41(2):179–83.

Varma PK, Puthuvassery Raman S, Unnikrishnan KP, et al. Intraoperative transesophageal echocardiography diagnosis of concomitant hypertrophic cardiomyopathy with anomalous insertion of a papillary muscle band to the interventricular septum in a patient for aortic valve replacement. J Cardiothorac Vasc Anesth. 2014;28(6):e56–8.

Zeineh NS, Eles G. Images in clinical medicine. Apical Hypertrophic Cardiomyopathy. N Engl J Med. 2015;373(19):e22.

Zhang LH, Fang LG, Yang J, et al. Infective endocarditis in patients with hypertrophic obstructive cardiomyopathy: five cases report. Zhonghua Xin Xue Guan Bing Za Zhi. 2012;40(3):209–13. Chinese.

Infective Endocarditis

9

Abstract

Infective Endocarditis is an inflammation of the valves and the endocardium. Vegetation formation is an essential evidence of infective endocarditis. The location, morphology, size, number, complications, and the mobility of the vegetation with the cardiac cycle must be assessed. Compared with transthoracic echocardiography, 3D TEE has much more advantages in examining infective endocarditis.

9.1 Mitral Valve Vegetation

A 63-year-old man with hypertension and severe MR suffered from shortness of breath and critical leg edema. Congestive heart failure was diagnosed. But after diuretic and inotropic agent therapy, symptoms worsened. Auscultation: irregular heart beat with a grade 3/6 systolic murmur over apex and left sternal border. ECG: atrial fibrillation, anterioseptal myocardial infarction and abnormal right axis deviation. Chest X ray: cardiomegaly with enlarged LV and right pleural effusion. Operation: MV replacement, repair of TV, atrial fibrillation ablation and ligation of RA and LA auricles.

Electronic supplementary material The online version of this chapter (doi:10.1007/978-981-10-0587-9_9) contains supplementary material, which is available to authorized users.

W.-H. Yin, M.-C. Hsiung, *Atlas of Perioperative 3D Transesophageal Echocardiography*,
DOI 10.1007/978-981-10-0587-9_9

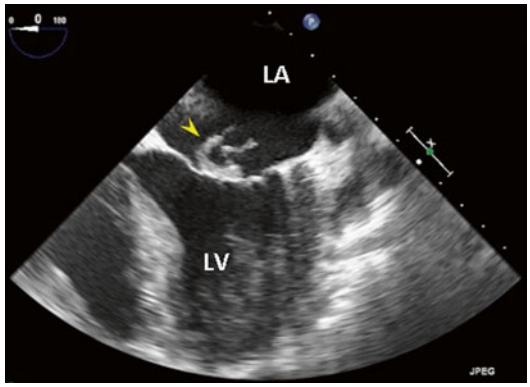

Fig. 9.1 Two-dimensional transesophageal echocardiography (2D TEE), four-chamber view, showed vegetation attached to the atrial side of both mitral leaflets (*arrow*) with AML flail into the LA

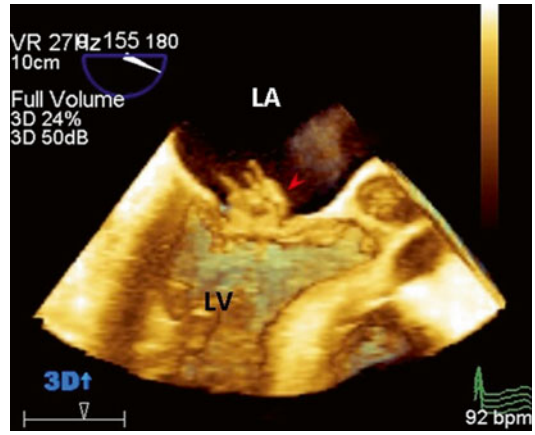

Fig. 9.3 3D TEE image, long-axis view, showed huge vegetation (*arrow*) attached to MV

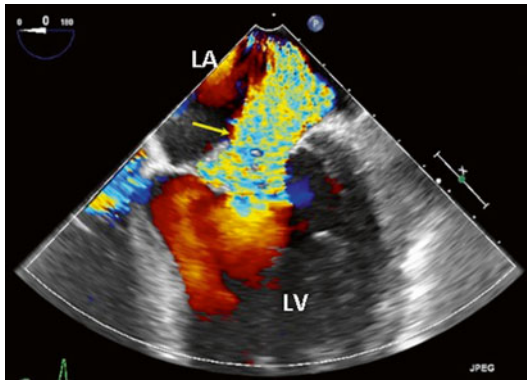

Fig. 9.2 2D TEE color Doppler, four-chamber view, showed severe eccentric MR (*arrow*) due to the flail leaflet

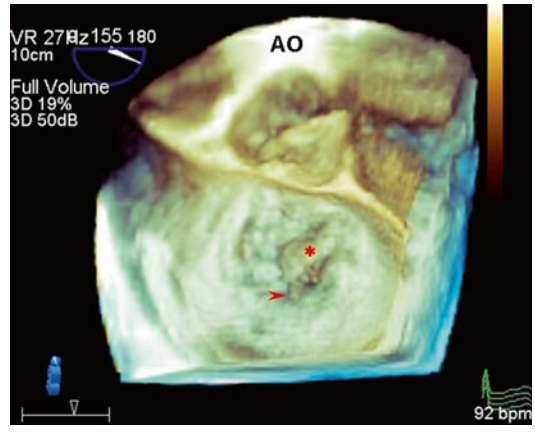

Fig. 9.4 3D TEE image, en face view, showed mitral vegetation (*) and flail of AML due to the rupture chordae (*arrow*)

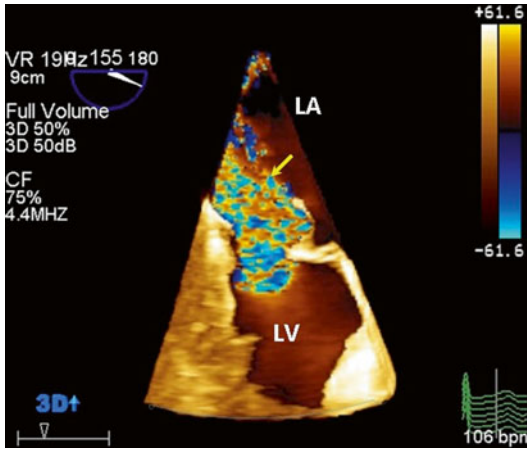

Fig. 9.5 3D TEE color Doppler, two-chamber view, showed severe eccentric MR (*arrow*) due to the flail leaflet

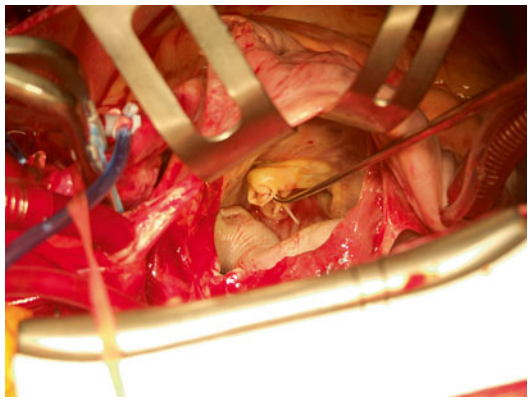

Fig. 9.6 Picture during operation showed the mitral vegetation

Tips

Mobile echodense masses attached to valvular leaflets and periannular abscesses are criteria for diagnosis of infective endocarditis.

9.2 Status Post Mitral Replacement Endocarditis

A 62-year-old woman had a history of rheumatic heart disease with mitral stenosis status post MV replacement 10 years ago and sick sinus syndrome status post permanent pacemaker. She suffered general weakness, chest pain and exertional dyspnea. Auscultation: regular heart beat. ECG: ventricular rhythm. Cardiac CT: marked cardiomegaly, lobulated masses over MV (2.2 cm × 1.5 cm at LA side, 1.8 cm × 1.3 cm at LV side with calcifications), engorged pulmonary arteries and right pleural effusion. Abdomen echo: engorged IVC and hepatic veins. Operation: redo MV replacement, repair of TV and pericardiectomy. Tissue culture of mitral vegetation confirmed micrococcus luteus.

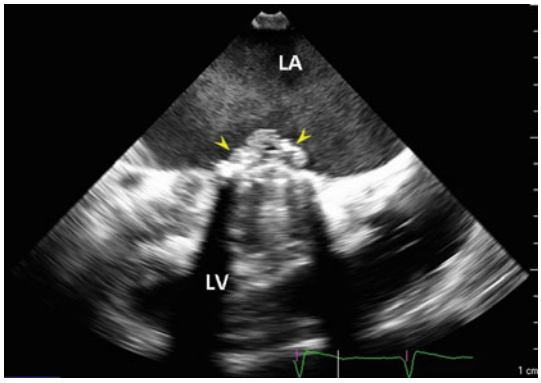

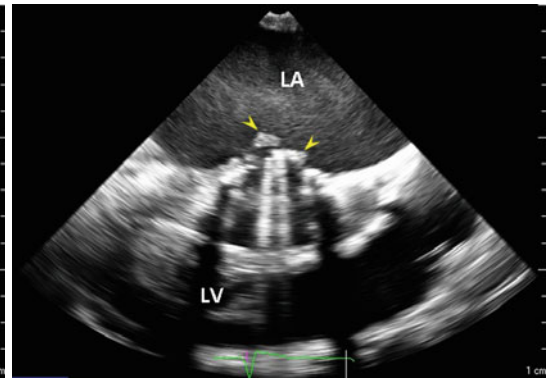

Figs. 9.7 and 9.8 Two dimensional transesophageal echocardiography (2D TEE), long-axis view in systole (*left*) and diastole (*right*), status post mechanical MV replacement, showed enlarged LA and irregularly shaped echogenic masses (*arrows*) attached to the atrial side of the mitral prosthesis

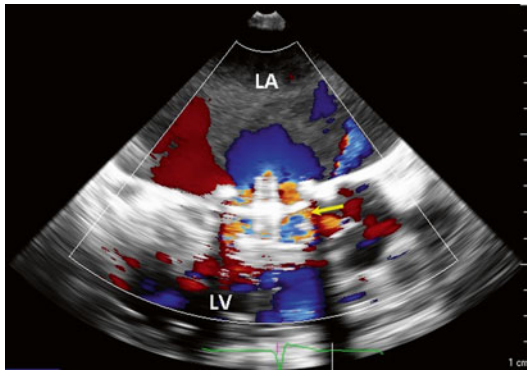

Fig. 9.9 2D TEE color Doppler, long-axis view, status post mechanical MV replacement, showed acceleration of mitral inflow (*arrow*)

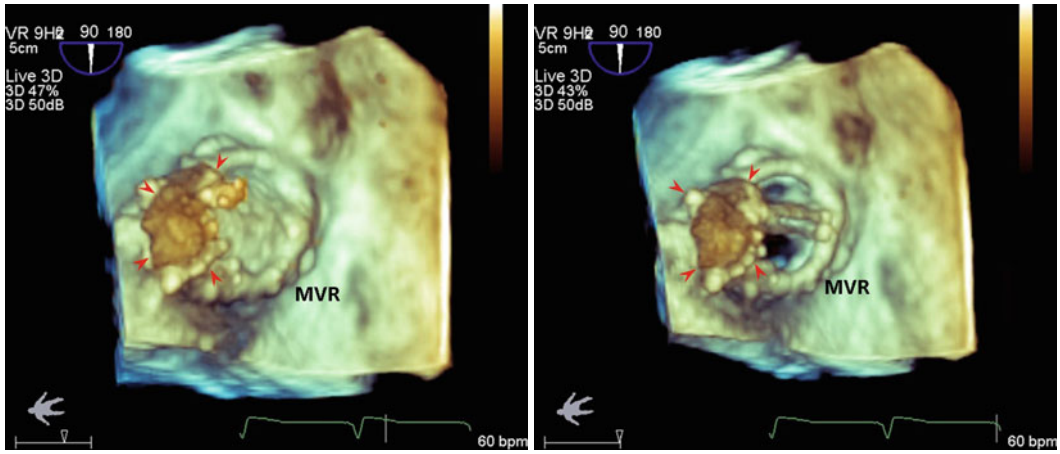

Figs. 9.10 and 9.11 3D TEE, en face view in systole (l*eft*) and diastole (*right*), status post mechanical MV replacement, showed the vegetation (*arrows*) was mobile and close to the prosthetic mitral annulus

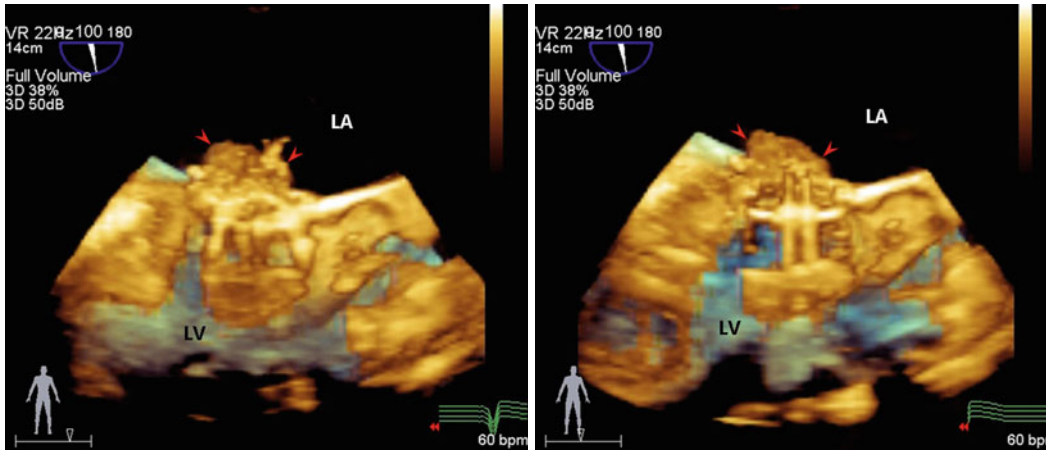

Figs. 9.12 and 9.13 3D TEE, long-axis view in systole (*left*) and diastole (*right*), status post mechanical MV replacement, showed a mobile vegetation (*arrows*) attached to the atrial side of the mitral prosthesis

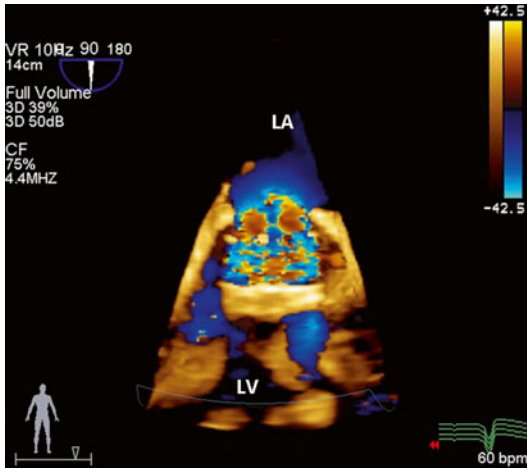

Fig. 9.14 3D TEE color Doppler, status post mechanical MV replacement, showed acceleration of mitral inflow

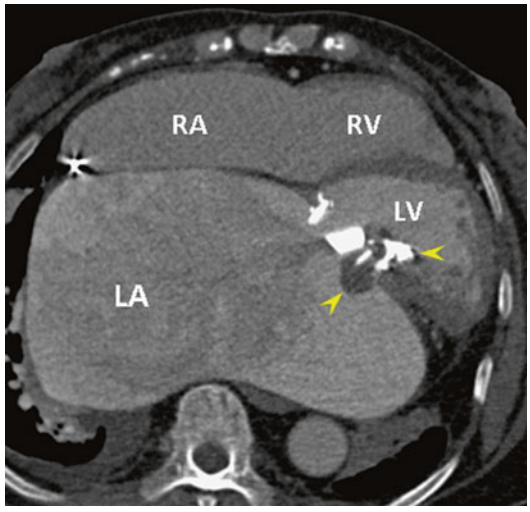

Fig. 9.15 Contrast-enhanced CT, status post mechanical MV replacement, showed marked cardiomegaly and lobulated masses (*arrows*) over both LA and LV sides of MV with calcifications

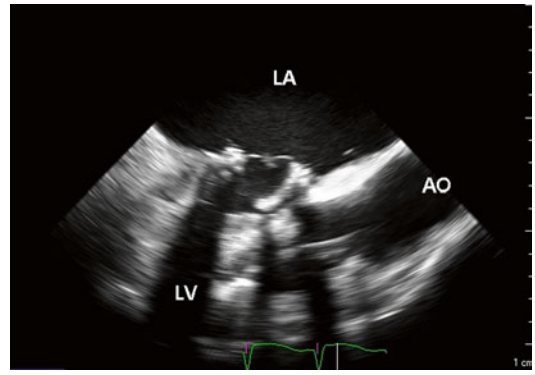

Fig. 9.16 2D TEE, long-axis view, status post re-do tissue MV replacement, showed normal prosthetic function

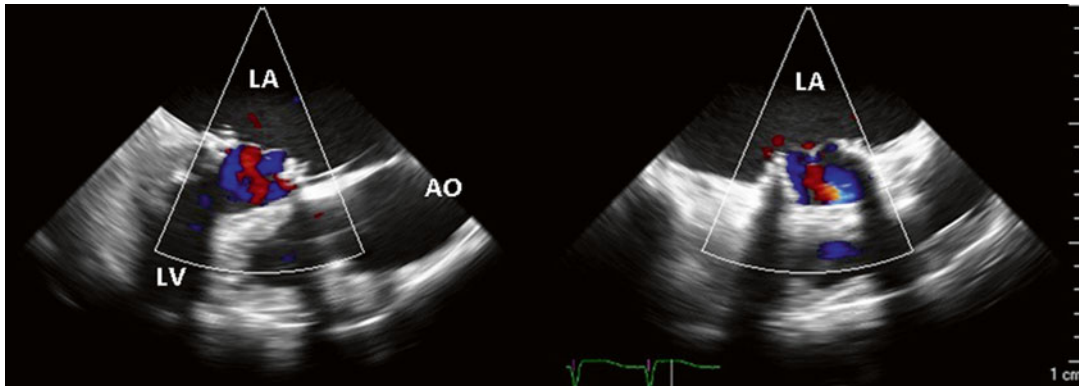

Fig. 9.17 2D TEE color Doppler, x-plane view, status post re-do tissue MV replacement, showed normal mitral inflow and minimal MR

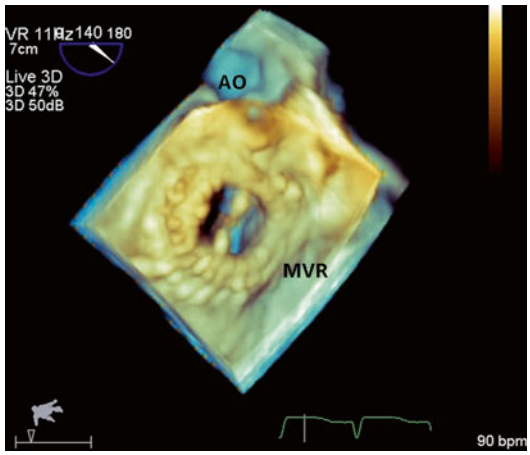

Fig. 9.18 3D TEE, en face view, status post re-do tissue MV replacement (*MVR*), showed normal prosthetic function

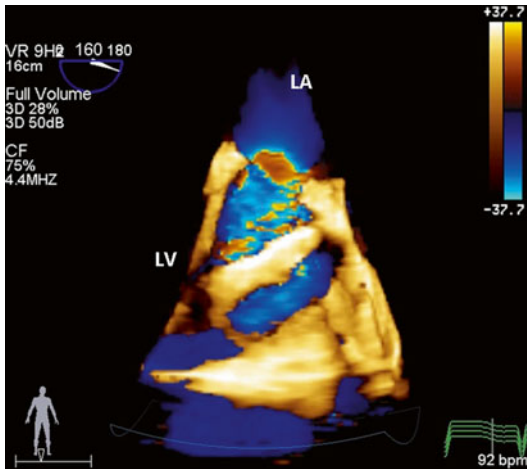

Fig. 9.19 3D TEE color Doppler, long-axis view, status post re-do tissue MV replacement, showed normal mitral inflow

Tips

The infection of prosthetic valve often involves the area around the sewing ring rather than valvular vegetation.

9.3 Bicuspid Aortic Valve Vegetation

A 57-year-old man without any previous medical history suffered from exertional shortness of breath. Auscultation: regular heart beat with a grade 2/6 systolic murmur over aortic area. ECG: LA enlargement, left axis deviation and LV hypertrophy. Chest X ray: cardiomegaly and bilateral pleural effusion. Cardiac catheterization: severe AR and pulmonary hypertension. Operation: AV replacement.

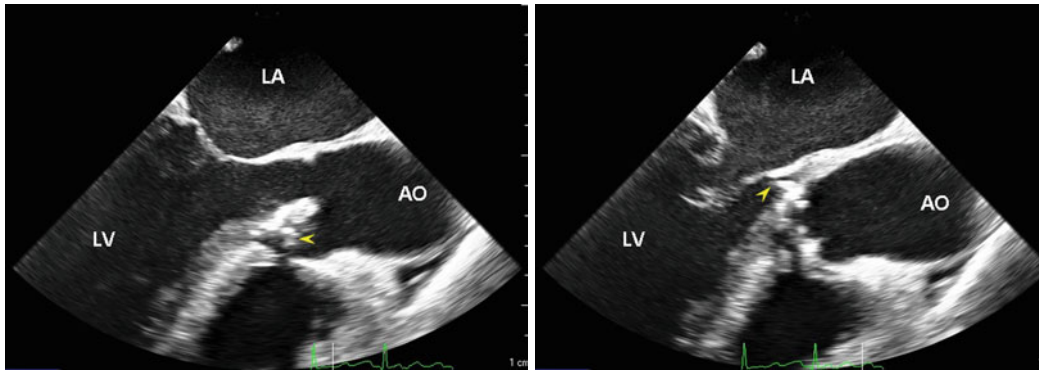

Figs. 9.20 and 9.21 2D TEE, long-axis view, showed systolic doming (*left*) and diastolic sagging (*right*) of AV with a vegetation (*arrows*) attached to it

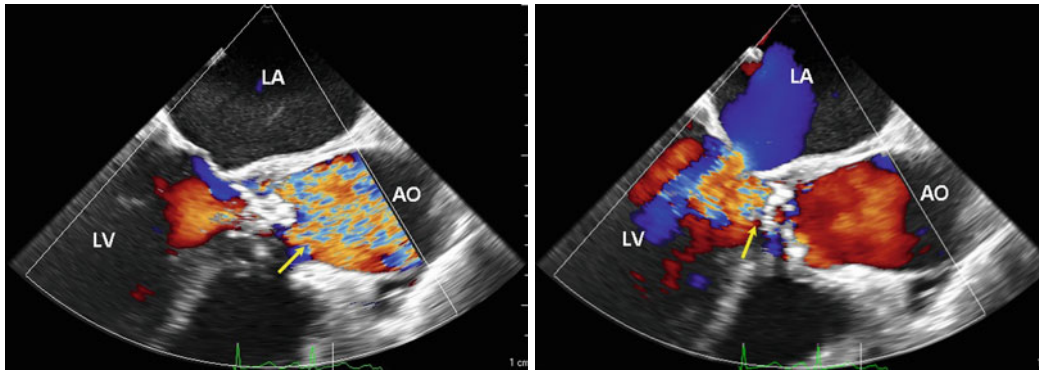

Figs. 9.22 and 9.23 2D TEE color Doppler, long-axis view, showed aortic stenosis (*AS*) with high-velocity LV outflow in systole (*left*) and severe AR in diastole (*right*)

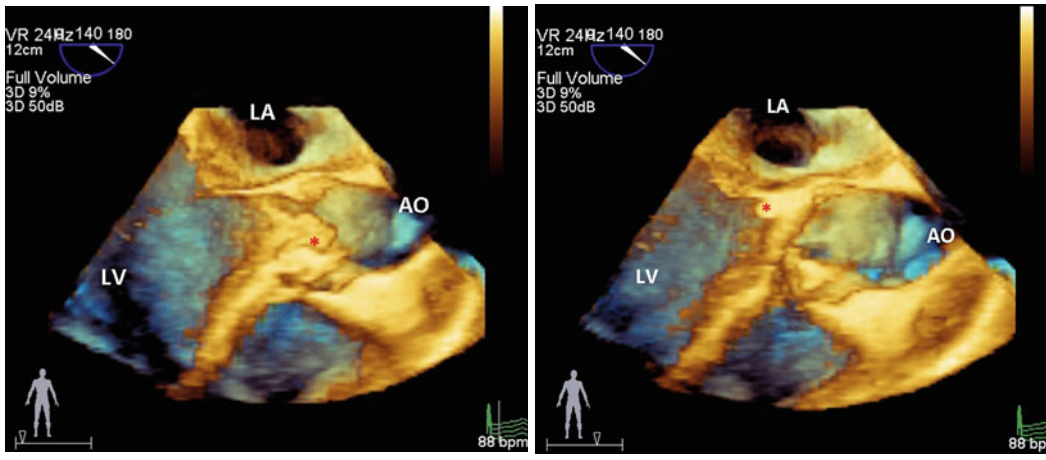

Figs. 9.24 and 9.25 3D TEE, long-axis view in systole (*left*) and diastole (*right*), showed AV vegetation (*) attached to the ventricular side of the leaflet with prolapse into the LV outflow tract in diastole

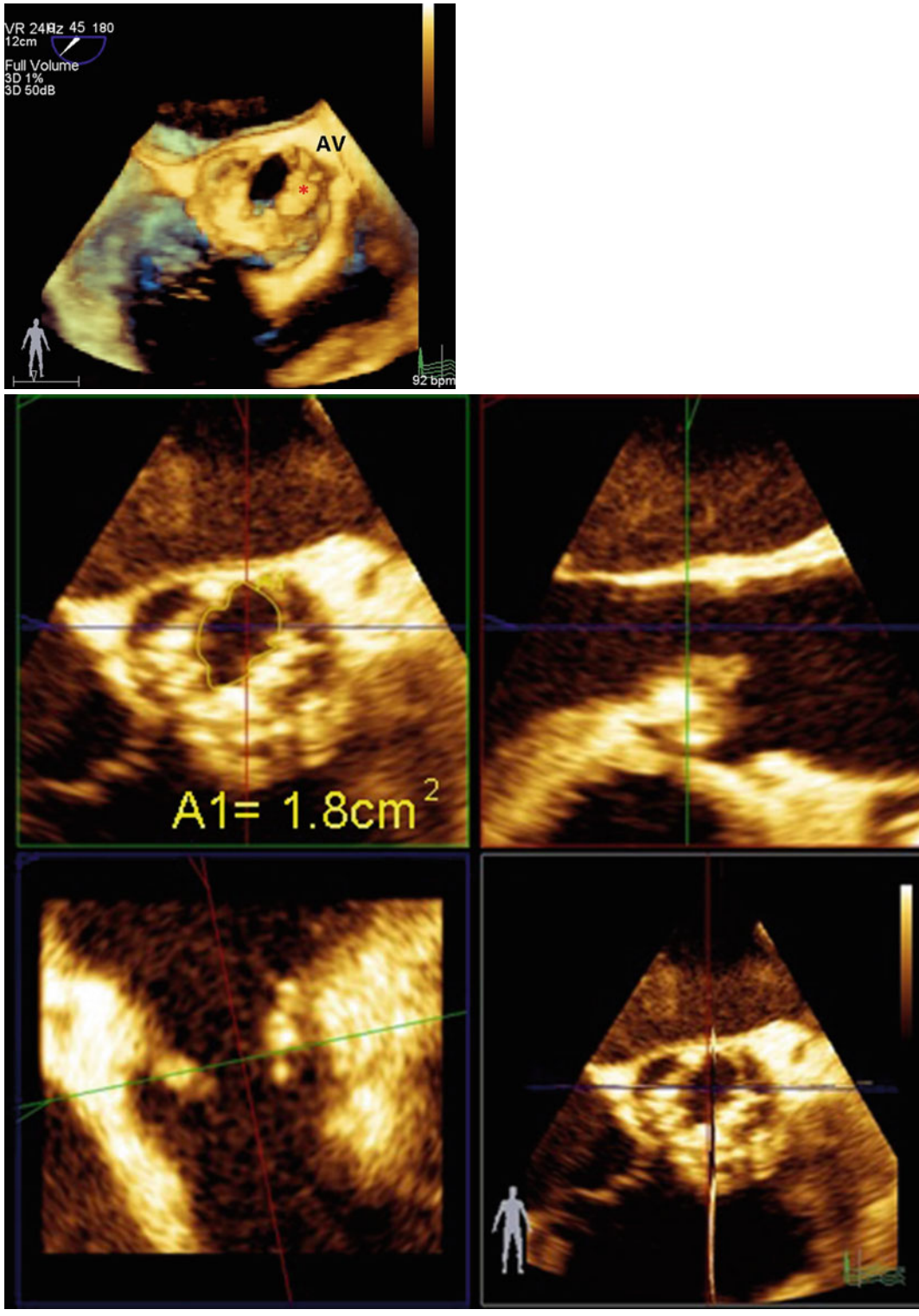

Figs. 9.26 and 9.27 3D TEE, short-axis view (*above*) and multi-planer reconstruction (*below*), showed bicuspid AV with vegetation (*) extension into the aortic root in systole and the AV area is 1.8 cm^2

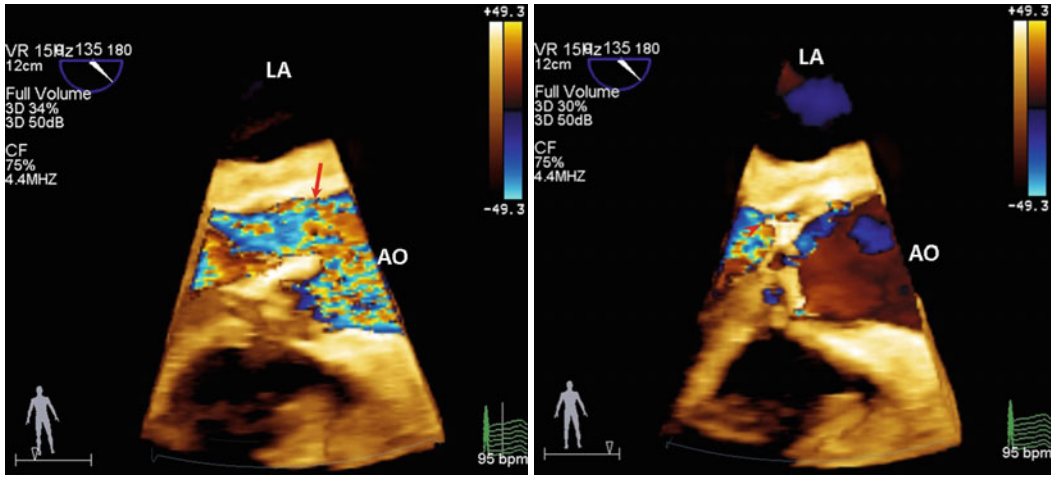

Figs. 9.28 and 9.29 3D TEE color Doppler, showed AS with high-velocity LV outflow (*arrow*) in systole (*left*) and severe AR in diastole (*right*) caused by AV vegetation (*arrow*)

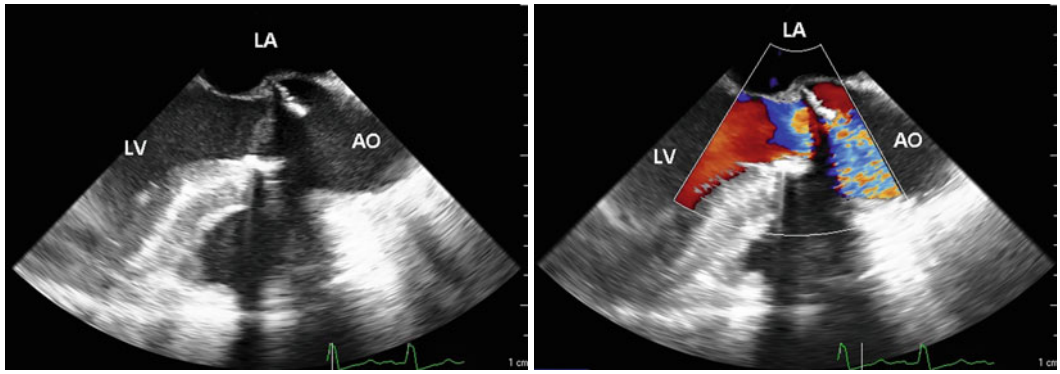

Figs. 9.30 and 9.31 2D TEE (*left*) and color Doppler (*right*), long-axis view, status post tissue AV replacement, showed normal prosthesis function and LV outflow

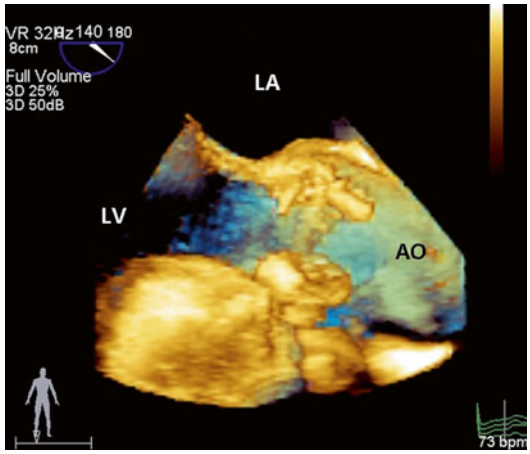

Fig. 9.32 3D TEE, long-axis view, status post tissue AV replacement (AVR), showed normal prosthesis function

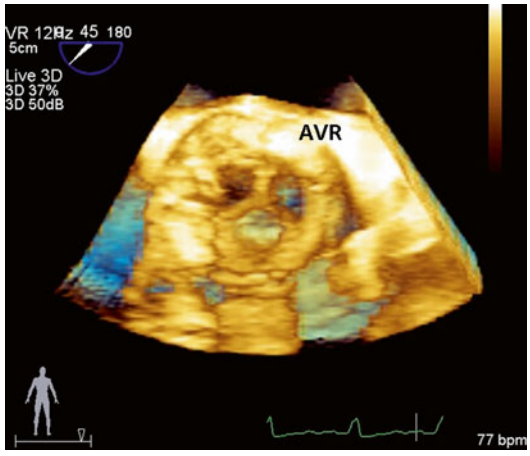

Fig. 9.33 3D TEE, short-axis view, status post tissue AVR, showed normal prosthesis function

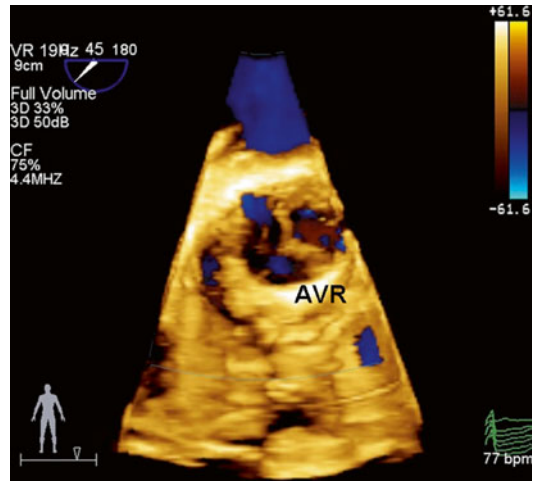

Fig. 9.34 3D TEE color Doppler, short-axis view, status post tissue AVR, showed normal LV outflow and minimal AR

Tips

An AV vegetation usually results in AR. A TEE examination is essential in detecting associated pathologies such as aortic abscess.

9.4 Ascending Aorta Vegetation

A 68-year-old woman has a history of coronary artery disease status post PCI, type two diabetes mellitus, bilateral pulmonary artery obstructive disease status post PTA with stent, end stage renal disease with regular hemodialysis and hyperlipidemia. She suffered from productive yellowish sputum and tarry stool, progressive shortness of breath and fever after dialysis. At emergency room, lab data showed leukocytosis and NT-pro BNP = 23202 pg/ml. Auscultation: irregular heart beat without significant murmur. ECG: sinus tachycardia and possible inferior ischemia. Chest X ray: pulmonary congestion, pneumonia and cardiomegaly. Chest CT: heavy calcification of coronary arteries. Operation: removal of vegetation in ascending aorta and CABG x1.

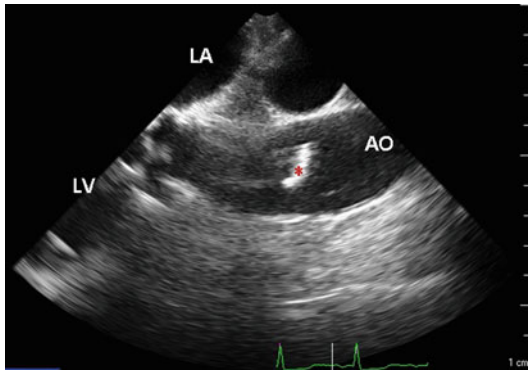

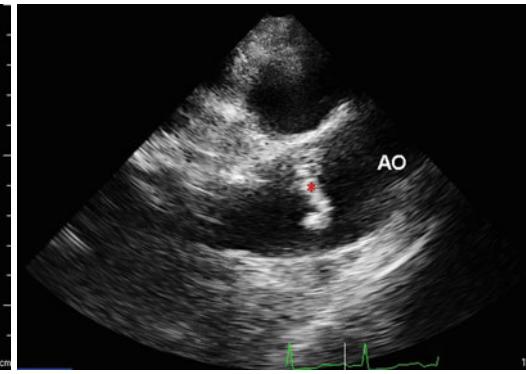

Figs. 9.35 and 9.36 Two-dimensional transesophageal ehcocardiagraphy (2D TEE), long-axis view, showed highly mobile vegetation (*) attached to the wall of ascending aorta

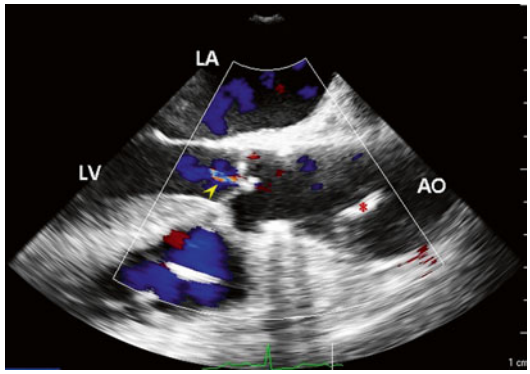

Fig. 9.37 2D TEE color Doppler, long-axis view, showed vegetation (*) in ascending aorta and mild AR (*arrow*)

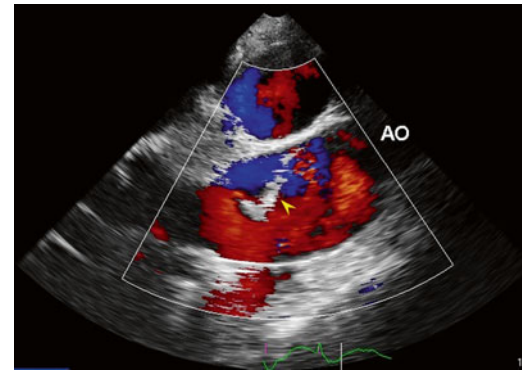

Fig. 9.38 2D TEE color Doppler, long-axis view, showed vegetation (*arrow*) in ascending aorta and flapping back and forth with cardiac cycle

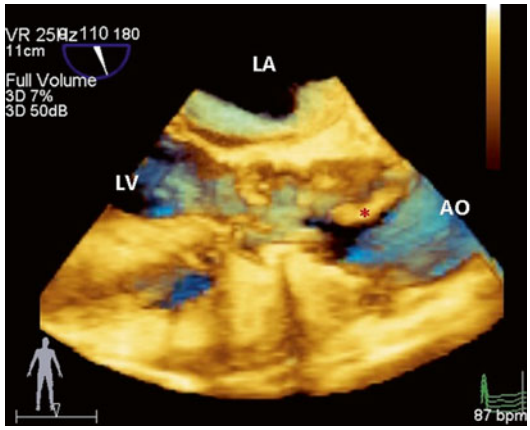

Fig. 9.39 3D TEE, long-axis view, showed highly mobile vegetation (*) attached to the wall of ascending aorta

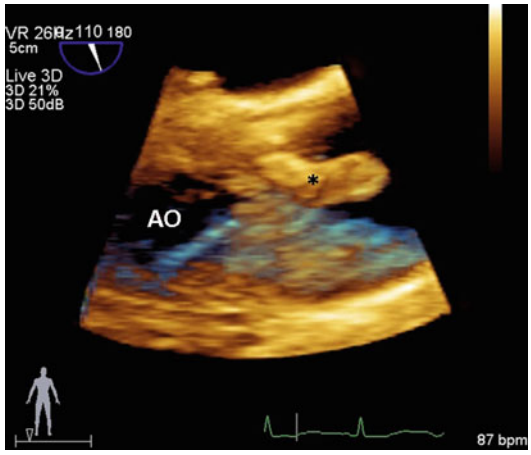

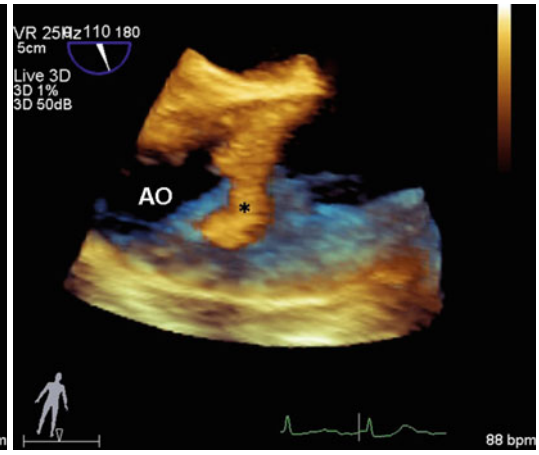

Figs. 9.40 and 9.41 3D TEE, zoom mode, showed highly mobile vegetation (*) attached to the wall of ascending aorta and flapping back and forth with cardiac cycle

Tips

Although TEE cannot define tissue pathology, the clinical presentation and image properties can help diagnosing vegetation and endocarditis.

9.5 Right Ventricular Outflow Tract Vegetation

A 49-year-old woman with old anterior septal myocardial infarction suffered from chest tightness and dyspnea. After being hospitalized, she experienced fever and Salmonella paratyphoin-A infection was found. Auscultation: regular heart beat without murmur. Cardiac catheterization: insignificant coronary artery disease. Chest CT: bilateral lung septic emboli, pericardial effusion with pericardial thickening and prominent pulmonary trunk with focal thickening over PV. Operation: emergency removal of RV outflow tract vegetation.

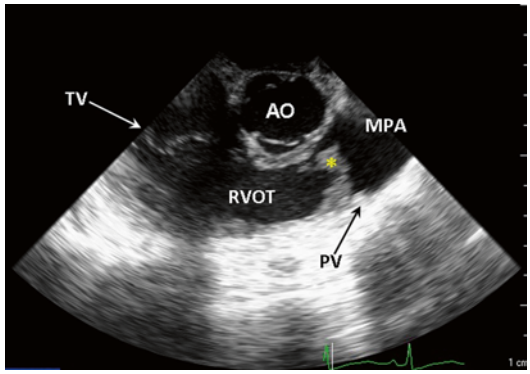

Fig. 9.42 Two-dimensional transesophageal echocardiography (2D TEE), short-axis view, showed a RV outflow tract vegetation (*) which was close to the PV. MPA, main pulmonary artery

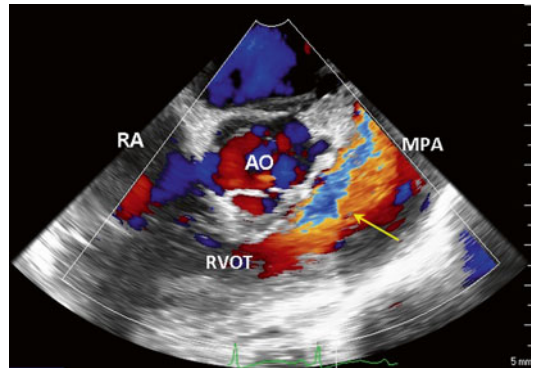

Fig. 9.44 2D TEE color Doppler, short-axis view, showed accelerated flow (*arrow*) in main pulmonary artery (*MPA*) caused by the RV outflow tract vegetation

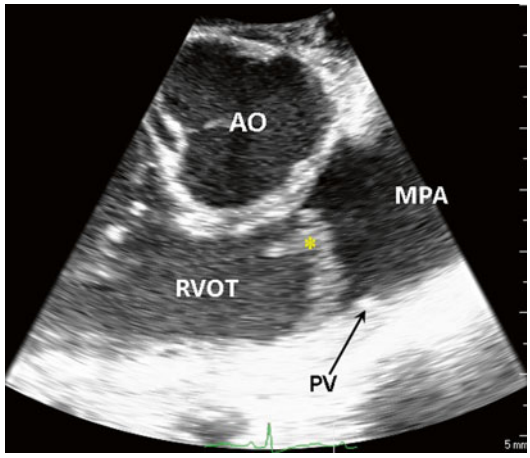

Fig. 9.43 2D TEE, zoom-mode of short-axis view, showed a RV outflow tract vegetation (*) which was close to the PV

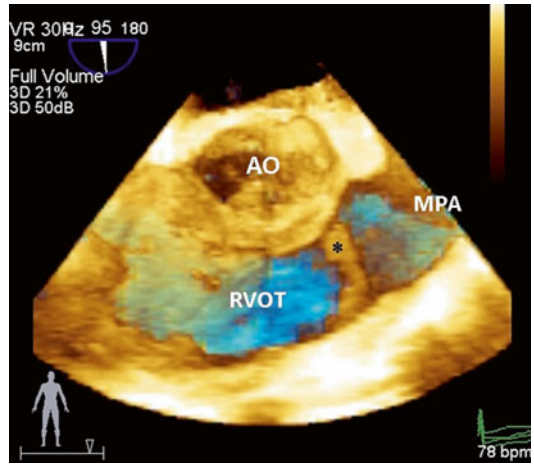

Fig. 9.45 3D TEE, short-axis view, showed a RV outflow tract vegetation (*) which was close to the PV

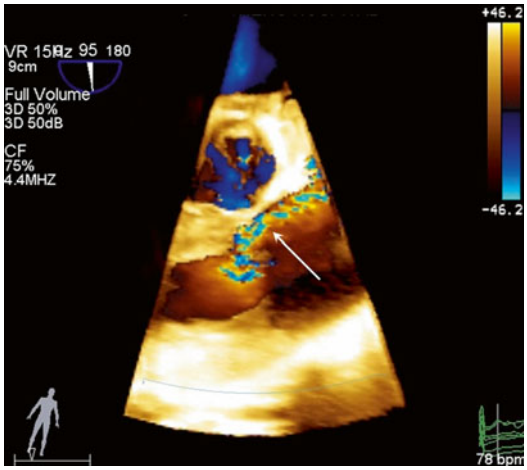

Fig. 9.46 3D TEE color Doppler, short-axis view, showed accelerated flow (*arrow*) in main pulmonary artery caused by the RV outflow tract vegetation

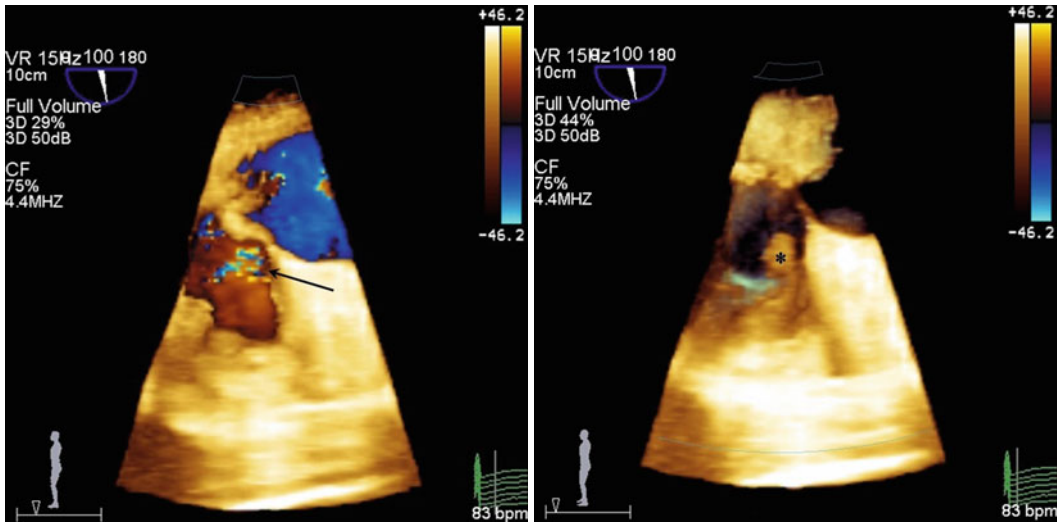

Figs. 9.47 and 9.48 3D TEE color Doppler (*left*) and color suppressed (*right*), view from RV perspective, showed accelerated flow (*arrow*) in main pulmonary artery caused by the RV outflow tract vegetation (*)

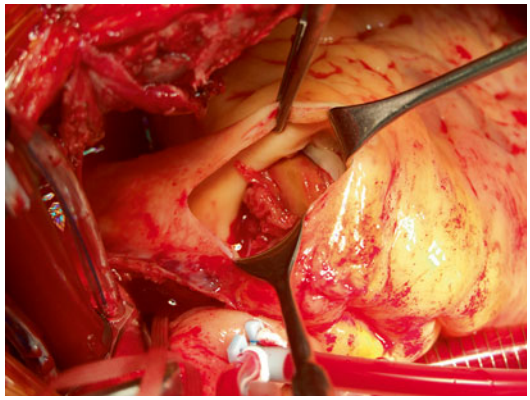

Fig. 9.49 Picture during the operation, the RV outflow tract vegetation was present

Tips

Although endocarditis often results in valvular vegetation, vegetation can arise from any portion of the heart.

9.6 Infective Endocarditis with Ventricular Septal Defect

A 27-year-old woman with heart murmur has run a fever since coming back from Thailand. Blood culture growth with MRSA. After antibiotics treatment, fever persisted. Auscultation: regular heart beat with a grade 2/6 systolic murmur. ECG: sinus tachycardia and nonspecific ST-T abnormality. Chest X ray: borderline cardiomegaly. Operation: TV repair and VSD patch repair.

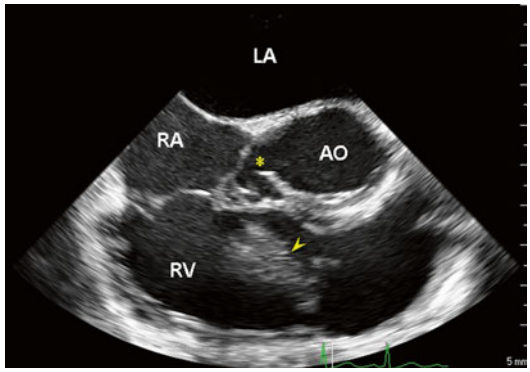

Fig. 9.50 Two-dimensional transesophageal echocardiogram (2D TEE), short-axis view, showed perimembranous ventricular septal defect (*) just lateral to the TV and huge TV vegetation (*arrow*)

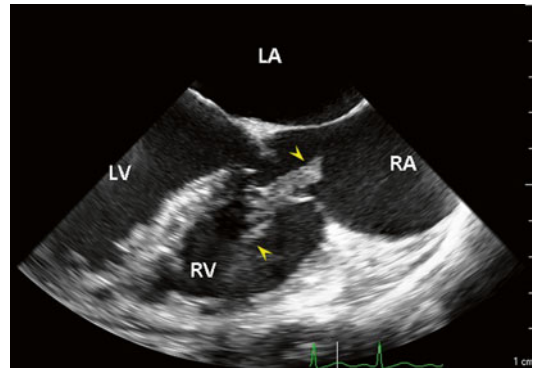

Fig. 9.52 2D TEE, modified four-chamber view, showed multiple highly mobile echodense masses (*arrows*) attached to both atrial and ventricular sides of the septal tricuspid leaflet

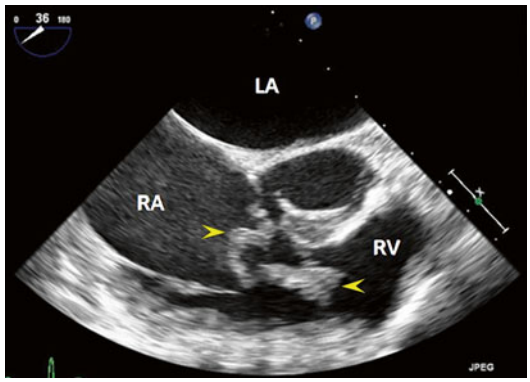

Fig. 9.51 2D TEE, short-axis view, showed multiple highly mobile echodense masses (*arrows*) attached to both atrial and ventricular sides of the septal tricuspid leaflet with its tail extended to the RV outflow tract

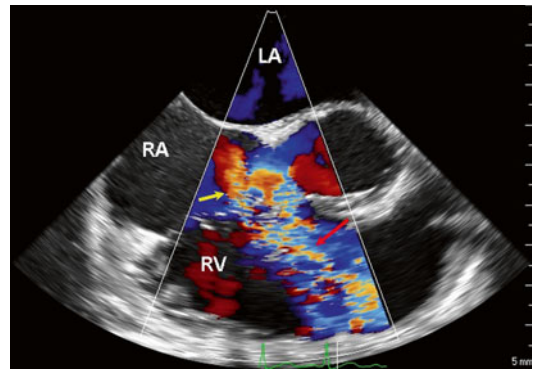

Fig. 9.53 2D TEE color Doppler, short-axis view, showed a left-to-right flow (*red arrow*) across the ventricular septal defect and mild to moderate TR (*yellow arrow*)

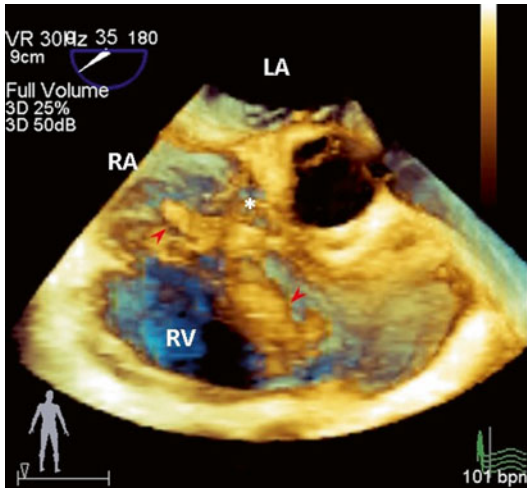

Fig. 9.54 3D TEE, short-axis view, showed a perimembranous ventricular septal defect (*) and vegetation (*arrows*) attached to both atrial and ventricular sides of septal tricuspid leaflet

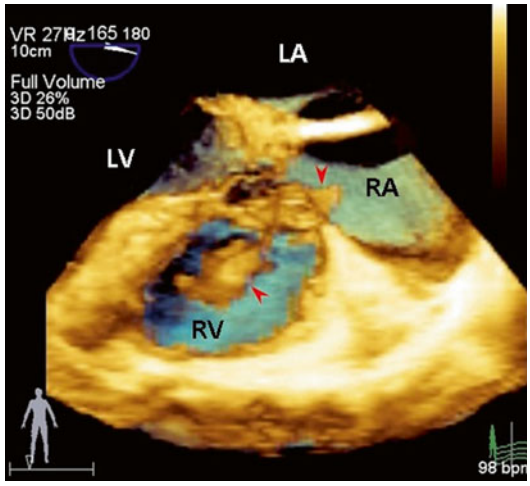

Fig. 9.55 3D TEE, modified four- chamber view, showed vegetation (*arrows*) attached to both atrial and ventricular sides of septal tricuspid leaflet

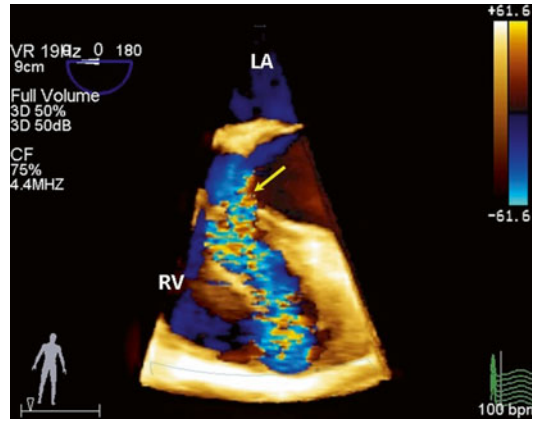

Fig. 9.56 3D TEE color Doppler, short-axis view, showed a left-to-right flow (*arrow*) across the ventricular septal defect

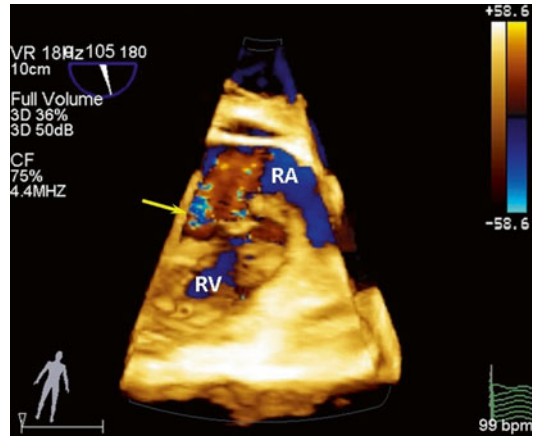

Fig. 9.57 3D TEE color Doppler, modified four-chamber view, showed a mild to moderate TR (*arrow*)

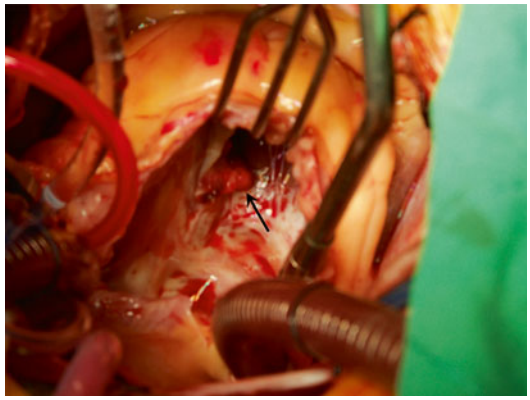

Fig. 9.58 Picture during operation, showed the septal tricuspid vegetation (*arrow*)

Tips

The differential diagnosis of a large, mobile, echodense mass includes thrombus or a tumor. The pathology should be confirmed by blood culture.

Suggested Reading

Allred C, Crandall M, Auseon A. The important but underappreciated transgastric right ventricular inflow view for transesophageal echocardiographic evaluation of cardiac implantable device infections. Echocardiography. 2013;30(1):E1–3.

Almdahl SM, Endresen PC, et al. Unusual left atrial vegetation. J Card Surg. 2014;29(5):638.

Anwar AM, Nosir YF, et al. Real time three-dimensional transesophageal echocardiography: a novel approach for the assessment of prosthetic heart valves. Echocardiography. 2014;31(2):188–96.

Barton TL, Mottram PM, Stuart RL, et al. Transthoracic echocardiography is still useful in the initial evaluation of patients with suspected infective endocarditis: evaluation of a large cohort at a tertiary referral center. Mayo Clin Proc. 2014;89(6):799–805.

Butler TC, Sedgwick JF, Burstow DJ. 3-D assesment of infecrive endocarditis with anterior mitral valve perforation and flail posterior leaflet. Int J Cardiol. 2015;185:249.

Chen SW, Tsai FC, Chou AH. Adult bicuspid aortic valve endocarditis with extensive paravalvular invasion attributable to disseminated varicella zoster infection. Ann Thorac Cardiovasc Surg. 2012;18(4):382–4.

Di Benedetto G, Citro R, Longobardi A, et al. Giant Candida mycetoma in an ascending aorta tubular graft. J Card Surg. 2013;28(5):557–60.

Harinstein ME, Marroquin OC. External coronary artery compression due to prosthetic valve bacterial endocarditis. Catheter Cardiovasc Interv. 2014;83(3):E168–70.

Liang M, Pasupati S, Jogia D. Post-transcoronary ethanol septal ablation (TESA) infective endocarditis complicated by aventricular septal defect. J Invasive Cardiol. 2011;23(8):348–50.

Ouyang H, Wu X, Zhang J. Giant vegetation in the right ventricle caused by Staphylococcus aureus and Candida mycoderma. Heart Surg Forum. 2014;17(1):E7–9.

Patel N, Azemi T, Zaeem F, et al. Vacuum assisted vegetation extraction for the management of large lead vegetations. J Card Surg. 2013;28(3):321–4.

Rap MI, Chacko A. Optimising the use of transoesophageal echocardiography in diagnosing suspected infective endocarditis. Acta Cardiol. 2015;70(4):487–91.

Suryaprabha T, Kaul S, Alladi S, et al. Acute posterior circulation infarct due to bicuspid aortic valve vegetation: an uncommon stroke mechanism. Ann Indian Acad Neurol. 2013;16(1):100–2.

Tanaka A, Sakamoto T, et al. Vegetation attached to the elephant trunk. Eur J Cardiothorac Surg. 2013;44(3):565–6.

Tanis W, Teske AJ, van Herwerden LA, et al. The additional value of three-dimensional transesophageal echocardiography in complex aorticprosthetic heart valve endocarditis. Echocardiography. 2015;32(1):114–25.

Vilacosta I, Olmos C, de Agustín A, et al. The diagnostic ability of echocardiography for infective endocarditis and its associated complications. Expert Rev Cardiovasc Ther. 2015;16:1–12.

Yong MS, Saxena P, Killu AM, et al. The preoperative evaluation of infective endocarditis via 3-dimentational tranesophageal echocardiography. Tex Heart Inst J. 2015;42(4):372–6.

Tumors and Mass Lesions

10

Abstract

This chapter deals with tumors and mass lesions. Cases of thrombus, myxomas, and thymoma are described.

3D TEE allows a full view and better understanding of the mass and its relation with the surrounding anatomic structures. An en face view of the LAA inlet from the LA can be provided to evaluate the LAA thrombus.

10.1 Left Atrial Thrombus

A 73-year-old man had a history of hypertension, hepatitis B and chronic atrial fibrillation. A LA thrombus was told by another hospital. Auscultation: irregular heart beat with a grade 3 systolic murmur over apex. ECG: atrial fibrillation with rapid ventricular response, clockwise rotation and non-specific STT change. Chest x ray: mild cardiomegaly. Cardiac catheterization: single vessel coronary disease. Operation: removal of LA thrombus, obliteration of LA appendage and atrial fibrillation ablation.

Electronic supplementary material The online version of this chapter (doi:10.1007/978-981-10-0587-9_10) contains supplementary material, which is available to authorized users.

W.-H. Yin, M.-C. Hsiung, *Atlas of Perioperative 3D Transesophageal Echocardiography*,
DOI 10.1007/978-981-10-0587-9_10

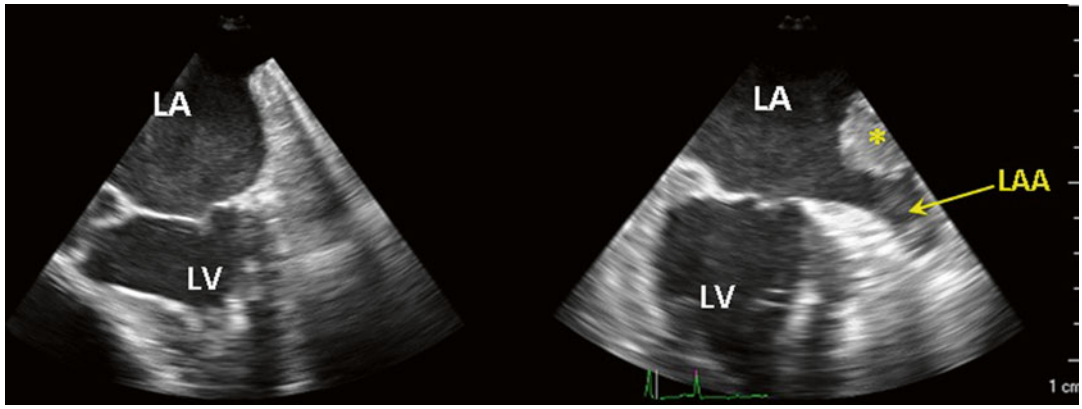

Fig. 10.1 Two-dimensional transesophageal echocardiography (2D TEE), x-plane view, showed dilated LA with a thrombus (*) in LA appendage (*LAA*)

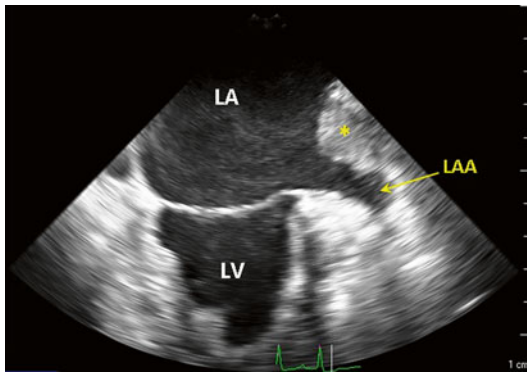

Fig. 10.2 2D TEE, two-chamber view, showed dilated LA with a thrombus (*) in LA appendage (*LAA*)

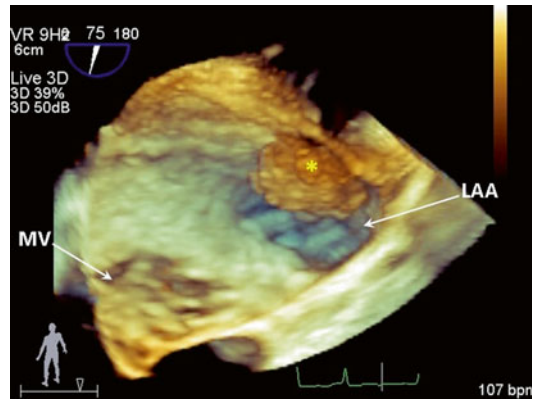

Fig. 10.4 3D TEE, view from LA perspective, showed a thrombus (*) in LA appendage (*LAA*)

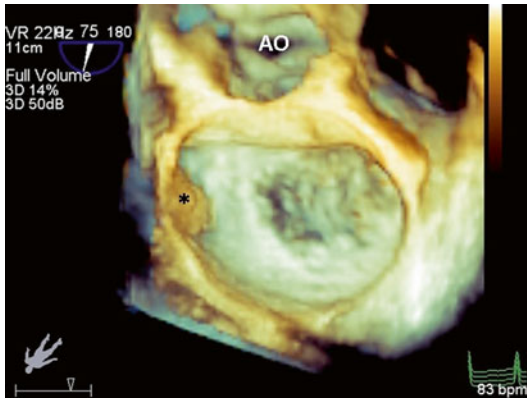

Fig. 10.3 3D TEE, en face view, showed a thrombus (*) in LA

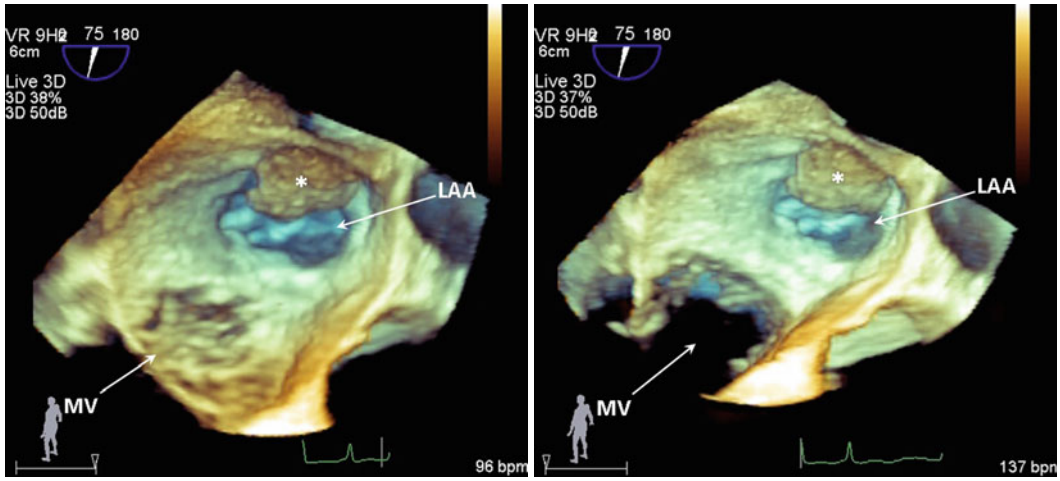

Figs. 10.5 and 10.6 3D TEE, view from LA perspective in systole (*left*) and diastole (*right*), showed a thrombus (*) in LA appendage (*LAA*)

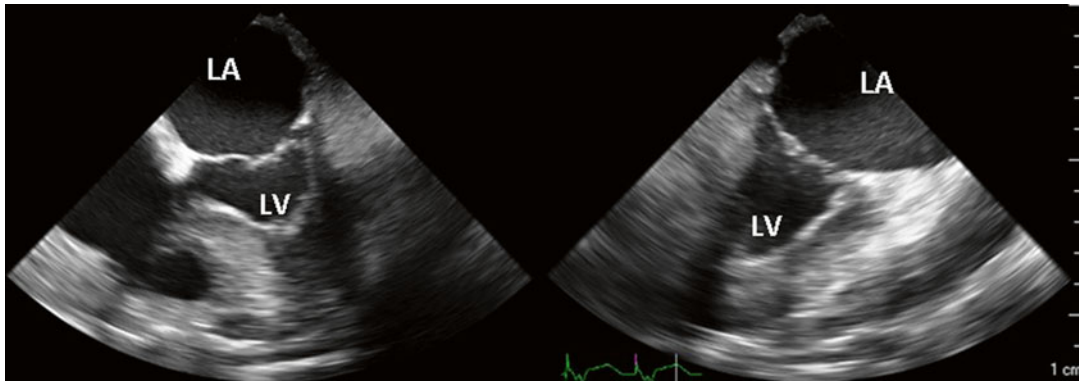

Fig. 10.7 2D TEE, x-plane view, status post removal of LA thrombus and obliteration of LA appendage, showed no more thrombus in LA

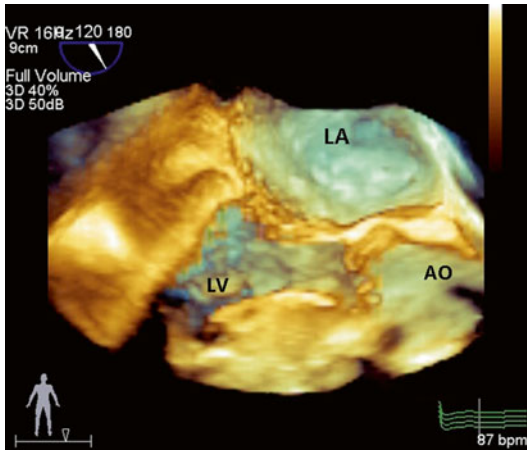

Fig. 10.8 3D TEE, long-axis view, status post removal of LA thrombus and obliteration of LA appendage, no more thrombus was in LA

Tips

In 2D TEE, two- and four-chamber views provide best images of LAA. But in 3D TEE, multiple viewing perspectives are available to evaluate the thrombus in LAA.

10.2 Left Atrial Myxoma

A 61-year-old man with medical-controlled type two diabetes mellitus suffered from dizziness with heart burn sensation. He was told having a LA tumor by other hospital. Auscultation: regular heart beat without murmur. ECG: non-specific ST-T change. Cardiac catheterization: single-vessel coronary artery disease. Operation: removal of LA tumor, patch repair of created ASD and CABG x1 (SVG to OM2). Pathological diagnosis: myxoma.

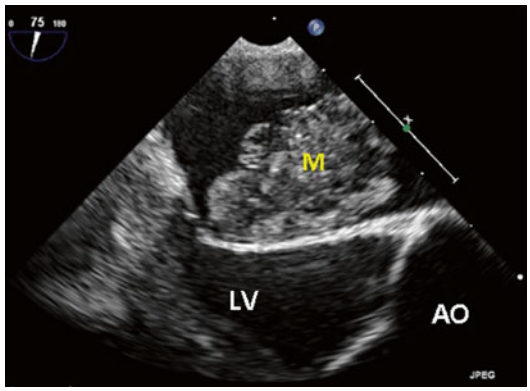

Fig. 10.9 Two-dimensional transesophegeal echocardiography (2D TEE), long-axis view, showed a highly mobile, grape cluster appearance myxoma (*M*) attached to anterior mitral leaflet

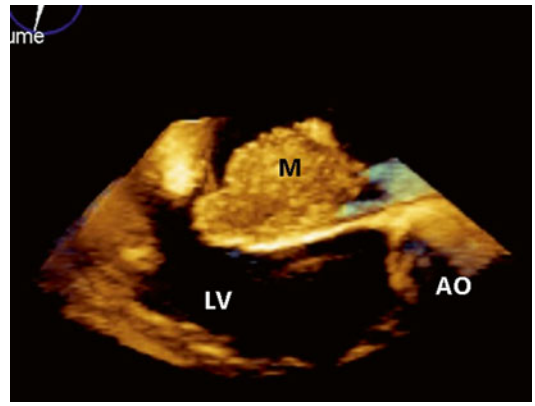

Fig. 10.11 3D TEE, long-axis view, showed the irregular LA myxoma (*M*) prolapse across the mitral annulus into the LV in diastole

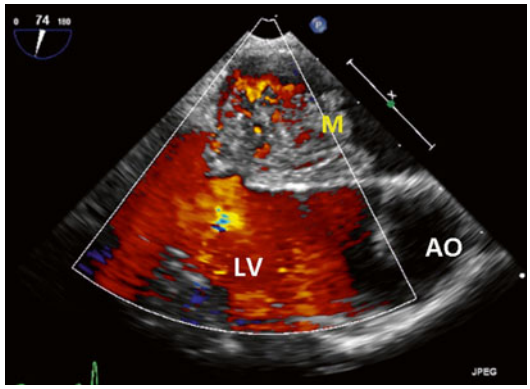

Fig. 10.10 2D TEE color Doppler, long-axis view, showed the LA myxoma (*M*) with flow across and caused eccentric MR

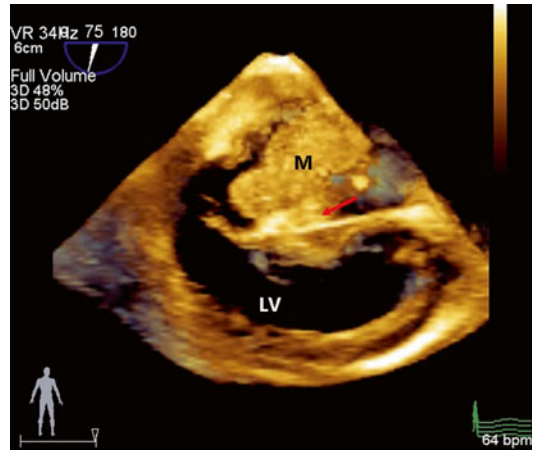

Fig. 10.12 3D TEE, showed the LA myxoma (*M*) arising from a stalk (*arrow*) attached to the anterior mitral leaflet

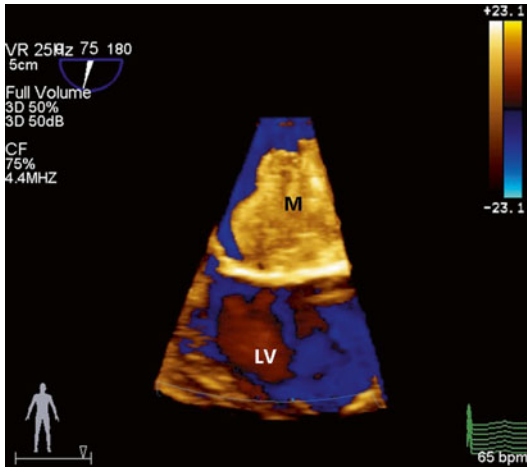

Fig. 10.13 3D TEE color Doppler, long-axis view, showed eccentric MR and normal LV diastolic filling

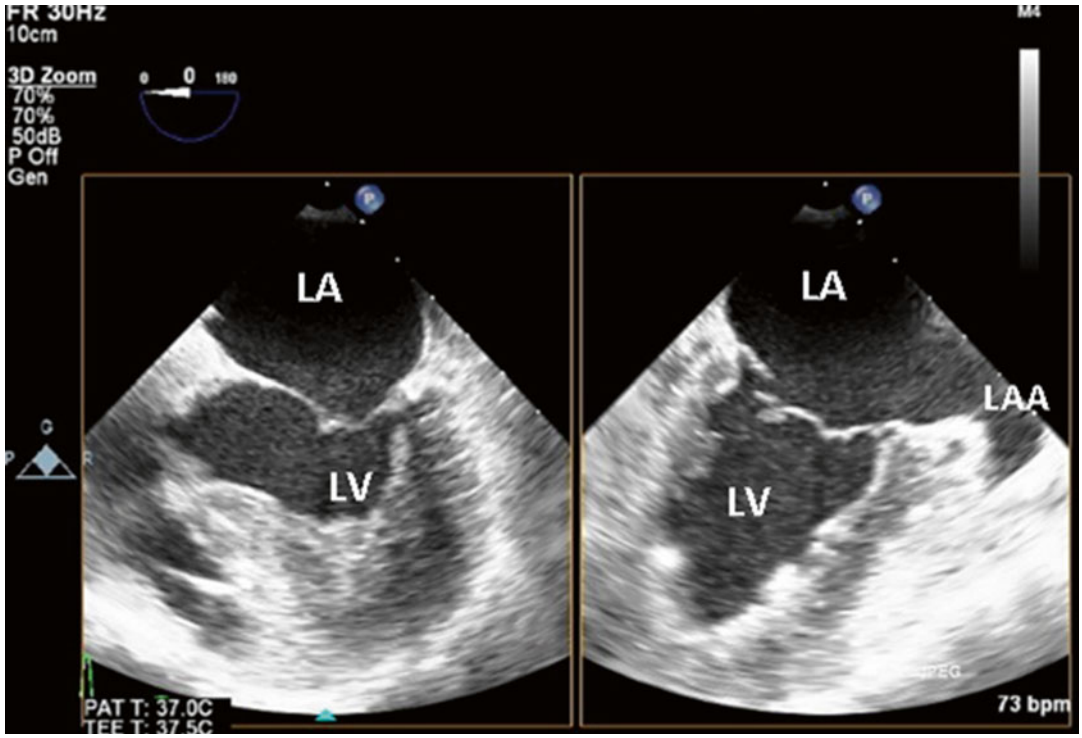

Fig. 10.14 2D TEE image, x-plane view, status post removal of LA tumor, showed clear LA with normal MV function

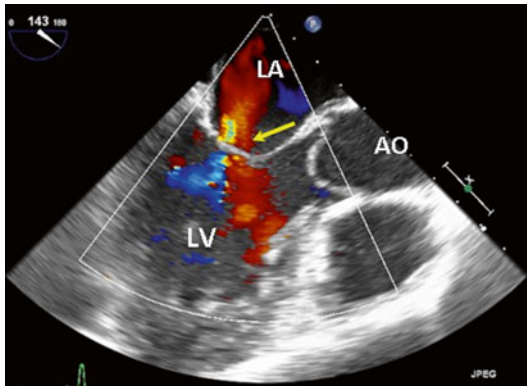

Fig. 10.15 2D TEE color Doppler, long- axis view, status post removal of LA tumor, showed mild MR (*arrow*)

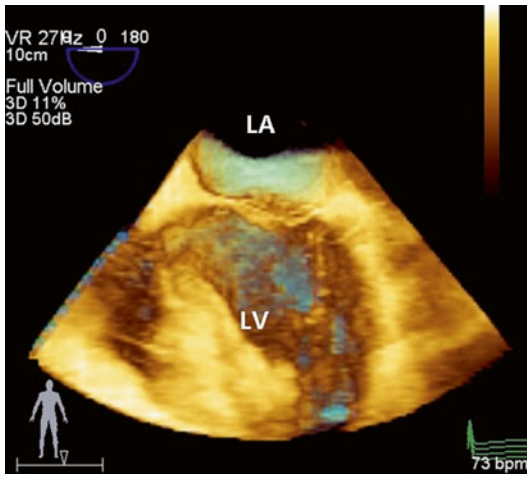

Fig. 10.16 3D TEE, five-chamber view, status post removal of LA tumor, showed clear LA with normal MV function

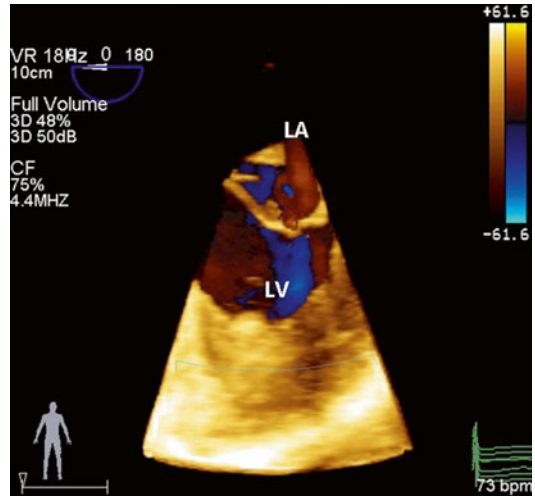

Fig. 10.17 3D TEE color Doppler, five-chamber view, status post removal of LA tumor, showed mild MR

Tips

Clinical presentation, location, attachment site, mobility, size and shape are key points to elaborate an intracardiac mass. Among which, determination of the attachment site is the most essential for surgical plan for resection.

10.3 Right Atrial Myxoma

A 50-year-old woman presented with RA tumor, numbness of bilateral hand and shortness of breath. Auscultation: regular heart beat. ECG: RA enlargement and right axis deviation. Catheterization: a large RCA branch gave blood supply to the huge RA tumor, positive tumor stain sign. Operation: RA tumor removal. Pathological diagnosis: myxoma.

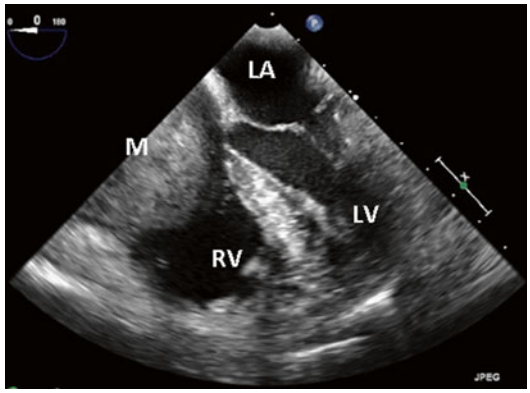

Fig. 10.18 Two-dimensional transesophageal echocardiography (2D TEE), modified four-chamber view, showed a huge mobile mass (*M*) in RA with dilated RA and RV

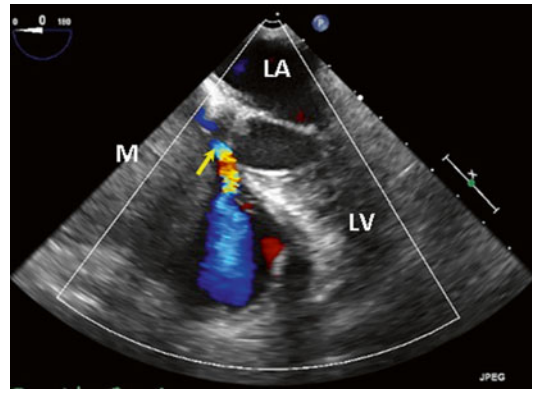

Fig. 10.20 2D TEE color Doppler, modified four-chamber view, showed accelerated tricuspid inflow (*arrow*), partial obstruction to RV diastolic filling, due to the atrial mass (*M*)

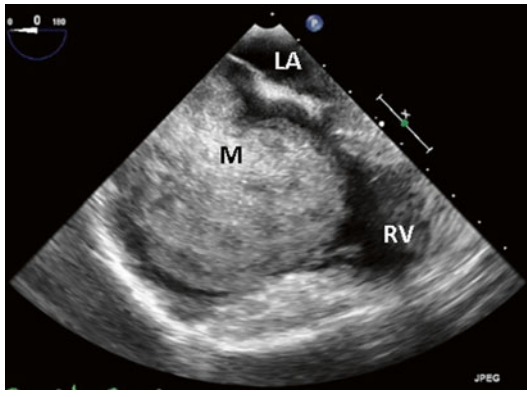

Fig. 10.19 2D TEE, modified four-chamber view, showed the mass (*M*) with non-homogeneous density attached to RA basal posterior wall

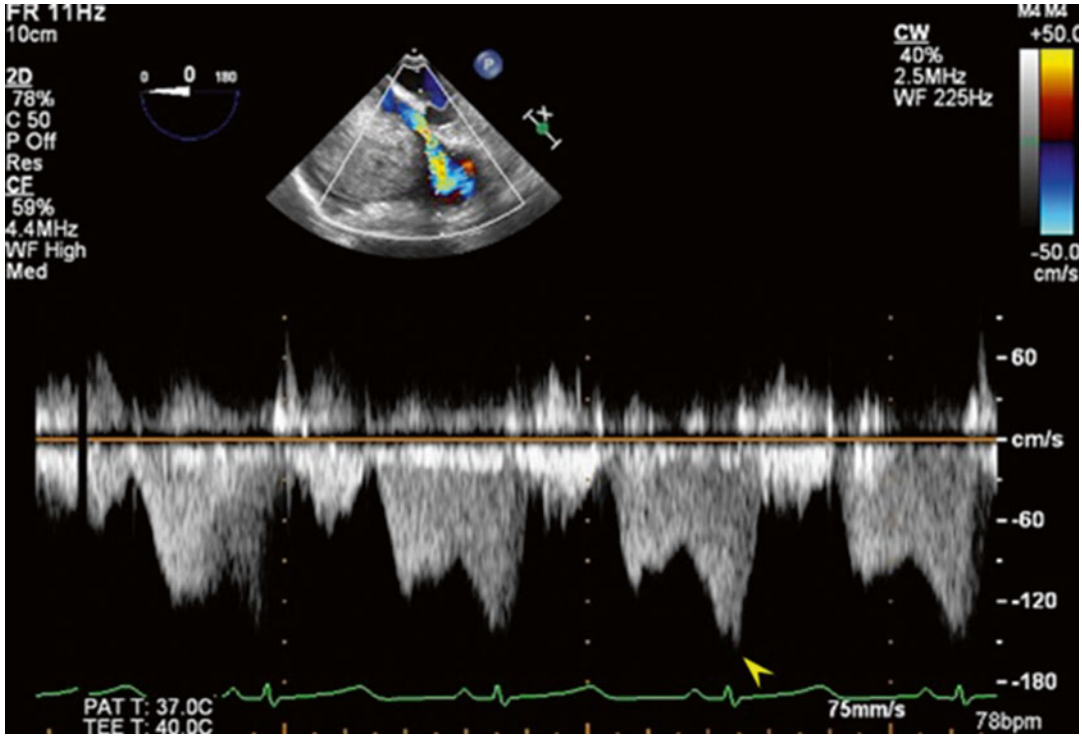

Fig. 10.21 2D TEE continuous-wave Doppler of TV, TS with high gradient tricuspid inflow (*arrow*) was present

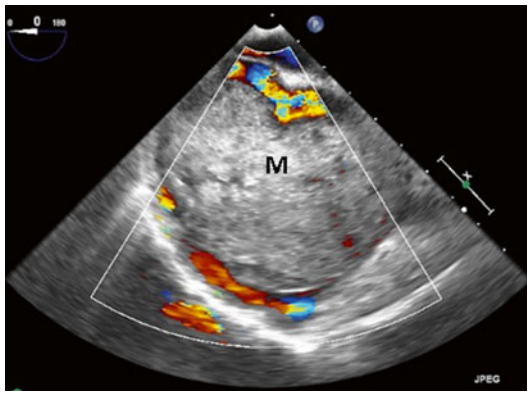

Fig. 10.22 2D TEE color Doppler, modified four-chamber view, showed the RA mass (*M*) had blood supply and nearly filled the chamber

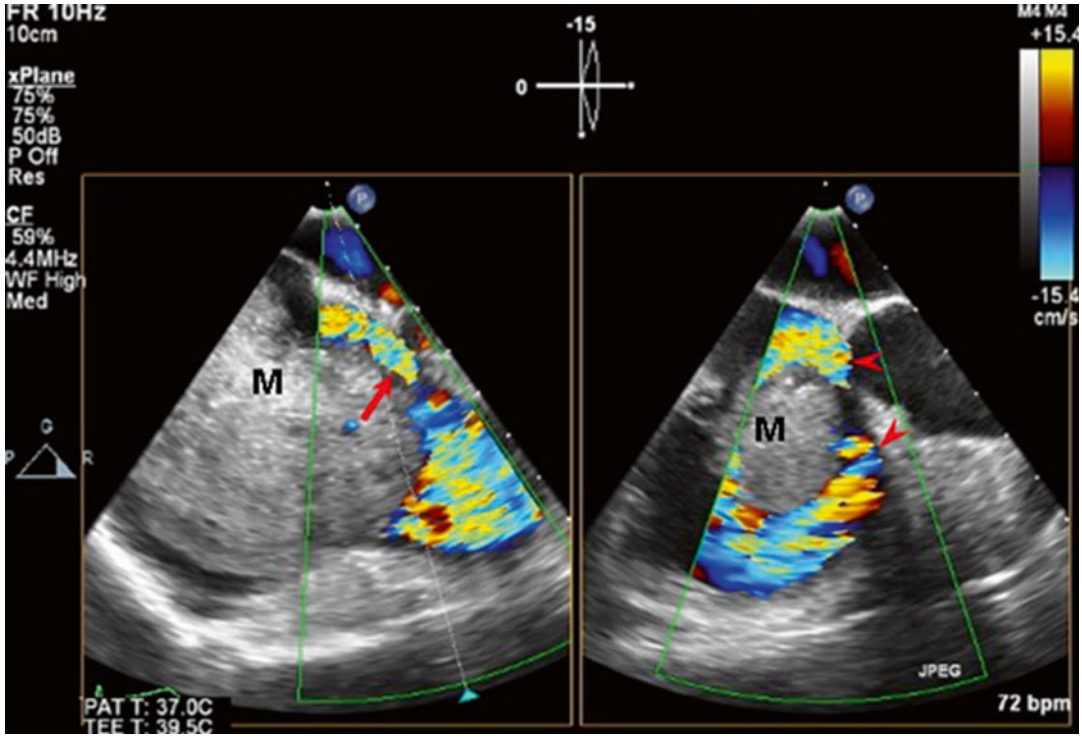

Fig. 10.23 2D TEE color Doppler, x-plane view, showed moderate TR (*arrows*) due to incomplete TV closure

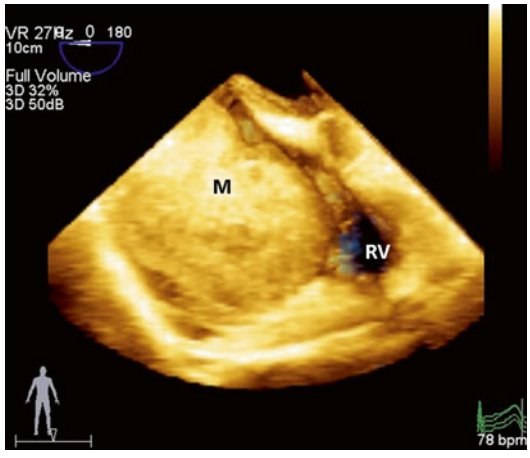

Fig. 10.24 3D TEE, modified four-chamber view, showed the huge mass (*M*) attached to RA basal posterior wall

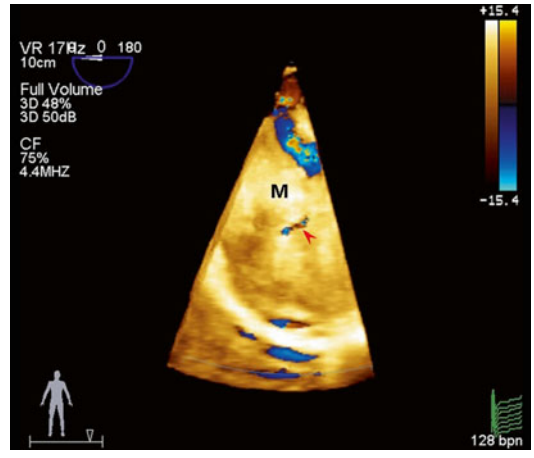

Fig. 10.25 3D TEE color Doppler, showed the RA mass (*M*) had blood supply (*arrow*)

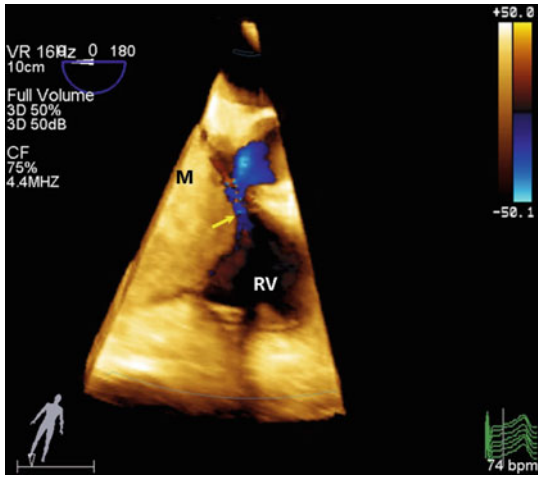

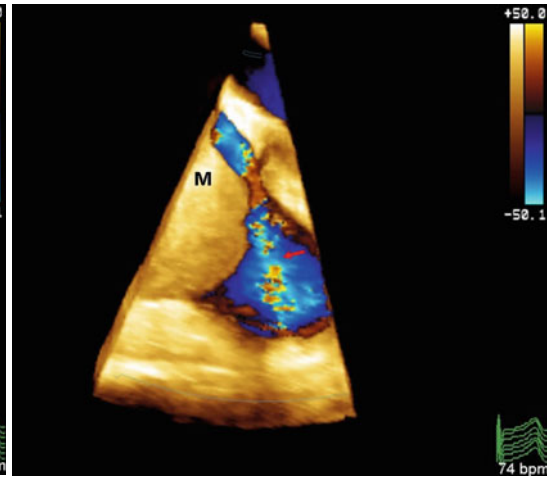

Figs. 10.26 and 10.27 3D TEE color Doppler, modified four-chamber view, showed moderate TR (*yellow arrow*) in systole due to incomplete TV closure (*left*) and accelerated tricuspid inflow (*red arrow*) in diastole as the mass (*M*) obstructed the tricuspid orifice (*right*)

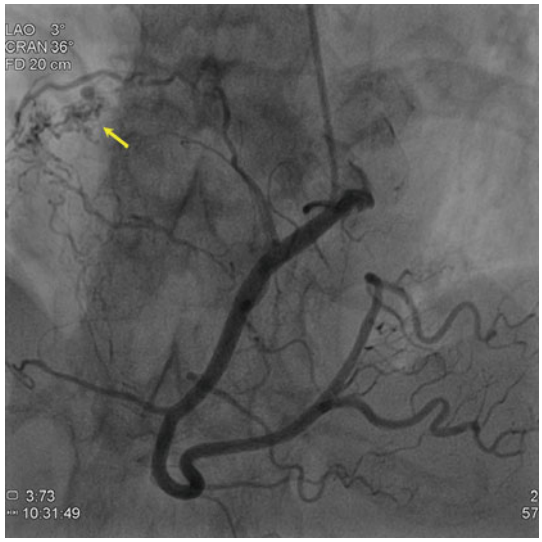

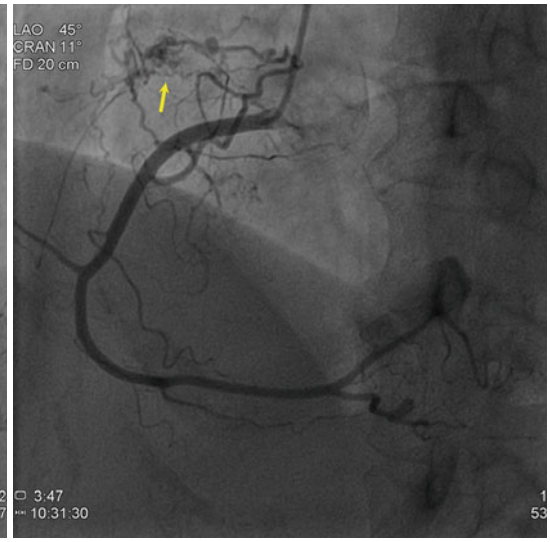

Figs. 10.28 and 10.29 Fluoroscopy of RCA, a large conus branch (*arrow*) gave blood supply to the RA tumor, positive tumor stain sign

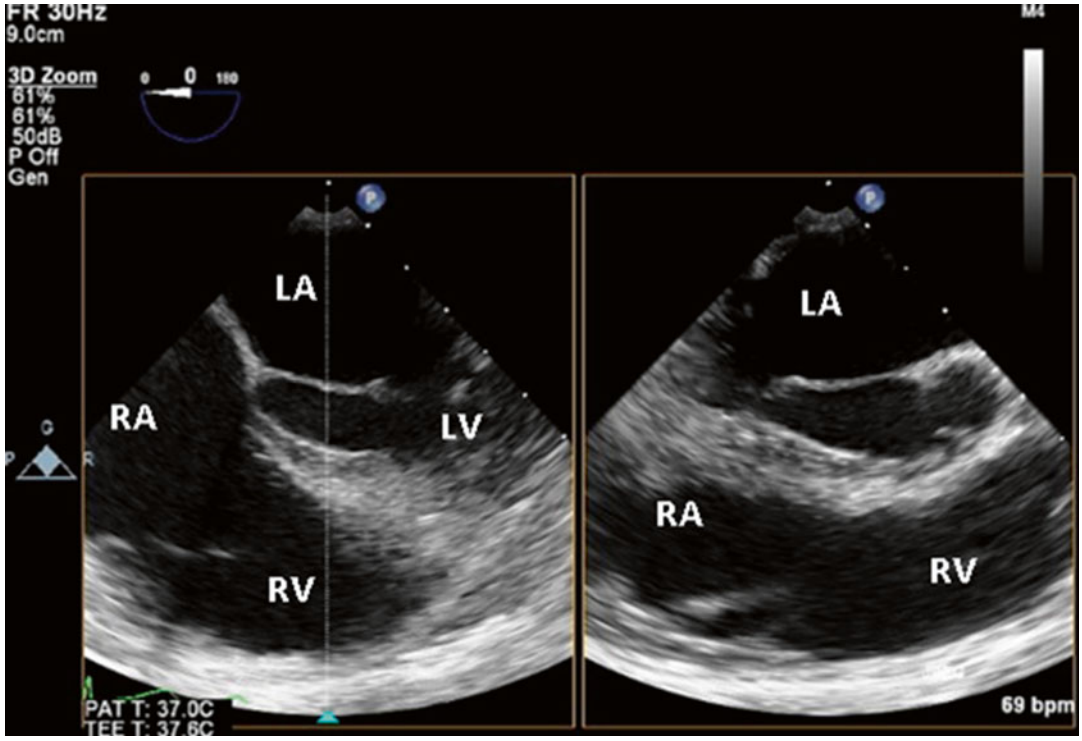

Fig. 10.30 2D TEE, x-plane view, status post removal of RA tumor, complete excision was documented

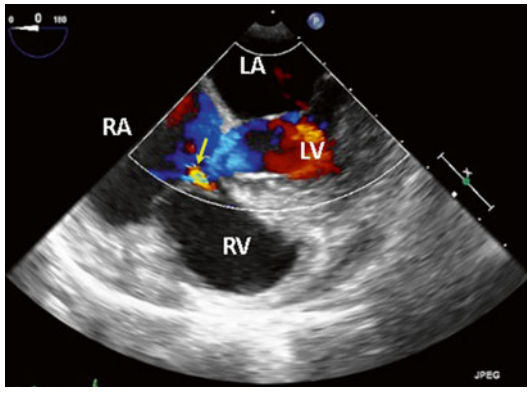

Fig. 10.31 2D TEE color Doppler, modified four-chamber view, status post removal of RA tumor, showed mild TR (*arrow*)

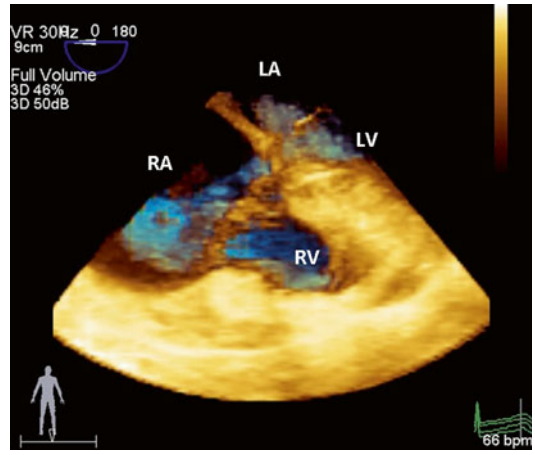

Fig. 10.32 3D TEE, modified four-chamber view, status post removal of RA tumor without residudal

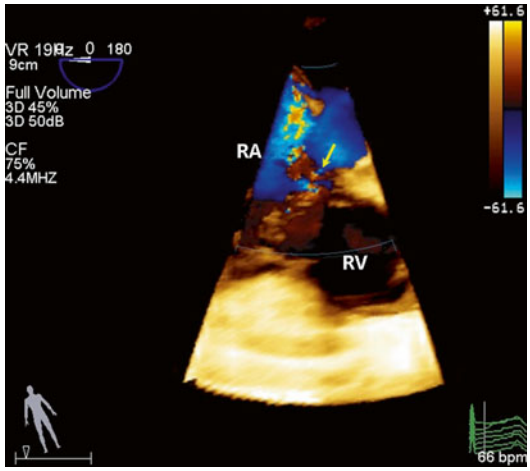

Fig. 10.33 3D TEE color Doppler, modified four-chamber view, status post removal of RA tumor, showed mild TR (*arrow*)

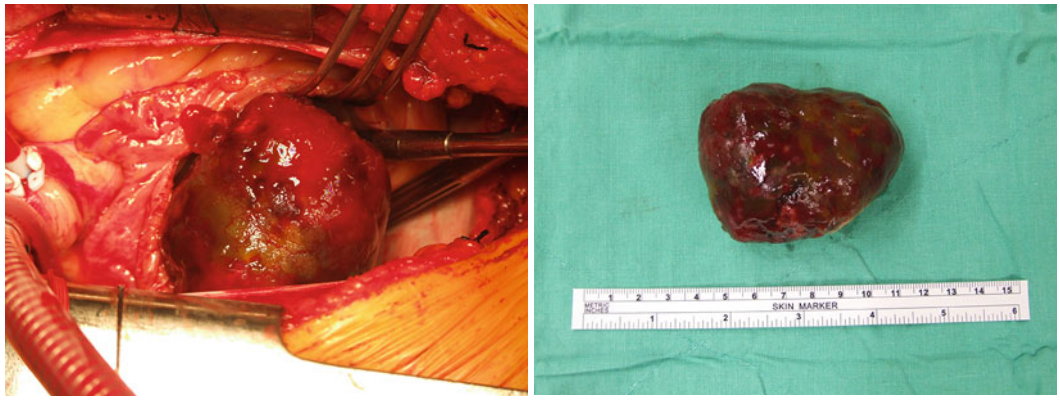

Figs. 10.34 and 10.35 Picture during operation (*left*) and gross specimen (*right*) showed the RV myxoma measuring 6 cm × 5 cm × 4 cm in fresh state

Tips

Myxomas are the most common primary cardiac tumor, which most often are single and arise from the fossa ovalis of the interatrial septum.

10.4 Invasive Thymoma Extending into Superior Vena Cava and Right Atrium

A 34-year-old man was in good health before. He suffered from facial flush, swelling and dyspnea recently. Lab data showed aspartate transaminase = 18 IU/L and creatinine = 0.88 mg/dl. Auscultation: regular heart beat without murmur. ECG: normal sinus rhythm. Chest X ray: increased soft tissue density at mediastinum with a space occupied lesion in left pulmonary hilum. Chest CT: a huge anterior mediastinal tumor (10 cm × 7.4 cm) with lung metastasis and superior vena cava (SVC) involvement. Operation: mediastinal tumor resection, wedge resection of right middle lobe lung tumor and SVC repair. Pathological diagnosis: thymoma, type B2, stage IV.

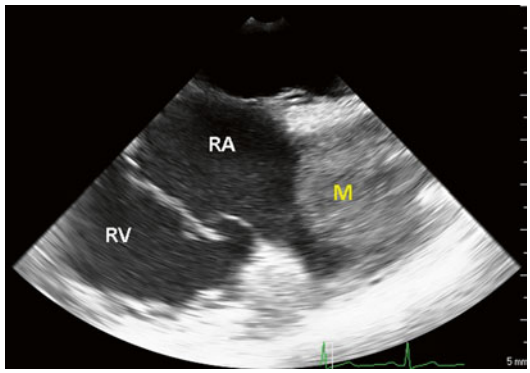

Fig. 10.36 Two-dimensional transesophageal echocardiography (2D TEE), showed an invasive thymoma (*M*) extending into the SVC and protruded into RA

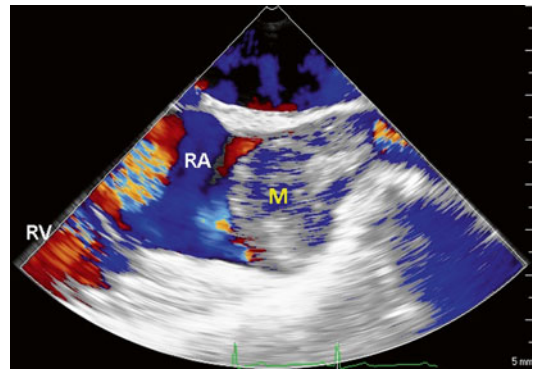

Fig. 10.37 2D TEE color Doppler, showed an invasive thymoma (*M*) extending into the SVC with occlusion

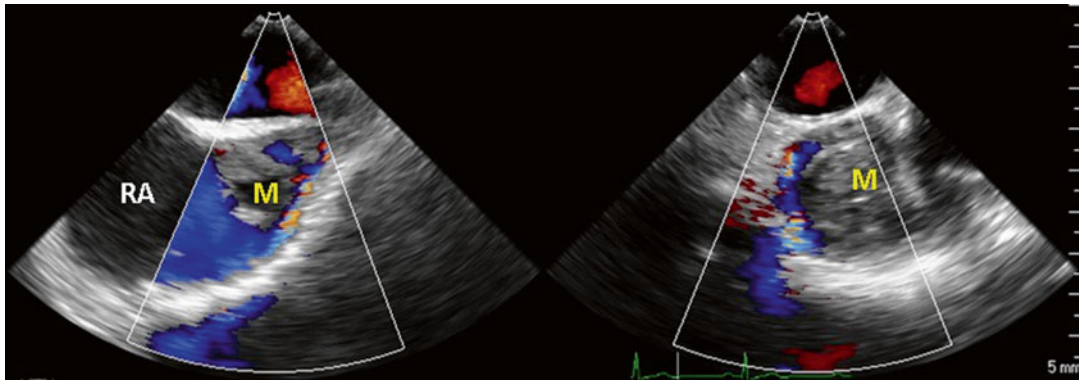

Fig. 10.38 2D TEE color Doppler, x plane view, showed SVC was occluded by the invasive thymoma (*M*)

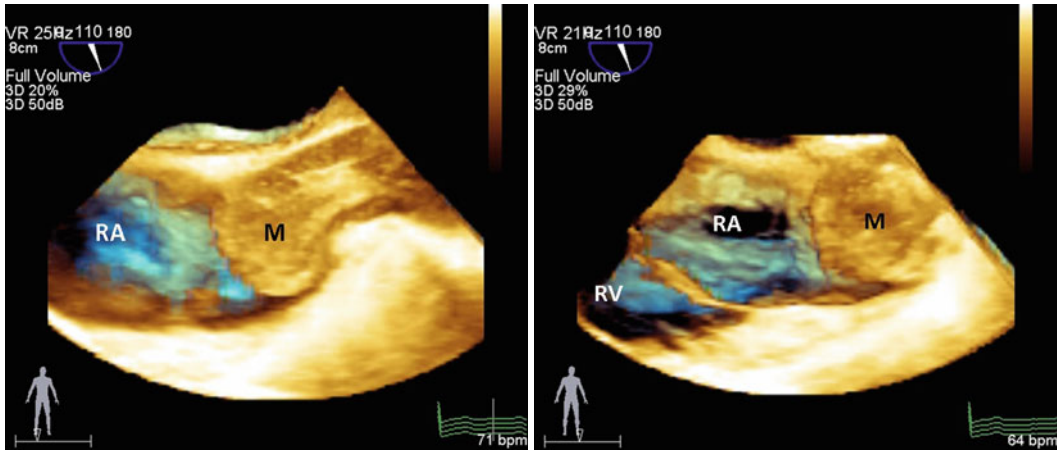

Figs. 10.39 and 10.40 3D TEE, showed the thymoma (*M*) extending into the SVC and protruded into RA

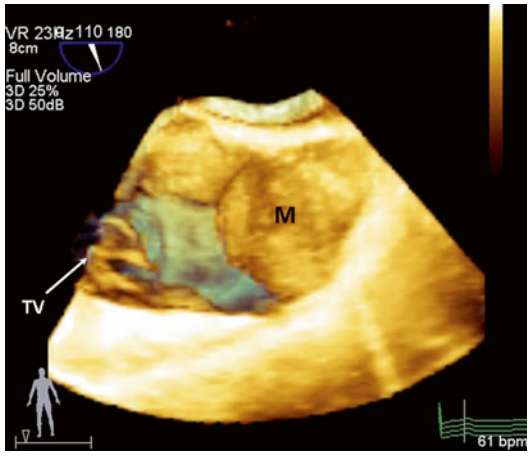

Fig. 10.41 3D TEE, showed the thymoma (*M*) extending into the SVC and protruded into RA

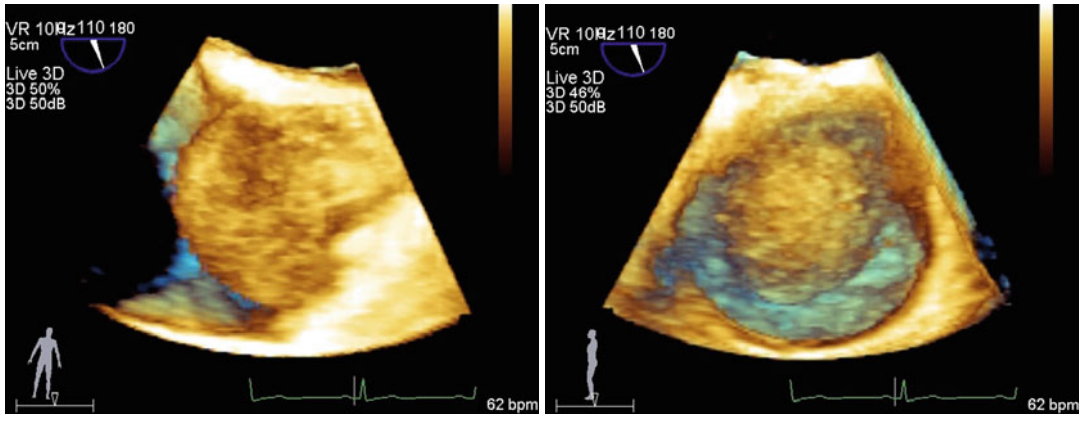

Figs. 10.42 and 10.43 3D TEE, zoom mode and perspective from RA to SVC (*right*), showed the thymoma almost filled the SVC and protruded into RA

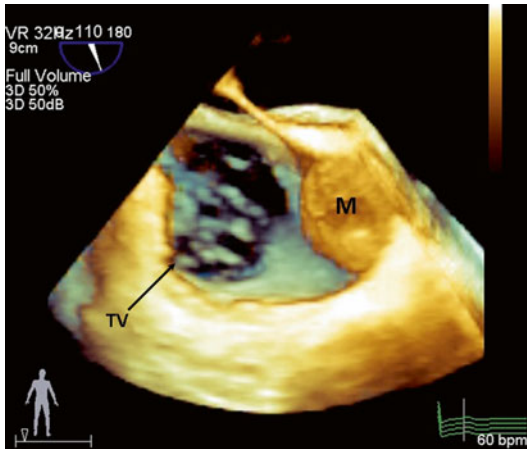

Fig. 10.44 3D TEE, perspective from RA to RV, showed the thymoma (*M*) protruded into RA

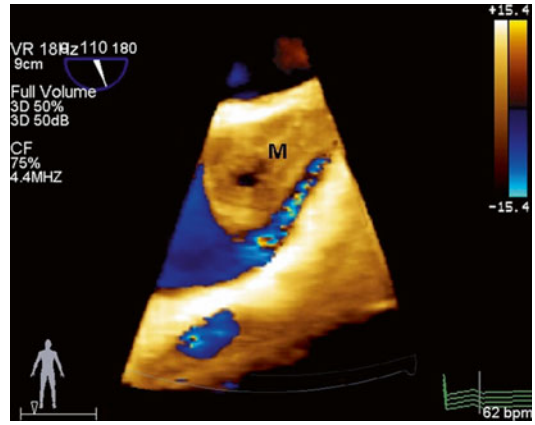

Fig. 10.45 3D TEE color Doppler, showed an invasive thymoma (*M*) extending into the SVC with occlusion

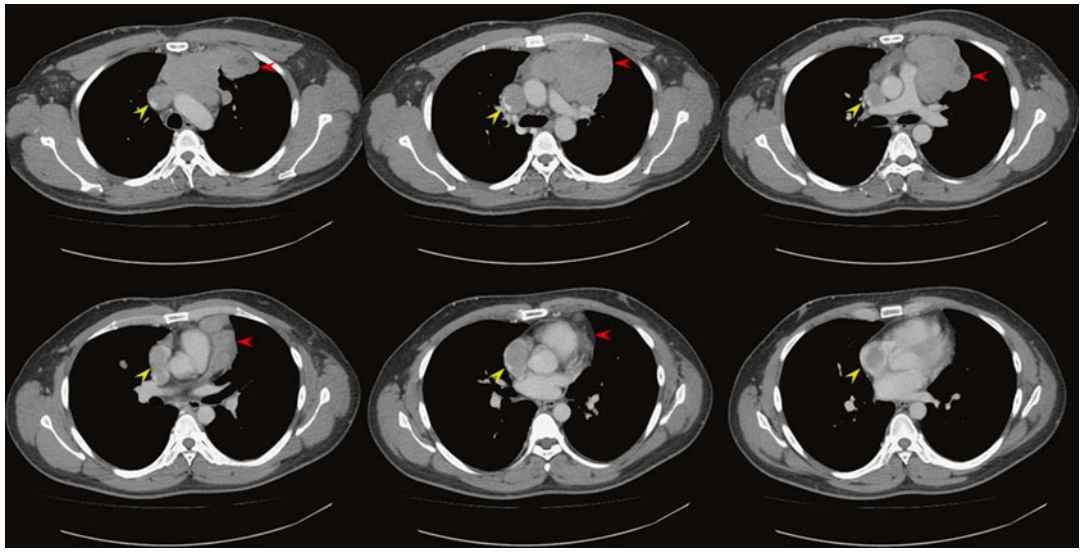

Fig. 10.46 Contrast-enhanced CT images, showed a huge anterior mediastinal tumor with lung metastasis (*red arrows*) and extended into the SVC and RA (*yellow arrows*)

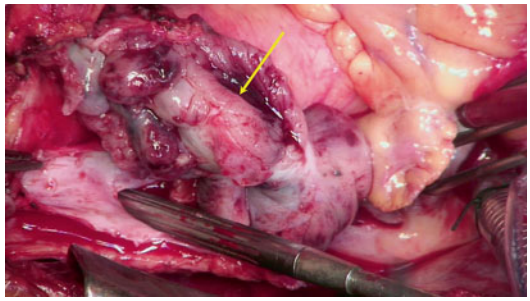

Fig. 10.47 Picture during tumor resection, showed the thymoma in SVC (*arrow*)

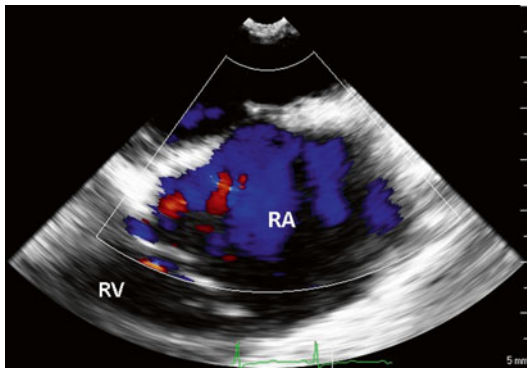

Fig. 10.48 2D TEE color Doppler, status post tumor resection, showed clear RA without residual thymoma

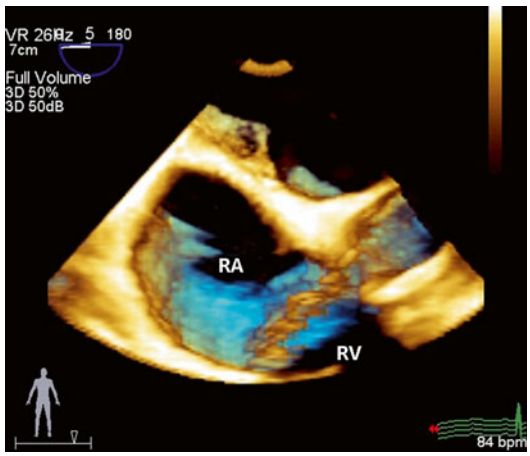

Fig. 10.49 3D TEE, status post tumor resection, showed clear RA without residual thymoma

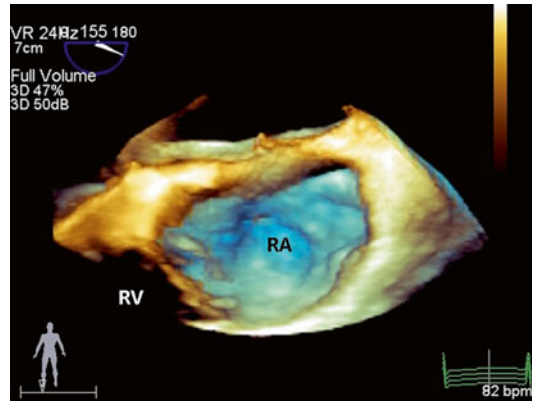

Fig. 10.50 3D TEE, status post tumor resection, showed clear RA without residual thymoma

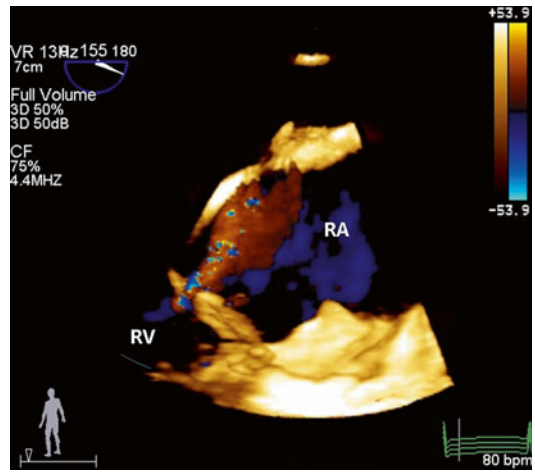

Fig. 10.51 3D TEE color Doppler, status post tumor resection, showed mild TR

Tips

Invasive thymoma commonly infiltrates neighboring mediastinal structures. The case with thymoma extension into the SVC and consequent SVC occlusion is rare.

Suggested Reading

Abdelaziz A, Abdelgawad A, et al. A new complication of transesophageal echocardiography: pulmonary embolization of a right atrial myxoma. J Thorac Cardiovasc Surg. 2015;149(5):e79–81.

Cannavà G, Currò A. Left atrial myxoma presenting as acute coronary syndrome. Int J Cardiol. 2015;190: 148–50.

De Giacomo T, Patella M, et al. Successful resection of thymoma directly invading the right atrium under cardiopulmonary bypass. Eur J Cardiothorac Surg. 2015; 48(2):332–3.

Melloni G, Bandiera A, et al. Thymoma with intravascular extension into the right atrium. Eur J Cardiothorac Surg. 2014;45(4):e126.

Nishizaki Y, Yamagami S, Daida H. Left atrial myxoma incidentally discovered on transesophageal echocardiography. Intern Med. 2015;54(5):535.

Ried M, Neu R, Schalke B, et al. Radical surgical resection of advanced thymoma and thymic carcinoma infiltrating the heart or great vessels with cardiopulmonary bypass support. J Ca rdiothorac Surg. 2015;10:137.

Yong-Qiang D, Jiang-Shui L, Xiao-Ming Z, et al. Surgical treatment of an invasive thymoma extending into the superior vena cava and right atrium. World J Surg Oncol. 2014;12:6.

Others

11

Abstract

The other cases are classified as this chapter including a patient received a HeartMate II and the other patient suffered aortic root perforation.

A HeartMate II is a LV assistant device which can be alternative to heart transplantation. Perforation of aortic root is an iatrogenic complication during atrial fibrillation ablation. The cases are both interesting and enjoyable.

11.1 HeartMate II

A 50-year-old man had a history of ischemic cardiomyopathy with congestive heart failure, old myocardial infarction with triple-vessel coronary artery disease status post PTCA and stenting, LV thrombus, hypertension and type two diabetes mellitus. He suffered from fever with chillness and exertional dyspnea. Auscultation: irregular heart beat with a grade 3/6 murmur over left sternal border. ECG: atrial fibrillation with moderate ventricular response, ventricular premature beats and right axis deviation. Chest X ray: cardiomegaly and bilateral pleural effusion. Cardiac catheterization: severe triple-vessel coronary artery disease, ischemic cardiomyopathy and refractory heart failure, NYHA Fc III-IV. Heart transplantation was advised, but due to pertinacity of severe hyperglycemia under oral hypoglycaenic agent status, he decided to have a HeartMate II implantation. Operation: CABG x1 (SVG to OM) and HeartMate II implantation.

Electronic supplementary material The online version of this chapter (doi:10.1007/978-981-10-0587-9_11) contains supplementary material, which is available to authorized users.

W.-H. Yin, M.-C. Hsiung, *Atlas of Perioperative 3D Transesophageal Echocardiography*,
DOI 10.1007/978-981-10-0587-9_11

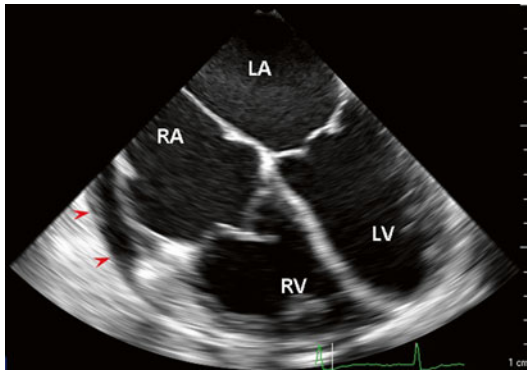

Fig. 11.1 Two-dimensional transesophageal echocardiography (2D TEE), four-chamber view, showed congestive heart failure with global systolic dysfunction, four-chamber dilation and moderate pericardial effusion (*arrows*)

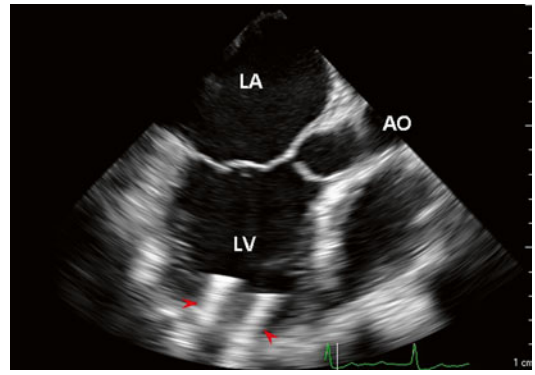

Fig. 11.3 2D TEE, long-axis view, status post implantation of LV assistant device, HeartMate II. The cannula (*arrows*) inserted into LV apex

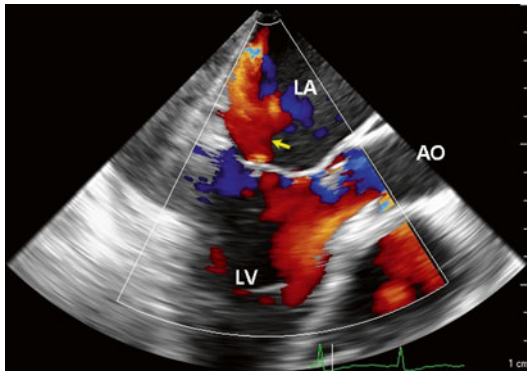

Fig. 11.2 2D TEE color-Doppler, long-axis view, showed congestive heart failure with moderate ischemic MR (*arrow*)

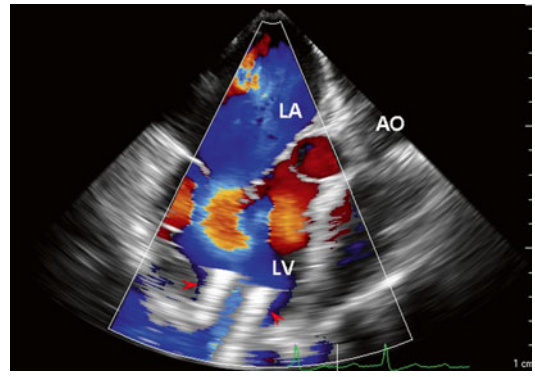

Fig. 11.4 2D TEE color Doppler, long-axis view, status post HeartMate II implantation. Flow out of the ventricle occurred through the HeartMate II (*arrows*)

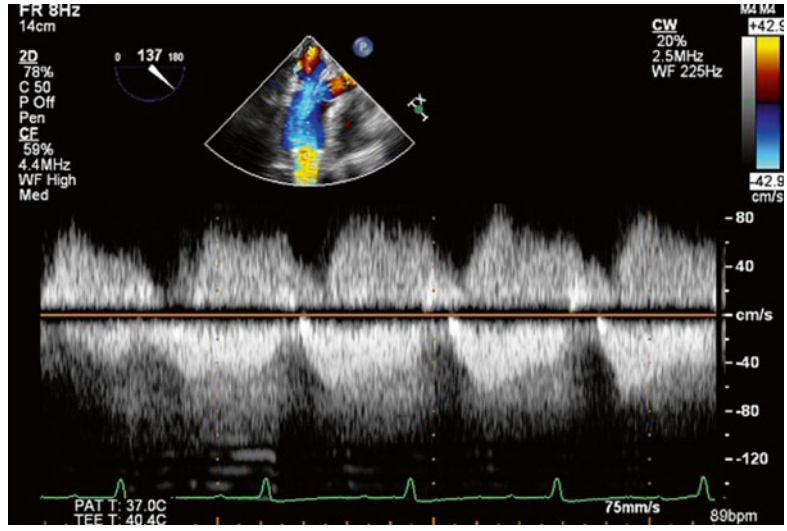

Fig. 11.5 2D TEE continuous-wave Doppler through the cannula, proper filling was confirmed

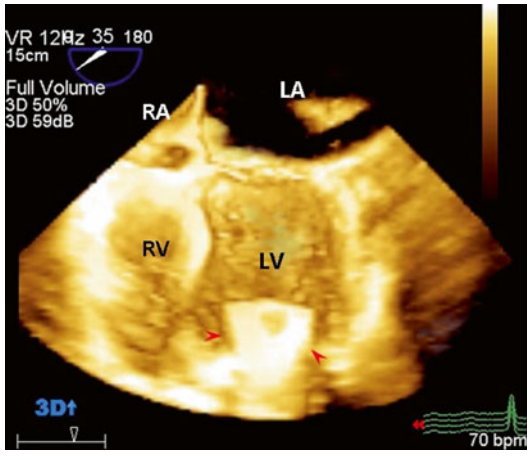

Fig. 11.6 3D TEE, four-chamber view, status post implantation of LV assistant device, HeartMate II. The cannula (*arrows*) inserted into LV apex

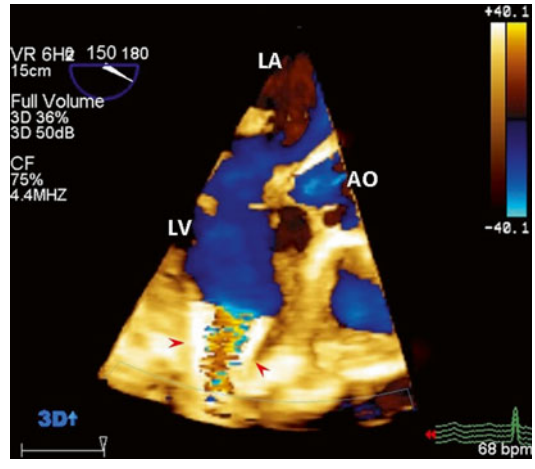

Fig. 11.7 3D TEE color Doppler, long-axis view, status post HeartMate II implantation. Showed diastolic flow in the apical cannula (*arrows*)

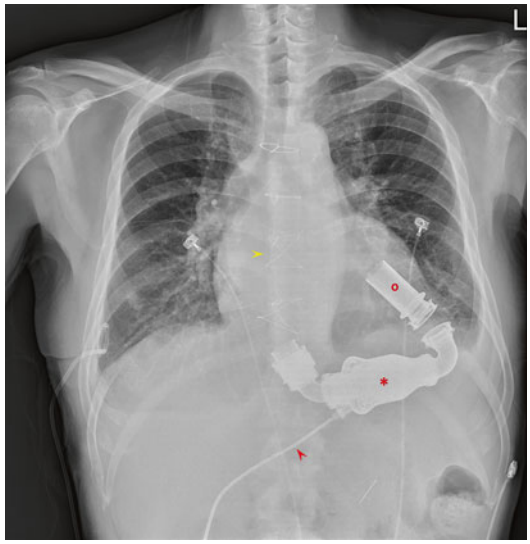

Fig. 11.8 Chest X ray showed the HeartMate II device was successfully implanted which included an outlet (o) inserted into LV apex, a pump (*), an inlet draining into ascending aorta (*yellow arrow*) and a wire (*red arrow*) connecting to external battery

Tips

A comprehensive TEE examination is essential both prior to and after the HeartMate II insertion to prevent any contraindication as well as to confirm the placement and function.

11.2 Iatrogenic Aortic Root Perforation

A 71-year-old man had a history of coronary artery disease status post PCI (LAD, LCX) and CABG x3 (SVG to first diagonal, posterior lateral branch of RCA and OM), severe MR and TR status post MV replacement and TV repair. He suffered from intermittent palpitation and exertional dyspnea. Auscultation: irregular heart beat without significant heart murmur. ECG: atrial fibrillation with tachycardia and old anterioseptal MI. He admitted for atrial fibrillation ablation. During procedure, the ablation lead pierced through from RA to aorta which resulted in aortic root perforation. Operation: emergent occluder implantation for aorta to RA iatrogenic fistula.

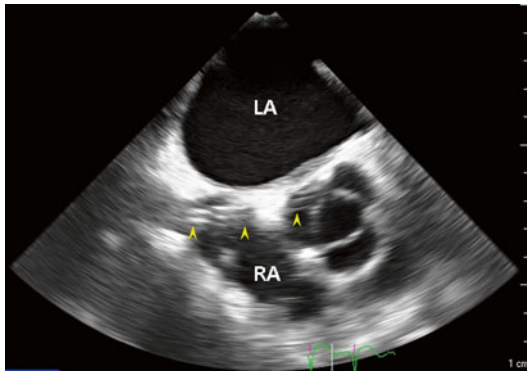

Fig. 11.9 Two-dimensional transesophageal echocardiography (2D TEE), short-axis view, during atrial fibrillation ablation, showed the ablation lead (*arrows*) went through from RA to aortic root at the level of the aortic sinus, just above the non-coronary cusp of the AV

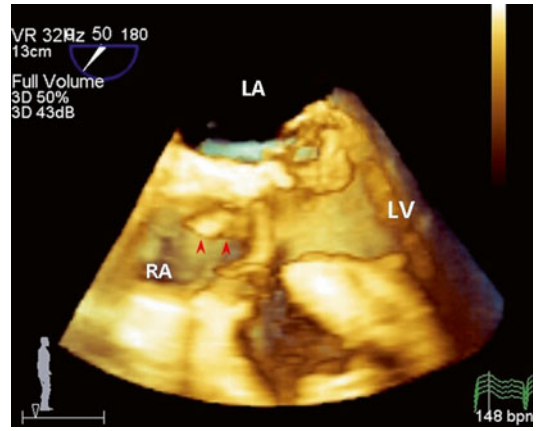

Fig. 11.11 3D TEE, modified five-chamber view, showed the ablation lead (*arrows*) pierced through from RA to aortic root

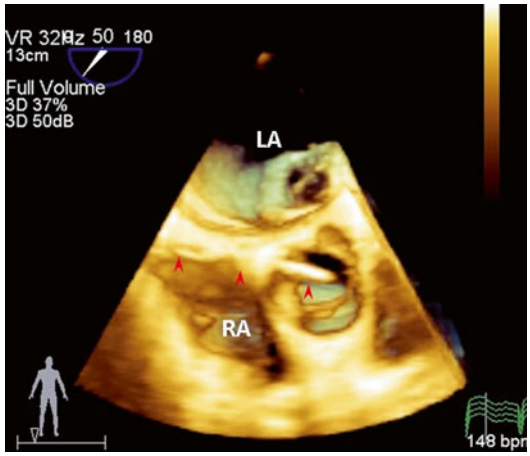

Fig. 11.10 3D TEE, short-axis view, during the procedure, showed the ablation lead (*arrows*) pierced through from RA to aortic root

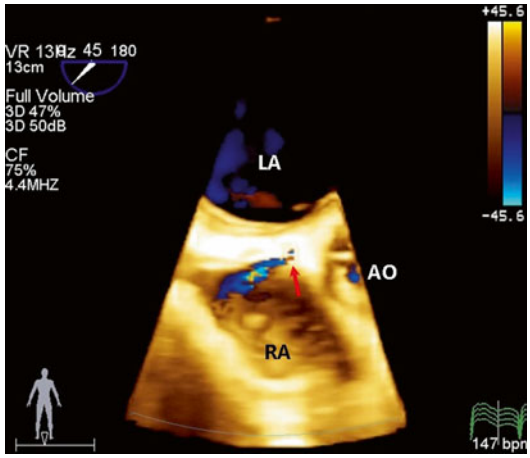

Fig. 11.12 3D TEE color Doppler, short-axis view, showed continuous flow (*arrow*) from aorta to RA

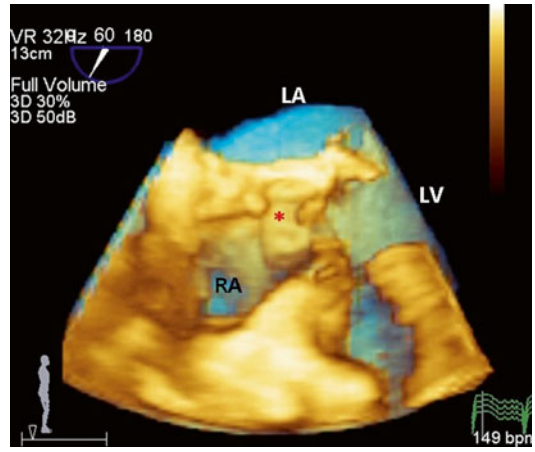

Fig. 11.14 3D TEE, modified five-chamber view, status post occluder (*) implantation

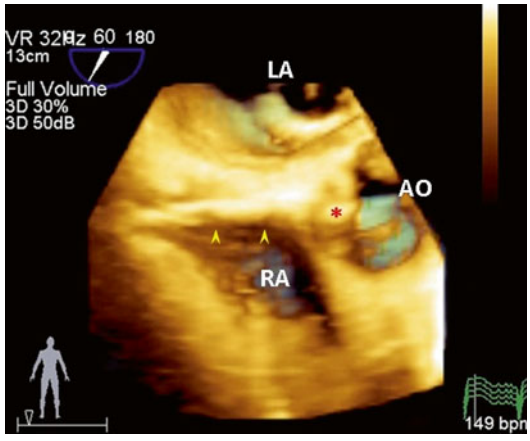

Fig. 11.13 3D TEE, short-axis view, showed the occluder (*) was transported by catheter (*arrows*) and deployed to occlude the iatrogenic aorta to RA fistula

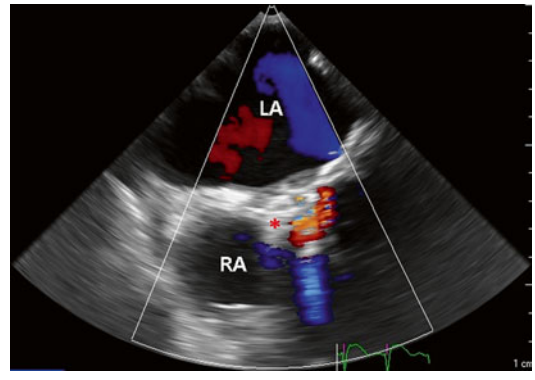

Fig. 11.15 3D TEE color Doppler, short-axis view, status post occluder (*) implantation without residual flow seen

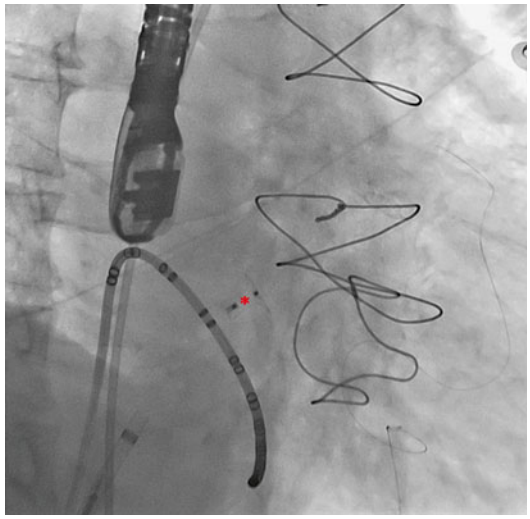

Fig. 11.16 Fluoroscopy status post occluder implantation, showed the deployed occluder (*arrows*)

Tips

TEE examination of aorta assists in the placement of ablation wire by preventing aortic injury and confirming proper positioning.

Suggested Reading

Bansal RC, Chandrasekaran K. Real time three-dimensional transesophageal echocardiographic evaluation of aortic valve perforation. Echocardiography. 2015;32(7):1147–56.

Cheng RK, Aboulhosn J, Nsair A. Percutaneous angioplasty of stenotic outflow graft anastomosis of HeartMate II. JACC Cardiovasc Interv. 2014;7(6):700–3.

Copeland H, Stoletniy L, et al. Implantation of HeartMate II left ventricular assist device in a single-lung patient. Ann Thorac Surg. 2015;99(6):2216–8.

Ho-Ping Y, An-Ning F, Shen-Kou T, et al. Transcatheter repair of iatrogenic aortic perforation complicating transseptal puncture for a catheter ablation of atrial arrhythmia. Acta Cardiol Sin. 2014;30:490492.

Pauwaa S, Raghuvir R, Kurien S, et al. Intermittent aortic insufficiency as an aid to diagnosing obstruction in a HeartMate II continuous-flow left ventricular assist device. ASAIO J. 2011;57(3):244–6.